To the Graduate Council:

I am submitting herewith a dissertation written by Michael Scott Kriger entitled "FUNDAMENTAL ASPECTS OF THE IONIZATION MECHANISMS IN FAST ATOM BOMBARDMENT/LIQUID SECONDARY ION, ELECTROSPRAY, AND ELECTROHYDRODYNAMIC MASS SPECTROMETRY." I have examined the final copy of this dissertation for form and content and recommend that it be accepted in partial fulfillment of the requirements for the degree of Doctor of Philosophy, with a major in Chemistry.

Kelsey D. Cook, Major Professor

We have read this dissertation
and recommend its acceptance:

Accepted for the Council:

Associate Vice Chancellor
and Dean of The Graduate School

# Fundamental Aspects of the Ionization Mechanisms in Fast Atom Bombardment / Liquid Secondary Ion, Electrospray, and Electrohydrodynamic Mass Spectrometry

A Dissertation

Presented for the

Doctor of Philosophy

Degree

The University of Tennessee, Knoxville

Michael Scott Kriger

May 1995

DEDICATION

To my wife Amanda,

for her unselfish love and support,

and

To my beautiful daughter,

Sarah Meghan

for the joy she has given me,

and

To my parents,

Glenn and Judy

for their love, encouragement and support for so many years.

## ACKNOWLEDGMENTS

Many individuals have contributed to the success of my research. I owe Professor Kelsey D. Cook many thanks for providing encouragement and guidance when times were tough and for teaching me how to be a research chemist. Dr. Albert A. Tuinman deserves many thanks for taking the time to teach me many aspects of mass spectrometry that I would not have known otherwise. I also owe special thanks to Dr. John Bartmess for the many helpful discussions. I owe Drs. Peter Todd, Tim Short and Roswitha Ramsey of Oak Ridge National Laboratory special thanks for all of their assistance and for allowing me access to their instrumentation. I also wish to thank Dr. J. Q. Chambers for allowing me access to the electrochemical instrument and for useful discussions about the preparation of conductive polymers and gold films. Past and present Cook research group members, including Bill Boggess, Steven Salvato, Martin Haddix, and Charles Coffey have provided memories that I will never forget.

I deeply appreciate the funding provided by the University of Tennessee Chemistry Department, the Science Alliance, the National Science Foundation, and the University of Tennessee Scholarly Research Incentive Fund that made this work possible.

## ABSTRACT

Surface activity effects in fast atom bombardment (FAB) and liquid secondary ion mass spectrometry (LSIMS) were investigated using two quaternary ammonium cations. It was shown that the intensity of tetradecyltrimethylammonium ($TTA^+$), a surface active cation, was initially strong and then decreased over the lifetime of the sample. The FAB signal from tetraethylammonium ($TEA^+$), a non-surface active quaternary ammonium cation, was shown to be initially weak followed by a short lived burst of high intensity prior to the end of the experiment. The reasons for this behavior were determined using a secondary ion imaging instrument to characterize the ion emission from the surface of the sample. The images revealed that $TTA^+$ yielded relatively uniform signal intensity from across the entire surface of the sample, while $TEA^+$ yielded non-uniform secondary ion emission across the surface of the sample. The explanation of the non-uniform $TEA^+$ emission was based on a Marangoni force. Marangoni forces drive less surface active solutes to the periphery of a sample. The $TTA^+$ signal was initially strong because of complete surface coverage from the beginning of the experiment. The $TEA^+$ signal was strong late in the experiment, because that was when the region of intense $TEA^+$ emission (due to changes in sample size) comes into the region of the source where ions are accepted into the analyzer.

A new micro-electrospray (ES) source was developed. The new source was tested using continuous infusion and capillary electrophoresis to deliver solution to the emitter. The new source used a small inner diameter fused

silica capillary with a mechanically shaped conical tip. The tip was chemically treated with a mercaptan reagent to improve the adhesion of a vapor deposited gold layer. These capillaries were shown to withstand over 100 hours of operation, to spray a variety of highly conductive aqueous and non-aqueous solutions, and to withstand harsh chemical treatment. The capillaries were also tested mass spectrometrically. Under continuous infusion conditions, as little as seven attomoles of cytochrome C was detected from an aqueous solution using flow rates less than 1 μl/minute. The charge state distribution of cytochrome C is known to change in the presence of methanol (methanol denatures cytochrome C). The extent of denaturation was investigated using solutions containing various amounts of methanol. Based on preliminary observations, the higher charge states of cytochrome C appear to be more heavily solvated than the lower charge states. The source was also evaluated as a capillary electrophoresis/ES interface. The four peptide components of an aqueous mixture were successfully separated and detected using the micro-ES source.

EH MS was used to probe the preferential solvation of the proton in a mixed solvent system containing 95/5 (v/v) water/glycerol. The EH source used previously to sample glycerol solutions was modified to contain a fused silica capillary to deliver aqueous (volatile) solutions to the emitter region. In a 95/5 (v/v) water/glycerol solution containing 40 mM HCl, the most intense peaks in the spectrum are the protonated glycerol dimer ($[G_2 + H]^+$) and trimer ($[G_3 + H]^+$). This indicates preferential solvation of the proton by glycerol, and is in good agreement with known gas and solution phase chemistry of the two solvents. The relative abundance of water clusters differed markedly from that reported in the literature for the gas-phase hydration of the proton; it

was therefore inferred that the distribution may reflect solution phase rather than gas phase chemistry.

Table of Contents


| | | |
|---|---|---|
| Chapter 1 | Introduction | 1 |
| 1.1 | FAB/LSIMS | 2 |
| 1.2 | Electrospray Ionization | 7 |
| | 1.2.1 Capillary Electrophoresis/Electrospray | 13 |
| 1.3 | Electrohydrodynamic Ionization | 19 |
| 1.4 | Solvation | 27 |
| | 1.4.1 Condensed-Phase Approaches | 31 |
| | 1.4.2 Mass Spectrometric Approaches | 33 |
| 1.5 | Summary and Objectives | 45 |
| Chapter 2 | Experimental Methods | 46 |
| 2.1 | FAB/LSIMS | 47 |
| | 2.1.1 Secondary ($2^{o}$) Ion Microprobe | 47 |
| | 2.1.2 VG ZAB-EQ | 50 |
| | 2.1.3 Electrochemical Polymerization of 3-methylthiophene | 52 |
| 2.2 | Electrospray Ionization | 55 |
| | 2.2.1 Finnigan-MAT Ion Trap | 55 |
| | 2.2.1.1 Electrospray Sources | 55 |
| | 2.2.1.2 Capillary Characterization Apparatus | 62 |
| | 2.2.2 Capillary Coating Procedure | 66 |
| 2.3 | Electrohydrodynamic Ionization Mass Spectrometry | 68 |
| | 2.3.1 AEI MS-902 | 68 |
| | 2.3.2 EH Source Modification | 74 |

| | | |
|---|---|---|
| 2.4 | Sample Preparation and Reagents | 79 |
| | 2.4.1 Sample Preparation for FAB/LSIMS | 82 |
| | 2.4.2 Sample Preparation for ESI | 82 |
| | 2.4.3 Sample Preparation for EH | 82 |
| Chapter 3 | Secondary Ion Emission From Solutions: Time Dependence and surface Phenomena | 84 |
| 3.1 | Temporal Behavior of FAB Spectra | 87 |
| 3.2 | Spatial Distribution of Solutes | 98 |
| 3.3 | Effects of Surface Activity | 111 |
| 3.4 | Electrochemical Polymerization on FAB Target to Improve Wettability | 118 |
| 3.5 | Conclusions | 122 |
| Chapter 4 | Durable Gold-Coated Fused Silica Capillaries For Use in Electrospray Mass Spectrometry and Capillary Electrophoresis/Electrospray Mass Spectrometry | 124 |
| 4.1 | Capillary Characterization | 127 |
| | 4.1.1 Capillary Durability | 127 |
| | 4.1.2 Spray Versatility | 133 |
| 4.2 | Mass Spectrometric Applications | 138 |
| | 4.2.1 Continuous Infusion Experiments | 138 |
| | 4.2.2 Figures of Merit | 151 |
| | 4.2.3 CE/ES/MS | 154 |
| 4.3 | Conclusions | 158 |

Chapter 5 Electrohydrodynamic Mass Spectrometry As A Probe of Solution Chemistry 159

5.1 Preferential Solvation 161

5.2 Cluster Distribution 180

5.3 Conclusions 205

Chapter 6 Conclusions and Suggestions for Future Work 207

List of References 213

VITA 231

LIST OF TABLES


| Table | Description | Page |
|---|---|---|
| 2.1 | Parts list for the Finnigan-MAT ITMS shown in Figures 2.4 and 2.5. | 57 |
| 2.2 | Parts list for the unmodified EH source shown in Figure 2.10. Materials are SS except as noted. | 71 |
| 2.3 | Parts list for the modified EH source shown in Figure 2.11. Materials are SS except as noted. | 73 |
| 2.4 | List of reagents used in these studies. | 80 |
| 3.1 | $TEA^+$ and $TTA^+$ information. | 99 |
| 4.1 | Solutions used to test the chemical stability of capillary coatings. | 128 |
| 4.2 | Counter electrode current and needle voltage data for first capillary used to test long-term stability, spraying 10 mM acetic acid (pH 3.5) at 0.2 μL/minute. | 130 |
| 4.3 | Counter electrode current and voltage data for a second capillary used to test long-term stability, spraying 10 mM acetic acid (pH 3.5) at 0.2 μL/minute. | 131 |
| 4.4 | Solutions used to test electrospray stability with 25 μm i.d. coated capillaries. | 139 |
| 4.5 | A comparison of the sensitivity enhancement factors for spraying 21 μM cytochrome C in 75% Methanol/24% water/1% acetic acid from Au-tipped | |

| | | |
|---|---|---|
| | capillaries with varying inner diameter. | 144 |
| 5.1 | Solvation enthalpies* (kJ $mol^{-1}$) of tetraalkylammonium ions in water and methanol at 25° C. | 163 |
| 5.2 | List of prominent ions appearing in EH mass spectra of 40 mM HCl in 95/5 (v/v) water/glycerol solvent mixture using a flow rate of 5, 7.5 and 10 μL/hour. Entries represent the average from at least 3 replicates and corresponding standard deviation (σ). | 167 |
| 5.3 | Solvent properties for water and glycerol. | 170 |
| 5.4 | Gas phase thermodynamic data for Reaction 5.1, involving protonated water clusters. | 187 |
| 5.5 | Calculated errors illustrating the poor fit at various temperatures and pressures. | 189 |
| 5.6 | Metastable decay data for clusters from a 40 mM HCl solution in 95% water and 5% glycerol (v/v). | 194 |
| 5.7 | Metastable decay free energy for the loss of water from protonated water clusters. Calculated using gas-phase free energy data from Kebarle. | 197 |

LIST OF FIGURES


| Figure | Description | Page |
|---|---|---|
| 1.1 | The FAB and LSIMS experiments. A primary particle beam impinges upon a sample and secondary ions are produced. The primary beam is neutral for FAB and ionic for LSIMS. | 3 |
| 1.2 | The ES experiment (shown for positive ions). The electric field at atmospheric pressure promotes the formation of small droplets which ultimately form unsolvated ions. $V_{es}$ is the voltage necessary to sustain stable spray. | 8 |
| 1.3 | Cross sectional view of the sheath flow interface used in CE/ES. Typical conditions are as follows: CE capillary dimensions of 25 to 100 μm i.d. X 365 μm o.d with flow rates on the order of 10 μL/hour; SS needle dimensions of 394 μm i.d. X 711 μm o.d.; sheath solvent delivered at flow rates on the order of 1 to 5 μL/minute; ES voltage 1 to 4 kV. | 16 |
| 1.4 | Cross sectional view of the liquid junction interface used in CE/ES. Typical CE and ES conditions are the same as those described in Figure 1.3. | 17 |
| 1.5 | A depiction of the EH experiment. The electric field in a vacuum promotes the desorption of ions from a sample reservoir. | 20 |
| 1.6 | Schematic diagram illustrating the primary and | |

| | | |
|---|---|---|
| | subsequent spheres of solvation around the cation $M^+$. | 29 |
| 2.1 | Schematic diagram of the wide angle secondary ion microprobe used to acquire secondary ion images and spectra. | 48 |
| 2.2 | Schematic diagram of the VG ZAB-EQ instrument used to acquire fast atom bombardment data. | 51 |
| 2.3 | Schematic diagram of the electrochemical apparatus used to polymerize 3-methylthiophene on the surface of a stainless steel FAB probe tip. | 54 |
| 2.4 | Schematic diagram of the Finnigan-MAT ion trap mass spectrometer and syringe pump used to acquire continuous infusion electrospray data. The source is shown using the gold coated capillaries described in section 2.2.2. See parts list in Table 2.1. | 56 |
| 2.5 | Schematic diagram of the Finnigan-MAT ion trap mass spectrometer and capillary electrophoresis instrument used to acquire the CE/ESI data. The source is shown using the gold coated capillaries described in section 2.2.2. See parts list in Table 2.1. | 58 |
| 2.6 | Cross sectional view of the system used for electrospray using a sheath solvent flow or nitrogen nebulization | 60 |
| 2.7 | Schematic diagram of the bench-top apparatus used to characterize the durability of the gold-coated tips and their versatility for spraying various | |

solutions. 63

2.8 Electron micrograph of a gold-coated 25 μm i.d. x 365 μm o.d. shaped fused silica capillary. The electron micrograph was obtained using an ETEC Autoscan (Los Angeles, CA) electron microscope. The micrograph was acquired by Mr. Richard Williams of the University of Tennessee Microscopy Laboratory under conditions yielding a magnification of 40X. The outer diameter at the tip after shaping is estimated to be 50 μm or roughly twice the inner diameter of the capillary. To avoid charging of non-conductive surfaces, only the conductive (gold-coated) portion of the capillary was mounted in the instrument to acquire the electron micrograph. 66

2.9 Schematic diagram of the AEI MS-902 instrument used to acquire the EH data. FFR = field free region. 69

2.10 Cross-sectional view of the unmodified EH source used with glycerol samples. Numbers refer to parts listed in Table 2.2. 70

2.11 Cross-sectional view of the modified EH source used with aqueous solutions. Dotted lines indicate wire connections. Numbers refer to parts listed in Table 2.3. 72

2.12 Cross sectional view of the positioning of the fused

| | | |
|---|---|---|
| | silica capillary within the Pt emitter. | 76 |
| 3.1 | Schematic diagram illustrating the sample orientation during the (a) LSIMS and (b) FAB experiments. | 88 |
| 3.2 | Normalized (to the most intense signal from $TTA^+$) intensities of m/z 256 ($TTA^+$) and m/z 93 ($[G + H]^+$) versus time from a 1 mM solution of TTAB in glycerol. Data from a FAB experiment using the VG ZAB-EQ. | 90 |
| 3.3 | FAB mass spectrum recorded from scan 1 of Figure 3.2. | 92 |
| 3.4 | FAB mass spectrum recorded from scan 50 of Figure 3.2. | 93 |
| 3.5 | Normalized (to the most intense signal from $TEA^+$) intensities of m/z 130 ($TEA^+$) and m/z 93 ($[G + H]^+$) versus time from a 1 mM solution of TEAI in glycerol. Data from a FAB experiment using the VG ZAB-EQ. | 94 |
| 3.6 | FAB mass spectrum recorded from scan 20 of Figure 3.5. | 95 |
| 3.7 | FAB mass spectrum recorded from scan 82 of Figure 3.5. | 96 |
| 3.8 | Intensity versus time for the rejuvenation experiment of (a) $TEA^+$ (m/z 130) and (b) $TTA^+$ (m/z 256) from 1 mM glycerol solutions. For comparison, the lighter trace in each figure corresponds to | |

protonated glycerol (m/z 93). Each figure is normalized to the most intense analyte ($TEA^+$ or $TTA^+$) signal. The arrows indicate when the fresh glycerol was added to the probe tip. Data acquisition was interrupted during this time period and re-started after re-inserting the probe tip into the instrument. 97

3.9 (a) Secondary ion image of m/z 256 ($TTA^+$) from 1 mM TTAB in glycerol, using white as the most intense and black as least intense. (b) Relative intensity of m/z 256 along cursor mark in image of part (a). 100

3.10 LSIMS Mass spectra acquired from the (a) center and (b) edge of the sample shown in the image of Figure 3.9. 101

3.11 LSIMS mass spectrum acquired late in the experiment from the center of the sample shown in the image of Figure 3.9. 103

3.12 (a) Secondary ion image of m/z 130 ($TEA^+$) from 1 mM TEAI in glycerol, using white as the most intense and black as least intense. (b) Relative intensity of m/z 130 along cursor mark in image of part (a). 104

3.13 LSIMS mass spectrum acquired at the (a) center and (b) edge of the sample shown in the image of Figure 3.12. 105

| | | |
|---|---|---|
| 3.14 | Secondary ion image of m/z 130 ($TEA^+$) (a) 15, (b) 32, and (c) 66 minutes after introduction of the sample, respectively. Each image is individually normalized to the most intense point in the image, which is indicated by white. | 106 |
| 3.15 | Secondary ion image of m/z 93 ($[G + H]^+$) (a) 15, (b) 32, and (c) 66 minutes after the introduction of the sample, respectively. Each image is individually normalized to the most intense point in the image, which is indicated by white. Except for the position of the respective maxima, no correlation is implied between the maximum intensities of m/z 130 (Figure 3.14) and m/z 93 in the respective images. | 107 |
| 3.16 | LSIMS Mass spectrum acquired at the center of the image shown in Figure 3.15c. | 109 |
| 3.17 | FAB mass spectrum acquired from a dry sample of $TEA^+$. | 110 |
| 3.18 | Successive (a) $TTA^+$, (b) $TEA^+$, and (c) $TTA^+$ secondary ion images from the same droplet of TEAI and TTAB in glycerol solution, acquired about 4 minutes between images. | 114 |
| 3.19 | Intensities of m/z 130 ($TEA^+$) and m/z 154 ($[NBA + H]^+$) versus time from 1 mM TEAI in m-nitrobenzyl alcohol sample from a FAB experiment. | 116 |
| 3.20 | Secondary ion image of (a) m/z 130 ($TEA^+$) and | |

(b) m/z 154 ([NBA + H]$^+$) from 1 mM TEAI in m-nitrobenzyl alcohol using white as the most intense and black as the least intense. 117

3.21 Cyclic voltammogram using a stainless steel electrode coated with poly-3-methylthiophene. The electrochemical cell consisted of a 0.1 M solution of tetraethylammonium perchlorate in acetonitrile, a Ag/AgCl quasi-reference electrode, and a Pt mesh counter electrode. 120

3.22 Total ion chromatogram from a thin film of glycerol applied to the surface of a stainless steel target coated with poly 3-methylthiophene. The amount of glycerol was not determined. 121

4.1 CE/ES interface using a sheath flow of solvent to establish electrical connection. 126

4.2 Collector current as a function of needle voltage while spraying methanol through a 25 μm i.d gold-coated capillary (Au) at a flow rate of 0.2 μL/minute and through a 150 μm i.d stainless steel needle (SS) at a flow rate of 1 μL/minute. The SS curve is offset +1 μA for clarity. 135

4.3 Collector current as a function of needle voltage while spraying 50:49:1 methanol:water:acetic acid (v/v/v) through a 25 μm i.d gold-coated capillary (Au) at a flow rate of 0.2 μL/minute and

through a 150 μm i.d stainless steel needle (SS) at a flow rate of 1 μL/minute. The SS curve is offset +1 μA for clarity. 136

4.4 Collector current as a function of needle voltage while spraying pure water at a flow rate of 0.2 μL/minute through a 25 μm i.d gold-coated capillary and a flow rate of 1 μL/minute through a 150 μm i.d stainless steel needle (SS). 137

4.5 Electrospray ionization mass spectra of 21 μM cytochrome C in 75% methanol/24% water/1% acetic acid (v/v/v) using a (a) 32 gauge stainless steel needle and a flow rate of 1 μL/minute and (b) 10 μm i.d gold-tipped capillary and a flow rate of 0.1 μL/minute. 3.2 picomoles of analyte were consumed using the SS needle and 0.32 picomoles of analyte were consumed using the Au-tipped capillary during the 9 second data averaging period. Numbers in the right hand corner represent absolute counts (of the most intense peak in the spectrum) in arbitrary units. 141

4.6 Electrospray ionization mass spectrum obtained from a 21 μM aqueous solution of cytochrome C using (a) a 32 gauge stainless steel needle with nitrogen nebulization and an infusion rate 1.0 μL/minute and (b) a 25 μm i.d. gold-tipped capillary and an infusion rate 0.1 μL/minute.

Numbers in the upper right hand corner of the spectra represent absolute intensity in arbitrary units. 142

4.7 Electrospray ionization mass spectrum obtained from a 21 μM solution of cytochrome C in 80% water/20% methanol (v/v) using a 25 μm i.d. gold-tipped capillary and an infusion rate 0.1 μL/minute. The inset represents an 8X magnification of the low m/z region of the spectrum. 145

4.8 Electrospray ionization mass spectrum obtained from a 21 μM solution of cytochrome C in 60% water/40% methanol (v/v) using a 25 μm i.d. gold-tipped capillary and an infusion rate 0.1 μL/minute. 146

4.9 Electrospray ionization mass spectra obtained from a 21 μM aqueous solution of cytochrome C using the methanol sheath source shown in Figure 4.1. The interface was tuned to optimize signal intensity for (a) high m/z ions and (b) low m/z ions. The methanol was delivered at a flow rate of 1 μL/minute and the 21 μM aqueous cytochrome C solution was delivered at a flow rate of 0.1 μL/minute. Numbers in the upper right hand corner of the spectra represent absolute intensity in arbitrary units. 148

4.10 Electrospray ionization mass spectrum obtained from a 21 μM aqueous solution of cytochrome C

using a 25 μm i.d. gold-tipped capillary and an infusion rate 0.1 μL/minute. The interface was tuned to optimize signal intensity for (a) high m/z ions and (b) low m/z ions. Numbers in the upper right hand corner of the spectra represent absolute intensity in arbitrary units. 150

4.11 Single scan (50 msec injection time) mass spectrum of cytochrome C obtained from a 0.17 μM aqueous solution (1% acetic acid). The spectrum was acquired under continuous infusion conditions at a flow rate of 0.05 μL/minute using a 25 μm i.d. gold-tipped capillary. 152

4.12 Plot of mass spectrometric response as a function of the cytochrome C concentration. A usable dynamic range of three orders of magnitude (minimum) is observed. All solutions were 99% water and 1% acetic acid. The line is described by the following equation: $y = 0.90x + 3.33$ with a correlation coefficient ($r^2$) of 0.9997. 153

4.13 Total ion current electropherograms for multiple injections of leucine enkephalin on a 50 μm i.d. gold-tipped capillary. 155

4.14 Electrospray ionization mass spectrum (single scan) from a 17 fmole injection of leucine enkephalin using capillary electrophoresis. 156

4.15 Total ion current (TIC) electropherogram for a

single injection of a mixture of leucine-enkephalin (2.16 picomoles), xenopsin (730 femtomoles), neurotensin (622 femtomoles), and bradykinin (536 femtomoles) on a 50 μm i.d. gold-tipped capillary. Peptides were injected electrokinetically (6 seconds at 20 kV) from an aqueous solution onto a 60 cm long fused silica column. The CE voltage was maintained at 20 kV. The two peaks adjacent to Leu-Enkephalin (one before and one after) were not identified. 157

5.1 Electrohydrodynamic ionization mass spectrum of 40 mM HCl in 95% water / 5% glycerol (v/v). Clusters are labeled as follows: $A_n = [G_n + H]^+$; $B_n = [(H_2O)_n + H]^+$; $C_n = [G_1 + (H_2O)_n + H]^+$; $D_n = [G_2 + (H_2O)_n + H]^+$; $E_n = [G_3 + (H_2O)_n + H]^+$ (where G denotes glycerol). See Table 5.2 for list of ions and their relative abundance. 162

5.2 Electrohydrodynamic ionization mass spectrum of (a) 40 mM tetramethylammonium ($TMA^+$) bromide and (b) 40 mM tetraethylammonium ($TEA^+$) bromide in 95/5 (v/v) water/glycerol solvent mixture. Solvated peaks are labeled in the spectra (where G denotes glycerol). 165

5.3 Electrohydrodynamic ionization mass spectrum of 40 mM HCl in a 90/10 (v/v) water/glycerol solvent mixture. Solvated peaks are labeled in the spectrum (where G denotes glycerol). Note the absence of

water clusters. M* is a metastable decay product corresponding to the loss of one glycerol molecule from the trimer cluster ($[G_3 + H]^+ \rightarrow [G_2 + H]^+ + G$). 171

5.4 Electrohydrodynamic ionization mass spectrum of 40 mM (a) KI, (b) NaI, (c) RbI and (d) CsI in 95/5 (v/v) water/glycerol. Solvated peaks are labeled in the spectra (where G denotes glycerol). Note the absence of water clusters. M* represents metastable decay ($n \rightarrow n-1$). 173

5.5 Electrohydrodynamic ionization mass spectrum of a 5 mol% NaI in 100% glycerol solution. Solvated peaks are labeled in the spectra (where G denotes glycerol). Note the absence of water clusters. 174

5.6 Electrohydrodynamic ionization mass spectrum of 18 mM HCl and 22 mM NaI in a 95/5 (v/v) water/glycerol solvent mixture. An = $[G + H]^+$; Bn = $[(H_2O)_n + H]^+$. 175

5.7 Plot of $\Sigma I[(H_2O)_n + H]^+$ divided by $\Sigma I[G_n + H]^+$ to illustrate that water clusters are detected after the addition of approximately 18 mM HCl to the 95/5 (v/v) water glycerol solution. Error bars represent the standard deviation of three replicates. 177

5.8 Electrohydrodynamic ionization mass spectrum of 40 mM HCl in a 95/5 (v/v) water/thioglycerol solvent mixture. $A_n = [TG_m + H]^+$; $B_n = [(H_2O)_n + H]^+$; $C_n = [TG + (H_2O)_n + H]^+$; $D_n = [TG_2 + (H_2O)_n + H]^+$; $E_n = [TG_3 +$

$(H_2O)_n + H]^+$; $F_n = [TG_4 + (H_2O)_n + H]^+$. 179

5.9 Plots of cluster relative intensity versus hydration number for the $[(H_2O)_n + H]^+$ series under different conditions of flow rate and accelerating voltage: ◊ = 5 μL/hour (8 kV needle potential); □ = 5 μL/hour (6 kV needle potential); Δ = 7.5 μL/hour (8 kV needle potential); o = 10 μL/hour (8 kV needle potential). Each series of clusters is normalized to the most abundant ion within that cluster. 181

5.10 Plots of cluster relative intensity versus hydration number for the $[G + (H_2O)_n + H]^+$ series under different conditions of flow rate and accelerating voltage: ◊ = 5 μL/hour (8 kV needle potential); □ = 5 μL/hour (6 kV needle potential); Δ = 7.5 μL/hour (8 kV needle potential); o = 10 μL/hour (8 kV needle potential). Each series of clusters is normalized to the most abundant ion within that cluster. 182

5.11 Plots of cluster relative intensity versus hydration number for the $[G_2 + (H_2O)_n + H]^+$ series under different conditions of flow rate and accelerating voltage: ◊ = 5 μL/hour (8 kV needle potential); □ = 5 μL/hour (6 kV needle potential); Δ = 7.5 μL/hour (8 kV needle potential); o = 10 μL/hour (8 kV needle potential). Each series of clusters is normalized to the most abundant ion within that cluster. 183

5.12 Sum-squares response surface showing the (log) sum squares error [$\Sigma(Y - Y)^2$] for the fit of Equations 5.3 to the experimental intensity ratios using literature values of $\Delta G$ and indicated temperatures and pressures. 188

5.13 Free energy cycle for the removal of protonated water clusters from bulk solution. 190

5.14 Free energy for removal of protonated water clusters $[(H_2O)_n + H]^+$ of varying n from bulk solution. Calculated from the free energy cycle using gas-phase $\Delta G$ values shown in Table 5.4. 192

5.15 Comparison of the stable protonated water cluster distribution (□) with the corrected water cluster distribution (◊). The ordinate of the corrected distribution represents the sum of the stable full energy ion intensities and the metastable ion intensities. 199

5.16 Dependence of the average proton hydration number on the number of glycerol molecules included in a mixed cluster under different conditions of flow rate and accelerating voltage: ◊ = 5 μL/hour (8 kV needle potential); □ = 5 μL/hour (6 kV needle potential); Δ = 7.5 μL/hour (8 kV needle potential); o = 10 μL/hour (8 kV needle potential). The average hydration number was calculated as

follows: Average Hydration Number = $\frac{\Sigma n i_n}{\Sigma i_n}$. 200

5.17 A plot of the distribution of water clusters having the general formula $[(H_2O)_n + H]^+$ up to n = 5 (◊) and the distribution of thioglycerol clusters having the general formula $[TG_n + H]^+$ (□) using the intensity of the $^{34}S$-containing isotope peak. Individual data points represent the average of 5 replicates and the error bars represent the standard deviation of the replicates. 202

5.18 Plots of cluster relative intensity versus hydration number for the $[TG_m + (H_2O)_n + H]^+$ series using (a) the $^{34}S$ isotope peak to determine intensity and (b) the monoisotopic masses to determine intensity. The symbols represent the following clusters: ◊ = $[TG_1 + (H_2O)_n + H]^+$; □ = $[TG_2 + (H_2O)_n + H]^+$; o = $[TG_3 + (H_2O)_n + H]^+$. Each series of clusters is normalized to the most abundant ion within that series. 203

# Chapter 1

## Introduction

The impact of desorption ionization (DI) mass spectrometry (MS) has been phenomenal over the past decade. The invention of fast atom bombardment (FAB) [1], electrospray (ES) [2], and matrix assisted laser desorption (MALDI) [3] has extended the mass range accessible for MS analysis at least two orders of magnitude. These DI methods have also extended the classes of compounds amenable to MS analysis to include thermally labile, non-volatile, high molecular weight species such as proteins and peptides. Each of the DI techniques relies on the desorption of ions from the condensed phase, either liquid or solid, to generate a mass spectrum containing the molecular ion (often protonated). FAB relies on a high energy projectile to eject ions into the gas phase, usually from a liquid solvent or "matrix." ES relies on a strong electric field to produce charged droplets from an analyte solution and subsequent ejection of analyte ions into the gas phase during droplet evaporation. Electrohydrodynamic (EH) [4] ionization relies on an electric field to generate gas-phase ions from solution in vacuum. MALDI relies on the interaction of the matrix with photons to eject ions into the gas phase. The matrix in this case is comprised of organic molecules that interact with the laser beam to absorb energy. These techniques are often referred to as "soft" ionization techniques because of the lack of fragmentation of the molecular ion. As typical for innovative techniques, the growth of applications using DI has progressed at a rate much faster than fundamental studies and our understanding of the ionization mechanisms that give rise to

the outstanding results.

The work presented in this dissertation is intended to extend our understanding of the fundamental aspects of the ionization mechanisms of FAB/liquid secondary ion MS (LSIMS) [5], ES, and EH MS. This chapter will provide an introduction to FAB, ES, and EH and a brief historical perspective of each. A more general discussion of mass spectrometry and state-of-the-art instrumentation/techniques can be found in a text by Watson [6] and recent reviews by Burlingame *et al.* [7,8].

Each of the DI methods used here relies on sampling ions directly from solution. Ions attributable to the solvent are often observed in DI spectra. In fact, mass spectrometry has been one of the preferred techniques for probing various aspects of solvation. This chapter will also provide a general discussion of solvation and some of the prominent mass spectrometric techniques and non-mass spectrometric approaches to studying solvation. Chapter 5 will address derivation of solution information from EH spectra.

## 1.1 FAB/LSIMS

FAB and LSIMS were actually derived from secondary ion (SI) MS, [9] whereby primary particles impinge upon a "dry sample" target to yield secondary ions. A general depiction of the bombardment process is shown in Figure 1.1. Particles originating from a primary particle source are directed towards and impinge upon a liquid sample, causing the ejection of neutral and ionic species into the gas phase. Bombardment of a dry (solid versus liquid) sample usually results in a large degree of fragmentation of the molecular ion and surface charging (especially for insulating organics), which can disturb

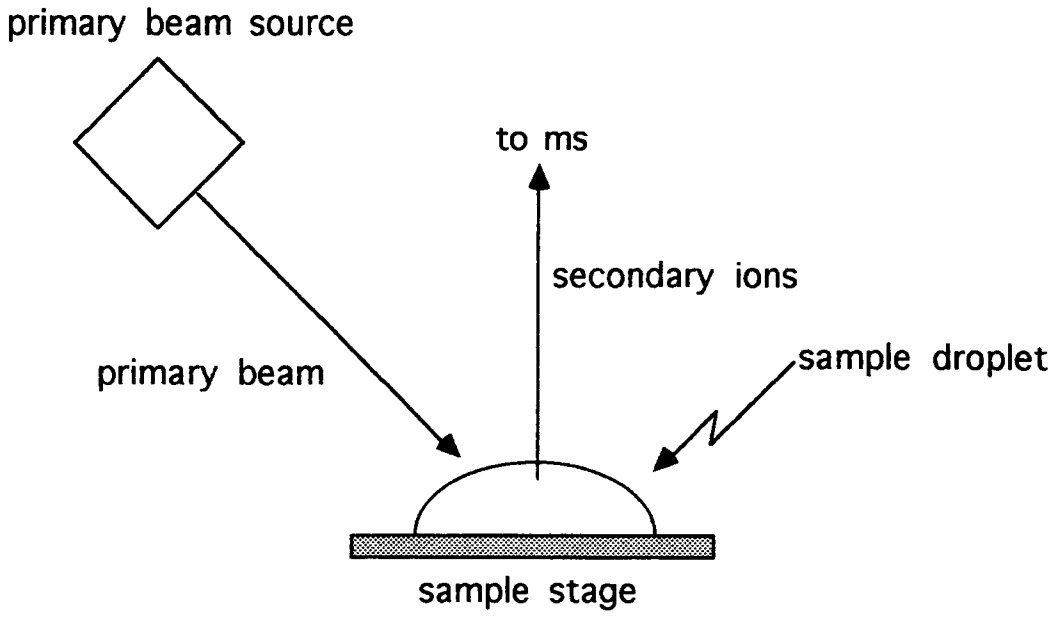



Figure 1.1. The FAB and LSIMS experiments. A primary particle beam impinges upon a sample and secondary ions are produced. The primary beam is neutral for FAB and ionic for LSIMS.

electric fields and therefore, ion sampling/focusing. In inventing FAB, Barber *et al.* [1] sought to overcome the surface charging effect by using neutral atoms instead of ions as primary particles. Rather than bombarding a solid surface, in FAB the analyte is dissolved in a liquid matrix to help overcome the problems encountered with fragmentation and charging in SI MS. The liquid matrix reduces the extent of fragmentation by absorbing some of the primary particle energy. The liquid matrix also provides a conductive medium so that charging is not a problem. FAB was quite successful and became the first ionization technique to yield mass spectra over long periods of time (sample lifetime on the order of 10 to 60 minutes) for molecules in the mass range 1,000 to 10,000 Daltons. This allowed analysis of solutes not previously detected with MS, including solutes of biological interest. [10,11,12,13] Shortly after the introduction of FAB, Aberth *et al.* [5] demonstrated that results obtained with FAB could be reproduced using a primary ion source with the analyte dissolved in a liquid matrix. The results were qualitatively similar to those observed with FAB for solutes such as peptides, lipids, nucleosides, and steroids. The name of "liquid secondary ion mass spectrometry" (LSIMS) was adopted and has since been used to describe SI MS using analytes dissolved in a liquid matrix. The advantages of using a primary ion beam rather than a primary neutral atom beam include primary beam focus and deflection capabilities.

Despite extensive and successful use of FAB and LSIMS for more than a decade, the ionization mechanism has not been completely understood. [14,15,16] A well-accepted and simple model of how secondary ions are generated from solution was adapted by Van der Peyl *et al.* [17] from the "collision cascade" model for desorbing atomic ions from a metal surface.

[18,19] The "collision cascade" model correlates secondary ion yields with primary energy deposited at the surface (directly proportional) and surface binding energy (inversely proportional) for desorbing atomic ions from a metal (electrically conductive) surface. The adapted model takes into account the series of events that finally leads to the ion ejection from solution. The primary particle impinging upon the liquid surface penetrates to a depth of 0 to 20 Angstroms (Å), [20,21] which allows for dissipation of kinetic energy through collisions with solvent and solute molecules. The region of energy dissipation is assumed to resemble a tear-drop shape. The secondary ion escape depth is approximately 10 Å below the surface. Several investigators have shown that increasing the primary beam energy up to approximately 15 - 20 keV provides an increase in sputtering efficiency [22,23,24,25] with an accompanying decrease in fragmentation [26,24] and an increase in the signal-to-background ratio. [23]

Controllable parameters such as the primary beam flux, [26,27,28,29] the primary beam energy, [22,23,24,25] and the choice of matrix have been investigated by several workers. Reynolds and Cook have even ranked the parameters in the order of their influence on the appearance of the FAB spectrum. [26] The choice of matrix has the largest influence on the appearance of the spectrum, followed by the primary beam flux and then the primary beam energy.

Choice of the liquid matrix is an important factor for successful FAB and LSIMS. Desirable properties of the matrix include: low volatility for vacuum compatibility, high viscosity, capable of dissolving the solute, and acidic for positive ion FAB or basic for negative ion FAB. [30] The more common solvents for FAB and LSIMS include glycerol, thioglycerol, [31] and 3-nitrobenzyl

alcohol. [32] A more complete list of solvents and their physical and chemical properties can be found in a compilation by Cook *et al.* [33] and reviews by De Pauw. [34,35]

Despite all of the investigations into the ionization mechanisms of FAB and LSIMS, it is still difficult to reproduce certain aspects of the FAB and LSIMS experiments. Specifically, FAB results display temporal behavior that is sometimes difficult to reproduce from day-to-day, from instrument-to-instrument, and even from analysis-to-analysis. This has been explained based on several factors, including evaporation rate, [36] sputtering rate, [37,38,39,40,41] sample preparation (size) [42,43] and surface phenomena. [44,45,46] It has been shown that FAB and LSIMS are extremely sensitive to surface active solutes (surfactants) and less sensitive to solutes that do not lower the surface tension of the liquid matrix ("non-surfactants"). Given the acceptance of the "cascade model" discussed above, and the fact that surfactants exist on the surface of the liquid, these observations appear reasonable. Several investigators have shown that surface active solutes yield an initially strong secondary ion signal followed by a gradual decrease in intensity. [e.g., ref 45] This decrease has been attributed to the depletion of the surface excess of surfactant due to sputtering and evaporation. Using species that are not surface active, the analyte secondary ion intensity has been shown to increase as the FAB experiment progressed. [e.g., ref 46] This behavior has not been as well explained or understood as the surfactant behavior. The understanding is further complicated by the irreproducibility of the time dependence of such behavior. Chapter 3 addresses the variation in time dependence for both surfactants and non-surfactants. Secondary ion images of the sample surface will be used to help explain the time dependence

of surfactant and non-surfactant ion signals in FAB and LSIMS.

## 1.2 Electrospray Ionization

Electrospray has a long history totally unrelated to mass spectrometry. The electrospray process has been utilized in spray painting, [47] crop dusting, [48] and fuel atomization. [49] Although Dole was the first to use ES in mass spectrometry, he did not recognize the capabilities and future of the technique. [50,51,52,53] It was not until 1984 that Fenn *et al.* [2] recognized the potential importance of ES as a mass spectrometric ionization technique. Electrospray has since become one of the most powerful techniques for the analysis of extremely high molecular weight, non-volatile, thermally labile molecules. A major difference between FAB and ES is the extent of charging. Typical FAB spectra contain singly charged species, while typical ES spectra contain analyte species with multiple charges. The multiple charging observed in ES makes possible the analysis of species having molecular weights in excess of the mass range of most mass spectrometers.

ES, which is one of the most recent developments in DI, relies on a strong electric field to generate ions from a mist of charged droplets formed from the dispersion of an analyte solution, as opposed to the bombardment process utilized in FAB. Through collisions at atmospheric pressure, ions within the droplets are stripped of solvent. A simplistic depiction of the ES experiment is shown in Figure 1.2, and can be described as several distinct steps. A liquid sample is delivered to the metallic needle at a flow rate typically on the order of 1-10 μL/minute. A potential of 3-4 kV applied between the needle tip and the counter electrode results in the dispersion of the liquid at

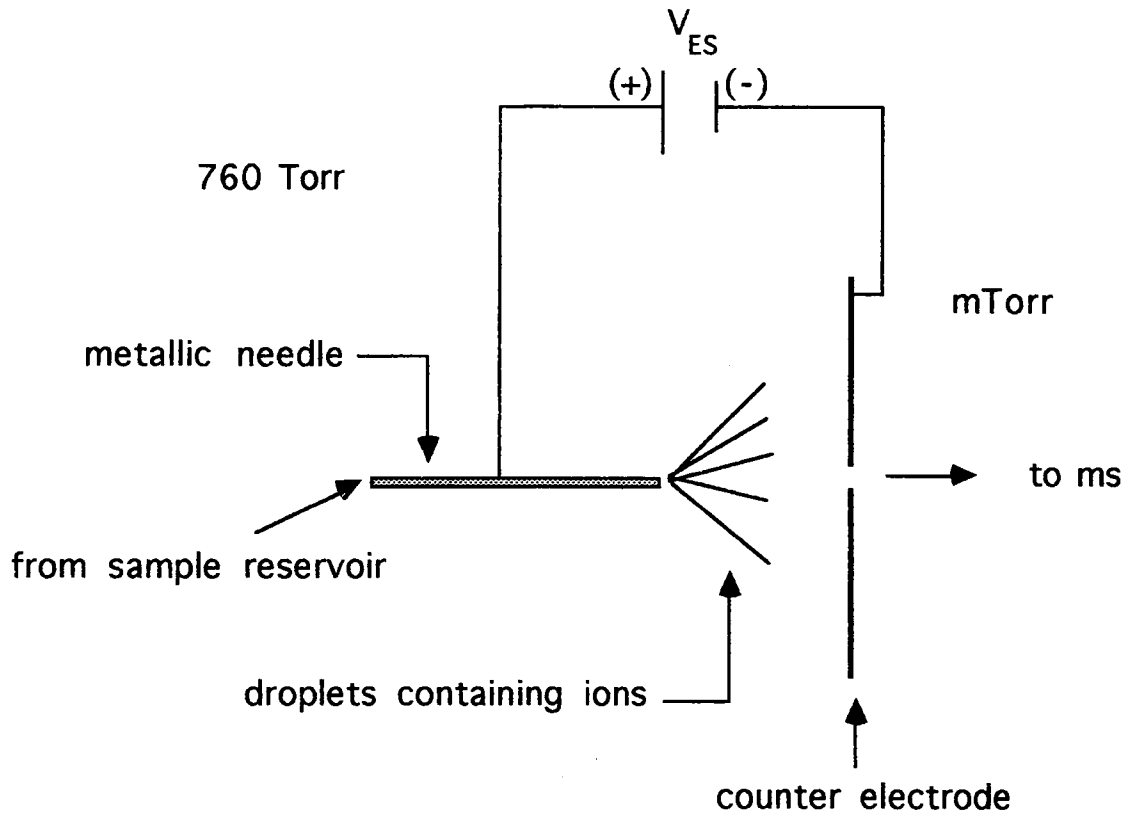



**Figure 1.2.** The ES experiment (shown for positive ions). The electric field at atmospheric pressure promotes the formation of small droplets which ultimately form unsolvated ions. $V_{es}$ is the voltage necessary to sustain stable spray.

the needle tip into a fine mist of highly charged droplets. These droplets undergo collisions with gases in the atmosphere causing evaporation of the solvent and ejection of unsolvated ions into the atmosphere. The ions are sampled into the mass analyzer via a small orifice located in the counter electrode (various geometries are used). The sampled ions are subsequently mass analyzed and detected.

Two models are commonly invoked to explain how unsolvated ions are derived from small droplets. The two models are the *charge residue model* of Dole *et al.* [50,51,52,53,54] and the *ion evaporation model* of Thomson and Iribarne. [55,56] Kebarle has recently reviewed the models (making comparisons of the model predictions with experimental evidence) and has concluded that "it is not possible to state with certainty which theory fits better with the available evidence." [57] A common view point of all models is the occurrence of Rayleigh explosions. Rayleigh explosions occur when the charge within a droplet, described by equation 1.1, is large enough to overcome the surface tension.

$$Q_R^2 = 64\ \pi^2\ \varepsilon_0\ \gamma\ r_R^3$$

Equation 1.1

where $\varepsilon_0$ is the permittivity of vacuum, $\gamma$ is the surface tension, and r is the droplet radius. The radius of the droplet changes as solvent is evaporated until the Rayleigh limit (equation 1.1) is met and then the droplet undergoes fission. From this point in the ionization process, the different models deviate and should be considered separately. The charge residue model argues that "naked" ions result from collision-induced solvent evaporation from small

droplets that contain only a single solute ion. The generation of the single ion within a small droplet is the result of a series of Rayleigh explosions caused by an excess of charge within a droplet. As the solvent continues to evaporate, the charge density continues to increase until the Rayleigh limit (described above) is reached. This process continues until only a single analyte ion is contained within the droplet and the remaining solvent is evaporated through collisions. [58] The ion evaporation model argues that "naked" ions are generated as a result of a strong electric field (field desorption) generated on the droplet surface from an excess of charged species in a small droplet. The model is based on theory that predicts the rate of ion emission from the charged droplet and is related to the ion solvation energy. Röllgen, however, has shown that the electric field generated at the droplet surface is not large enough to desorb an ion. [59,60] Both models, however, have been useful in reconciling results and neither model has been proven definitively. Common to both models, however, is the "small droplet" theme where ions are generated late in the spray process from small droplets, rather than early in the spray process from relatively large droplets. Several detailed descriptions of how the charged droplets are formed have been presented elsewhere. [61,62]

Despite the many reports of ES applications, fundamental aspects that influence the spray performance and sampling efficiency continue to be examined. These factors include solution ionic strength and analyte concentration, [63,64,65,66] solvent volatility, [67,68] solvent dielectric constant, solution flow rate, [69,70] solution pH, [71,72,73] and source temperature. [74,75,76] The extent of these influences on the ES performance (e.g., flow rate) can vary from one instrument to another depending on the source arrangement and geometry. Some of these limitations, however, have

been overcome. For example, the use of a sheath nebulization gas has overcome problems associated with high flow rates (encountered in some applications) and the use of a sheath solvent has overcome the problem of low flow rates (also encountered in some applications). In addition to those improvements, sharpening the emitter tip [64] and using a discharge suppression gas such as $SF_6$ [67] has allowed for stable spray of aqueous solutions prior to the onset of a corona discharge. Problems related to solution conductance and analyte concentration (if too high) have been reduced by using a sheath solvent for dilution. Source modifications have also allowed for careful control of source temperature.

As a result of some of the changes mentioned above, fundamental studies of aqueous and non-aqueous solutions are possible. For example, proteins are known to change conformation as a function of solution pH, temperature, and solvent composition. One of the more recent observations made of ES spectra of proteins has been a shift to higher charge state distributions with increases in solution pH and temperature. [see for example references 58 and 77] Chait *et al.* have attributed these shifts to known solution chemistry changes in the protein conformation. [77] Another example of solution chemistry has been the evidence for spray-induced oxidation of the solvent observed by Turecek; [76] in the case of methanol, this should result in the formation of formaldehyde and protons. This observation is important, because generation of protons within the ES plume has the effect of changing the pH of the ES droplet and also the chemistry (such as conformation) of the solute contained within the droplet. Proteins are also known to change conformation with changes in solvent composition, such as the addition of methanol. These changes have been observed as shifts in

charge state distribution (an increase in the number of protons) in ES spectra obtained from proteins in methanolic solutions. [58,78,79,80]

Over the past several years micro-electrospray sources (sources operated at low flow rates) have also been developed as attempts to alleviate some of the physical and chemical limitations of conventional ES sources. For example, conventional ES sources have difficulty spraying purely aqueous solutions. Conventional ES sources also require flow rates on the order of 1 to 10 μL/minute, thereby consuming large amounts of sample. Flow rates using the micro-ES sources have been reduced to less than 1 μL/minute [81] and stable spray is now possible from highly conductive aqueous solutions without the need for nebulization or a discharge suppresser gas. [67] The ability to spray highly conductive aqueous solutions also extends the range of ES applications to include capillary electrophoresis. The use of small diameter (typically 5 to 50 μm i.d.) fused silica capillaries (encountered in CE) in place of conventional emitters (typically 100 to 150 μm i.d.) has proven advantageous in several electrospray ionization (ES) mass spectrometric (MS) applications. [58,81,82,83,84] Sensitivities are much better and limits of detection are orders of magnitude lower because of the improved sampling efficiency (presumably from the smaller droplets) obtained from the micro-ES sources. [84] For example, Wahl *et al.* [84] have shown improvements in sensitivity on the order of thirty fold (compared to conventional sources) and limits of detection on the order of attomoles when using small i.d. capillaries (conventional source limit of detection has been on the order of femtomoles). Successful use of small i.d. capillaries for ES has been a large part of the driving force behind many attempts to couple capillary electrophoresis and electrospray. These attempts and their shortcomings are addressed in section 1.2.1 below.

### 1.2.1 Capillary Electrophoresis/Electrospray

Capillary electrophoresis (CE) is a separation method capable of providing extremely efficient separation of solutes from extremely small sample volumes (in a short time period) based on their electrophoretic mobility in an applied electric field. [85] Solutes are introduced into the "entrance" end of a fused silica capillary filled with an aqueous buffer solution. The entrance end of the capillary is subsequently immersed in a reservoir of the buffer solution connected to a high voltage power supply through an immersed wire. The exit end of the fused silica capillary is immersed in a second buffer reservoir that is connected to ground. A high ionic strength buffer is necessary to establish electroosmotic flow within the capillary by creating an electrical double layer along the walls of the fused silica capillary. Solutes move through the capillary via electroosmotic flow until they elute from the exit end of the capillary. Typical CE detection is accomplished on-line by removing a small portion of the polyimide coating near the exit end of the capillary. This region of the fused silica capillary functions as the "sample cell" for absorption spectrophotometry (UV/VIS). The buffer reservoir at the exit end of the capillary is not necessary when coupled to ES.

Although micro-ES seems well suited as a mass spectrometric interface to capillary electrophoresis, this coupling has been a challenge for several years. There are some limitations and incompatibilities associated with each technique. For example, CE buffers typically consist of high concentrations (mM) of non-volatile salts dissolved in water. In contrast to solutions

providing the best CE performance, ES performance has been best for solvent systems containing a large fraction of a volatile organic solvent such as methanol. The reduced surface tension and increased volatility of methanol allows for more efficient removal of the solvent from the analyte (see discussion above about Rayleigh explosions). ES performance is also best in the absence of species such as sodium and potassium and other species that might compete with the analyte for charge.

Several electrospray sources have been developed to overcome these difficulties. [86,87,88,89,90,91] Recall from above that electrical connection is necessary in CE to establish the potential difference between the capillary entrance and exit ends and is also necessary in ES to establish a stable spray. The original CE/ES MS interface utilized a vapor-deposited layer of silver on the outer surface of the CE capillary exit terminus (ES emitter) to establish the electrical connection necessary for both CE and ES. [86] This design was limited because CE flow rates were below optimum requirements by this source which resulted in frequent spray instabilities. This interface, as a consequence of not incorporating a conically shaped emitter, also precluded the use of high ionic strength buffers typically used in CE. The shape and outer diameter of the emitter better focus the electric field and are important for the successful spray of aqueous solutions. [92] Furthermore, the silver layer had a short lifetime presumably due to electrochemical reactions of the silver. This source design has since been abandoned.

A second variation of the sheathless design developed by Smith *et al.* [93] and Jorgensen *et al.* [94] utilized a vapor deposited layer of gold on an etched fused silica capillary. The fused silica tip is etched with hydrofluoric acid or drawn before coating to provide sharper edges and enhanced field

focusing. Shaping the capillary terminus in this manner is not very precise and weakens the capillary tip (fused silica is brittle after the polyimide coating is removed), but facilitates stable ES with highly conductive solutions (including aqueous solutions without organic co-solvent). [64] This design eliminated the problems associated with electrochemical reaction of silver on the previous sheathless design, but physical adhesion of the metallic layer was still problematic. This design also eliminated the problems associated with flow rates by utilizing smaller i.d. fused silica capillaries. Despite the short lifetime of the gold coating, this interface has been used extensively.

A third attempt at interfacing CE and ES MS, which removed many of the limitations experienced with the silver and gold metallized tips, utilized a coaxial liquid sheath flow. [88] In this arrangement, the CE capillary terminus (ES emitter end) was positioned within and extended slightly beyond a concentric metal tube. A sheath liquid (typically methanol or methanol/water flowing at 1-5 μL/minute; compatible with conventional ES) flows through the annulus of the concentric tube and comes into direct contact with the exit end of the CE capillary. The necessary CE and ES voltages are established by applying the high voltage to the concentric metal tube (Figure 1.3). This coaxial flow set-up was further refined to include a conical-shaped tip at the CE terminus (ES emitter) end of the fused silica capillary. [84] This conical shape (shown in Figure 1.3) helped to focus the electrical field and stabilize the ES process. The sheath flow interface, however, introduces dilution (typical CE flow rates are ≤ 1 μL/minute and sheath flow rates are on the order of 1-5 μL/minute) and the addition of other ionizable or charge-carrying species (solvent, buffer, impurities) that compete for charge during the ES process. The dilution and ionization competition has the effect of reducing the

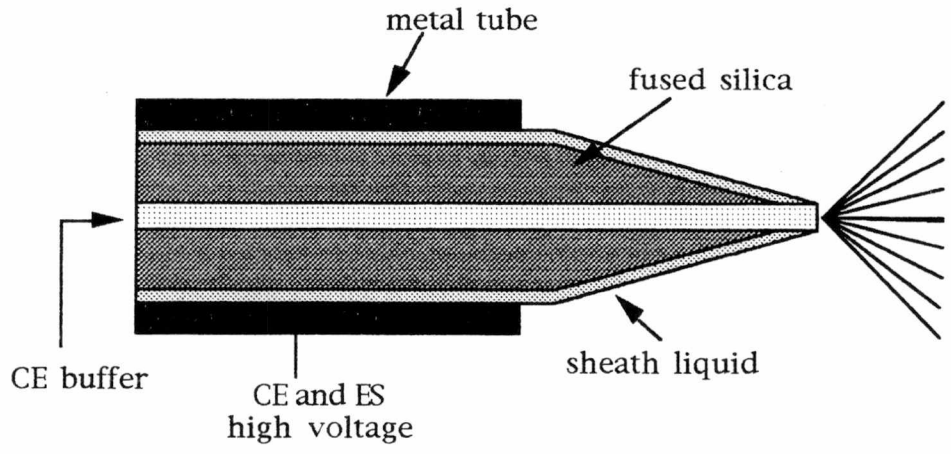



**Figure 1.3.** Cross sectional view of the sheath flow interface used in CE/ES. Typical conditions are as follows: CE capillary dimensions of 25 to 100 μm i.d. X 365 μm o.d with flow rates on the order of 10 μL/hour; SS needle dimensions of 394 μm i.d. X 711 μm o.d.; sheath solvent delivered at flow rates on the order of 1 to 5 μL/minute; ES voltage 1 to 4 kV.

analyte sensitivity. [81] Other problems may result from changes in analyte solubility or molecular conformation when using sheath fluids with high organic solvent content. [58]

A fourth interface, introduced by Henion *et al.*, [89] utilizes a liquid junction to establish the necessary electrical connection and provide an additional make-up flow of CE buffer to be compatible with ES requirements. In the liquid junction arrangement, the CE capillary terminates in a reservoir (low volume union tee) of the buffer positioned remote from the ES emitter (Figure 1.4).

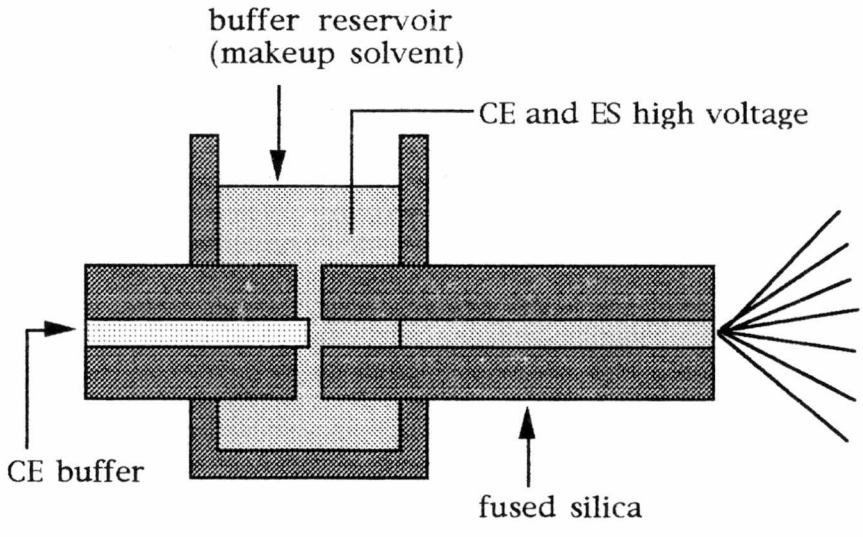



**Figure 1.4.** Cross sectional view of the liquid junction interface used in CE/ES. Typical CE and ES conditions are the same as those described in Figure 1.3.

The solution exits the buffer reservoir via a short section of fused silica capillary which functions as the ES emitter. The electric potential necessary for CE and ES is established by applying high voltage to the reservoir. Like the sheath liquid interface, this design suffers from dilutions. Gale and Smith [81] have also developed a micro-ES source using a fused silica capillary and a metallic fitting remote from the emitter to establish electrical connection for continuous infusion experiments. Van Berkel *et al.* [95] have taken advantage of remote connections to study electrochemical reactions via ES.

A fifth interface, developed by Zare *et al.* [96], is accomplished by inserting a small (25 μm diameter) gold wire in a 75 to 100 μm i.d. capillary at the CE exit end to establish the necessary electrical connection for CE and ES; while this risks clogging small capillaries and may distort the electric field at the tip, it has provided a useful CE/ES interface.

Work continues in this area in attempts to improve methods of making electrical connection and extend the range of usable CE buffers. [93] Some of the latest work [84] has taken the direction of extremely small internal diameter (i.d.) capillaries for CE/ES and continuous infusion experiments. Despite the limitations of each method described above, good separations of a variety of proteins and peptides at the attomole level of detection have been demonstrated. [84] The multitude of approaches and attempts described above is a strong indication of the importance and potential of CE/ES. Chapter 2 describes a novel procedure for shaping the capillary terminus and the specific procedure used to chemically modify the fused silica surface prior to vapor deposition of the gold. The results of coating characterization, including durability and versatility, and MS results obtained using the metallized capillary for ES and CE/ES on an ion trap mass spectrometer are

presented in Chapter 4.

## 1.3 Electrohydrodynamic Ionization

EH ionization is perhaps the "softest" DI technique. EH avoids depositing an excess of internal energy (usually resulting in fragmentation) into the ion through a bombardment process such as in FAB or a desolvation process such as in ES. [97] A major difference between ES and EH is the desorption of ions directly in vacuum in the latter technique. EH relies on an electric field, on the order of $10^6$ V $cm^{-1}$, to desorb ions from solution located at the tip of the emitter, as shown in Figure 1.5. [97] This applied electric field is stronger than in ES, and results in the desorption of preformed ions (solutes that exist in solution as charged species) into the gas phase for mass analysis.

EH was first introduced by Evans and Hendricks as a technique for generating ions directly from liquid metal alloys. [4] Evans continued to develop EH and chose glycerol, doped with NaI supporting electrolyte, as a solvent for organic solutes because of its ability to dissolve a wide range of organic solutes and its low vapor pressure. The supporting electrolyte served to increase solution conductance (which promotes ion emission rather than spraying of charged droplets) and a source of cations for forming "preformed" ions. The low solvent vapor pressure was necessary for vacuum requirements within an ion source. [98] Biological materials such as glutathione and neomycin [99] could be sampled after cationization via $Na^+$ attachment or protonation in the solution phase. Later applications of EH indicated that some ions were sampled as solvated species and some of the ion/solvent clusters underwent desolvation after emission. These observations were useful in

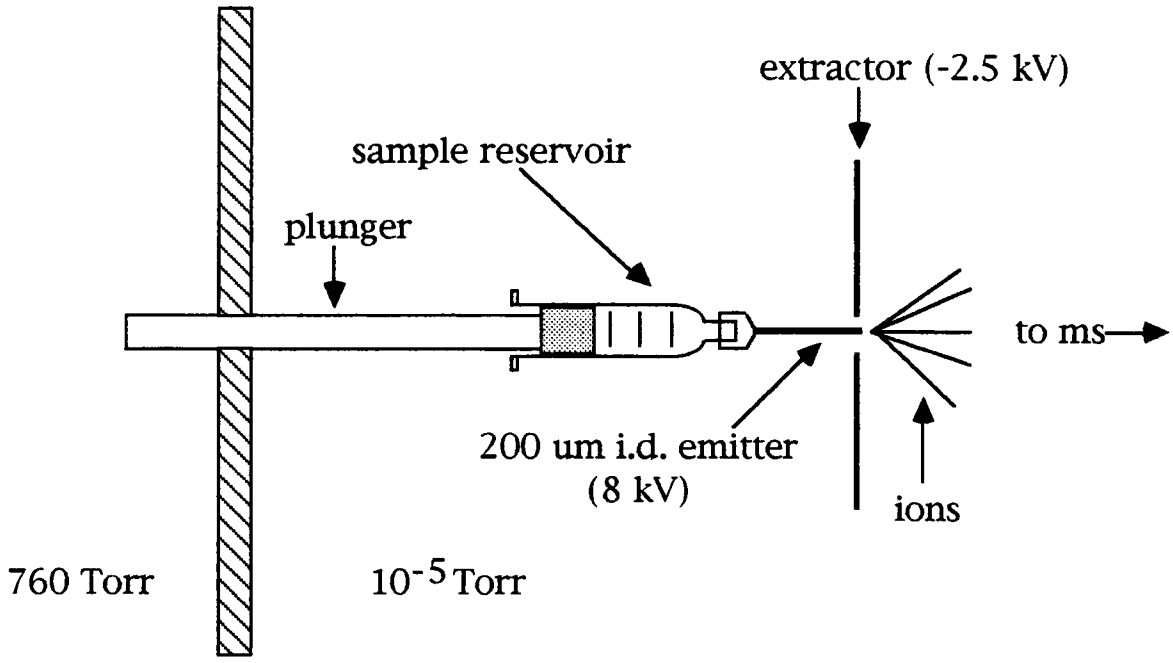



Figure 1.5. A depiction of the EH experiment. The electric field in a vacuum promotes the desorption of ions from a sample reservoir.

determining the role and influence of solution chemistry on the sampling process and the appearance of the EH mass spectrum. [99,100,101]

Evans also observed substantial differences in the sampling behavior of cations such as $Na^+$ and $Ba^{+2}$. Peaks attributable to $Na^+$ (and solvent adducts) obtained from solutions containing $Na^+$ were readily detected. [99,101] In contrast, $Ba^{+2}$ ions were only detected under "detuned" conditions. This was explained as follows. Ions are accelerated into the mass analyzer with kinetic energy determined by an accelerating electric potential applied to the emitter. If the ion loses part of its mass (e.g., through evaporation of a solvent molecule), the ion kinetic energy must decrease proportionately. The instrument used in these experiments utilized an electrostatic (energy) analyzer (ESA) to remove ions without the selected kinetic energy. Therefore, when an ion exits the source region (accelerating voltage region) and experiences a subsequent loss in mass, it can only be detected when the electrostatic analyzer (ESA) is detuned to allow ions with energy less than that corresponding to the full accelerating potential to pass through to be detected. Only under these circumstances were doubly charged, solvated $Ba^{+2}$ ions detected. It was apparent that doubly charged ions were more heavily solvated than the singly charged ions and consequently underwent substantially more in-flight desolvation (unimolecular metastable decay) than the singly charged species. These initial observations suggested EH could be used to probe ion/solvent interactions. The phenomenon of ion/solvent interactions (solvation) will be discussed in detail in section 1.4.

Cook continued the work of Evans and began to characterize and develop the ionization process to probe solution chemistry. [97] In one of the first studies by Cook and Chan, the ligand exchange reactions of Ru(II),

Cr(III), and Cr(II) bipyridyl complexes revealed that EH spectra reflected the known solution chemistry stability trends for these complexes. [102] This observation further established that EH could be a suitable probe of solution-phase chemistry. Work in the area of crown ether complexes with cations gave further evidence that EH could be used to probe solution-phase chemistry. [103] In a study of competitive equilibria, the relative abundance of 18-crown-6 complexes with a variety of cations observed in the EH mass spectrum of ions sampled from glycerol correlated well with known solution chemistry of the same complexes in aqueous and methanolic solutions.

The relationship between species present in solution and those observed in the mass spectrum can be complicated by fragmentation. In a direct comparison study of the extent of fragmentation of some diquaternay ammonium salts using FAB and EH, more fragmentation occurred during the FAB bombardment process than occurred during the EH desorption process. [104] This observation is important because it suggests that the EH mass spectrum, uncomplicated by fragmentation, is a more accurate reflection of solution chemistry than FAB. For ammonium chloride and a series of methylammonium chlorides (1-4 methyl groups), [105] the extent of solvation decreased with increasing cation size and there was a corresponding increase in sampling efficiency. This was reconciled based on a shielding argument. The charge density and the degree of solvation is expected to be smaller for the larger cations due to a more efficient shielding of the ion center. Both the barrier to desorption and the likelihood of in-flight desolvation are reduced.

Another example of the manifestation of solvent effects in EH sampling studied within the Cook research group addressed the determination of polymer average molecular weights. Other DI techniques, such as FAB, can

give rise to bias of the polymer average molecular weight due to fragmentation of large polymer molecules to make smaller ones. Since EH spectra normally contain little or no evidence of fragmentation, EH should provide an accurate average molecular weight of polymeric materials, provided that there is representative sampling. EH did provide an accurate average molecular weight for the polymer poly(ethylene glycol) (PEG; $HO(CH_2CH_2O)_nH$). [106] Metal adducts of the polymer (e.g., $Na^+$ attachment) were detected and used to calculate the average molecular weight from the distribution observed in the mass spectrum. Metal adducts of the polymer could be detected from polymer material exceeding the mass range of the instrument; the attachment of multiple cations shifted the m/z ratio into the operating mass range of the instrument. These ions were readily sampled despite their multiple charge; the long polymer chains apparently shield the metal charge centers from strong interaction with the solvent. In contrast to the accurate results obtained for PEG, for the polymer poly(ethyleneimine) (PEI; $H_2N(CH_2CH_2NH)_nH$) average molecular weights based on the distribution observed in the EH mass spectrum, were well below the values specified by the manufacturer. [107] Other techniques (field desorption, FAB, plasma desorption, and laser desorption/time-of-flight) have provided average molecular weights in only slightly better agreement with the specified values. Unlike the PEG oligomers, the PEI oligomers have nitrogen atoms that can interact with the solvent through hydrogen bonding. This hydrogen bonding (solvation) leads to poor and biased sampling of the larger PEI oligomers by EH and to some degree other mass spectrometric methods. Branching may have also influence the sampling behavior by increasing oligomer solvation.

The polymer oligomer work also identified another possible factor that

can lead to complications in interpretation of EH mass spectra as direct reflections of solution-phase chemistry. The site of ion emission in EH is the surface of the meniscus formed at the tip of the emitter. Ions must arrive at the surface by a combination of convection and diffusion. [108,109,110] Convection, the flow of solution to the tip of the emitter, should not lead to any bias. However, smaller solutes may diffuse faster than larger solutes, thus introducing a bias against heavier solutes such as the heavier (more highly solvated) oligomers of PEI (and probably, to some extent, PEG). The measured sampling efficiency (signal intensity divided by concentration) of PEI was shown to be time dependent and was found to decrease systematically with increasing size and charge. [107] This time dependence was examined in more detail using a homologous series of tetraalkylammonium salts to probe the effects of ion pairing, solvation, surface activity, and mass transport. [109] At the onset of EH emission, the more hydrophobic and less solvated higher molecular weight species are preferentially desorbed from the surface of the meniscus. Since these larger ions diffuse through the solution more slowly than the smaller species they are gradually depleted from the surface with a corresponding decrease in relative intensity. Ion pairing can also have a dramatic effect on the sampling behavior of ions from solution. The influence of ion pairing on EH and FAB sensitivity was established using a diquaternary ammonium cation and various anions. The trend in percent ion pairing correlated reasonably well with trends in enthalpy of hydration for the anions (acetate, nitrite, chloride, bromide, nitrate, iodide, perchlorate). [26,111]

Studies to alleviate some of the bias observed in EH spectra were undertaken by Murawski and Cook in investigating solvent systems other than

glycerol. [112,113] The change from glycerol solution to aqueous solutions was also necessary to study the kinetics of enzymatic hydrolysis of peptides. As part of this attempt to eliminate the need for a viscous solvent such as glycerol, Murawski incorporated a bonding tool (i.d. 12.5 or 25 μm) made of either tungsten carbide or titanium carbide in place of the platinum capillary used with glycerol solutions. Other precautions, such as increasing the spacing between the emitter and extractor, were also taken to reduce the chances of sparking from such a large electric field (and probably increased source pressure). One aspect considered was the energy spread of ions (ion/solvent clusters) sampled from aqueous solution. Ions desorbed from solution have a finite range of kinetic energies know as the kinetic energy spread. This work indicated that the energy spread of ion/solvent clusters generated from aqueous solution was much narrower than the energy spread of ion/solvent clusters generated from glycerol solution. Careful tuning was necessary to match the ion energy with the electrostatic analyzer (ESA) energy. This effect was attributed to collisional cooling during the desorption process. [108] This work also revealed that ion/solvent clusters containing water and having the general formula $[(H_2O)_n + Na]^+$ could be detected only when 100% water was employed as the solvent. The stability of the EH emission, however, was poor when purely aqueous solutions were used, making quantitative interpretation of results difficult. In fact the emission instability from the purely aqueous solutions forced a change to a solvent system that contained a less volatile co-solvent. Thiodiethanol was chosen as a co-solvent for biological work because it does not interfere with enzymatic activity and improved the sampling stability. Although the stability of this solution was not as good as with pure glycerol, enzymatic hydrolysis reactions

were monitored. [113,114]

The time dependence of the enzymatic hydrolysis within the ion source was monitored to obtain structural information about the peptide. The sequence of peptides can be determined by sequential cleavage of peptide amino acids by an enzyme (e.g., carboxypeptidase-Y). The rate of amino acid cleavage (kinetics information) can be determined by monitoring the intensity of peaks attributed to the amino acid as a function of time. The monitoring of enzymatic hydrolysis reactions of peptides is currently being pursued by another group member using thioglycerol co-solvent and a flow injection variation of the source described in section 2.3.2. [115] Salvato has acquired kinetics information for the enzymatic (carboxypeptidase-Y) hydrolysis of the pentapeptide leucine-enkephalin that agrees qualitatively with data obtained from a more conventional spectrophotometric technique. [115]

Other reports of EH work come from Dobychin *et al.*, [116,117] Mil'man *et al.*, [118] Zolotoi *et al.*, [119,120] Alexandrov *et al.*, [121,122] and Mahoney *et al.* [123,124] using source pressures much higher than for conventional EH work. The data obtained at the higher source pressure more closely resembles ES spectra than EH spectra. The latest report of EH was by Fenselau *et al.* using a membrane introduction system. [125] These reports have not specifically addressed the role of solvation, although ion/solvent clusters are certainly present. Mahoney, for example, used the clusters generated from EH as primary ions for bombardment experiments. The work of Fenselau involved sampling ions from a highly aqueous solution. Only glycerol ion/solvent clusters were evident in the spectra although the solution contains 80% water.

Clearly from the brief description of EH results to date, a common theme

has been the soft ionization mechanism and spectra reflecting solution chemistry. For these reasons, EH appears to be a viable mass spectrometric ionization method for probing ion/solvent interactions in solution without grossly disrupting the micro-environment. The ion/solvent interaction, solvation, and the competition among solvents (in a multi-solvent system), for sites around the ion, competitive solvation, will be discussed in section 1.4 below. Results assessing the utility of EH ionization as a probe of condensed phase solvation and competitive solvation are presented and discussed in Chapter 5.

## 1.4 Solvation

For many years, the solvent was believed to simply provide an inert medium for chemical reactions. Only over the past 50 years has it been recognized that the chemical and physical properties of most solutes are affected by the solvent and that the chemical and physical properties of most solvents are affected by the addition of a solute. This interaction of solutes with solvents (solvation) comprises an enormous area of research that has intrigued chemists for many years. Of the 3 phases of matter (gas, liquid, and solid), the liquid phase is the least understood despite the majority of chemistry taking place in solution and the fact that nearly 3/4 of the earth's surface is covered by water. During the past several decades an abundance of research has been directed towards obtaining a better understanding of both aqueous and non-aqueous solution chemistry (especially on a microscopic or molecular level).

Many experimental and theoretical approaches have been utilized to

probe the structure, dynamics, and energetics involved in interactions of solutes with solvents; it would be a near impossible task to compile a complete review of such work. This section is intended to describe some of the more recent experimental approaches (and chemical systems) used to probe clusters and some of the general shortcomings. Prior to discussing the experimental approaches, it is necessary to provide a working definition of solvation and competitive or preferential solvation. The chemical species of interest and the species interacting with the solvent is referred to as the solute and is either a neutral or ionic atom or molecule. The solvent is a liquid capable of interacting with and dissolving the solute. This interaction of the solute with the solvent is known as solvation and is the result of short- and long-range electrostatic energies such as dipole moment, polarizability, and basicity. [126,127,128] The first moment of charge distribution is called the dipole moment. Two point charges having opposite signs separated by some distance R have a dipole moment extending along the line from positive to negative charge. [129] Polarization energies are due to changes in the electron distribution within the solute and solvent molecules when they come within the influence of each other. The electric fields arising from permanent moments of either the solute or solvent molecule will induce moments in the other molecule. The induced moments will lead to an attraction between the solute and solvent molecules. [129] The basicity of the solvent is also important in cluster chemistry. A Brönsted-Lowry base is a species capable of accepting a proton and a Lewis base is one capable of donating a pair of electrons. In the case of competition for the proton, the stronger Brönsted-Lowry base will be protonated. If the solution contains more than a single solvent component, the solvents can compete for interaction with the solute based on the

energetics of the interactions mentioned above. This phenomenon is known as competitive or preferential solvation. A single solute entity is certainly not limited to interactions with only a single solvent molecule and usually interacts with many solvent molecules. Figure 1.6 below is a very simplistic illustration of solvation showing the proximity and arrangement of solvent molecules around a single solute (in this case an ionic solute).

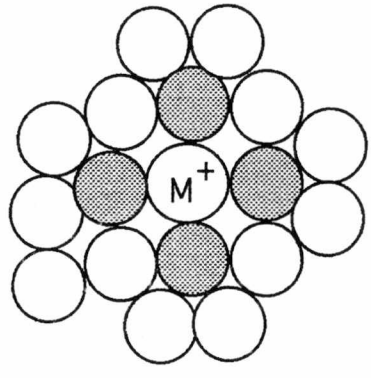



Figure 1.6. Schematic diagram illustrating the primary and subsequent spheres of solvation around the cation $M^+$.

The shaded spheres in direct contact with the ion are considered to be in the primary solvation sphere, while the other spheres (unshaded) are not in direct contact with the cation and are considered to be in the secondary and subsequent solvation spheres. The volume of space directly surrounding the solute can only accommodate a certain number of solvent molecules, termed the primary solvation number, related to the size and coordination number of both the solute and the solvent. Typical values for the primary solvation

number range from 4 to 8. [126] Once this volume is full (often referred to as a closed primary solvation sphere) solvent molecules can still interact with the solute, but at larger distances. These interactions are considered to take place in the secondary and subsequent solvation spheres of the solute. The secondary solvation shell can be considered to be the volume surrounding the solute, that is one solvent molecule removed. The third, fourth, etc. solvation shell simply implies that the solvent molecules are in a volume separated from the solute by two, three, etc. other solvent molecules. In solution, the solvation spheres subsequent to the primary sphere can form extended networks. This extension is due not only to the interaction of the solute with the solvent, but also due to interaction of solvent molecules with one another through, for example, hydrogen bonding. For solutions containing multiple solvents (e.g., a binary solvent system), the picture becomes more complicated due to competition among the solvent components for sites within the primary solvation sphere. The primary and subsequent solvation spheres can contain solvent molecules from both components, for example, of a binary solvent system. The individual solvation shells are not limited to only a single solvent component in a mixed solvent system, and clusters containing more than a single solvent component are referred to as mixed solvent clusters.

Investigations of solute/solvent (solvation) interactions can generally be classified as either bulk phase measurements or gas phase measurements. Bulk phase measurements are those done directly in solution, such as calorimetry. Information obtained, such as heat of solution, often reflects an average of all interactions that take place in solution (ion/solvent interactions, solvent/solvent interactions, counterion/solvent interactions, solvent restructuring, etc.) Conversely, gas-phase measurements are capable

of isolating one interaction of interest (e.g., ion/solvent interaction). Contributions from the bulk solvent and from counterions are eliminated. Gas-phase approaches of studying solvation (e.g., mass spectrometry) are capable of providing step-wise thermodynamic information or microscopic detail of the structure ion/solvent clusters. To obtain microscopic information directly, it is necessary to distinguish discrete clusters from one another. The bulk phase approaches are generally not capable of resolving the discrete clusters in solution. Mass spectrometric approaches are capable of resolving the contributions from discrete clusters, however, these are gas-phase measurements. An approach capable of sampling ion/solvent clusters directly from solution and subsequently resolving the individual clusters would be ideal. Some of the current approaches for probing such solute/solvent interactions in the condensed and gas phases are presented below.

### 1.4.1 Condensed-Phase Approaches

One of the more prominent experimental approaches to studying condensed-phase solvation has been and continues to be nuclear magnetic resonance (NMR) spectroscopy. [130] NMR spectroscopy has been quite successful at probing the structure and dynamics of electrolytic solutions in single and multi-component solvent systems. [126,131,132] NMR measurements are based on either chemical shifts or relaxation time measurements. The NMR relaxation techniques have become more prominent for probing the microscopic properties of electrolyte solutions because they allow the study of dynamics and structure of electrolyte solutions on a microscopic level. [131] The relaxation approach relies on the decay of a longitudinal or transverse

component of the nuclear magnetization towards equilibrium values following a radio frequency perturbation pulse. The longitudinal or spin-lattice relaxation time ($T_1$) is related to the energy of interaction of the particular relaxation ($E_i$) and a molecular correlation time ($\tau_c$). Structural properties are determined from $E_i$ and dynamics information is determined from $\tau_c$. Another advantage of using the relaxation time approach is the ability to separate inter- and intramolecular contributions. Knowledge of the two contributions leads to separation of ion/solvent, ion/ion, and solvent/solvent interactions. Despite being able to differentiate between the interactions and providing qualitative information about the environment of the ion, NMR is not capable of resolving contributions from discrete clusters or providing quantitative thermodynamic information. NMR has been a successful approach for probing preferential solvation of alkali salts in binary mixtures of the following solvents with water: N-methylformamide, tetrahydrofuran, ethanol, methanol, acetonitrile, and dimethylsulfoxide. [130,131] Others have studied the preferential solvation of both the halogens and alkali cations in mixtures of methanol, ethanol, acetone, and other non-aqueous solvents. [see reference 134] A few excellent reviews of the NMR techniques have recently appeared in the literature. [131,133,134]

While NMR has been one of the more prominent techniques for probing condensed phase solvation, a multitude of other spectroscopic techniques have also been used to study the interaction of solutes with solvents. [135,136,137,138] These techniques include time resolved infrared spectroscopy [139,140,141], ultraviolet/visible spectroscopy [142,143], time-resolved photoelectron spectroscopy [144,145], electron spin resonance (ESR) spectroscopy [146,147], laser related spectroscopy (hole burning and

photolysis) [148,149], Raman spectroscopy [150,151] and neutron scattering. [138,152,153,154] Each of these approaches involves varying degrees of energetic interrogation of the ion/solvent clusters in solution. Energetics of the ion/solvent interactions are often derived from the magnitude of the signal, while structural and solvent preference information is often derived from changes in spectral characteristics such as a wavelength shift. The dynamics of solvent arrangement are derived from time based signals. Solvation phenomena also play an important role in electrochemistry, especially at electrode interfaces, and numerous electrochemical approaches to probing solute/solvent interactions have been reported in the literature. [155,156,157,158,159,160,161] All of these electrochemical and spectroscopic techniques provide qualitative information about the microscopic environment of the solute in a solvent or solvent mixture. In no case does this information resolve contributions to the microscopic environment from individual solvent molecules (*e.g.*, $[(H_2O)_5 + H]^+$ *versus* $[(H_2O)_6 + H]^+$), rather the information is the average of all solvent molecules within the micro-environment of the solute.

Instead, these techniques are generally used to <u>infer</u> microscopic chemistry from the bulk average properties of the various clusters present in solution. Consequently, the complexity of solution dynamics has generally precluded a full understanding of condensed-phase solute/solvent interactions on a microscopic or molecular level.

### 1.4.2 Mass Spectrometric Approaches

An alternative approach utilized for probing solute/solvent

interactions is mass spectrometry. [162,163,164] The more prominent mass spectrometric techniques and their shortcomings are discussed below. In contrast to the bulk phase methods discussed above, mass spectrometric probes provide insight into the structure and energetics of individual clusters on a microscopic or molecular level. Calorimetry, a bulk phase technique, is capable of providing heats of solution (solvation), but not step-wise heats or free energies of solvation (energy requirements for sequential addition of solvent molecules to the solute). Determination of these step-wise thermodynamic values was made possible through pioneering work in the field of mass spectrometry by Kebarle with high pressure mass spectrometry [165] and pulsed high-pressure mass spectrometry (PHPMS).[166,167] The apparatus and experimental conditions have, of course, been described by Kebarle. [166] Briefly, methane gas at pressures on the order of 4-5 Torr containing known amounts of solvent at pressures on the order of 25-100 mTorr is allowed to flow into a thermostated stainless steel ion source. Original experiments (HPMS) utilized a continuous electron beam (constant filament current), while the improved source (PHPMS) utilizes a pulsed (2000-eV,5 nA) electron beam. The change to the pulsed source ensured equilibrium rather than steady-state conditions. The electron beam is pulsed on for 4 to 180 μsec and off for 2 to 4 msec. The protons created by a given electron pulse react and reach equilibrium as they diffuse towards the walls of the field free ion source. Ions that come into the vicinity of a very narrow slit (3 mm x 0.01 mm) are carried by gas flow into an evacuated region pumped by a high-capacity pump, where neutrals are pumped away. The ions are focused by electric fields and accelerated into a sector instrument for mass analysis. For species such as the alkali salts, ions are created and introduced into the region of

high vapor pressure by thermionic emission from a filament that has been coated with the salt of interest. Considering how the core ion is generated and the manner in which the interaction of the ion with the solvent occurs, this technique can be considered to be strictly a gas phase approach. This approach is limited to studying those ions that can be created by electron ionization or thermionic emission and precludes studying solutes of biological importance such as proteins. The classes of solvents that can be studied, while there certainly are many, are limited to those with appreciable vapor pressure.

Another mass spectrometric approach used to obtain reaction rate constants and equilibrium thermodynamic data has been the flowing afterglow. [168,169,170,171,172] In this apparatus the carrier gas (often helium) at high velocity ($10^4$ cm/sec) passes through a reactor tube on the order of 8 cm in diameter and 1 meter in length. The pressure in this tube is typically 0.5 Torr. Ions are obtained by electron ionization (electrons are generated by a heated filament upstream in the tube). Neutral reactant gases are introduced through one or more nozzles downstream of the filament. The ions are sampled by bleeding a small part of the gas through a small orifice into a region of high vacuum and detected by a quadrupole mass analyzer. The chemical systems amenable to flowing afterglow instruments are similar to those amenable to HPMS. The ions must be created by electron ionization and the solvents must have appreciable vapor pressure.

A limitation to the HPMS, PHPMS, and flowing afterglow systems is the inability to determine ion concentrations in situ. Ion concentrations are determined by bleeding gas through a small orifice into a region of high vacuum for mass analysis. In contrast, the pulsed, trapped ion cyclotron

resonance (ICR) spectrometer has the advantage of detecting the ion concentrations in situ and does not depend on a sampling leak. [173,174,175,176] In this experiment, information about rate constants and equilibrium thermodynamic data can be obtained. The ICR arrangement creates ions in a rectangular cell (dimensions of the order of 1 in. x 1 in. x 3.5 in.) by pulsed (on the order of 10-50 msec) electron ionization. The gas pressure within the cell is typically $10^{-6}$ Torr or less. The ions created by electron ionization are trapped in the cell by large magnetic fields and small static voltages. After a given time of reaction within the cell, the concentration of ions is determined by irradiating the ions with an RF at their cyclotron frequency, and detecting the resulting power absorption or image current.

Gas phase approaches, such as the mass spectrometric techniques discussed above, offer two "advantages" over the bulk phase measurements: 1.) the elimination of the influence of the counterion on solvation and 2.) the elimination of the influence of the bulk solvent properties on solvation. While the gas phase techniques certainly eliminate these influences, in reality they are present in solution and must be considered. From the gas phase measurements, solution phase characteristics are only inferred and not measured directly. Despite these potential complications, HPMS, PHPMS, flowing afterglow, and ICR experiments have proven to provide valuable kinetics and thermodynamic data.

Through careful control of the solvent vapor pressure and source temperature, these methods can provide the information necessary to determine the enthalpy and entropy of solvation for the stepwise addition of individual solvent molecules to the core ion (Reaction 1.1). The equilibrium

constant (K) for reaction 1.1 can be estimated using equation 1.3:

$$H^+(H_2O)_n = H^+(H_2O)_{n-1} + H_2O$$

Reaction 1.1

$$K_{n,n-1} = \frac{I_{n-1}P_s}{I_n}$$

Equation 1.3

where $P_s$ represents the water vapor pressure and $I_{n-1}$ and $I_n$ represent the relative intensity of the ions detected in the mass spectrum (this approach assumes that the partial pressure of ionic species ($P_n$) is proportional to the corresponding ion intensity($i_n$)). The temperature dependence of this equilibrium constant is represented by the van't Hoff relation shown in Equation 1.4:

$$\ln K = -\frac{\Delta H}{RT} + \frac{\Delta S}{R}$$

Equation 1.4

where $\Delta H$ is the solvation enthalpy and $\Delta S$ is the entropy. If $\Delta H$ and $\Delta S$ are temperature independent, a van't Hoff plot ($\ln K$ vs $\frac{1}{T}$) has a slope equal to $-\frac{\Delta H}{R}$ and an intercept of $\frac{\Delta S}{R}$. The slope and intercept allow for calculating the free energy using equation 1.1.

Since the pioneering work of Kebarle in studying gas-phase hydration in the 1960's, this area of mass spectrometry and interest in cluster science has continued to expand. HPMS, PHPMS, flowing afterglow, and ICR continue to

make an impact on the field (gas-phase thermodynamic and kinetics information is still obtained from these techniques), however, others have turned their attention to additional types of mass spectrometric approaches. In the early 1980's Barber *et al.* developed FAB/LSIMS. [1] As discussed above, one of the features of FAB is the ability to sample ions from a liquid matrix. As a result of the liquid matrix (and probably not one of the original intentions for FAB/LSIMS), clusters containing the solvent are generated along with the solute of interest. [177] An excellent review by Sunner detailing the ionization process, the desorption process, the nature of preformed ions and ionic cluster formation in FAB/LSIMS has recently appeared. [178] While FAB is capable of generating ion/solvent clusters from solution, there has been evidence for dominance of gas-phase chemistry in determining the appearance of the spectrum. [179,180,181] Kebarle has obtained FAB spectra from neutral binary mixtures of compounds commonly used as FAB matrices (triethanolamine, diethanolamine, 4-octylamine, 1,2,4-butanetriol, glycerol, and 4-nitrobenzyl alcohol) having a range of gas-phase basicities. [181] The results indicated that the spectrum of the compound with the lower gas-phase basicity was suppressed. Kebarle also obtained spectra for basic analyte pairs (An1 and An2) dissolved in glycerol. [179] For the pairs of analytes where An1 had the higher solution-phase basicity but the lower gas-phase basicity, it was observed that peaks attributed to protonated An1 were suppressed by An2. Kebarle concluded that gas-phase energetics dominate over solution-phase energetics in the FAB experiment. Regardless of whether gas- or solution-phase energetics dominate the spectrum, an excess of internal energy is imparted into the cluster via the bombardment event. The excess of internal energy has the effect of causing fragmentation and disrupting solvation

spheres. While these shortcomings have limited the use of FAB as an approach to probing ion/solvent clusters, other aspects of solution chemistry, such as surface activity, can be probed. [178]

Another commonly encountered technique for probing clusters is free jet vapor expansion followed by a primary ionization event such as EI or photoionization. This technique usually generates solvent clusters with very low internal energy and correspondingly little unimolecular (metastable) dissociation. [182,183,184,185] By expanding rapidly to avoid cluster growth due to cooling during the expansion process, chemistry representative of pre-expansion vapor equilibria can be probed. Again, like the HPMS and PHPMS techniques, this technique appears to represent gas-phase as opposed to solution-phase chemistry. While the species ultimately detected must be ionic, the chemistry is due primarily to neutrals present in the vapor expansion. Again, the chemical systems probed are limited to solvents having appreciable vapor pressure over a wide range of temperatures.

Another of the more recent developments in the study of solvent clusters has come from the use of collision induced dissociation (CID) to probe the enthalpies of solvation for non-equilibrium systems. [186,187,188,189] Initial work using CID to probe protonated water clusters was qualitatively in godd agreement with the accepted equilibrium values reported in the literature. [187] These experiments, however, were done at unknown temperatures which made precise and definitive comparisons of thermodynamic data difficult. Dalleska *et al.* [189], however, have been able to measure the stepwise solvation enthalpies of protonated water clusters (and hydrated metal ions; e.g., $Cu^{+m}(H_2O)_n$) using CID experiments that are in good agreement with the equilibrium values reported by Kebarle. Dalleska utilized

a guided ion beam mass spectrometer to perform these experiments. In this approach cluster ions are formed in a 1 m long flow tube operating at pressures on the order of 0.4 to 0.7 Torr with a helium flow rate of 3,500-15,000 mL/min. $He^+$ and $He^*$ are formed in a microwave discharge source for reaction downstream with water, and the metal ions are formed from a dc discharge by argon ion sputtering of a cathode fabricated from the metal of interest. The source contains a buffer gas pressure sufficient to thermalize the clusters both vibrationally and rotationally. Ion clusters are then extracted into a magnetic sector instrument for mass selection. The mass selected ion clusters are slowed to the desired kinetic energy and focused into an octopole ion guide that radially traps the ions. The octopole passes through a gas cell containing xenon collision gas. After exiting the gas cell, product and unreacted cluster ions drift to the end of the octopole and are focused into a quadrupole for mass analysis. The absolute reaction cross sections for protonated water clusters and hydrated metal clusters with xenon were determined for energies ranging from thermal to 20 eV (center of mass energy). The absolute uncertainties in cross section magnitudes were estimated to be ±20% and the relative uncertainties were estimated to be ±5%. The CID threshold approach to determining enthalpies of solvation is an alternative to the equilibrium method of HPMS and PHPMS. [188,189,190] This method, however, requires careful consideration of multiple collisions, cluster internal energy, and dissociation lifetimes to agree well with results obtained from equilibrium conditions. Collision cross-sections are based on single collision conditions. To obtain such conditions, data are collected at several pressures and then extrapolated to zero pressure (single collision conditions). Multiple collisions have the effect of imparting more energy than expected

into the cluster. The clusters exiting the ion source are also assumed to be in their ground electronic state so that the internal energy can be described by a Maxwell-Boltzmann distribution of rotational and vibrational states corresponding to 298 K. Also, the dissociation must occur within the time frame of the experiment ($10^{-4}$ seconds on the instrument used) to be detected.

Other developments in the area of cluster science at the molecular level (microscopic level) have come from Castleman and co-workers. [191,192] Primary ionization events (necessary to generate species detectable by mass spectrometry), as mentioned above, often impart an excess of internal energy into the core ion or the cluster. As a result of the primary ionization event it has become clear to Castleman and others that molecules may undergo reorientation. This reorientation of molecules has generated a great deal of interest in the area of cluster structure and dissociation dynamics. [193,194,195,196,197,198,199,200,201,202] One of the more recent instrumental developments in this area of research has been the use of laser based reflectron time-of-flight (TOF) mass spectrometry. [203] Castleman and Wei have used this technology to probe cluster dynamics of hydrogen bound systems such as ammonia and van der Waals interactions with systems such as xenon. Neutral clusters are formed in a supersonic expansion from a pulsed nozzle having a diameter of 150 μm. The neutral clusters are then ionized using a Nd:YAG laser source operating at 355 nm with a pulse length of 6 nsec. The ions formed by multiphoton ionization are accelerated in an electric field to several kilo-electronvolts and directed through a field-free region toward a reflectron. Ions are then reflected through another field-free region towards the detector. The reflectron is necessary to resolve precursor ions from fragment ions. The resolution of the two kinds of ions allows for

determination of kinetic energy releases (energy released during the dissociation process) and decay fractions (the extent of decay) of the dissociating cluster in the field-free regions. Thermodynamic values, however, are calculated from the translational energy of the cluster, the rotational energy of the cluster, and the CID threshold. The CID threshold is measured directly, but the translational and rotational energies of the cluster are based on the assumption that the cluster is thermalized within the source prior to the dissociation reaction.

A few other mass spectrometric techniques have been used to study ion-solvent interactions. Cook and Murawski have reported the apparent preferential solvation of $Na^+$ ions (sampled by EH) by glycerol in mixed water/glycerol solutions. Clusters having the general formula $[(H_2O)_n + Na^+]$ were only detected from 100% aqueous solutions of NaI. The relative abundance of the pentamer (n = 5) cluster was larger than that of other clusters and suggests that this cluster, possessing a closed (full) solvation shell, is more stable than the other clusters. [112] Since that time, other reports of clusters generated by EH ionization have appeared from Fenselau [125] and Mahoney. [204] Fenselau utilized the EH technique to sample ions from a membrane introduciton system but did not specifically address the clusters detected in terms of ion/solvent interactions. It is interesting to note, however, that despite water being the major solvent component in the mixture of water/glycerol, only clusters attributed to glycerol are observed in the mass spectrum. Mahoney has used an aqueous solution of ammonia to generate massive clusters for use as a primary ion source. While the source does generate clusters, Mahoney does not specifically address the role of ion/solvent interactions.

Since the introduction of electrospray (and ion spray and thermospray) ionization many investigators have focused their attention on the role of the solvent in the ionization process and mechanism. This research has considered the role the solvent plays in the ionization mechanism, [57,205,206,207] the study of ion-solvent clusters formed by the ionization process, [64,65,72,208,209] and the effect the solvent can have on the appearance of the spectrum. [58,68,74,210] The ES technique, like EH and FAB, samples ions directly from solution. However, like FAB, HPMS, and PHPMS there are some complications that should be considered. The very nature of the ES sampling process requires that the droplets undergo many collisions at atmospheric pressure to remove the solvent molecules from the solute. While this is advantageous for ES in general (improves the ionization efficiency), it makes interpretation of the relationship between ion-solvent clusters initially present in solution and the appearance of the spectrum difficult. In fact, the goal in most ES applications is complete desolvation. Despite the desire to completely desolvate the analyte for analytical ES, the possibility exits to detect solvated species. [see ref. 64, for example] The ion-solvent clusters that survive the ionization process, however, enter the instrument with ill-defined internal energy, but less than needed to remove a solvent molecule. Despite these shortcomings, ES has provided some useful information concerning interaction of solutes ranging from metal ions to large biomolecules with solvents such as methanol and water. For example, several investigators have used ES to study the solvation of aqueous solutions of alkali and transition metal salts. [65,211,212,213,214,215] Another example of the use of ES to probe ion/solvent interactions comes from the observation that the charge state distribution of large biomolecules changes as the composition of the solvent

changes (the composition of methanol changes). [58]

From the above discussion of the various approaches to probing the structure, dynamics and energetics of clusters, it is clear that cluster science is an enormous field of research. While the above discussion falls short of being inclusive of all work to date (Castleman and others have published reviews of solvation and clustering [162,163,216]), it does provide an indication of some of the shortcomings of the techniques and methods currently being used to probe the chemistry of clusters and the chemical systems amenable to the techniques. In general, the condensed phase techniques (optical spectroscopy and NMR) provide useful information about bulk phase properties and attempt to infer microscopic chemistry from this information. While the mass spectrometric techniques have also provided extremely useful information, there are also shortcomings such as those stemming from the energetic primary ionization process, the gas phase creation of ion-solvent clusters, and the complicated relationship between the observed spectrum and clusters present in solution. EH ionization offers an alternative approach to the methods described above. Results obtained using a newly modified EH source are presented in Chapter 5. These studies will assess the potential of EH as a viable alternative approach for sampling and probing ion/solvent interactions in solution.

## 1.5 Summary and Objectives

The primary objective of the research efforts presented in this thesis has been to provide a better understanding of the ionization mechanisms involved in (FAB)/(LSIMS), ES, and EH MS. The FAB/LSIMS investigation was aimed at gaining a better understanding of the time dependence of spectra. The ES investigation was directed towards a better understanding of the ionization process, improving existing methods for electrospraying conductive aqueous solutions, and interfacing the method with CE. The EH work has focused on the development of an approach capable of probing solution-phase solvation. The role of solution chemistry has been important in explaining the results presented in this thesis. While only the EH work presented in Chapter 5 specifically focuses on the ion/solvent interactions, the work presented in Chapters 3 and 4 are also indirectly related to the role the solvent plays in the ionization mechanism.

# Chapter 2

## Experimental Methods

Four mass spectrometers (VG ZAB-EQ, Extrel Triple Quadrupole, AEI MS-902, and Finnigan-MAT Ion Trap) were used to acquire the MS data presented in this dissertation. Each instrument is described and an instrument schematic is provided within this chapter in the order in which the results and discussion are presented in subsequent chapters. The wide variety of mass spectrometers described below is a reflection of the different information obtained from each. For example, the Extrel secondary ion microprobe provides information about the spatial distribution of secondary ions originating from the surface of a liquid sample. The VG ZAB-EQ was used in parallel with the secondary ion microprobe to provide information about the time dependence of secondary ions originating from the surface of a liquid sample under normal FAB conditions. The AEI MS-902 has for many years been dedicated to electrohydrodynamic ionization mass spectrometry and was a logical choice for the studies of ion/solvent clusters generated from solution. The Finnigan-MAT Ion Trap was used for the electrospray applications so that results obtained from a "conventional" ES source could be compared to results obtained using the ES source developed at the University of Tennessee and described below.

## 2.1 FAB/LSIMS

### 2.1.1 Secondary ($2^o$) Ion Microprobe

The Oak Ridge National Laboratory (ORNL) wide angle secondary ion microprobe, used to acquire secondary ion spectra and images from liquid matrices, has been described in detail previously. [217,218] The microprobe was designed and constructed by the Todd group at ORNL. Briefly, it consists of a cesium ion ($Cs^+$) primary ion gun with a focusing objective lens and raster capability; a wide angle secondary ion source; an Extrel (Pittsburgh, PA) triple quadrupole mass filter (used in these studies as a single MS, rather than in the tandem mode); and a post-analysis acceleration detector (PAD). Figure 2.1 shows a schematic diagram of the wide angle secondary ion microprobe. Control and data acquisition are performed using an 80286-based computer, with software developed at ORNL by the Todd group. Secondary ion images reported here are based on the peak intensity of mass-resolved secondary ions.

The analyte is dissolved in an appropriate solvent such as glycerol or nitrobenzyl alcohol and a thin layer is applied to the copper sample stage within a 1-$cm^2$ area. Glycerol and nitrobenzyl alcohol are viscous liquids with low vapor pressure. The low vapor pressure is necessary to obtain the high vacuum necessary within the ion source housing. The primary ($1^o$) ion beam, which has a diameter of approximately 100 μm, is rastered across the surface of the sample. The rastering is accomplished by computer control of a set of

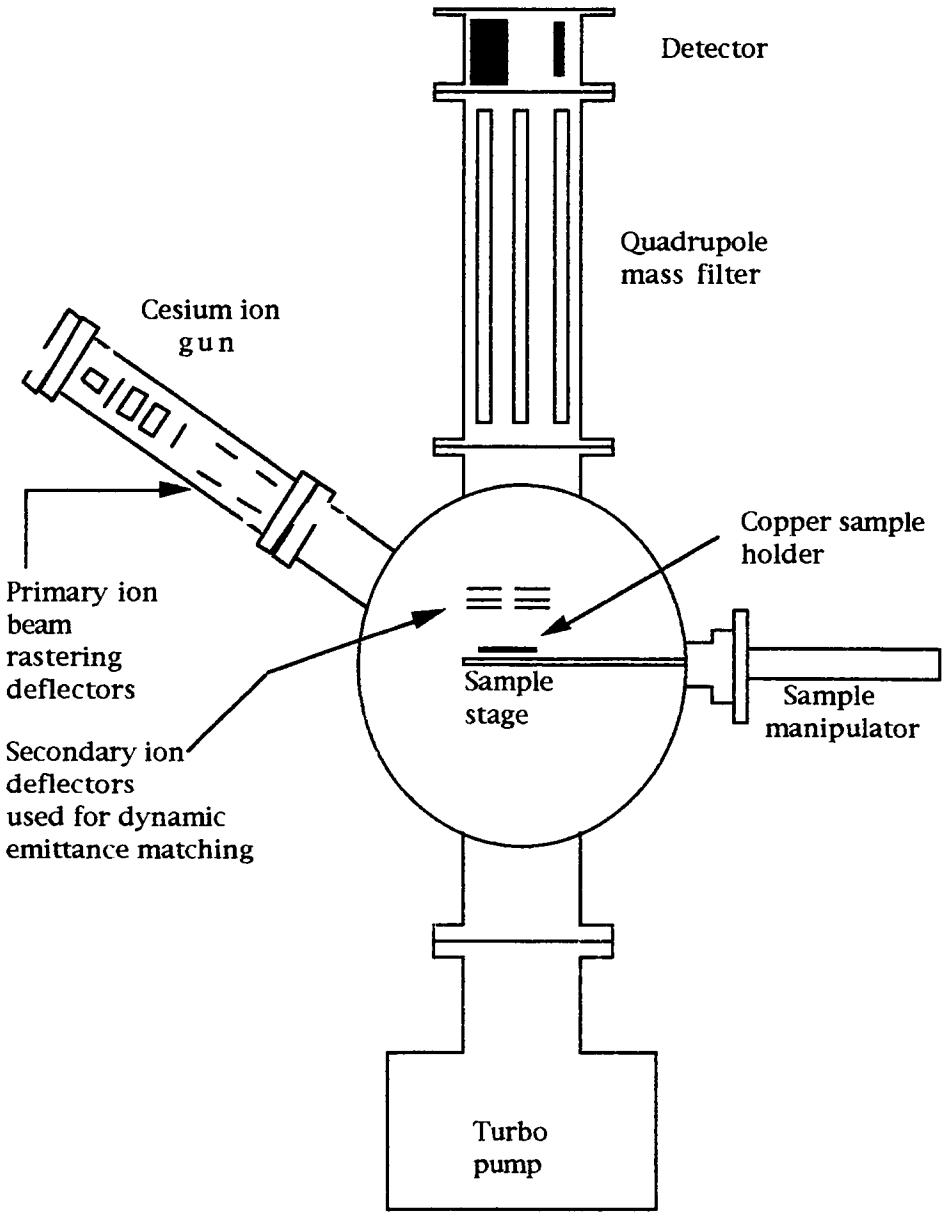



**Figure 2.1.** Schematic diagram of the wide angle secondary ion microprobe used to acquire secondary ion images and spectra.

deflectors located adjacent to the ion beam exit aperture of the $Cs^+$ ion gun (or $1^o$ gun). The rastering generates $2^o$ ions from only a small area of the sample at any given time. This area is determined by the size and location of the $1^o$ ion beam. $2^o$ ions are only transmitted into the mass spectrometer for mass analysis from a very narrow region on the sample termed the field of view of the mass analyzer. The rastering of the $1^o$ ion beam obviously changes the location from which $2^o$ ions are being generated. Therefore, a technique by which the $2^o$ ions are deflected into the field of view of the mass spectrometer must be employed. This is accomplished by varying the potentials of a set of $2^o$ ion deflectors located within the ion source. The potential of the deflector plates (computer controlled) is varied to adjust the $2^o$ focal point synchronously with the rastering of the $1^o$ ion beam across the surface of the sample. This "moving focus technique" is referred to as dynamic emittance matching (DEM). [217,219]

The following instrumental conditions were employed: 6 keV $Cs^+$ primary ion beam; 3 nA primary ion current; 10-eV secondary ion kinetic energy; -6 kV PAD dynode voltage; -1.3 kV multiplier voltage. The data acquisition rate was 50 kHz. 128 intensity measurements at a selected mass-to-charge ratio (m/z) (single ion monitoring mode, SIM) are obtained and averaged prior to deflection of the 100-μm $1^o$ beam spot to the next position on the sample. The time required to obtain data for a 200 x 200 pixel image over a 1-$cm^2$ area was approximately 2 minutes. Alternatively, a full spectrum over the mass range 50 to 300 Daltons could be obtained from a single point on the sample in about 2 seconds by acquiring a single intensity measurement at each m/z. The primary ion gun was allowed to warm up for a minimum of 1

hour prior to collecting data.

For secondary ion imaging experiments, a thin film of sample was applied to approximately 1-$cm^2$ of a 20-mm x 100-mm copper plate which was mounted horizontally on the sample stage. This assembly was inserted via a pre-vacuum chamber into the source housing. The source housing operating pressure is typically on the order of $10^{-7}$ Torr. Data collection started immediately after inserting the probe into the source housing and continued for approximately 1.5 hours. Reported ion intensities in mass spectra represent peak heights from a single scan of the mass range. Reported images represent averages of 128 intensity measurements at each of 40,000 pixels during a single "raster excursion" of the 1-$cm^2$ area.

### 2.1.2 VG ZAB-EQ

Fast atom bombardment (FAB) data were obtained with a VG Analytical (Manchester, UK) ZAB-EQ mass spectrometer (Figure 2.2) using the standard VG FAB source and a VG 11-250J data system. The instrument was operated at an acceleration potential of 8 kV and with a mass resolution of at least 1000 (10% valley definition). Research grade Xe (MG Industries, North Branch, NJ) was used with an Ion Tech (Middlesex, UK) atom gun, operating with 1.0 mA emission current at 8.0 kV. The FAB gun was allowed to warm up for at least 1 hour prior to data acquisition. Under these conditions, the beam area was determined by Boggess to be 0.28 ± 0.02 $cm^2$, [110] so the 0.071 $cm^2$ area of the brass FAB target was fully and uniformly exposed to the primary atom beam.

For the FAB experiments, approximately 2 mg of a glycerol solution

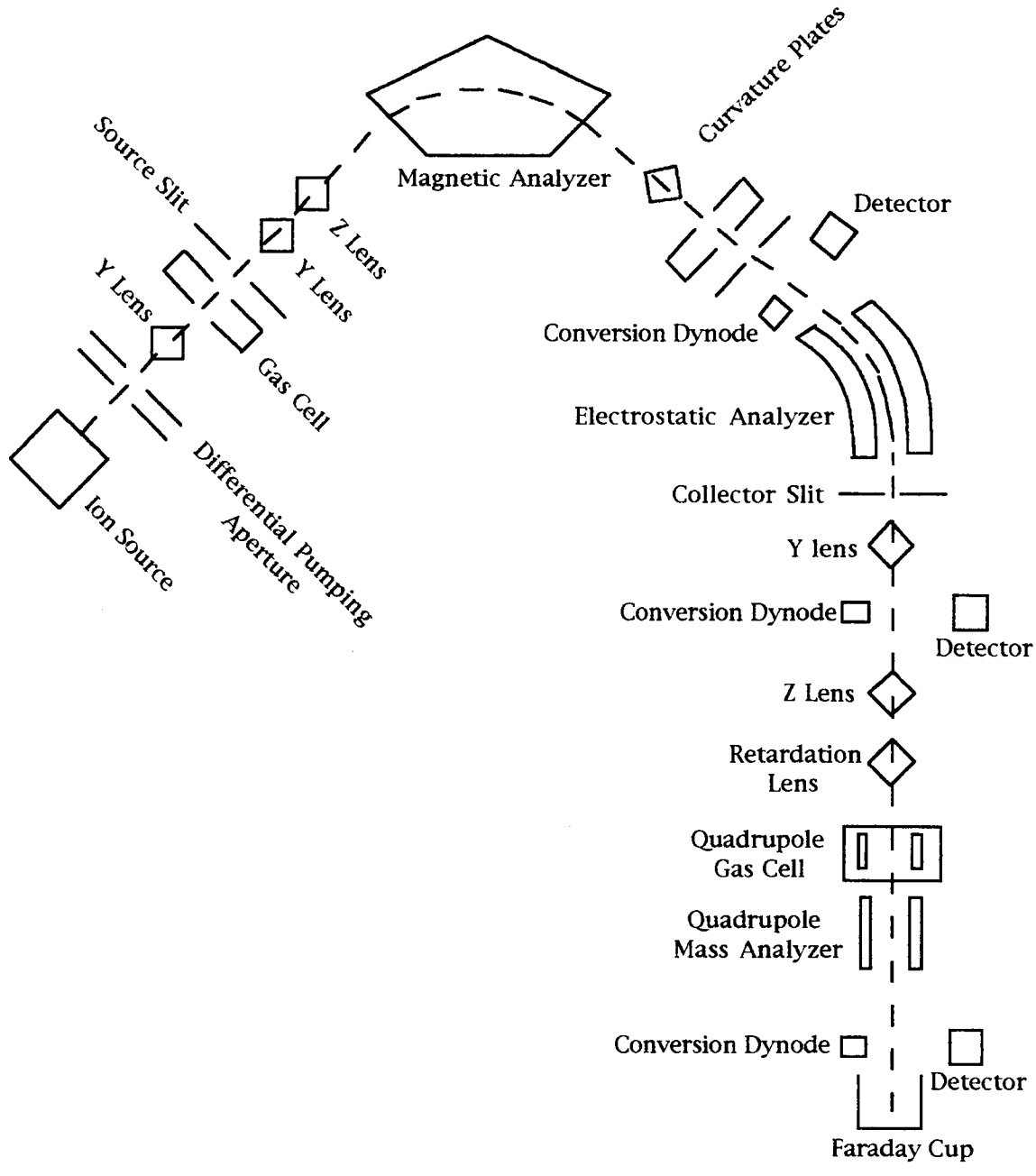



**Figure** 2.2. Schematic diagram of the VG ZAB-EQ instrument used to acquire fast atom bombardment data.

were loaded onto the flat end of a cylindrical target by dipping. The FAB probe was then inserted into the source via a pre-vacuum stage. The operating pressure of the source housing was typically on the order of $10^{-6}$ Torr. Data collection began immediately after inserting the probe into the source high vacuum housing. Each sample was run to dryness, requiring approximately 1 hour.

Data were acquired in the histogram mode of operation. In this mode, the data system calculates m/z centroids from intensity versus time profiles. The mass spectrum is then stored and presented as a bar graph (histogram) of peak intensity as a function of the m/z centroid. Spectra were obtained using a 10 second/decade magnet scan over the mass range 50-500. Plots of intensity versus time were reconstructed from these scans, rather than by single ion monitoring. Reported ion intensities represent peak heights. Reported FAB mass spectra represent a single scan over the entire mass range indicated above. The intensity versus time profiles ("ion chromatograms) were generated from the individually stored mass spectra.

### 2.1.3 Electrochemical Polymerization of 3-methylthiophene

Liquid "beading" is a problem commonly encountered in applying a liquid to a metal surface. Unless the surface is wetable (solvent/surface interactions exceed surface tension [solvent/solvent] interactions) when a liquid (e.g., glycerol) is applied to a metal surface, it will form a droplet rather than a thin uniform layer. This affects FAB because this droplet can sag and meander across the surface of the probe tip. The sagging and meandering can effect the time dependence and reproducibility of FAB spectra. One method of

overcoming the "beading" effect is to coat the surface of the metal with a chemical that improves the wettability of the surface. In the case of FAB mass spectrometry, this material must be conductive to allow for the application of the accelerating voltage and so that surface charging does not occur. Electrochemical polymerization of 3-methylthiophene has been shown to provide a conductive and hydrophilic layer on metal surfaces. [220] Therefore, in an attempt to overcome the "beading" effect when applying the liquid matrix, the FAB target was coated with poly(3-methylthiophene) using the procedure described below.

As shown in Figure 2.3, the apparatus consisted of an electrochemical cell (beaker) and a three electrode system consisting of a stainless steel working electrode (0.32 cm diameter planar electrode), a platinum mesh counter electrode, and a Ag/AgCl wire (quasi-reference electrode). The polymerization solution contained 0.01 M 3-methylthiophene and 0.1 M tetraethylammonium perchlorate dissolved in acetonitrile. No special precautions were taken to remove dissolved gases, such as oxygen, from the solution. The 3-methylthiophene was vacuum distilled at 140 Torr prior to use to improve purity. The electrode potentials were controlled using a Bioanalytical Systems BAS 100 Electrochemical Analyzer (Lafayette, IN) operating in the cyclic voltammetry mode. The potential was initially set to 0 mV, then cycled to +1100 mV at a scan rate of 50 mV/second, and then returned to 0 mV at the same scan rate. This cycle was repeated as necessary (minimum of twice) to provide a black film that completely covered the FAB probe tip surface. While the thickness of the layer was not determined, complete coverage of the surface was determined by visual inspection. A special Teflon sheath (Figure 2.3) was constructed to shield the sides of the FAB probe tip

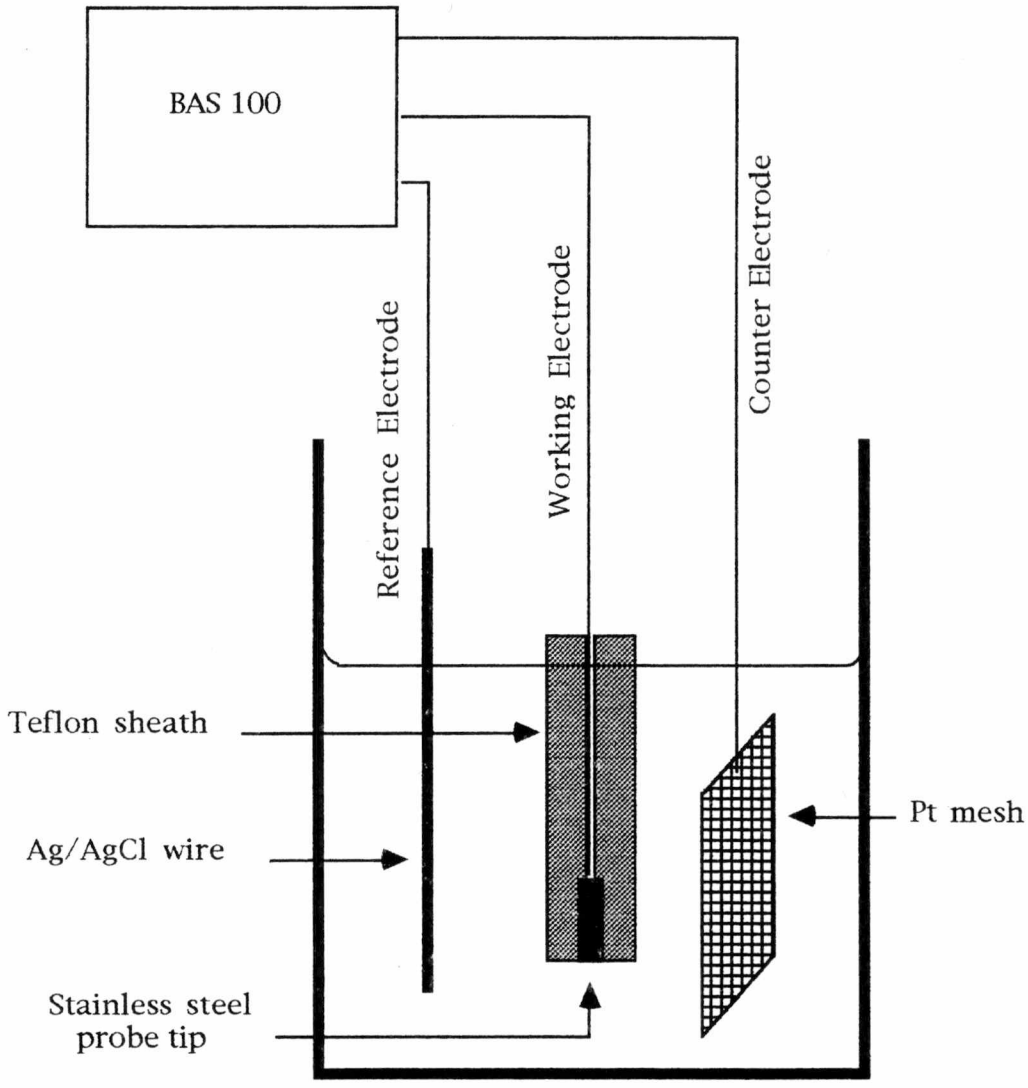



**Figure 2.3.** Schematic diagram of the electrochemical apparatus used to polymerize 3-methylthiophene on the surface of a stainless steel FAB probe tip.

from the polymerization reaction, thereby improving the efficiency of electrochemical deposition at the useful, flat surface.

## 2.2 Electrospray Ionization

### 2.2.1 Finnigan-MAT Ion Trap

ES mass spectrometric experiments were performed using a Finnigan-MAT ITMS (San Jose, CA) (Figures 2.4 and 2.5) modified for ES. [221] Ions were injected for periods ranging from 10 to 500 msec and then subjected to an RF "heating" cycle (typically ramped from 50 to 400 mV for 50 msec followed by 300 msec at 1800mV) to promote desolvation. [222] Resonance ejection [223] was used in all cases to extend the normal m/z range (i.e., m/z 650) by factors up to five.

#### 2.2.1.1 Electrospray Sources

Two classes of electrospray (ES) mass spectrometric experiments were performed. In continuous infusion, a syringe pump was utilized to deliver solution to the electrospray source. The second class utilizes a powerful separation technique, capillary electrophoresis (CE), to deliver solution to the electrospray source.

In all cases the ES emitter was positioned 0.5 to 2.5 cm away from the front aperture plate of the ion trap (IT) to maximize analyte signals. For most ES applications, a gold-tipped fused silica capillary (10-50 μm i.d. x 365 μm o.d. x 50-60 cm; see section 2.2.2 below for preparation procedure) was placed within

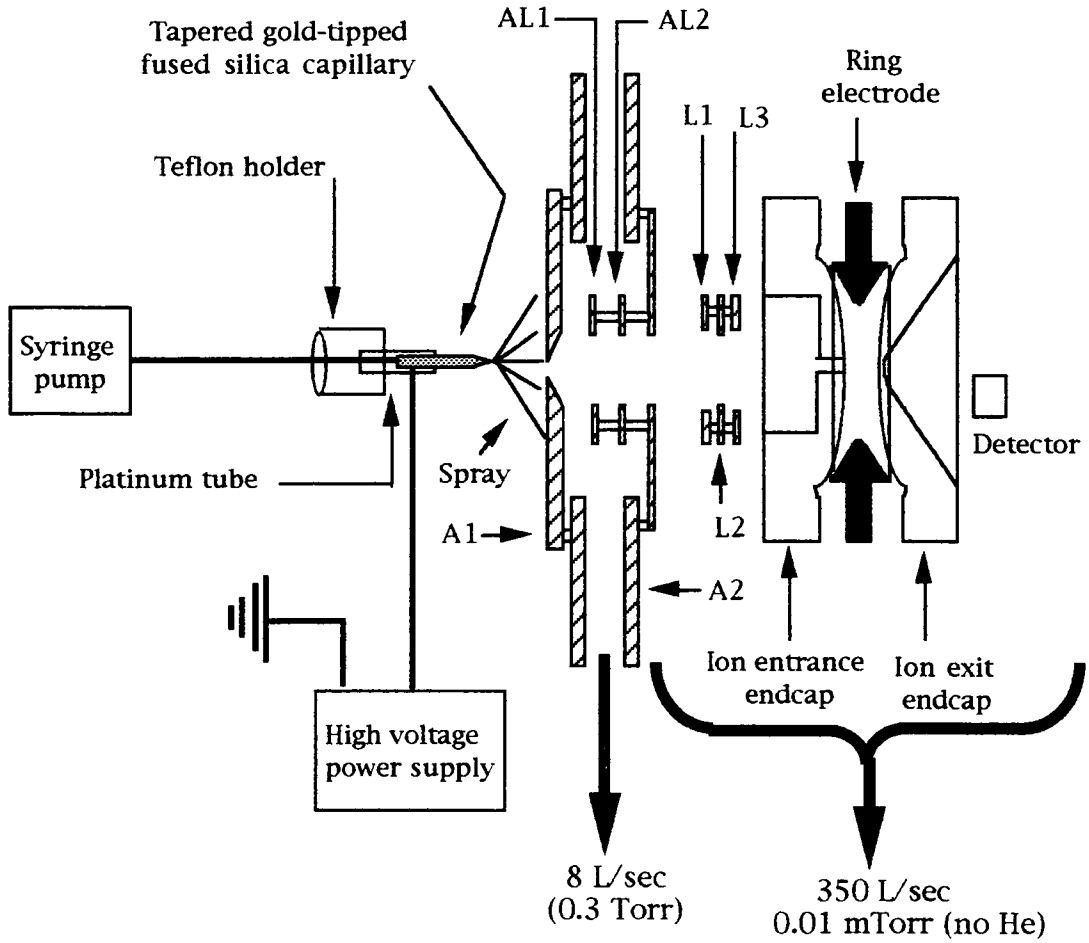



**Figure 2.4.** Schematic diagram of the Finnigan-MAT ion trap mass spectrometer and syringe pump used to acquire continuous infusion electrospray data. The source is shown using the gold coated capillaries described in section 2.2.2. See parts list in Table 2.1.

Table 2.1. Parts list for the Finnigan-MAT ITMS shown in Figures 2.4 and 2.5.

| Identifier | Description (typical voltages) |
|---|---|
| A1 | entrance aperture plate (+100 volts) |
| A2 | exit aperture plate (ground potential) |
| AL1 | interface lens (+100 - 200 volts) |
| AL2 | interface lens (+100 - 200 volts) |
| L1 | lens #1 of 3 element lens (+100 - 200 volts) |
| L2 | lens #2 of 3 element lens (+100 - 200 volts) |
| L3 | lens #3 of 3 element lens (+100 - 200 volts) |
| ring electrode | ion trap ring electrode (-1.8 to - 2.0 kV) |

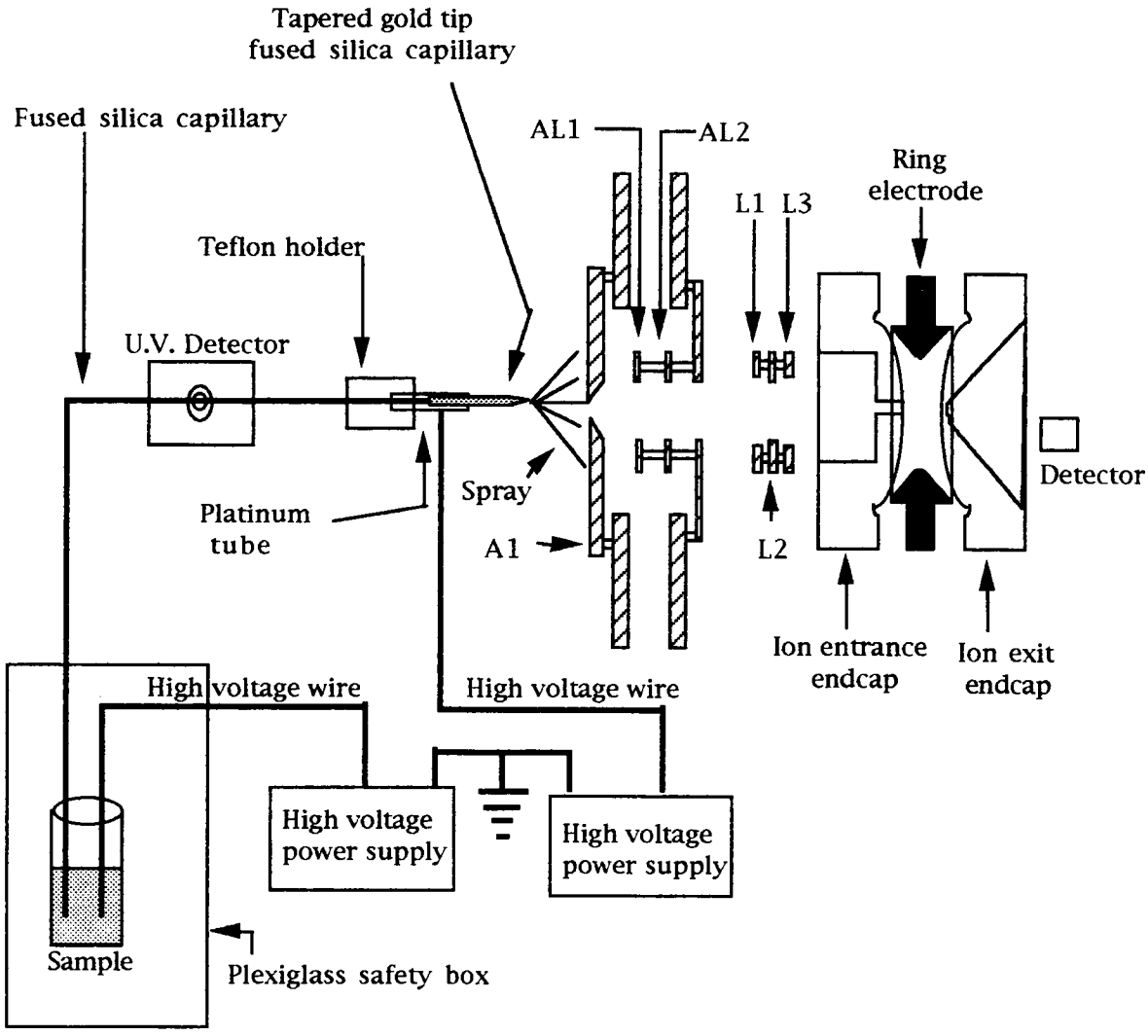



Figure 2.5. Schematic diagram of the Finnigan-MAT ion trap mass spectrometer and capillary electrophoresis instrument used to acquire the CE/ESI data. The source is shown using the gold coated capillaries described in section 2.2.2. See parts list in Table 2.1.

a platinum capillary (394 μm i.d. x 711 μm o.d. x 2.54 cm; Hamilton, Reno, Nevada), with the coated tip projecting roughly 1 cm beyond the end of the Pt tube. Approximately 2 cm of the fused silica capillary was gold coated. The Pt tube was used to establish electrical contact while avoiding crushing and scratching the gold-tipped capillary. A small quantity of silver conducting paint (Micro-Circuits Company, New Buffalo, MI) was applied to secure the gold-coated capillary within the Pt tube and to ensure good electrical contact. High voltage (+1.5 to +4.5 kV) from a Universal Voltronics (Mount Kisco, NY; model BAP 16-1.5) power supply was applied to the platinum tube using an alligator clip. The counter electrode was the stainless steel entrance aperture (+100 V; 100 μm i.d.) into the mass spectrometer. In some comparison experiments, 27 gauge (150 μm i.d. x 520 μm o.d.) or 32 gauge (100 μm i.d. x 228 μm o.d.) dome-tipped stainless steel needles (Hamilton, Reno, NV) were used as the emitter. A nitrogen nebulizer system was also used for comparisons. It was comprised of a 32 gauge needle concentric within a 22 gauge needle (394 μm i.d. x 711 μm o.d.; Hamilton), with nitrogen (60 p.s.i.; flow rate on the order of several liters/minute; at ambient room temperature) passing through the annulus (Figure 2.6). Graphite ferrules were used to secure the needles within the union tee and the ES potential was applied directly to the union. Comparisons between various sources were made using identical data acquisition parameters.

In direct infusion experiments, solution was supplied to the ES emitter using a Harvard Apparatus (South Natick, MA) model 11 or 22 syringe pump with a gas-tight Hamilton syringe connected to the capillary or needle using a 1/16 inch zero dead volume union (VICI, Houston, TX) and Teflon ferrules (Chromatography Research Supplies, Inc., Addison, IL). Flow rates ranged

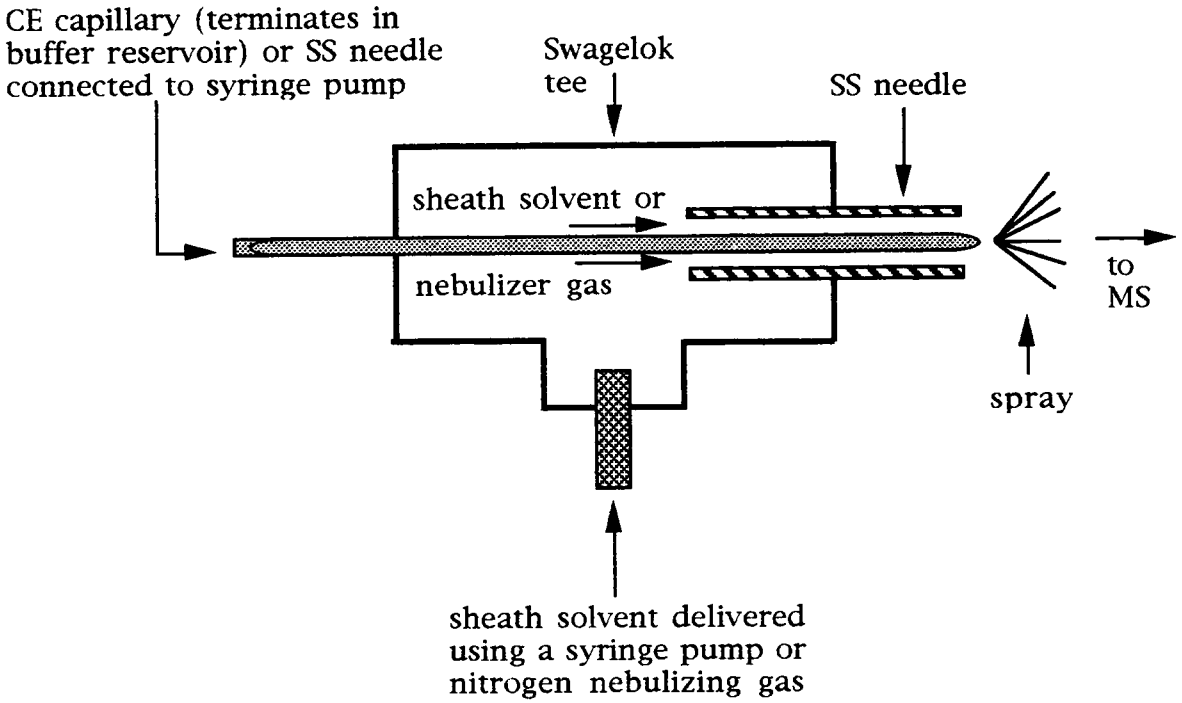



Figure 2.6. Cross sectional view of the system used for electrospray using a sheath solvent flow or nitrogen nebulization.

from 0.05 μL/minute for the gold-tipped capillaries to 1 μL/minute for the 32 gauge stainless steel needle.

The CE apparatus consisted of a Spellman (Plainview, NY) CZE 1000R high voltage power supply, safety interlock box, and an ISCO (Lincoln, NE) S500 UV absorbance detector. The safety interlock box was designed and constructed of Plexiglas at ORNL. It contained the sample and buffer reservoirs. If the door to the box was open, the high voltage was automatically turned off to prevent possible electrical shock. Separations were performed using a 60 cm long, 365 μm o.d. X 50 μm i.d. gold-tipped fused silica capillary. The coated terminus served as the CE exit (low voltage) end and was maintained at a potential of +2 to +3 kV to produce the electrospray. To provide the bias necessary to drive the electrophoresis, the buffer reservoir potential was maintained at -22 kV (Figure 2.5). The CE mobile phase was a 10 mM aqueous acetic acid solution having a pH of 3.4. All injections were made electrokinetically for 5 seconds at an applied voltage of -10 kV (relative to ground) from aqueous solutions. For chromatographic experiments (only), the inside of the column was coated with 3-aminopropyltriethoxysilane (Pierce, Rockford, IL) by the method of Moseley *et al.* [224] to minimize interaction of the positively charged analyte species with the negatively charged wall of the fused silica capillary. The gold outer coating was applied prior to chemically modifying the inner surface of the capillary. This order of capillary preparation required extreme care so that the gold tip was not broken. Future preparation should include coating the inner wall of the capillary prior to preparing the gold tip.

### 2.2.1.2 Capillary Characterization Apparatus

The experimental apparatus depicted in Figure 2.7 was used to characterize the durability of the gold-coated tips and their versatility for spraying various solutions. The emitter was positioned 1.5-2.0 cm from, and perpendicular to, a 3.5 cm x 3.5 cm x 1 mm thick stainless steel collector plate which served as the counter-electrode. This plate was grounded through a Keithley (Cleveland, OH) model 600A electrometer, thus providing a measure of the electrospray current. Two measures of spray quality were assessed. With the room light dimmed, a good quality backlit spray took on the appearance of a steady cone-shaped (cone angle $\approx 60^{o}$) mist that disappeared due to evaporation prior to striking the collector plate. Backlighting was accomplished by shining light from an illuminator (American Optical Corp.) at an angle just less than $180^{o}$ to the observer. A steady collector current (*ca.* 1 μA) observed with the electrometer provided a second indication of stable electrospray. In all experiments utilizing the bench-top apparatus depicted in Figure 2.7, 25 μm i.d. X 365 μm o.d. fused silica capillaries of lengths ranging from 20 to 50 cm were used. Continuous infusion was maintained at a flow rate of 0.2 μL/minute using a model 11 Harvard Apparatus syringe pump and a 25 μL Hamilton gas-tight syringe connected to the fused silica capillary using a 1/16 inch stainless steel Swagelock (Solon, OH) union and Teflon ferrules. The gold-coated fused silica capillary was positioned within a Pt tube and a small amount of silver conducting paint was applied as described above for ES applications. A Fluke (Model 408B, John Fluke Mfg. Co. Inc., Seattle, WA) power supply was used to supply the high voltage necessary to maintain ES. After connecting the fused silica capillary to the syringe, the syringe pump was

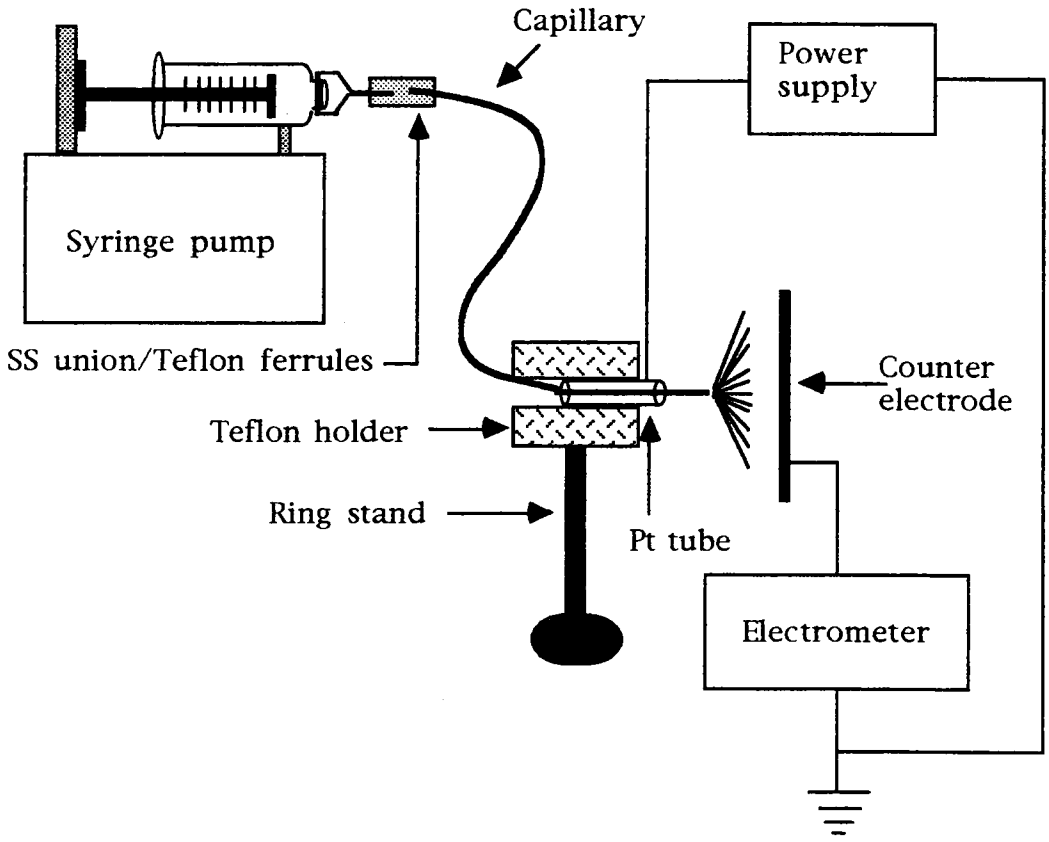



Figure 2.7. Schematic diagram of the bench-top apparatus used to characterize the durability of the gold-coated tips and their versatility for spraying various solutions.

turned on to establish the necessary flow. Once a droplet formed at the tip of the capillary, the high voltage was turned on. The high voltage was initially set to 0 kV and then adjusted in 100 V increments until the droplet was dislodged from the tip of the capillary. The voltage necessary to dislodge the droplet is typically several hundred volts higher than necessary to maintain stable electrospray. Following the removal of the droplet, the voltage was decreased to the minimum voltage necessary to maintain stable electrospray.

### 2.2.2 Capillary Coating Procedure

As mentioned in the introduction, a variety of methods for generating metallic coatings on fused silica capillary have been explored. These methods have either chemical or physical limitations. For example, silver coatings have a short lifetime due to electrochemical reactions that occur during the ES process. Other coatings are limited in their physical adhesion to the fused silica. Several of these coatings were tested in the Cook laboratory, including vapor deposited silver and gold on untreated fused silica and their shortcomings were confirmed. The coating produced by adapting a procedure described by Goss *et al.* [225] for an electrochemical application, has proven to be chemically and physically stable under a variety of conditions that will be presented later in this thesis. The University of Tennessee Research Corporation is currently considering applying for a patent for the technology described below (including the chemical treatment and the shaping procedure).

One end of a polyimide-coated fused silica capillary (typically 10-50 μm i.d. x 365 μm o.d. x 12-60 cm long; Polymicro Technologies, Inc., Phoenix, AZ)

was shaped by gently applying pressure to the capillary tip with fine grit sandpaper (600 W grit; Sandpaper Incorporated, Rockland, MA) held between the thumb and forefinger while spinning the capillary at full speed (≈ 6000 r.p.m.) in a bench top mini-lathe (Unimat-S1 Model DB200, American Edestaal, NY). A number 4 size collet was used to hold the capillary in the lathe. If more than 4 mm of the fused silica extended beyond the collet, it was difficult to prevent breaking the tip. In general, the outer diameter of the tip of a shaped capillary can be reduced to approximately twice the inner diameter. Shaping the tip beyond this diameter usually resulted in breaking the capillary. This treatment proceeded for about 10 min, until a profile like that in Figure 2.8 was achieved. The capillary was removed from the lathe, and *ca.* 1 cm of polyimide coating was burned off (starting at the shaped end) using a butane lighter or match. The shaped end of the capillary terminus (polyimide removed) was immersed in acetone for 1 minute while ultrasonically cleaning (Sonicor Model G-1080/ET-1/PC-1, Farmingdale, NY). The capillary was next flushed with several capillary volumes (depending on the length, one capillary volume is approximately 25 μL) of methanol using a syringe connected to the untreated end of the capillary with a 1/16" Swagelock union with Teflon ferrules. The shaped, uncoated end of the capillary was then cleaned by immersing (to a depth just adequate to cover the portion of capillary not coated with polyimide) for 20 minutes at 70°C in "Piranha solution" (1:4 mixture of 30% $H_2O_2$ and concentrated sulfuric acid). Extreme care should be taken when working with Piranha solution. The mixing of sulfuric acid with hydrogen peroxide is exothermic and should be done at small volumes. Typically 2 mL of piranha solution were prepared at one time. The capillary was then rinsed and flushed with several capillary volumes (minimum of 50 μL) of deionized

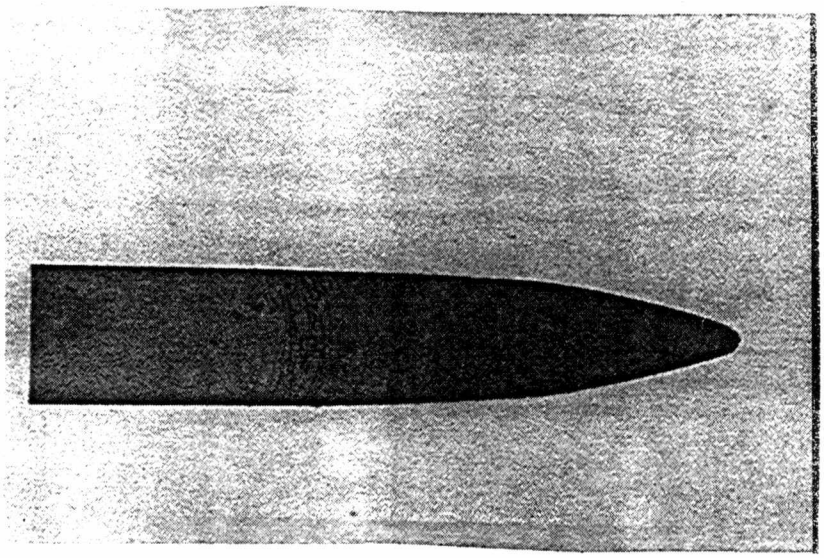


**Figure 2.8.** Electron micrograph of a gold-coated 25 μm i.d. x 365 μm o.d. shaped fused silica capillary. The electron micrograph was obtained using an ETEC Autoscan (Los Angeles, CA) electron microscope. The micrograph was acquired by Mr. Richard Williams of the University of Tennessee Microscopy Laboratory under conditions yielding a magnification of 40X. The outer diameter at the tip after shaping is estimated to be 50 μm or roughly twice the inner diameter of the capillary. To avoid charging of non-conductive surfaces, only the conductive (gold-coated) portion of the capillary was mounted in the instrument to acquire the electron micrograph.

distilled water (Milli-Q Deionizer, Millipore Corp., Bedford, MA; minimum resistance: 15 MΩ/cm), the outside was blown dry with argon gas, then the capillary was dried in an oven at 105 °C for 10 min.

After cleaning, *ca.* 4 cm of the capillary (shaped end) was immersed in a boiling coating solution (vessel equipped with a reflux condenser) for 10 minutes. The reaction vessel was a 250 mL round-bottom flask containing a solution prepared as follows below. The coating solution was comprised of 5 g (3-mercaptopropyl)trimethoxysilane dissolved in 200 g 2-propanol and 5 ml deionized distilled water. Following reaction, the outer surface of the capillary was rinsed with 2-propanol and the coating was cured in an oven at 105 °C for 10 minutes. The coating process (immersion, rinse, cure) was repeated two additional times to assure complete reaction of the fused silica surface. No precautions were taken to prevent the coating or Piranha solution from entering the inside of the capillary via capillary action during the reaction or cleaning process.

Finally, the capillary was coiled into a *ca.* 6 cm o.d. circle, and all but the reacted tip was covered with aluminum foil. The coil was mounted on a rotator within a Denton (Cherry Hill, NJ) model DV-515 bell jar evaporator. Following evacuation to $6 \times 10^{-5}$ Torr, the capillary was gold coated by vapor deposition using a flash power of 70 W while rotating at approximately 30 rpm to ensure uniform coating of the exposed surface. Approximately 25 milligrams of gold was placed in a tungsten basket located within the bell jar. The gold layer thickness was estimated to be on the order of 1000 Å (thicker layers tended to peel from the capillary surface). The coated capillary was inspected with a 3X microscope to confirm complete coverage. Incomplete coverage was never observed.

## 2.3 Electrohydrodynamic Ionization Mass Spectrometry

### 2.3.1 AEI MS-902

Electrohydrodynamic mass spectra were obtained with an AEI MS-902 mass spectrometer (Figure 2.9) equipped with a VG Update electronics console (VG Analytical, Altrincham, UK) and a Vector II data system (Teknivent, Maryland Heights, MO). The ionization source (Figure 2.10) used to acquire data from glycerol samples (described previously [100,226]) was modified to allow sampling of aqueous solutions. The modified EH source is shown in Figure 2.11 for comparison with the unmodified source and is described below. The mass spectrometer was operated with the slits fully open (resolution *ca.* 300; 10% valley definition) for maximum throughput. Magnet scans over the range 10-500 Daltons using a linear 30 second/scan were acquired in the histogram mode of operation (defined earlier). Mass spectra represent the average of either 15 or 30 minutes of acquisition (roughly 15 or 30 spectra).

Tandem MS was accomplished using the "linked scan control" of the VG Update electronics console. By scanning the magnetic field (B) and the electrostatic field (E) simultaneously at a constant B/E ratio, information can be gained about metastable fragmentation within the first field free region (FFR 1; region between the ion source and the ESA shown in Figure 2.9). To use the "linked scan control," the instrument is tuned as normal (the mode selector set to "scan" and "magnet") to allow the full energy precursor ion to be detected . The ion energy will be nominally 8 keV, but the exact ion energy is noted from the panel meter on the control console (set in the "voltage" position). With the panel meter on the control console still set to "voltage," the

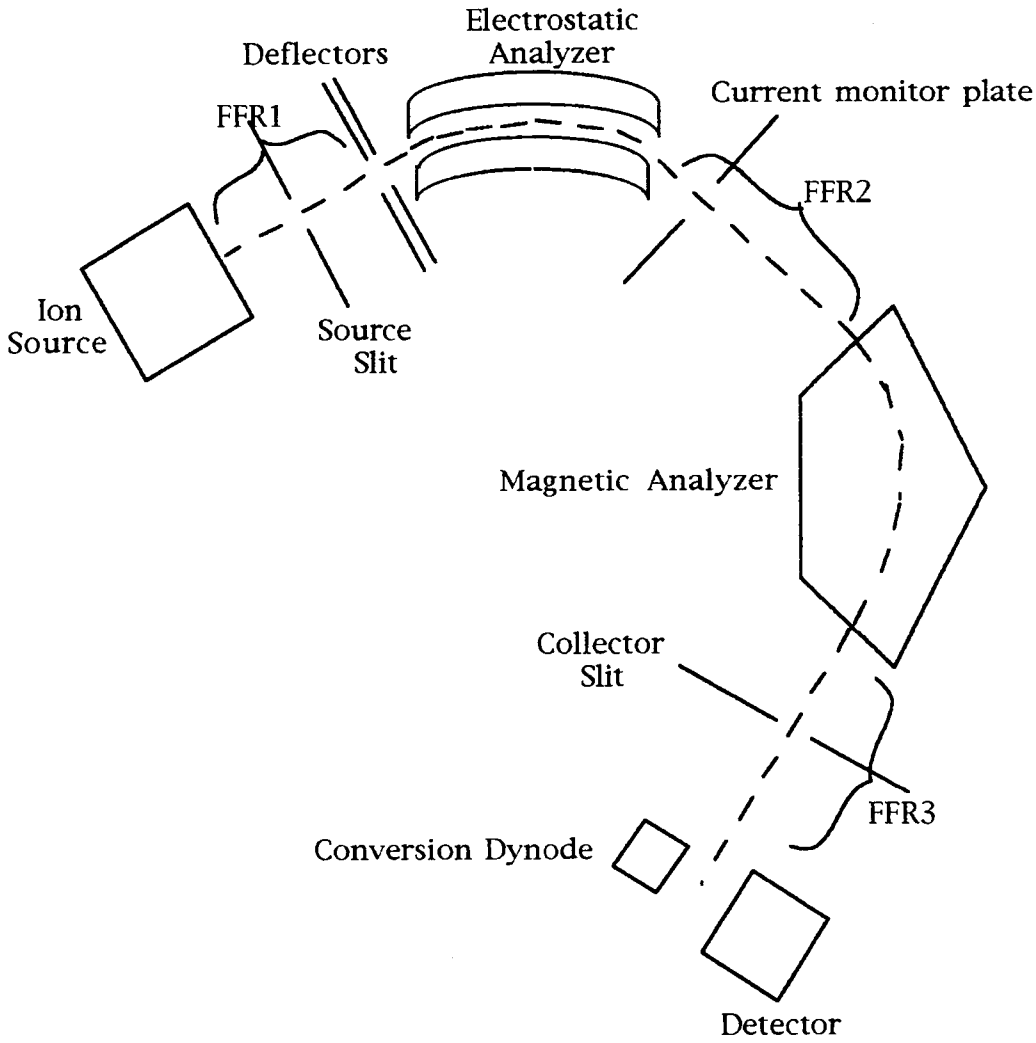



**Figure 2.9.** Schematic diagram of the AEI MS-902 instrument used to acquire the EH data. FFR = field free region.

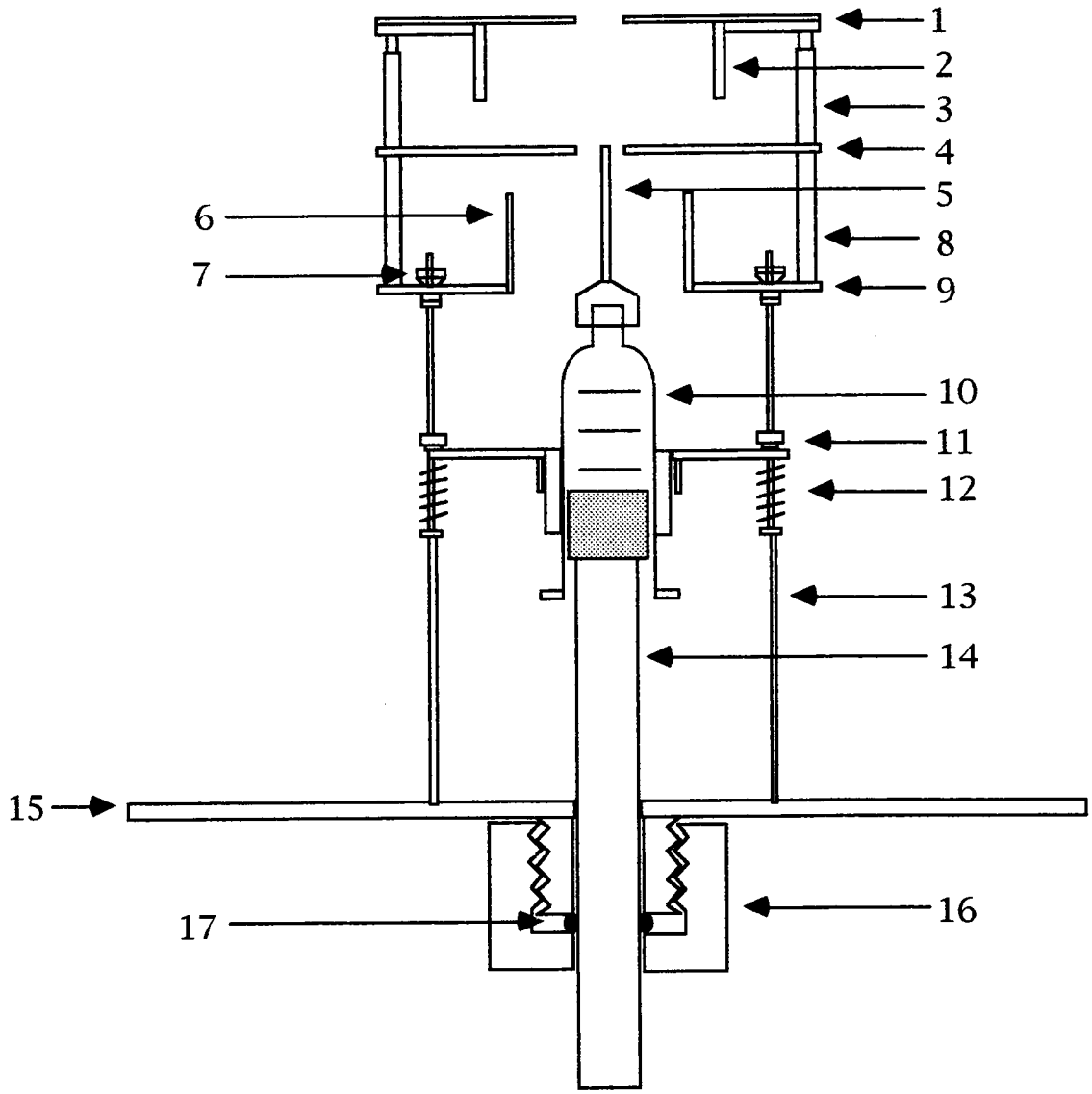



**Figure 2.10.** Cross-sectional view of the unmodified EH source used with glycerol samples. Numbers refer to parts listed in Table 2.2

Table 2.2. Parts list for the unmodified EH source shown in Figure 2.10. Materials are SS except as noted.

| Number | Description |
|---|---|
| 1 | collector plate (ground potential) |
| 2 | sputter shield |
| 3 | Delrin insulator |
| 4 | extractor (5 mm orifice; -2.5 kV potential) |
| 5 | platinum emitter (0.2 mm i.d.; + 8 kV potential) |
| 6 | sputter shield |
| 7 | nut used to affix extractor assembly to post |
| 8 | Delrin insulator |
| 9 | stainless steel base plate |
| 10 | 0.5 mL glass syringe |
| 11 | nut used to position Pt tube within extractor |
| 12 | spring |
| 13 | source mounting posts |
| 14 | syringe plunger |
| 15 | stainless steel vacuum flange |
| 16 | nut used to establish vacuum seal of o-ring with plunger |
| 17 | rubber O-ring to ensure vacuum seal |

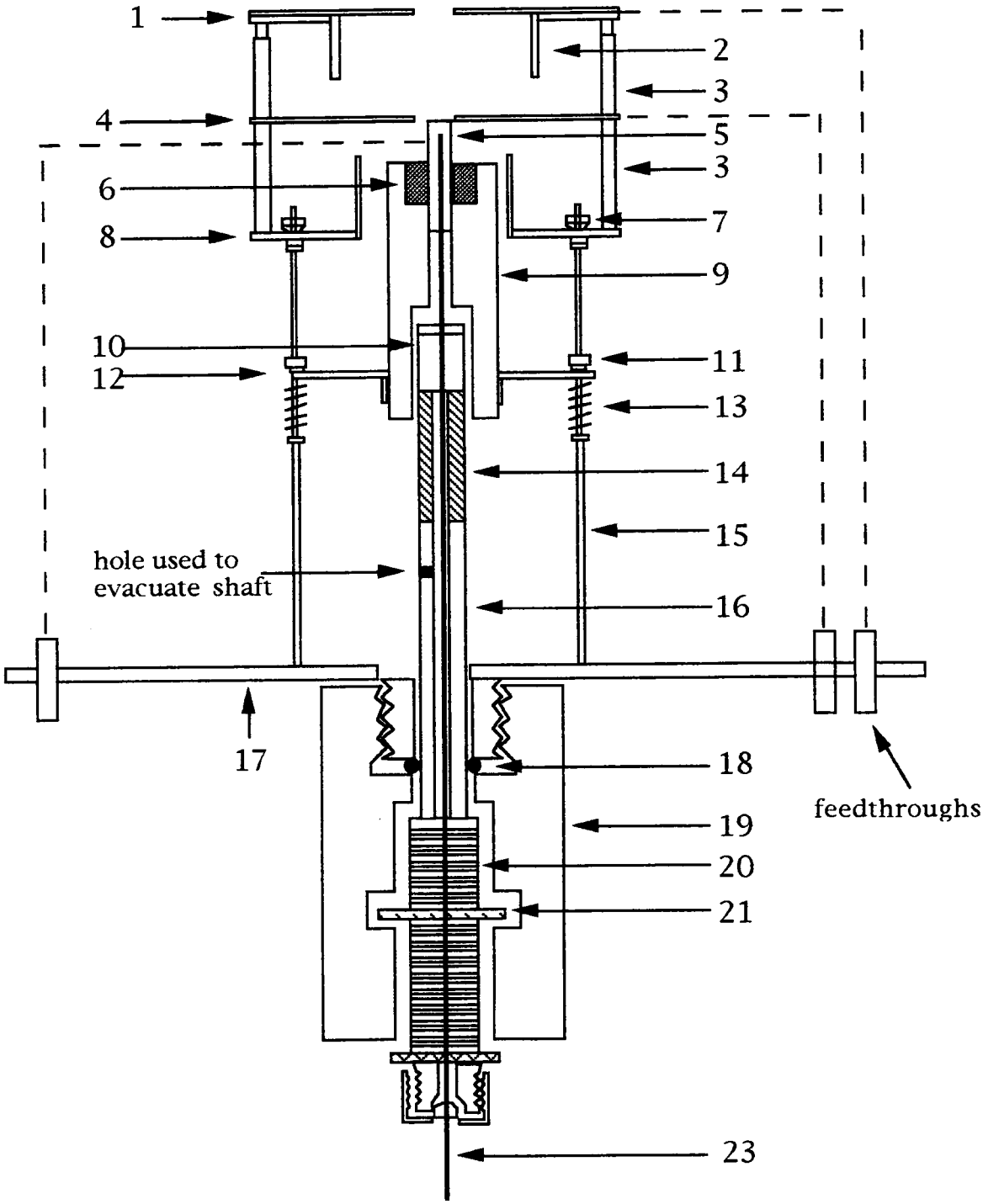



Figure 2.11. Cross-sectional view of the modified EH source used with aqueous solutions. Dotted lines indicate wire connections. Numbers refer to parts listed in Table 2.3.

Table 2.3. Parts list for the modified EH source shown in Figure 2.11. Materials are SS except as noted.

| Number | Description |
|---|---|
| 1 | collector plate (ground potential) |
| 2 | sputter shield |
| 3 | Delrin insulator |
| 4 | extractor (5 mm; -2.5 kV potential) |
| 5 | platinum emitter (0.2 mm i.d.; + 8 kV) |
| 6 | brass cylinder (+ 8 kV; used to establish electrical connection with Pt emitter) |
| 7 | nut used to affix extractor assembly to post |
| 8 | stainless steel base plate |
| 9 | Teflon support sleeve |
| 10 | stainless steel Swagelock (1/16") union (used to hold fused silica securely in capillary positioner) |
| 11 | nut used to position Pt tube within extractor |
| 12 | stainless steel support for Teflon sleeve |
| 13 | spring |
| 14 | Delrin insulator |
| 15 | source mounting posts |
| 16 | positioner shaft (portion of capillary positioner assembly) |
| 17 | stainless steel vacuum flange |
| 18 | rubber O-ring to ensure vacuum seal to positioner shaft |
| 19 | capillary positioner base (aluminum) |
| 20 | threaded portion of capillary positioner shaft (brass; 40 threads per inch) |
| 21 | knurled nut used to move positioner shaft in/out |
| 22 | brass union (shown with Teflon ferrule) |
| 23 | 25 μm i.d. X 150 μm o.d. fused silica capillary (polyimide coated; 50 cm long) |

linked scan control is set to Daughter (B/E), indicating that fragments from the precursor ion in FFR1 will be detected. Using the ESA coarse and fine helipots located on the linked scan control unit of the console, the ion energy is returned to the original value so that the precursor ion is again transmitted through the instrument. The panel meter on the control console is then set to "mass", and the mass is adjusted (using the mass helipots on the linked scan control unit of the console) to the precursor ion mass (a single point calibration). The scan control box of the console is set to scan linearly from low mass to high mass. The low mass can start at any point below the mass of the precursor ion and the high mass must end several mass units above the precursor ion mass so that the precursor ion is certain to be detected. Linked scan spectra were acquired using a Gould model ES1000 electrostatic recorder (Valleyview, OH). A minimum of 5 scans were recorded for each precursor ion and the relative intensities reported represent an average peak height from at least 5 scans.

### 2.3.2 EH Source Modification

The electrohydrodynamic (EH) ionization source previously described was modified (Figure 2.11) to facilitate direct introduction of largely aqueous samples. Sample from a reservoir outside of the evacuated source reaches the Pt emitter (200 μm i.d. x 365 μm o.d.; Hamilton, Reno, Nevada) by vacuum-induced flow through a polyimide-coated fused silica capillary (25 μm i.d. X 150 μm o.d. X 50 cm; Polymicro Technology Inc., Phoenix, Arizona) which passes through the vacuum flange and terminates inside the platinum capillary (anode). When fused silica capillaries were treated as described above for ES

and then used for EH, the gold was removed, possibly by field desorption at the higher EH potentials (compared with ES). Thus uncoated capillaries were used.

The sample reservoir was a disposable glass vial inserted into a Teflon holder sitting on top of a Plexiglas shelf connected to the mass spectrometer. This configuration ensured electrical insulation. Flow rates (except where noted) were maintained by the pressure differential between the outlet and inlet of the capillary. Flow rates were estimated based on the time it took for solution to travel the length of a 50 cm column. The time was established by immersing the end of the capillary outside vacuum in a solution and timing how long it took for the onset of emission (monitored mass spectrometrically). In this configuration, the flow rate was determined to be approximately 5 μL/hour for solutions containing 5% (v/v) glycerol in water. Compared with earlier versions of the source, the silica capillary allows for quicker and easier changing of samples without breaking vacuum and more stable operation with volatile solutions.

The positioning of the fused silica capillary within the Pt emitter is crucial for stable emission and is accomplished using the capillary positioner shown at the bottom of Figure 2.11. The capillary positioner moves the shaft and capillary tip relative to the stationary Pt tube. In operation, this was optimized as described below.

A small amount of low-volatility co-solvent such as glycerol is essential for successful operation of the modified source, presumably in order to maintain electrical contact to the solution through retention of a small reservoir (a few nL) of liquid at the emitter tip (Figure 2.12). The shape of the Pt emitter, which has been described previously, [226] is also important in establishing ion emission. Configured as shown, the source pressure using an

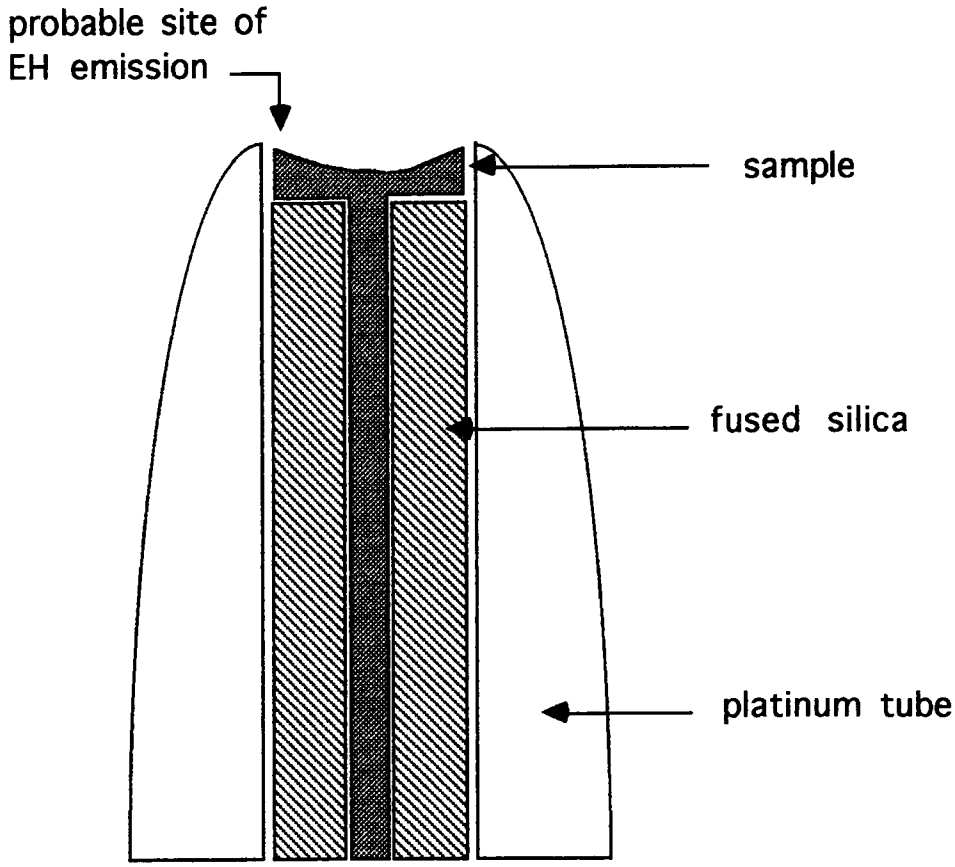



Figure 2.12. Cross sectional view of the positioning of the fused silica capillary within the Pt emitter.

Edwards 6 inch Diffstak diffusion pump with a liquid nitrogen cold trap was $2 \times 10^{-5}$ Torr and the analyzer pressure using a turbomolecular pump (Balzers model 360 TCP) was $8 \times 10^{-7}$ Torr for 5% glycerol solutions.

To operate the modified source, the platinum emitter was first positioned within the brass cylinder used to establish the electrical connection. One end of the fused silica was then square cut using an etching tool manufactured by Alltech Chromatography. The opposite end of the 50 cm capillary was inserted through the platinum emitter and fed through the remainder of the capillary positioner until it passed beyond the positioner base. The fused silica capillary was allowed to extend beyond the tip of the platinum emitter several centimeters while attaching the lens assembly to the mounting posts. The fused silica capillary was then pulled from the end outside of the vacuum flange so that only a few mm of capillary extended beyond the Pt emitter. The fused silica capillary was then secured in place using Teflon ferrules and the stainless steel Swagelock union attached to the positioner shaft (#10 in Figure 2.11) and the brass Swagelock union attached to the positioner base (the Swagelock union attached to the positioner base was used to maintain vacuum within the source, while that on the shaft assured positioning). Using a 3X magnifying glass and the positioning nuts (#11) shown in Figure 2.11, the platinum emitter was aligned in the center and in the plane of the extractor electrode. Using the capillary positioner nut (#21), the fused silica capillary was then lowered until the end just disappeared into the Pt emitter. The source assembly was then mounted in the source housing and secured using two screws. The two high voltage leads (emitter and extractor) were connected to the appropriate high voltage feedthroughs and the coaxial collector cable was connected to the collector plate via a low voltage feedthrough. The fused silica

capillary end protruding beyond the positioner base was placed into the analyte solution located in the Teflon holder described above. While adding liquid nitrogen to the trap for improved pumping speed, the source was evacuated to a pressure of 1 mTorr using an Edwards (model 550) belt driven mechanical pump. After reaching a pressure of 1 mTorr, the mechanical pump was valved off and the isolation valve between the source and the diffusion pump was opened.

Once the source pressure reached 5 x $10^{-5}$ Torr, the ion emission could be started in the following manner. With the isolation valve between the source and analyzer closed, the platinum capillary potential was adjusted to +8 kV and the extractor to -2.0 kV. The collector plate and emitter currents were monitored to ensure that ions were being emitted from the Pt emitter. Typical needle currents ranged from 2 - 5 μA and collector currents ranged from 0.1 - 1 μA. Then the isolation "ball" valve was opened so that ions could enter the analyzer region. The magnet was set (not scanning) to pass the base peak in the mass spectrum (typically the proton bound dimer of glycerol at m/z 185). The emitter and extractor potentials were then adjusted to provide a maximum in ion intensity prior to adjusting the position of the fused silica capillary within the Pt emitter. Once the maximum ion intensity was obtained, the fused silica capillary position within the Pt emitter was adjusted using the capillary positioner to obtain an even larger ion intensity. The ion deflector plates were then adjusted to ensure maximum transmission. Finally, the emitter and extractor potentials were further adjusted to ensure the maximum in ion intensity was being observed. As a bench-mark, the signal from the proton bound glycerol dimer from a 40 mM solution of HCl in 95% water and 5% glycerol (v/v; see sample preparation below) should be approximately 5 volts

(50% of full scale) when using the following conditions: +8 kV needle potential, -2.5 kV extractor potential, +2.6 kV electron multiplier potential, -5 kV conversion dynode potential, 2 x $10^{-7}$ amps-full-scale FA-3 setting, and 10 millisecond filtering.

The experiments described above are for normal operating conditions of the source and analyzer. In some cases it was necessary to deviate from the normal operating conditions. For example, in some of the results discussed in Chapter 5, the needle potential was changed from 8 kV to 6 kV and the ESA was set to pass ions with 6 keV kinetic energy. In some experiments (noted in Chapter 5) it was necessary to increase the flow rate above that obtained with vacuum induced flow. This was accomplished using the Harvard syringe pump described above. In this case, the fused silica capillary protruding from the positioner base was connected to the stainless steel needle of a 25 μL gas tight SGE syringe using a low dead volume Swagelock union, stainless steel ferrules, and PEEK ("PEEK" = polyetheretherketone; Alltech Chromatography, Deerfield, Illinois) tubing. The flow rate was adjusted to 7.5 or 10 μL/hour for comparison with the vacuum-induced flow rate of approximately 5 μL/hour.

## 2.4 Sample Preparation and Reagents

A list of reagents used in these studies is provided in Table 2.4 below. Reagents listed in Table 2.4 were used as received from the indicated manufacturer except where noted.

Table 2.4. List of reagents used in these studies.

| Reagent | Supplier | Purity |
|---|---|---|
| acetic acid | Mallinckrodt | Analytical Reagent |
| acetone | Mallinckrodt | Analytical Reagent |
| acetonitrile | Mallinckrodt | Analytical Reagent |
| 3-aminopropyltriethoxy silane | Pierce | > 96% |
| ammonium acetate | Mallinckrodt | Analytical Reagent |
| argon | National Welders | |
| boric acid | Mallinckrodt | Analytical Reagent |
| cytochrome C (type V, bovine heart) | Sigma | > 95% |
| dibasic sodium phosphate | Fisher | Reagent Grade |
| Bradykinin | Sigma | > 98% |
| ethanol | Midwestern Grain | 95 % |
| glycerol | Mallinckrodt | Analytical Reagent |
| hydrochloric acid | Mallinckrodt | Analytical Reagent |
| hydrogen peroxide (30%) | Mallinckrodt | Analytical Reagent |
| HPLC water | Baker | HPLC Grade |
| isopropyl alcohol | Mallinckrodt | Analytical Reagent |
| leucine enkephalin | Sigma | |
| methanol | Mallinckrodt | Analytical Reagent |
| (3-mercaptopropyl) trimethoxysilane | Aldrich | 95 % |

| Reagent | Supplier | Purity |
|---|---|---|
| monobasic sodium phosphate | Sigma | Reagent Grade |
| 3-methylthiophene[a] | Aldrich | 99% |
| 3-nitrobenzyl alcohol | Aldrich | 98% |
| nitrogen | Liquid Air, National Welders | |
| Neurotensin | Sigma | > 95% |
| potassium hydroxide | Mallinckrodt | Analytical Reagent |
| sodium dihydrogen phosphate | Mallinckrodt | Analytical Reagent |
| sodium iodide | Aldrich | Reagent Grade |
| sulfuric acid | Mallinckrodt | Analytical Reagent |
| tetrabutylammonium perchlorate | Fluka | > 98% |
| tetradecyltrimethyl-ammonium bromide | Sigma | Reagent Grade |
| tetraethylammonium bromide | Eastman | Reagent Grade |
| tetraethylammonium iodide | Eastman | Reagent Grade |
| thioglycerol | Sigma | 98% |
| p-toluenesulfonic acid | Aldrich | 99% |
| Xenopsin | Sigma | > 97% |

[a] 3-methylthiophene was vacuum distilled to improve purity as indicated in section 2.1.3.

### 2.4.1 Sample Preparation for FAB/LSIMS

All samples were prepared to yield analyte concentrations of 1 mM. All glycerol samples were vacuum degassed (pressure about 1 x $10^{-3}$ Torr) for a minimum of 8 hours under low heat and constant stirring.

### 2.4.2 Sample Preparation for ESI

Protein and peptide solutions were prepared using HPLC grade solvents (J.T. Baker, Phillipsburg, NJ) and were filtered through 0.22 μm polyvinylidene fluoride filters (Alltech Associates, Inc., Deerfield, IL) prior to use. Analyte concentrations are given within the ESI chapter.

### 2.4.3 Sample Preparation for EH

Distilled water was passed through a Milli-Q water purification system (Millipore Corporation, Bedford, MA) to obtain a minimum resistance of 15 MΩ $cm^{-1}$, and was used to prepare all aqueous solutions used in the EH studies. A mixed solvent solution roughly 40 mM in HCl was prepared by adding 0.33 mL of concentrated HCl (12.1 M) to a 100 mL volumetric flask containing approximately 50 mL of distilled deionized water, adding 5 mL of glycerol and then diluting to 100 mL using distilled deionized water. Mixed solvent solutions roughly 40 mM in tetramethylammonium or tetraethylammonium bromide were prepared by adding the appropriate amount of salt to a 100 mL volumetric flask, adding approximately 50 mL of distilled deionized water, then adding 5 mL of glycerol, and finally diluting to 100 mL with distilled deionized water. A

5 mol % (0.65 M) solution of NaI in glycerol was prepared by dissolving 0.81 grams of NaI in 10 grams of glycerol. This solution was vacuum degassed (pressure about 1 x $10^{-3}$ Torr) for a minimum of 8 hours under low heat and constant stirring to remove dissolved gases. A mixed solvent solution roughly 40 mM in NaI was prepared by adding 0.6 grams of NaI to a 100 mL volumetric flask, adding approximately 50 mL of distilled deionized water, then adding 5 mL of glycerol, and finally diluting to 100 mL with distilled deionized water. A mixed solvent solution containing 40 mM HCl in a 95% water and 5% thioglycerol was prepared as described above for the 40 mM HCl solution in 95% water and 5% glycerol, substituting thioglycerol for glycerol. Solutions containing various amounts of NaI and HCl within the same solution were prepared from 40 mM stock solutions of each containing 95% water and 5% glycerol. The total concentration of HCl and NaI was always maintained at 40 mM. For example, a solution containing 20 mM HCl and 20 mM NaI could be prepared by mixing equal volumes of the individual 40 mM stock solutions. The aqueous solutions were not degassed prior to use.

# Chapter 3

## Secondary Ion Emission From Solutions: Time Dependence and Surface Phenomena

FAB is considered to be one of the most important ionization techniques (among several other ionization techniques such as ES and thermospray) wherein solution chemistry plays an important role in the ionization mechanism and the appearance of the mass spectrum. [30,39,227] Solution-phase chemistry, such as ion-pairing, [111] condensation reactions, [41,228] and the formation of cations stabilized by the matrix have been studied using FAB. [110,229,230]

Solute-characteristic secondary ions in FAB and SIMS arise either from ionic species in solution or from addition of a cation or anion to a neutral species to form an ionic species. The addition of an ion, most commonly a proton, to the neutral species can occur either in solution [231] or in the dense gas phase region [179] directly above the solution, known as the selvedge.

Other solute-characteristic secondary ions produced during the FAB or LSIMS desorption process include solvated ions. Solvent-characteristic secondary ions usually result from the protonation or attachment of other cations or anions to the solvent molecules. For example, when glycerol is used as the solvent, protonated solvent clusters (e.g., dimer and trimer) are evident in the mass spectrum. Glycerol is one of the solvents commonly used in FAB and LSIMS.

LSIMS and FAB mass spectra of solutions are time-dependent, i.e., the relative intensities of various secondary ions change during the course of an

experiment. Generally, the time dependence of any particular solution is difficult to reproduce from instrument-to-instrument and even from analysis-to-analysis on a given instrument.

The time dependence has been studied by a number of workers, and appears to be a result of many factors, including primary particle induced damage, [37,38,39,40,41] evaporation, [36] sample size, [232] surface phenomena, [44,45,46] etc. In pioneering work on FAB MS of liquid samples, Ligon and Dorn found that the relative intensity of solute-characteristic secondary ions from glycerol solution correlates with relative surface activity. [45] Lacey and Keough later showed that the role of surface activity appeared to vary with time; [46] over the course of sample life, the intensity of secondary ions characteristic of compounds that are less surface active increases to a maximum and may dominate the SIMS spectrum toward the end of the experiment.

From these studies an active role of mass transport in FAB has been assigned to surface phenomena. [44,45] The effect was best demonstrated by Ligon and Dorn. [45] When the projection of the primary SIMS particle beam on the sample is smaller than the droplet of sample solution, surface tension drives surface active solutes toward the spot where the primary beam strikes the droplet. Ligon referred to this phenomenon as "side filling." In the parlance of colloid chemistry, mass transport driven by surface forces is known as a Marangoni effect. [233,234]

To understand the role of surface effects on sensitivity, it is important to recognize that the forces involved in surface phenomena extend only about 0.5-1 nm below the surface, so surfactants are not "pulled" to the surface; [233,234,235] rather, they must arrive at the surface by some mechanism (e.g.,

diffusion), after which surface phenomena may dominate. The net force, i.e. surface tension, is always directed *in the plane of the surface.* That is, surface effects cannot be used to explain the mass transport of solute from the bulk to the surface. An alternative mechanism, diffusion, is a slow process in the time domain of the FAB experiment; in a classic test of Gibb's theory of enhanced surface concentration, McBain found that surfactants required hours to reach equilibrium surface concentration in quiescent water. [235] Diffusion coefficients in glycerol are about $10^4$ times smaller than in water, so the time frame for diffusion should be even longer. [236] Furthermore, in FAB and SIMS the surface is continually sputtered away, unlike the case in McBain's experiments. Practically speaking, there is simply insufficient time during the course of a FAB experiment for the surface to be replenished by diffusion of the solute to the surface. [40] Ligon [45,237] recognized this fact and further concluded that the mechanism of mass transport within the bulk of the droplet could not be clearly discerned from his experiments; he hypothesized that mechanical mixing and convection were necessary to replenish the surface supply of solute.

In contrast to results obtained from solutions containing involatile solutes, when volatile amines are introduced onto the surface of glycerol via the gas phase, the effects of surface phenomena are not apparent. [180] Under such circumstances, amine-characteristic secondary ion intensity is found to correlate with the Henry's law concentration of free base and is independent of the relative surface activity of the respective amine. This conclusion is consistent with observations that FAB and SIMS sampling depths ordinarily encompass more than the surface monolayers. [237,238] In this context, the persistent and prominent role of surface phenomena and mass transport in

FAB spectra of involatile compounds dissolved in glycerol may appear anomalous.

This collection of disparate observations may be summarized simply. First, FAB and SIMS spectra of glycerol solutions are time-dependent, but the time dependence is difficult to reproduce and is by no means well understood or defined. Second, apparently definitive experiments have supported opposite conclusions concerning the role of surface activity in secondary ion emission. The most readily identifiable mechanisms for mass transport of solute from the sample bulk to the surface, mixing and convection, are by nature non-selective, yet apparently lead (in combination with Marangoni effects) to highly selective emission of nonvolatile surface analytes.

In this chapter, the time dependence of FAB spectra is compared with image data from a wide-angle secondary ion microprobe. [217] This instrument has made it possible to determine the spatial distribution of secondary ion emission from sample droplets. Secondary ion image data will used to gain insight into the time dependence of FAB data. Work in this chapter involved collaboration with Dr. Peter J. Todd at Oak Ridge National Laboratory, and has recently appeared in the literature. [239]

## 3.1 Temporal Behavior of FAB Spectra

In addition to other obvious differences, the two mass spectrometers used in these experiments differ in sample orientation and exposure. Samples in the imaging SIMS source are oriented horizontally (Figure 3.1a), which

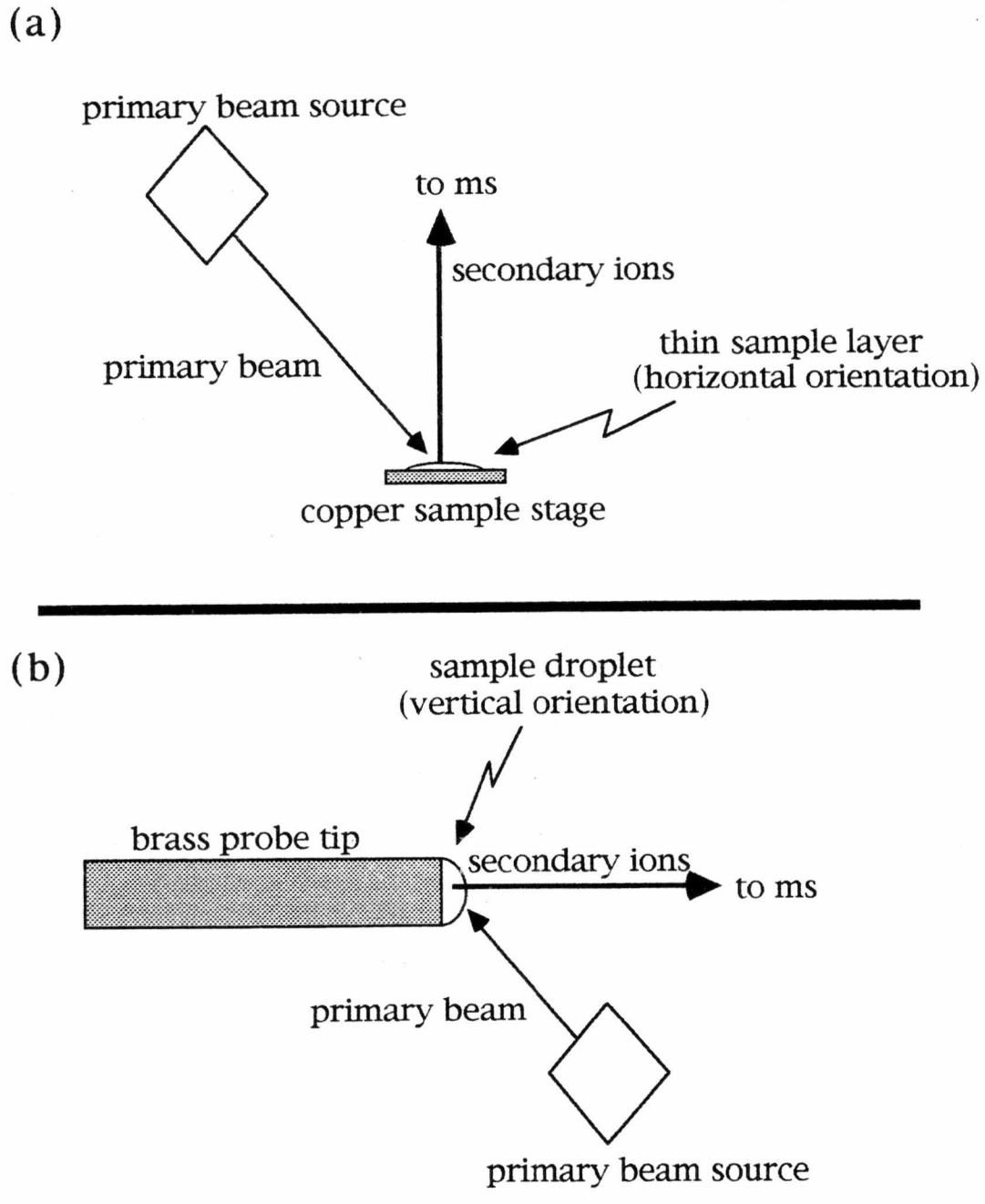



Figure 3.1. Schematic diagram illustrating the sample orientation during the (a) LSIMS and (b) FAB experiments.

prevents "sagging" or "drooping" of the sample droplet under the influence of gravity. [44] The primary ion currents are low, and exposure is intermittent. Thus, the dose experienced by the sample during the 2 minutes necessary to acquire data for an image is well below the "static SIMS" limit ($<10^{14}$ ions/cm$^2$) [9,44] ("static SIMS" implies that surface analysis is done along the x-y direction (within the plane of the sample) and not along the z direction or the depth axis of the sample [6]). Furthermore, exposure to the 100-$\mu$m-diameter primary beam at any point on the sample is intermittent because the beam is rastered across the sample. In contrast, the ZAB employs a vertical sample orientation for FAB (Figure 3.1b) and heavy continuous primary particle flux ($\approx 10^{12}$ to $10^{14}$ particles/second•cm$^2$) [44,240] over the entire sample. Gravity-induced flow and the high FAB sputtering rate account for the shorter persistence of FAB spectra ($\approx$ 1 hour) compared to the LSIMS spectra (> 1 hour). The acceptance aperture [38] of double-focusing instruments like the ZAB is similar to that of the quadrupole SIMS instrument; i.e., detected ions are limited to those originating from a rather narrow zone (probably $\leq$ 1 mm$^2$) of indeterminate position on the sample.

Despite these differences, FAB and LSIMS spectra obtained using the respective instruments are qualitatively similar; that is, the same ions are evident in spectra from both instruments (see below). However, as will be seen below, the quality of the match in relative intensities depends on the time of comparison.

Figure 3.2 shows the temporal behavior of the intensity of ions at m/z 256 (tetradecyltrimethylammonium cation ($C_{14}H_{29}N^+(CH_3)_3$, $TTA^+$) and m/z 93 (protonated glycerol, $[G+H]^+$) in FAB spectra of a 1 mM solution of tetradecyltrimethylammonium bromide (TTAB) in glycerol. The $TTA^+$ intensity

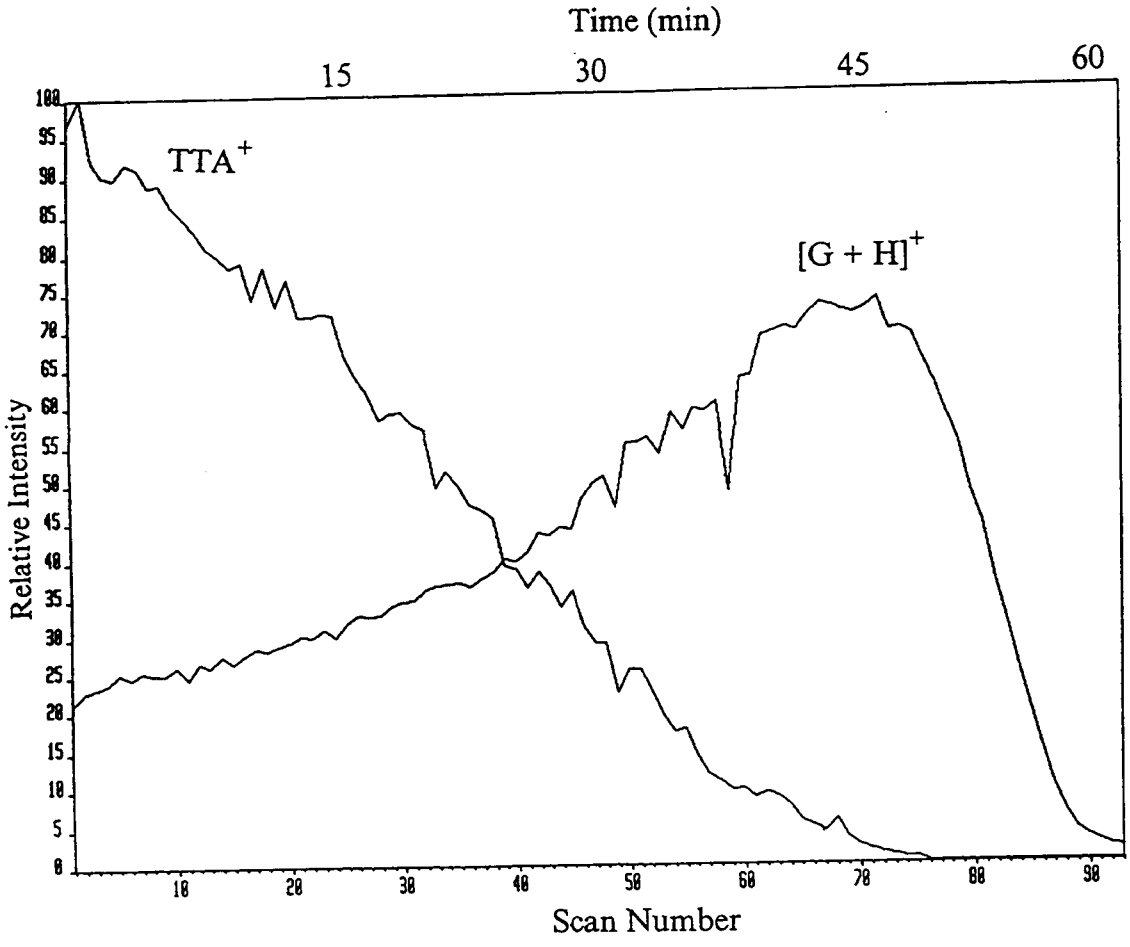



Figure 3.2. Normalized (to the most intense signal from $TTA^+$) intensities of m/z 256 ($TTA^+$) and m/z 93 ($[G + H]^+$) versus time from a 1 mM solution of TTAB in glycerol. Data from a FAB experiment using the VG ZAB-EQ.

initially dominates the spectrum, as shown in Figure 3.3; ions characteristic of glycerol (e.g. m/z 93, 185,...) are present, but at low intensity. After approximately 25 minutes of exposure, $TTA^+$ is still prominent, but protonated glycerol becomes the base peak in the spectrum, as shown in Figure 3.4. As bombardment continues beyond 25 minutes, $TTA^+$ disappears from the spectra, and eventually glycerol ion intensities also fall to the level of background. Similar behavior has been reported elsewhere. [40]

Figures 3.5 - 3.7 show data from an analogous experiment using a 1 mM solution of tetraethylammonium iodide (TEAI) in glycerol. Figures 3.5 and 3.6 show that the intensity of $TEA^+$ is at first low and fairly constant. $TEA^+$ intensity gradually rises until the spectrum is characterized by a short-lived burst of high intensity. Even at the peak intensity for $TEA^+$, the spectrum still contains ions derived from glycerol, as shown in Figure 3.7.

Emission of $TEA^+$ from a sample originally 1 mM TEAI in glycerol could be restored after the precipitous decrease demonstrated in Figure 3.5 by the simple application of pure glycerol to the probe tip and re-exposure to the primary atom beam (Figure 3.8a). Furthermore, the temporal behavior (including persistence) of the rejuvenated sample was similar to that shown in Figure 3.5, although the intensity of $TEA^+$ ions (relative to solvent ions) was typically half that for the original sample. For TTAB samples, no such rejuvenation was observed; FAB of a "rewetted" sample provided at best a weak, short lived, TTAB spectrum (Figure 3.8b). For both solutions, if a sample was allowed to dry in vacuum without primary particle bombardment, the temporal behavior following rewetting was observed to be similar to that shown in Figures 3.2 and 3.5.

The fact that $TEA^+$ intensity can be rejuvenated indicates that TEAI is

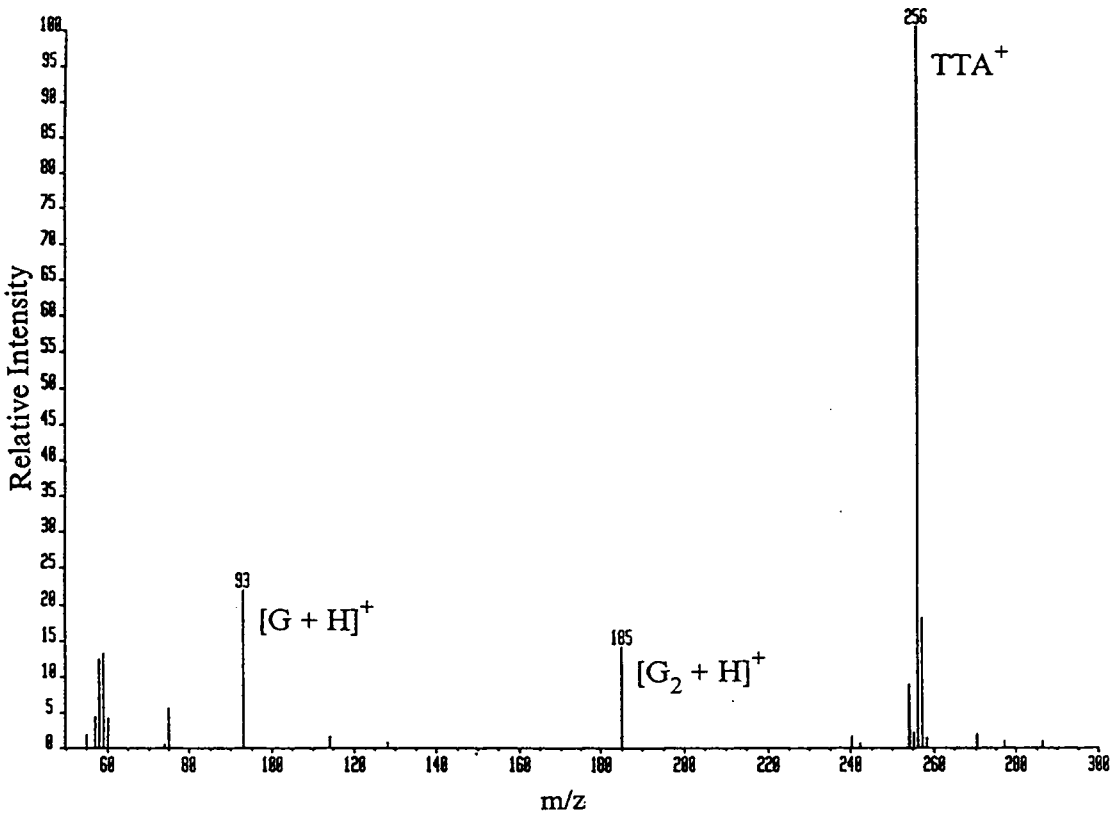



Figure 3.3. FAB mass spectrum recorded from scan 1 of Figure 3.2.

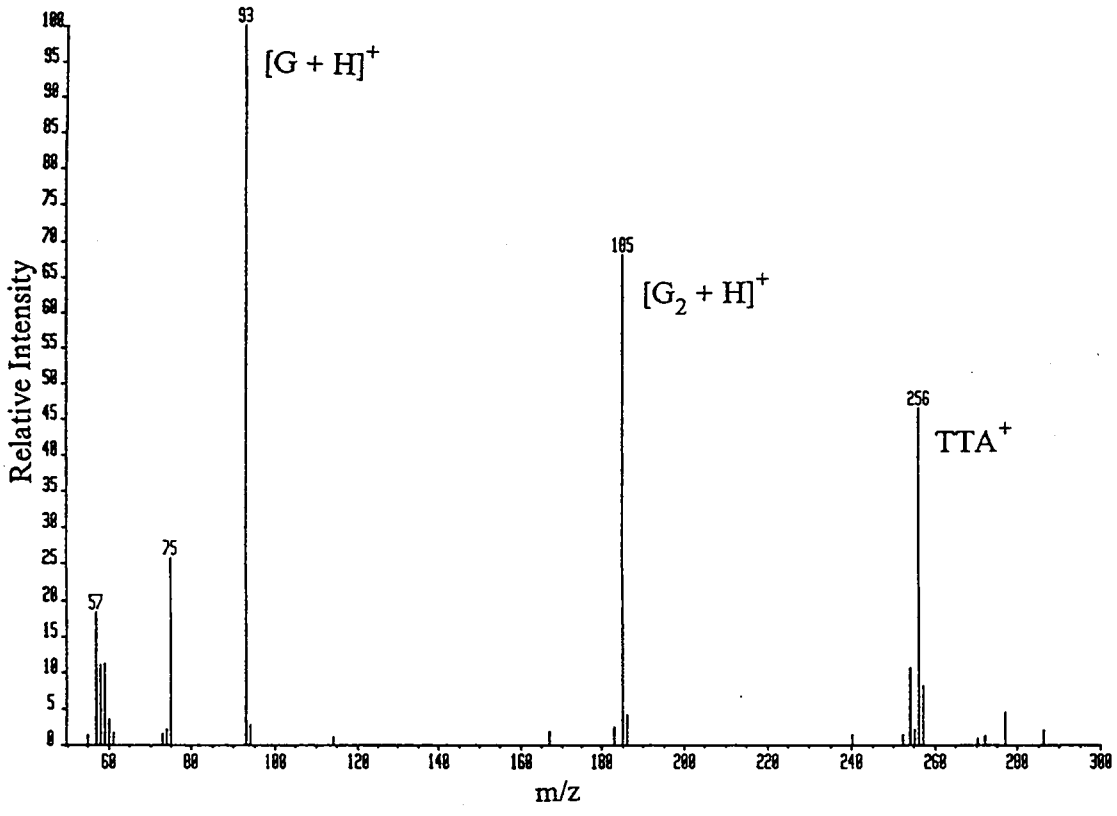



Figure 3.4. FAB mass spectrum recorded from scan 50 of Figure 3.2.

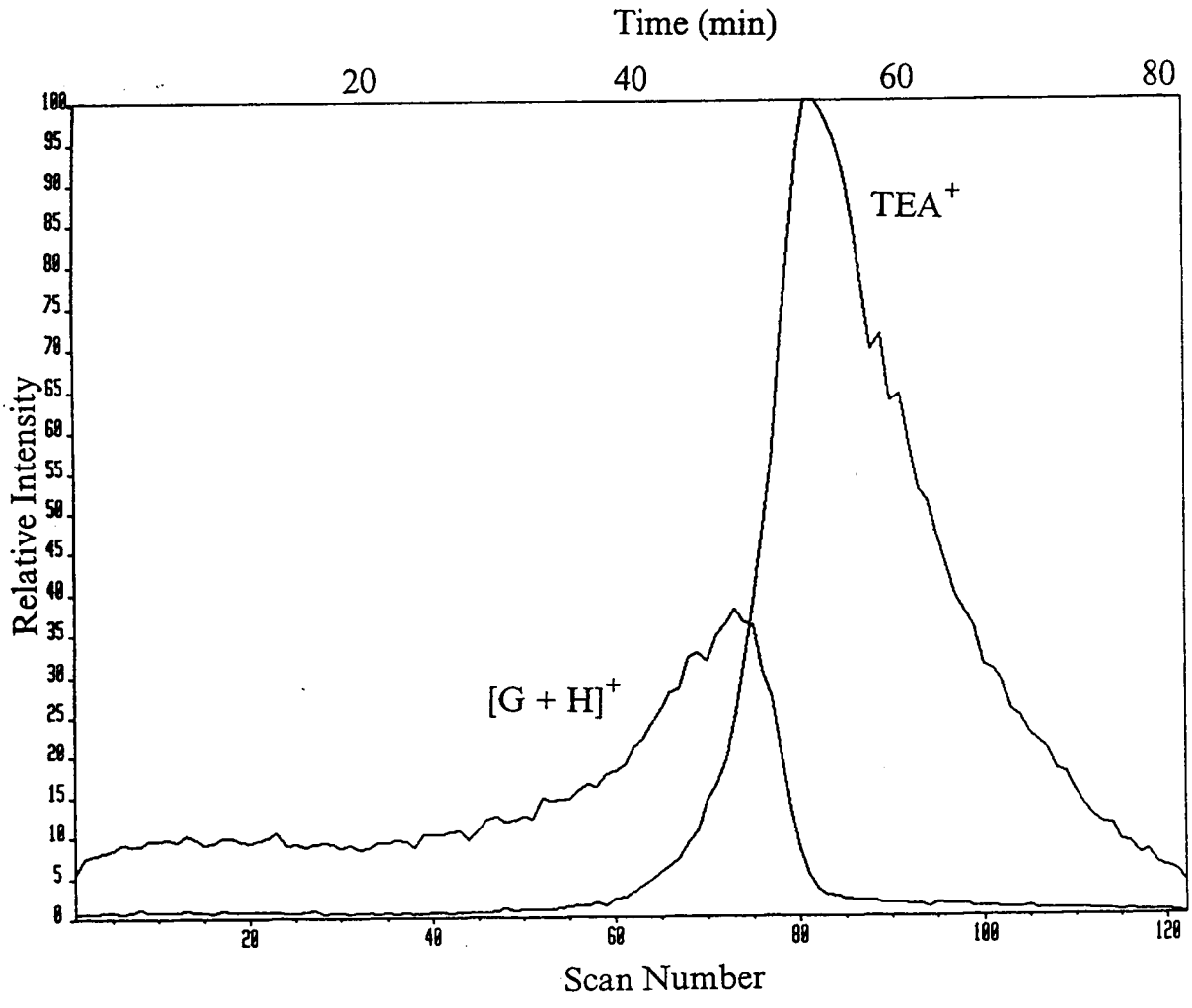



Figure 3.5. Normalized (to the most intense signal from $TEA^+$) intensities of m/z 130 ($TEA^+$) and m/z 93 ($[G + H]^+$) versus time from a 1 mM solution of TEAI in glycerol. Data from a FAB experiment using the VG ZAB-EQ.

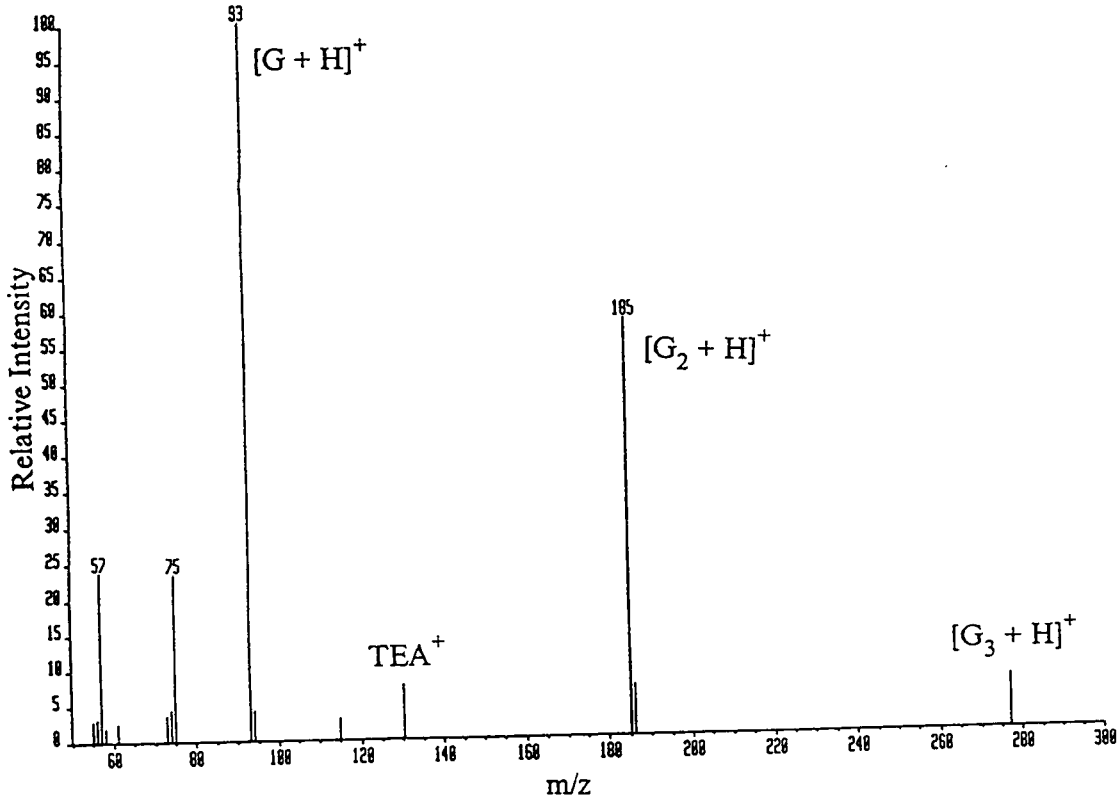



Figure 3.6. FAB mass spectrum recorded from scan 20 of Figure 3.5.

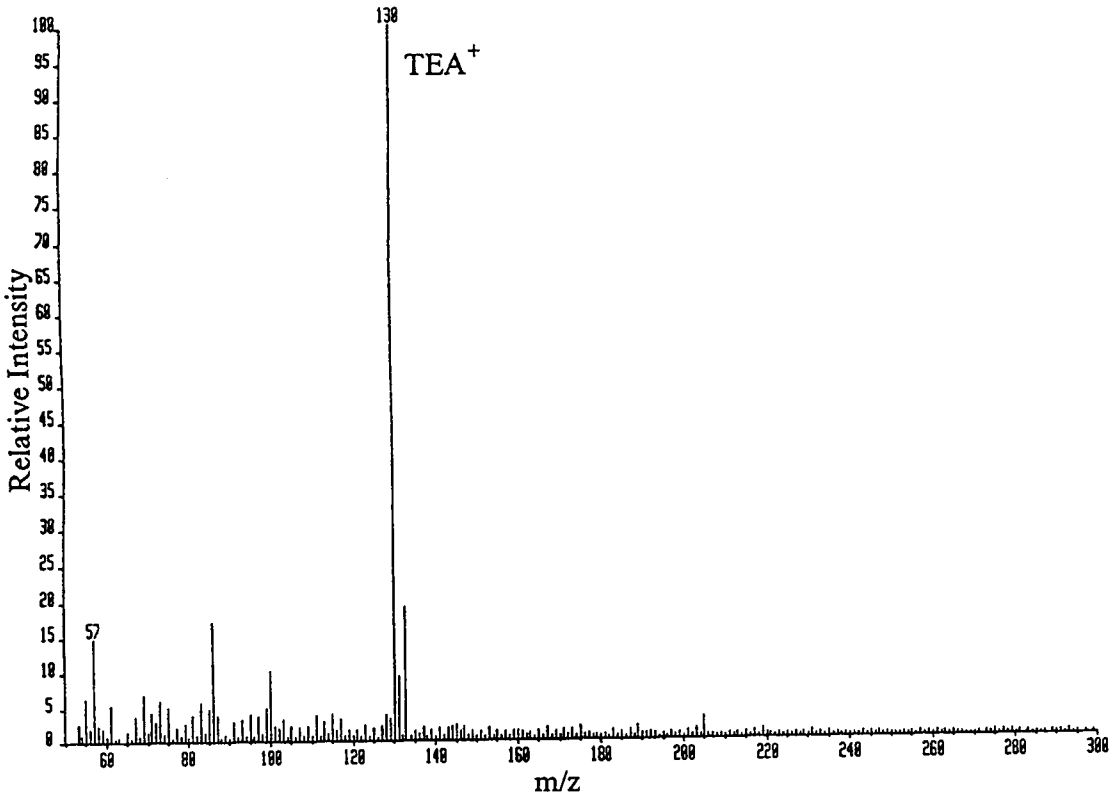



Figure 3.7. FAB mass spectrum recorded from scan 82 of Figure 3.5.

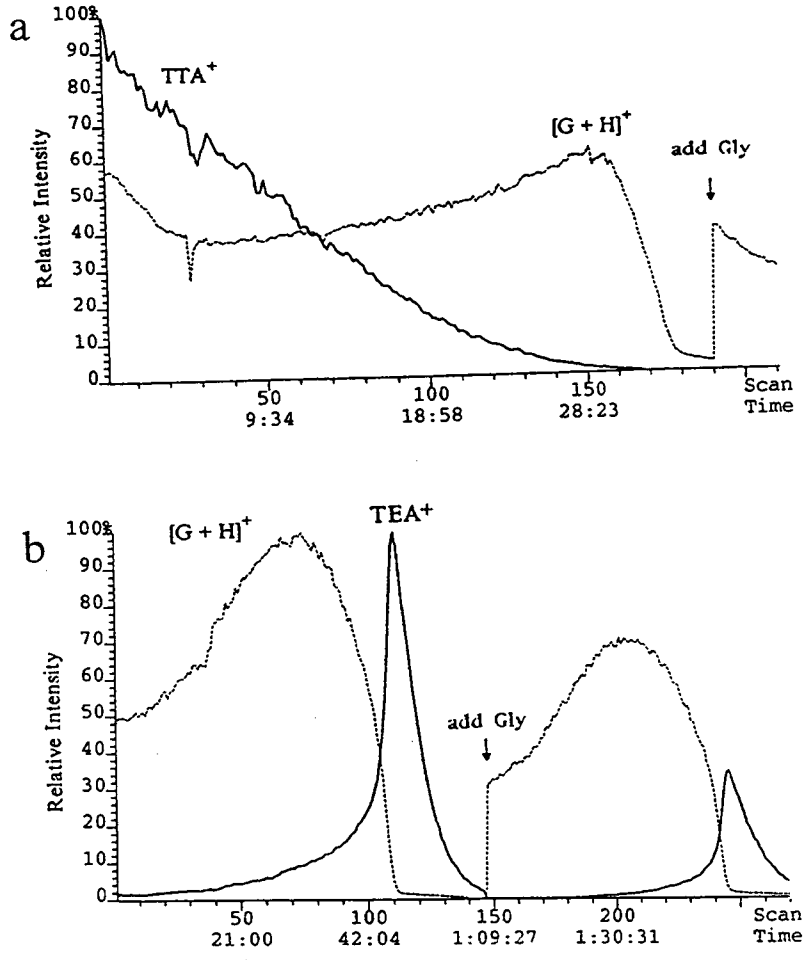



Figure 3.8. Intensity versus time for the rejuvenation experiment of (a) $TEA^+$ (m/z 130) and (b) $TTA^+$ (m/z 256) from 1 mM glycerol solutions. For comparison, the lighter trace in each figure corresponds to protonated glycerol (m/z 93). Each figure is normalized to the most intense analyte ($TEA^+$ or $TTA^+$) signal. The arrows indicate when the fresh glycerol was added to the probe tip. Data acquisition was interrupted during this time period and re-started after re-inserting the probe tip into the instrument.

removed at a rate less than the combined sputtering and evaporation rate of pure glycerol. Conversely, decay of the $TTA^+$ signal and its failure to be rejuvenated indicates that TTAB is removed at a rate greater than that of glycerol. $TTA^+$ is more hydrophobic than $TEA^+$ because of the longer alkyl chain length (tetradecyl *vs* methyl). Tanford has shown that the heat of solvation (enthalpy of solvation) becomes increasingly more positive for increasing alkyl chain length. [241] While the heat of solvation is not known for $TTA^+$, based on the discussion of Tanford, it is certainly more positive than heat of solvation for $TEA^+$ (Table 3.1). This suggests a weaker interaction of the $TTA^+$ (compared to $TEA^+$) with the solvent and hence, $TTA^+$ should be easier to remove from solution. In contrast, the more negative enthalpy of solvation for $TEA^+$ suggests a stronger interaction between the ion and the solvent and consequently $TEA^+$ should be more difficult to remove from solution. The surface tension values in Table 3.1 for $TTA^+$ and $TEA^+$ reveal that $TTA^+$ is more surface active (in water) and should be more readily sputtered from solution than $TEA^+$. Surface diffusion is far more rapid than bulk diffusion, therefore, the bulk diffusion coefficients (Table 3.1) of the two ions should not contribute very much to the differences observed in sampling behavior. The reason for these differences in sampling rate and their relation to the relative analyte surface activities is not immediately clear, but the dominating mass transport processes which contribute can be identified from imaging data.

## 3.2 Spatial Distributions of Solutes

Using the imaging capabilities of the SIMS microprobe to explain the temporal behavior of FAB spectra is subject to severe restrictions. The

Table 3.1. $TEA^+$ and $TTA^+$ information.

| Species | $\Delta H_s$[a] (kJ $mol^{-1}$) | Surface Tension[b] (dyne $cm^{-1}$) | Diffusion Coefficient (x $10^{-5}$ $cm^2$ $s^{-1}$) |
|---|---|---|---|
| $TEA^+$ | -493.5 (-508.7) | 70.5 | 0.858[c] |
| $TTA^+$ | | 68.6 | 0.094[d] |

[a] enthalpy of solvation in methanol (water). Methanol and water data taken from ref. [242].

[b] data obtained from 50 μM solutions of analyte in water. Taken from ref. [243].

[c] data for aqueous solution. Taken from ref. [244].

[d] data for aqueous solution. Taken from ref. [245]

substantial differences in primary ion flux density between the FAB and SIMS experiments must be considered. This will be discussed in detail below. However, as noted above, differences in the respective spectra caused by these differences between primary particle parameters are minor; that is, the same ions are present in both spectra, even though their relative abundances differ. This appears to be the case for liquids [5] in general. To emphasize this point, secondary ion mass spectra are included with images for comparison with the FAB spectra.

Figure 3.9a shows a map of the intensity at m/z 256 ($TTA^+$) from a 1 mM glycerol solution of TTAB. The intensity of $TTA^+$ is fairly uniformly distributed across the surface of the sample, as can be seen from Figure 3.9b, which is a Cartesian plot of $TTA^+$ intensity along the horizontal line indicated across the center of the image. Individual spectra obtained near the middle and the edge of the sample, as shown in Figure 3.10, are very similar to each other and to

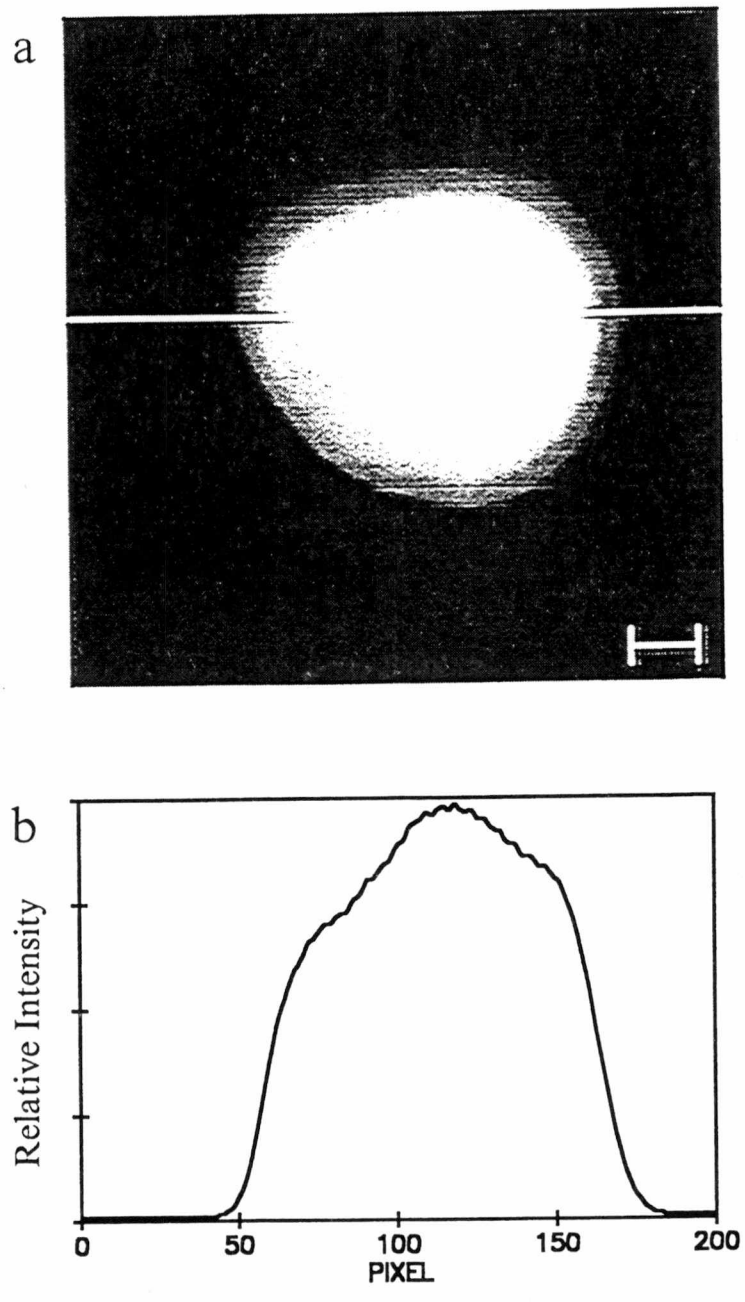



Figure 3.9. (a) Secondary ion image of m/z 256 ($TTA^+$) from 1 mM TTAB in glycerol, using white as the most intense and black as least intense. (b) Relative intensity of m/z 256 along cursor mark in image of part (a).

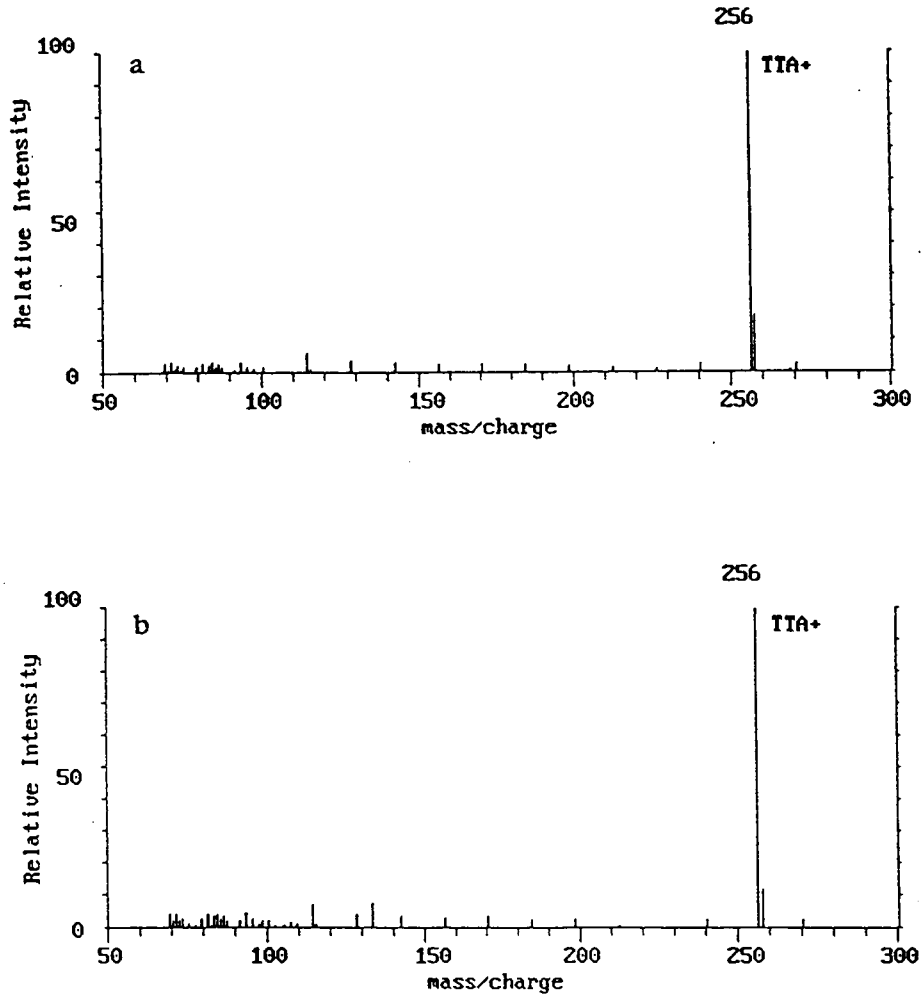



Figure 3.10. LSIMS mass spectra acquired from the (a) center and (b) edge of the sample shown in the image of Figure 3.9.

the FAB spectrum of Figure 3.3. In contrast with the FAB data, the spectra shown in Figure 3.10 persisted for the duration of the experiment (because of low primary ion doses), with no observable change in relative abundances. Figure 3.11 is a mass spectrum acquired late in the imaging experiment revealing the similarity to the spectra of Figure 3.10. At no point in the SIMS experiment was a spectrum similar to that shown in Figure 3.4 obtained, even when the primary beam was "parked" in one position and repetitive spectra scanned. At the low doses employed for this static SIMS experiment, the TTAB could not be appreciably depleted during sputtering (the duration of the experiment was in excess of 1 hour).

The secondary ion image of $TEA^+$ obtained from a glycerol solution of TEAI is shown in Figure 3.12a. The image is dramatically and revealingly different from that shown in Figure 3.9. $TEA^+$ is preferentially emitted from the periphery of the sample droplet. The magnitude of $TEA^+$ intensification near the rim is evident from the intensity profiles of Figure 3.12b. Near the center of the sample, the spectrum roughly parallels the "normal" FAB spectrum; i.e., Figures 3.13a and 3.6 are qualitatively similar. Significantly, spectra recorded from the periphery of the droplet, like that shown in Figure 3.13b, closely resemble that shown in Figure 3.7, the FAB spectrum near the maximum in $TEA^+$ emission.

A series of SIMS images of the sample used for Figure 3.12 was taken over a period of time. Over the course of the experiment, the images of Figure 3.14 show the distribution of $TEA^+$ emission, while Figure 3.15 shows the distribution of m/z 93 emission characteristic of glycerol, mainly for reference. As the droplet shrinks, the original "doughnut" shape of intense $TEA^+$ emission gradually fills. The filling corresponds to the shrinking of the

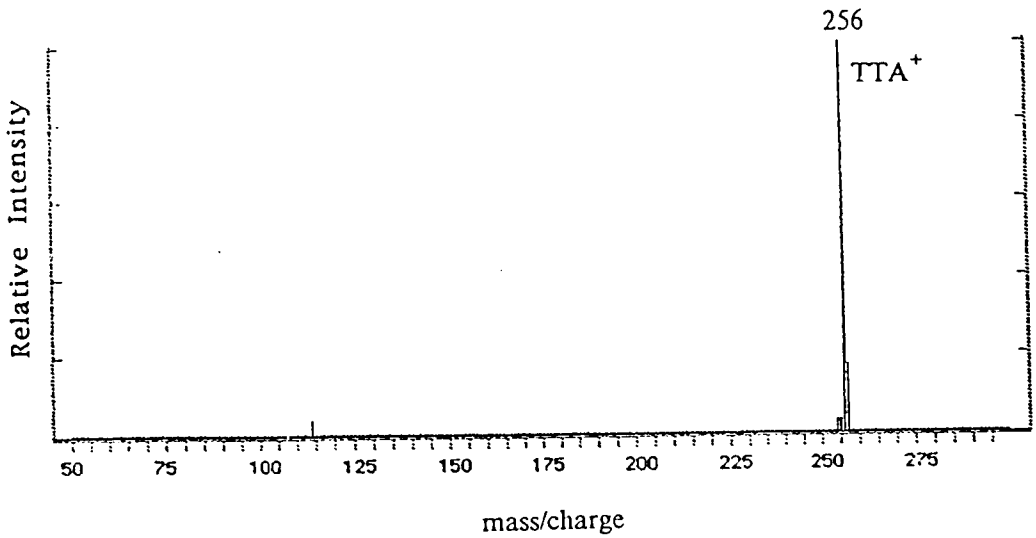



Figure 3.11. LSIMS mass spectrum acquired late in the experiment from the center of the sample shown in the image of Figure 3.9.

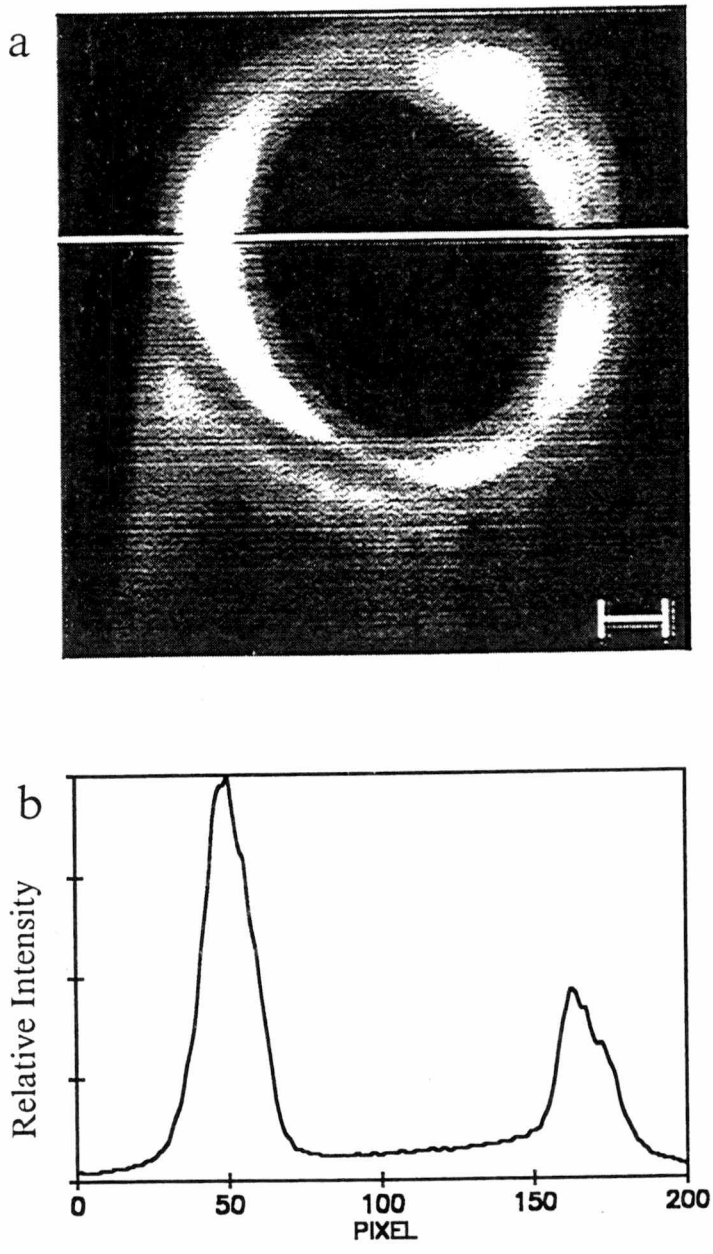



Figure 3.12. (a) Secondary ion image of m/z 130 ($TEA^+$) from 1 mM TEAI in glycerol, using white as the most intense and black as least intense. (b) Relative intensity of m/z 130 along cursor mark in image of part (a).

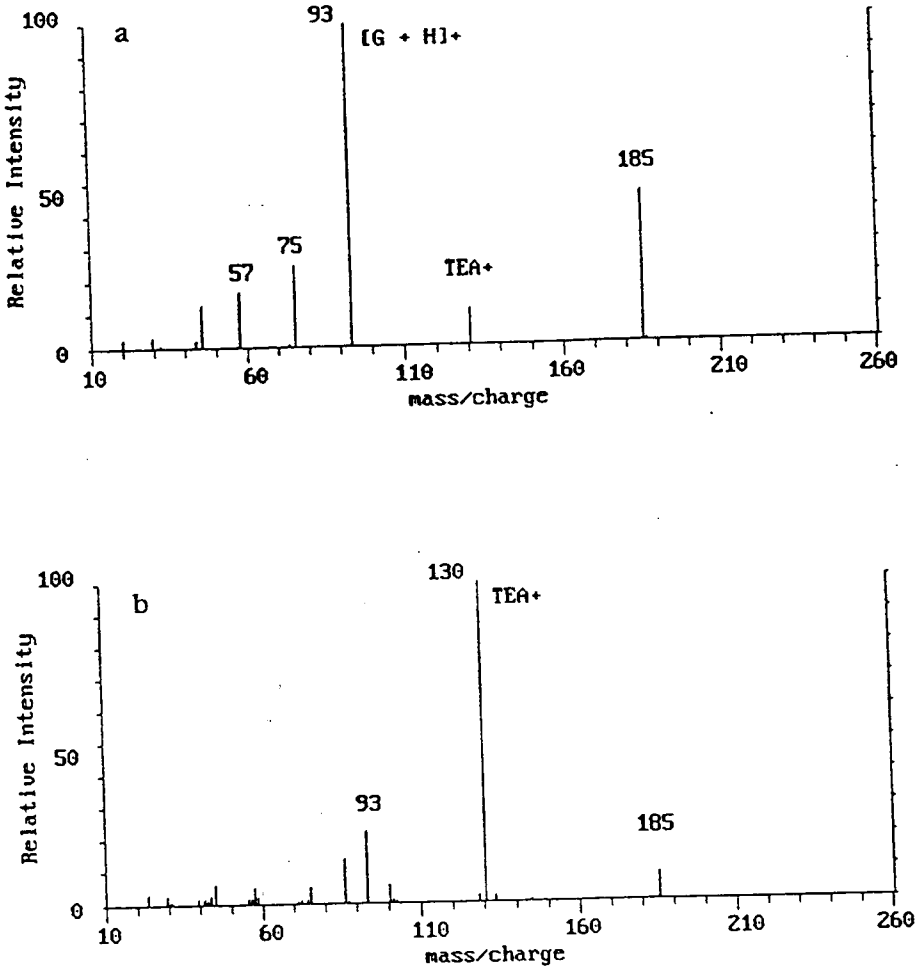



Figure 3.13. LSIMS mass spectrum acquired at the (a) center and (b) edge of the sample shown in the image of Figure 3.12.

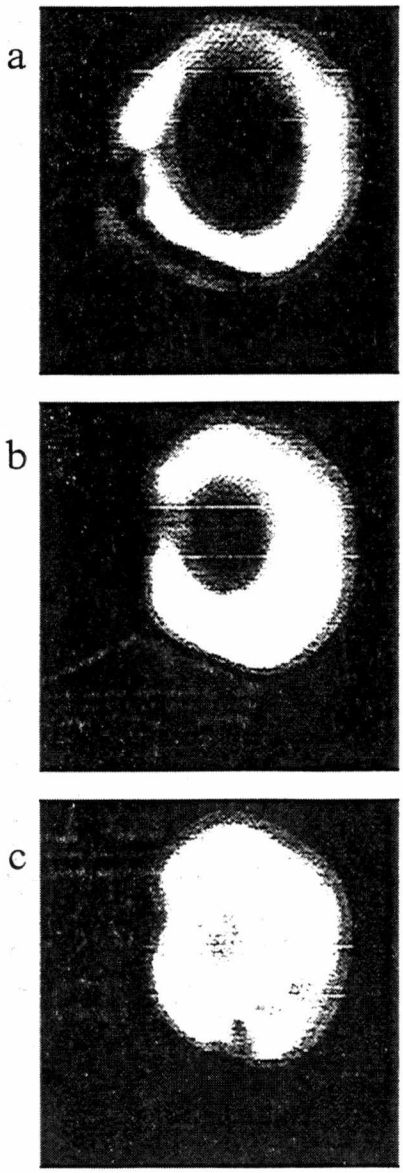



Figure 3.14. Secondary ion image of m/z 130 ($TEA^+$) (a) 15, (b) 32, and (c) 66 minutes after introduction of the sample, respectively. Each image is individually normalized to the most intense point in the image, which is indicated by white.

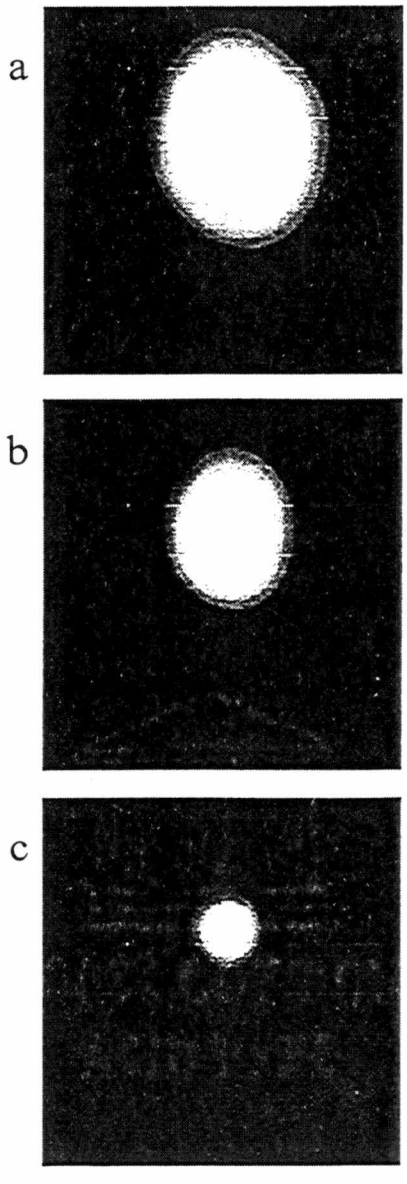



**Figure 3.15.** Secondary ion image of m/z 93 ($[G + H]^+$) (a) 15, (b) 32, and (c) 66 minutes after the introduction of the sample, respectively. Each image is individually normalized to the most intense point in the image, which is indicated by white. Except for the position of the respective maxima, no correlation is implied between the maximum intensities of m/z 130 (Figure 3.14) and m/z 93 in the respective images.

region of intense emission of m/z 93. The intensity of $TEA^+$ (relative to $[G + H]^+$) increases correspondingly until the spectrum shown in Figure 3.16 (taken at the "droplet" center after "doughnut" collapse) resembles the LSIMS spectrum shown in Figure 3.13b (on the "doughnut" edge) and the FAB spectrum shown in Figure 3.7.

Figures 3.14 and 3.15 can be used to explain, in part, why the FAB spectrum of $TEA^+$ is time-dependent. In FAB as in LSIMS, emission from the center of the droplet should initially consist primarily of characteristic glycerol ions. If the center of the FAB target is the object point of the mass spectrometric ion optics, then only late in the experiment will the "doughnut" of intense $TEA^+$ emission reach this focal region. Thus, as the hole fills in, the intensity of $TEA^+$ increases, as in Figure 3.5. Such time dependence would also be observed using the SIMS spectrometer if the (100 micron diameter) focal region had been "parked" at the droplet center via computer controlled deflectors within the secondary ion source. This experiment, however, would be too slow to be practical (flux too low) and was not attempted. With FAB, where primary particle flux is higher than for static SIMS, [246] once the sample dries characteristic secondary ion emission is only slightly above background due to damage and possibly charging (Figure 3.17). This explains the rejuvenation experiments wherein addition of glycerol restored characteristic emission. In contrast, static SIMS permits spectra to be obtained even from dry samples. That is why the hole in the "doughnut" gets smaller in Figure 3.14, but the diameter of the doughnut hardly changes at all.

The center of the doughnut may not coincide with the ion axis on some instruments or samples so that the spike of high intensity is seen at a different

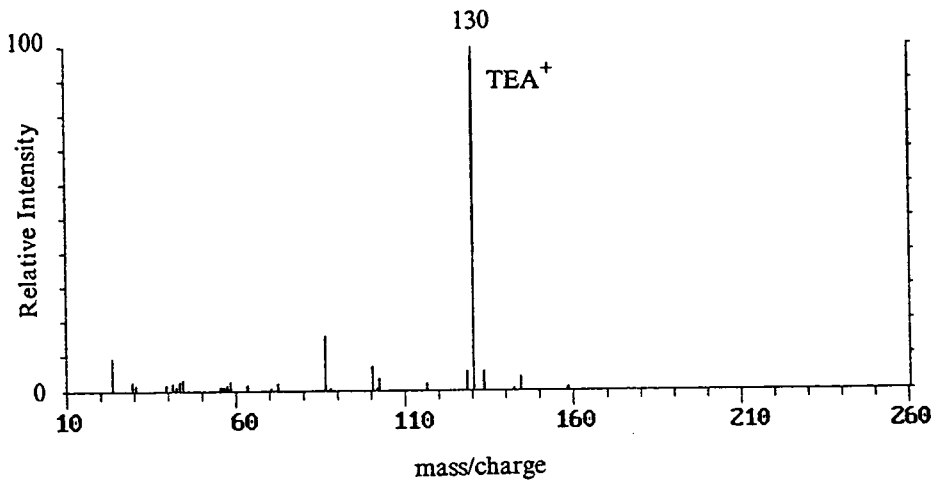



Figure 3.16. LSIMS mass spectrum acquired at the center of the image shown in Figure 3.15c.

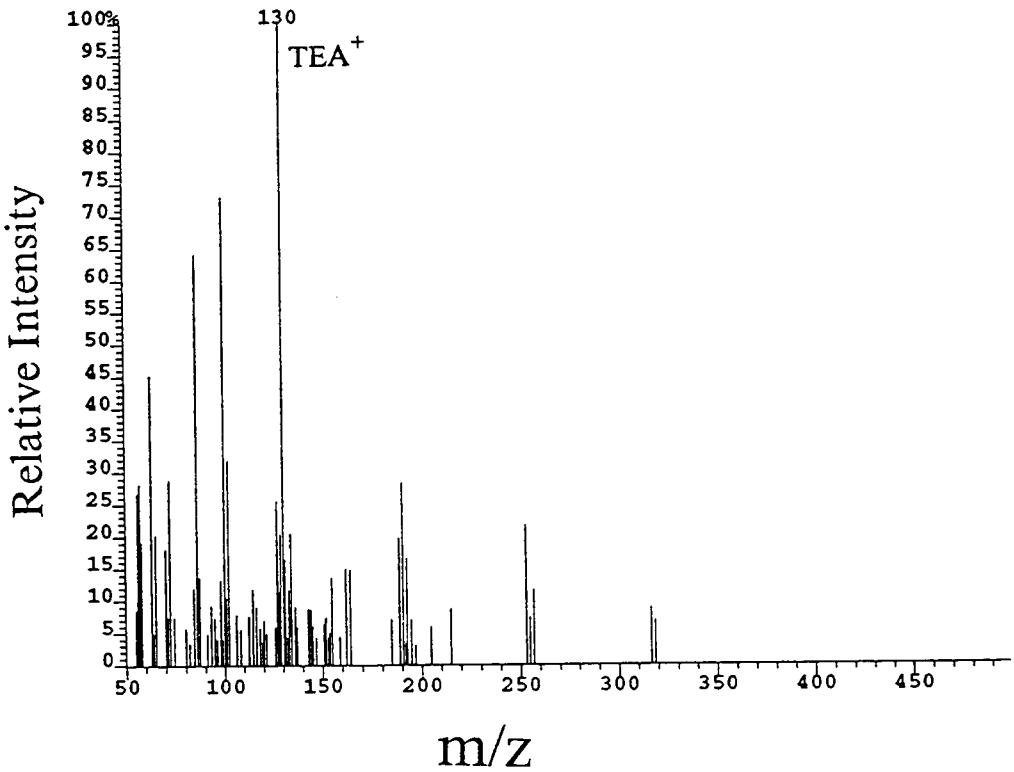



Figure 3.17. FAB mass spectrum acquired from a dry sample of $TEA^+$.

time during the course of the FAB experiment. Differences in evaporation rate due to differences in sputtering rate, pumping, thermal properties, and sample thickness also contribute to variability. Thus, for the same solution, a different time dependence may be observed. For studies in which the mass spectrometer focus is readjusted between measurements, it may be difficult to see differences between results from surfactants and nonsurfactants. Given the wide range of variables involved, it is not surprising that time dependence is difficult to reproduce from instrument-to-instrument. By contrast, the computer controlled ion optical properties of the SIMS instrument made images like those of Figures 3.9, 3.12, 3.14, and 3.15 remarkably reproducible.

While heterogeneous emission is characteristic for TEAI solutions, emission from TTAB solutions is reproducibly homogenous. Furthermore, temporal behavior of spectra from these solutions appears to arise mainly from changes in concentration due to preferential sputtering of TTAB, rather than ion optical effects. This contention is supported by the continuous decrease in intensity at m/z 256 under FAB conditions (Figure 3.2); by the results of rejuvenation experiments, which fail to yield a significant FAB spectrum after redeposition of glycerol (suggesting near depletion of TTAB); and by the homogenous emission of $TTA^+$ from the droplet (Figure 3.9).

## 3.3 Effects of Surface Activity

A simple and justifiable assumption is that the surface activity of TTAB is greater than that of TEAI in glycerol; this is certainly the case in water, another protic solvent (Table 3.1). By surface activity, it is meant that when a surface active molecule is on the surface, it has the effect of lowering the

surface tension of the liquid. Surface free energy is lowered by a surface excess concentration of such a solute.

As noted earlier, diffusion from the bulk is not a sufficiently rapid mechanism to replenish material sputtered from the surface during the course of a FAB experiment. [237] Therefore, surface active molecules must arrive at the surface by some mechanism other than diffusion through the bulk. By the same token, diffusion is not sufficiently rapid to reduce any surface excess concentration of solute that may be present on the surface of the glycerol solution due to evaporation of glycerol itself. As reported by Todd *et al.*, [232] a primary beam current density of about 10 $\mu A/cm^2$ will provide a rate of sputtering equal to the rate of glycerol loss from evaporation at normal room temperature. The flux density that corresponds to this, $6 \times 10^{13}$ atoms/$cm^2$-s, is a fairly typical value for a FAB experiment.

The drying behavior of TEAI solutions is much like that of brine solutions. It is well-known that hydrophilic salts tend to raise the surface tension of water. [233] As the solution evaporates, salt precipitates at the periphery, leaving a residue behind the shrinking droplet. Consistent with this phenomenon, secondary emission of $TEA^+$ is more intense from the periphery of the shrinking droplet than from the center until the very end of the experiment, when the sample has dried. For both brine and TEAI/glycerol solutions, precipitation occurs at the periphery. Excess salt on the surface (remaining after evaporation of solvent) is, therefore, transported rapidly across the surface to the periphery by a Marangoni effect.

The reproducible images shown in Figures 3.14 and 3.15 rule out any significant role for convection and mechanical mixing as mechanisms of mass transport of solute to the surface; such processes would tend to destroy the

surface heterogeneity. Figure 3.18 confirms the absence of mixing and convection (at least for the SIMS experiment where spatial resolution is available) even from a mixture containing TTAB, TEAI, and glycerol. The image of the three component system (a mixture of the surfactant and nonsurfactant in glycerol) clearly indicates that $TEA^+$ is emitted from the edge and $TTA^+$ is uniformly emitted from the sample surface. The images of the mixture sample (Figure 3.18) appear very much like the images from the samples containing only a single solute (Figures 3.9 and 3.12). By excluding important roles for bulk diffusion, mechanical mixing, and convection, only sputtering, evaporation, and Marangoni effects remain as mass transport mechanisms.

Due to the surface activity of TTAB, the Marangoni effect will tend to cause TTAB to be uniformly spread across the glycerol surface as it is enriched at the surface by evaporation. This surface spreading can account, at least in part, for the relatively rapid FAB sputtering of TTAB compared with TEAI.

With such a model, a very long time may be required for the system to reach a steady state, especially in the FAB experiment. As long as the rate of analyte removal (by sputtering) exceeds the rate of replenishment (mainly by solvent evaporation), steady state will never be reached and the sample will be depleted. The lower flux used in SIMS experiments results in slower rates of analyte and sample removal (compared to FAB). In part, the faster rate of sample removal in FAB may result from heating of the surface due to high primary particle flux densities. While sputtering increases linearly with primary particle flux, evaporation of glycerol increases exponentially with any temperature increase caused by elevated primary particle flux density. [232] From Figure 3.2, the steady state of $TTA^+$ emission and presumably of

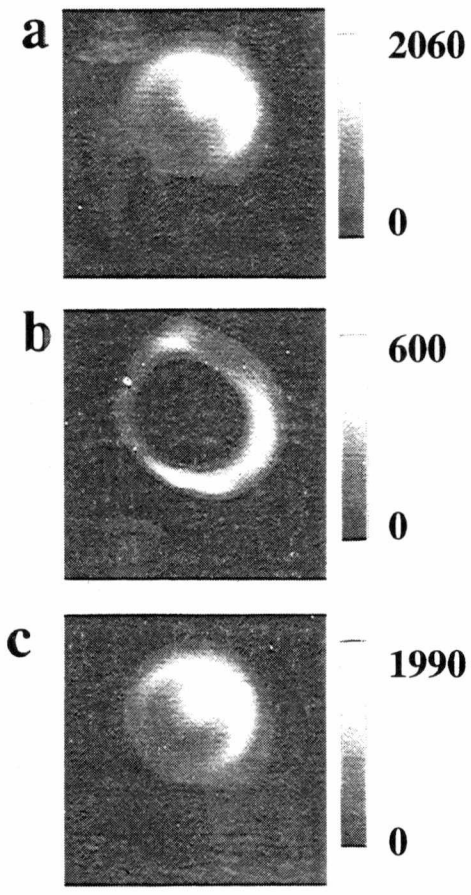



Figure 3.18. Successive (a) $TTA^+$, (b) $TEA^+$, and (c) $TTA^+$ secondary ion images from the same droplet of TEAI and TTAB in glycerol solution, acquired with about 4 minutes between images.

surface concentration is never reached in the FAB experiments. Because the sputtering rate is much lower in SIMS, the steady state of TTAB surface concentration is maintained throughout the experiment. Consistent with this fact, the SIMS spectrum of TTAB solution is essentially independent of time.

Sputtering and evaporation are well-known processes of sample depletion. Whether heterogeneous secondary ion emission from liquid samples is a common phenomenon is less obvious. Figure 3.19 shows the temporal behavior of $TEA^+$ and protonated m-nitrobenzylalcohol (m-NBA) [247] from a 1 mM solution of TEAI in NBA under FAB conditions. The peak in $TEA^+$ intensity (attributed to bringing the high-concentration region into focus) is similar to that of Figure 3.6 but less steep. The difference in slope may be a result of any of a number of factors, including different rates of evaporation and sputtering. Figure 3.20 shows the distribution of emission of $TEA^+$ and $[NBA + H]^+$, respectively. While NBA has chemical and physical properties very different from glycerol (such as viscosity and volatility), [33] the behavior of emission of $TEA^+$ from the NBA solution is very much like that from glycerol, and the images of samples from both solutions show similar distributions.

By presumption that matrix evaporation is the main method of mass "transport" to the surface of normal samples, it becomes possible to explain why the effects of surface activity are absent when solutes are admitted via the gas phase. With solutes that are at equilibrium with the vapor, both the surface distribution and bulk concentration of solute are controlled by gas-phase mass transport. Even though Marangoni effects may be rapid in the context of a FAB or SIMS experiment, gas-phase mass transport is far more rapid.

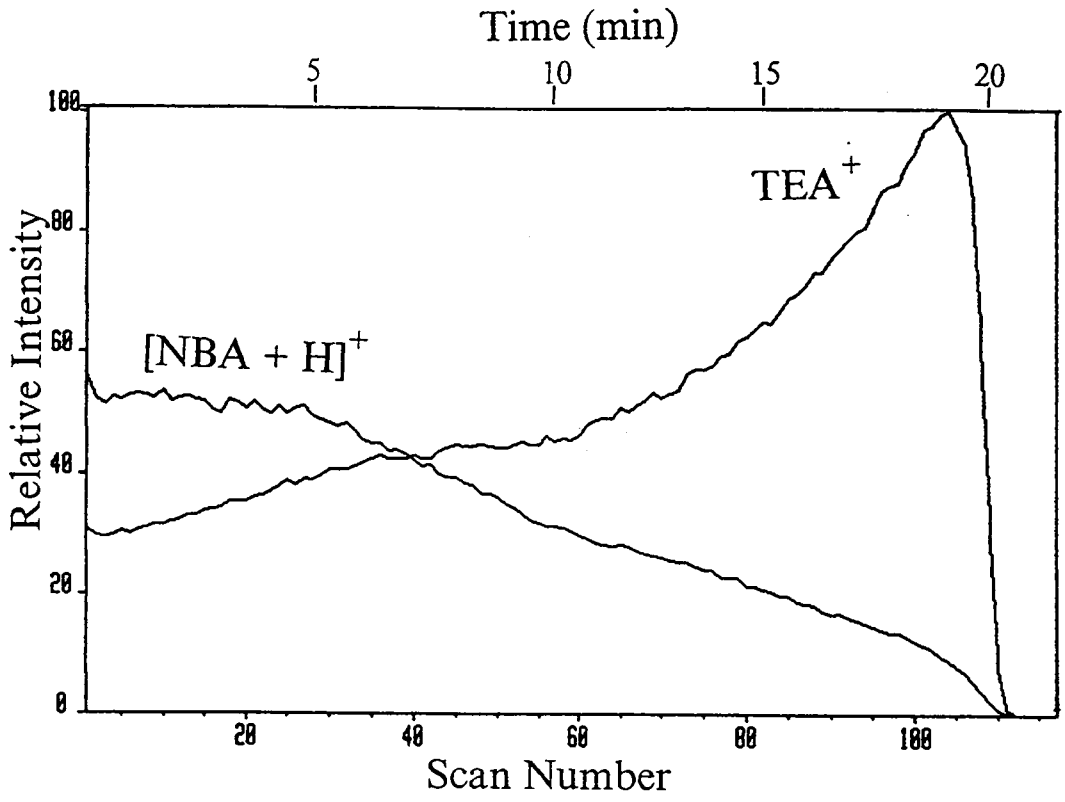



Figure 3.19. Intensities of m/z 130 ($TEA^+$) and m/z 154 ($[NBA + H]^+$) versus time from 1 mM TEAI in m-nitrobenzyl alcohol sample from a FAB experiment.

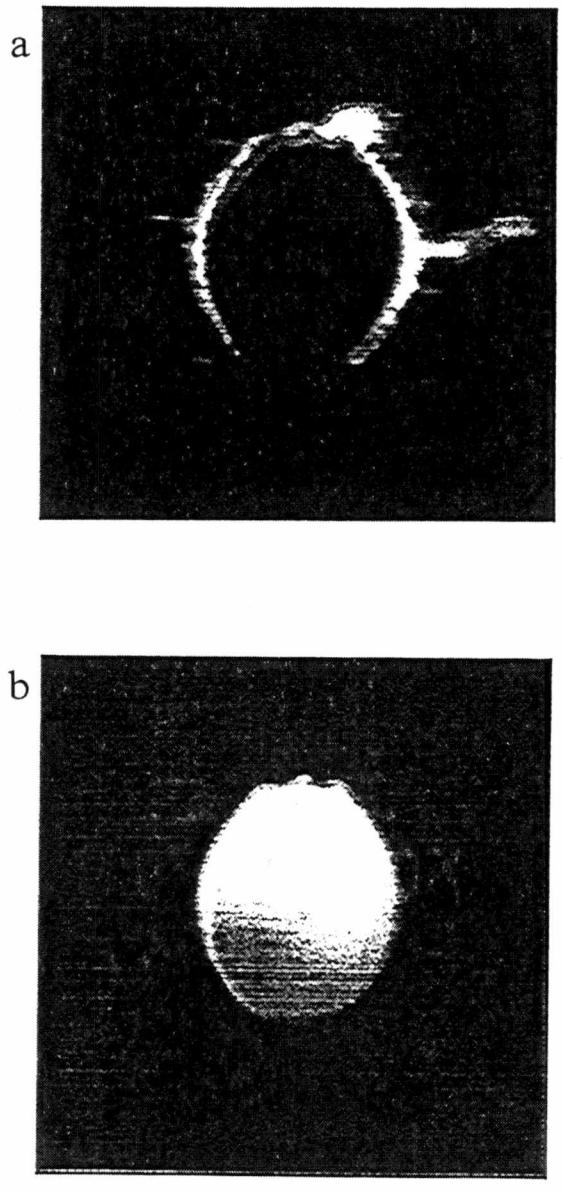



Figure 3.20. Secondary ion image of (a) m/z 130 ($TEA^+$) and (b) m/z 154 ($[NBA + H]^+$) from 1 mM TEAI in m-nitrobenzyl alcohol using white as the most intense and black as the least intense.

## 3.4 Electrochemical Polymerization on FAB Target to Improve Wettability

Wettability is another manifestation of surface tension. As noted above, it is difficult to reproduce FAB and LSIMS time dependence from run-to-run and from instrument-to-instrument. A possible contributor to the time dependence is the manner in which the sample is applied to the FAB target. In the FAB experiments, a droplet of the analyte solution is placed on the probe tip and then inserted into the vacuum chamber. This droplet can wander across the surface of the FAB probe tip as it shrinks due to sputtering and evaporation. A means of reducing the wandering and improving the reproducibility of FAB spectra would be to create a wettable probe tip surface. Common FAB solvents (e.g., glycerol), are organic and would require an organic surface. The wettable surface, however, must be electrically conductive so that charge will not accumulate on the probe tip surface and distort electric field lines or cause arcing and sparking within the source (also to assure application of the accelerating potential to the probe tip).

A first attempt at making the surface wettable was an electrochemically produced conductive organic polymer film (preparation described below) on the surface of a stainless steel target. [220] The stainless steel FAB target was positioned within a Teflon sheath as shown in Figure 2.3 so that only the end was exposed to the electrochemical cell. The Teflon shielded SS electrode was immersed in a coating solution that contained 0.01 M 3-methylthiophene and 0.1 M tetraethylammonium perchlorate dissolved in acetonitrile. Using the three electrode system described in section 2.1.3, the potential of the SS

"working" electrode was scanned from 0 mV to +1100 mV at a scan rate of 50 mV/second, and returned to 0 mV also at the same rate. The SS electrode was visually inspected for complete coverage of the surface with a black poly-3-methylthiophene film. The cycle was repeated as necessary (minimum of twice) to obtain complete coverage of the SS surface. After the surface was completely covered with poly-3-methylthiophene, a cyclic voltammogram like that shown in Figure 3.21 could be obtained when the "polymer electrode" was immersed in a solution of 0.1 M tetraethylammonium perchlorate in acetonitrile and the potential cycled from 0 mV to +1100 mV at a scan rate of 50 mV/second and returned to 0 mV at the same scan rate. The sharp increase in current near +1100 mV is indicative of a conductive layer on the stainless steel surface. [220] The wettability of the poly-3-methylthiophene coating was tested by applying a thin film of glycerol across the surface. A thin, uniform layer of glycerol on the surface clearly revealed that the poly-3-methylthiophene coating was wettable. The same result was not observed when a thin layer of glycerol was applied to the surface of an untreated SS probe tip; the glycerol immediately beads on such a probe tip. Using pure glycerol, the coating was tested for physical and chemical tolerance under normal FAB conditions. The coating survived numerous FAB experiments. The ion current dependence on time (total ion chromatogram) shown in Figure 3.22 reveals that the experiment time is much shorter when the sample is applied as a thin film rather than as a droplet. The amount of glycerol applied as a thin film was not determined, however, so the shorter experiment time may be attributed to the application of less material to the surface of the probe tip. This preliminary work should only be interpreted as evidence for a wettable probe tip surface that might prove useful for FAB experiments. This

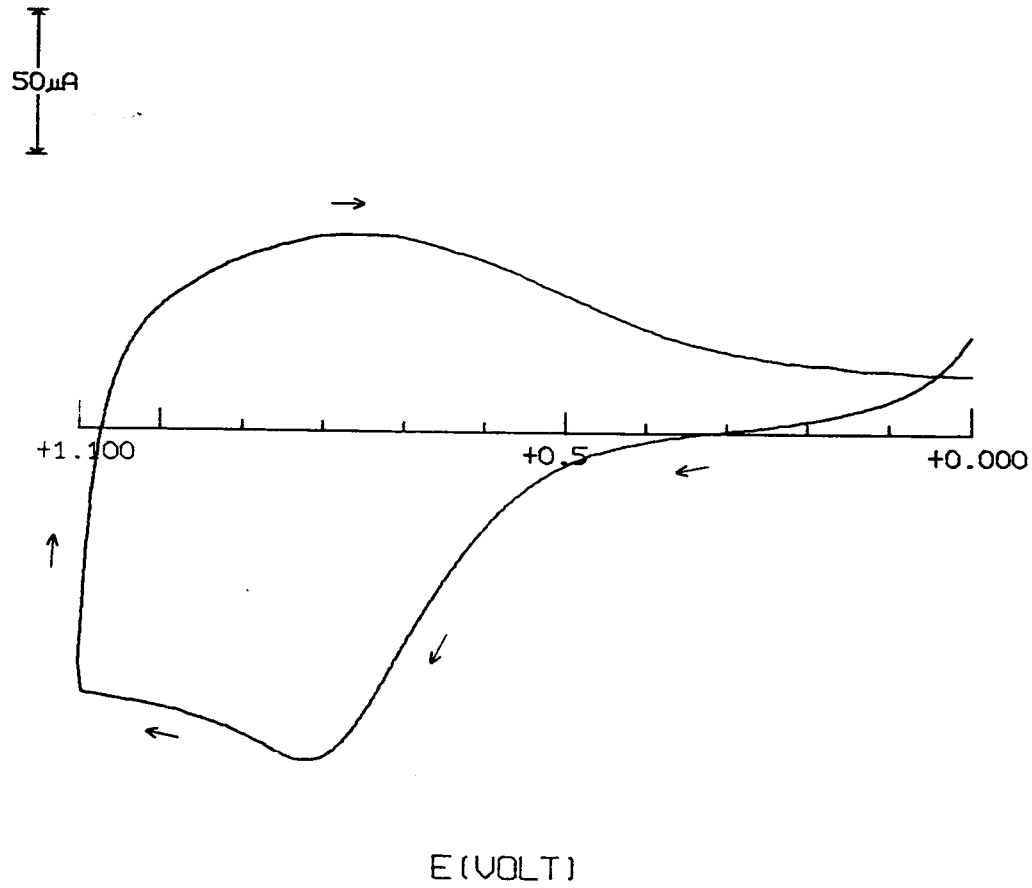



Figure 3.21. Cyclic voltammogram using a stainless steel electrode coated with poly-3-methylthiophene. The electrochemical cell consisted of a 0.1 M solution of tetraethylammonium perchlorate in acetonitrile, a Ag/AgCl quasi-reference electrode, and a Pt mesh counter electrode.

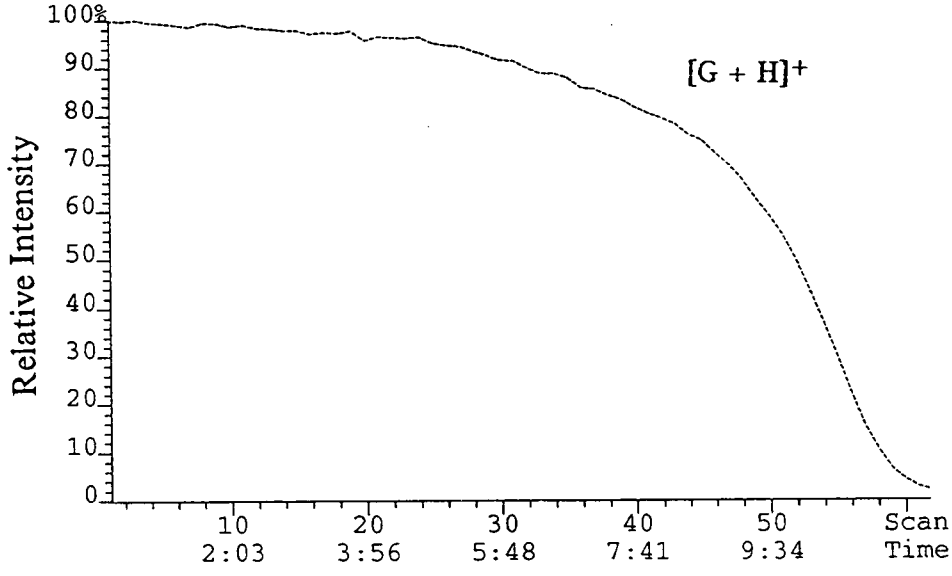



Figure 3.22. FAB total ion chromatogram from a thin film of glycerol applied to the surface of a stainless steel target coated with poly 3-methylthiophene. The amount of glycerol was not determined.

preliminary study needs to be extended to establish the possible advantages of using a wettable probe tip for FAB experiments.

While the conductive polymer provides a wettable surface, simple acid etching (immersing the tip in concentrated nitric acid for several minutes) of the surface also provides a wettable surface. For routine analysis, the easiest approach (in this case, acid etching) will most likely be used. These wettability studies and the development of new FAB/LSIMS probe tips to improve sensitivity and reproducibility were truncated short of completion. Suggestions for continuation of this project are made in Chapter 6.

## 3.5 Conclusions

The most important finding of this work is that concentrations and secondary ion emission from liquid solutions can be heterogeneous across the surface. The time dependence of FAB spectra can be explained on the basis of this heterogeneity, plus variation in analyte mass transport (mainly from Marangoni effects) and sampling efficiencies. As noted earlier, diffusion coefficients in glycerol are generally so small that diffusion through the bulk solution cannot be a viable mass transport mechanism to establish surface/bulk equilibrium during the course of a FAB or SIMS experiment. [237] By the same token, the slow diffusion of solutes in glycerol, in conjunction with glycerol evaporation, necessarily results in enrichment of involatile solute near the surface. When the presence of excess solute on the surface increases the surface tension, the solute is driven to the periphery by a Marangoni effect. For surfactants, the solute is dispersed across the surface by the same forces, as has been recognized by Ligon (and by others in studies not

related to MS). [44] He coined the term "side filling" to mean replenishment of solute at the site of primary ion bombardment driven by surface forces.

Practically speaking, the images make it possible to reconcile diverse sets of data and diverse conclusions reported in the literature. At the same time, it is clear that results obtained from solution samples without accounting for time dependence may well be ambiguous.

# Chapter 4

## Durable Gold-Coated Fused Silica Capillaries For Use In Electrospray Mass Spectrometry and Capillary Electrophoresis/Electrospray Mass Spectrometry

A major focus of electrospray has been the analysis of large molecules not previously amenable to MS. ES is also a potentially valuable tool for studying solution chemistry. Ion solvation studies such as those discussed in section 1.4 have been reported. [64,208] Under normal ES conditions, however, the droplet undergoes many collisions during the desolvation process which can complicate interpretations of the spectra to reflect solution phase solvation. The observed number and distribution of solvent molecules attached to the solute does not necessarily reflect the number or distribution prior to the ionization process. While ES is not ideally suited for probing discrete ion/solvent interactions, it is well suited for probing solvent effects on the solute chemistry. For example, recall from section 1.2.1 that the distribution of charge states (the number of protons per molecule) observed in the ES mass spectra of proteins (e.g., cytochrome c) changes as a function of the solvent composition, pH, and temperature. [58,76,77,78,79,80]

Many of the more important and interesting ES samples are complex aqueous mixtures requiring some sample pre-treatment prior to MS analysis. In analytical chemistry, complex mixtures often require some method of separation, such as liquid chromatography or capillary electrophoresis, prior to analysis to provide useful information. This problem is further aggravated in ES of proteins by the charge state distribution, making the spectrum of each

component complex. As already indicated in section 1.2.2, the CE separation typically requires a high ionic strength aqueous buffer solution for optimum performance. This solution is not entirely compatible with the optimum conditions for conventional ES; conventional ES performance has been best when the analyte is sprayed from methanol or methanol/water (greater than 50%, by volume, methanol). Recall from the discussion of section 1.2 that parts of the ionization mechanisms rely on Rayleigh explosions and solvent evaporation. Methanol is more volatile than water and has a lower surface tension, and should therefore, provide more efficient ionization. Another consideration in coupling CE and ES stems from the differences in flow rates. Recall from section 1.2.2 that the flow of solution (generated by the applied voltage) through the capillary in CE is on the order of 10 μL/hour and typical conventional ES sources require flow rates on the order of 1 to 10 μL/minute. The most common source used to overcome the differences in flow rates has been the sheath design shown in Figure 4.1. Despite these differences in solution composition and flow rates, a great deal of effort has been directed towards the development of an ES source capable coupling the two techniques. This chapter presents the source characterization results, sensitivity and limit of detection results (compared to a conventional ES source), and CE/ES results using a newly developed micro-source. In the course of these studies, results related to the solvent composition effect on the charge state distribution and protein conformation were also observed. This chapter will attempt to make clear whether the extent of solvation is due to the change in solvent or the conformation of the protein.

While section 2.2.2 describes the procedure for preparing the gold-coated silica capillaries, this chapter and a resulting publication [248] describe

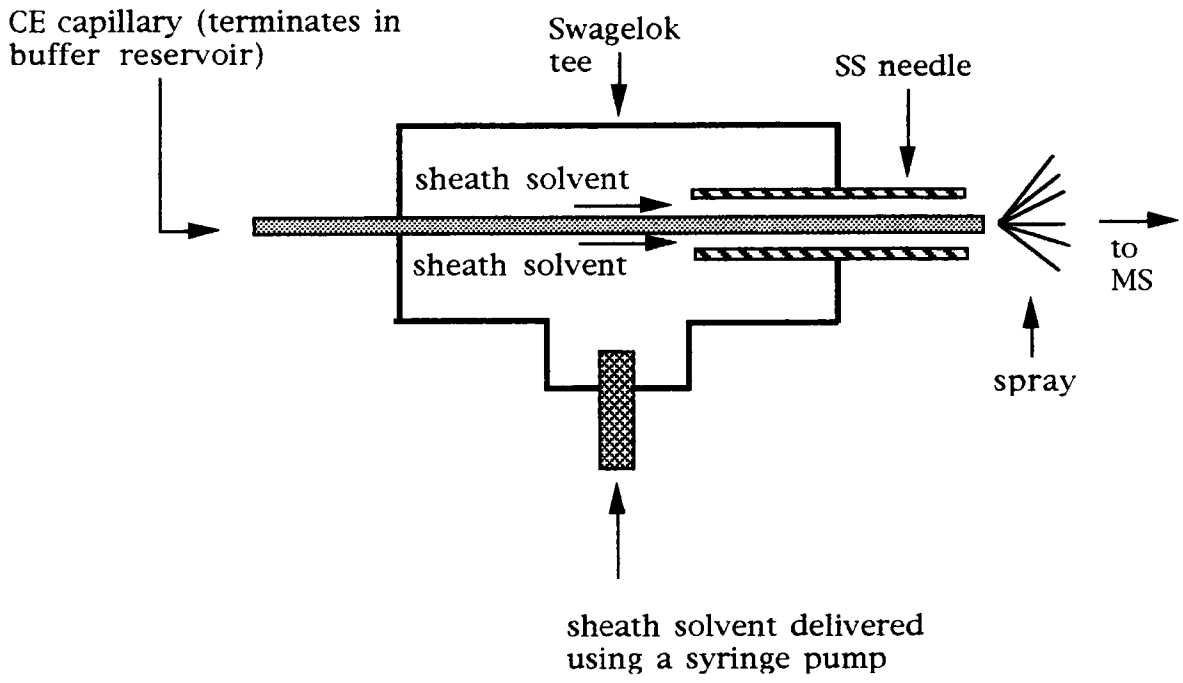



**Figure 4.1.** CE/ES interface using a sheath flow of solvent to establish electrical connection.

the characterization and evaluation of the capillaries for continuous infusion ES MS and CE/MS using an ion trap mass spectrometer (ITMS) also described in Chapter 2. The University of Tennessee Research Corporation is currently considering applying for a patent on the gold-coated fused silica capillary technology. Applications work presented in this chapter was accomplished through collaboration with Dr. Roswitha Ramsey at the Oak Ridge National Laboratory.

## 4.1 Capillary Characterization

### 4.1.1 Capillary Durability

In a preliminary test of coating stability, treated capillaries were sonicated for 1 minute in the various solvent systems shown in Table 4.1. Microscopic inspection (3X magnification) after sonication revealed perceptible coating deterioration only by aqua regia and Piranha solution. In a second test, physical adhesion was assessed by application and removal of a piece of adhesive cellophane tape. As reported by Goss *et al.*, [225] gold deposited on untreated silica was easily removed by adhesive tape, whereas there was no perceptible deterioration or removal of the gold layer from a capillary reacted with (3-mercaptopropyl)trimethoxysilane prior to gold coating, as outlined in Chapter 2 above.

The coating longevity under normal electrospray conditions was also evaluated. A 10 mM solution of acetic acid in water (pH 3.50) was sprayed (by infusion from a syringe pump) at 0.2 μL/minute from a single 25 μm i.d. X 365

Table 4.1. Solutions used to test the chemical stability of capillary coatings.[a]

| SOLUTION[b] | STABLE | UNSTABLE |
|---|---|---|
| WATER | XXX | |
| METHANOL | XXX | |
| ETHANOL | XXX | |
| 2-PROPANOL | XXX | |
| ACETIC ACID BUFFER (10 mM; pH = 3.5) | XXX | |
| CONCENTRATED HCl (12.1 M) | XXX | |
| AQUA REGIA | | XXX |
| PIRANHA SOLUTION [1:4 (v/v) mixture of 30% $H_2O_2$:$H_2SO_4$] | | XXX |
| AMMONIUM ACETATE BUFFER (10 mM; pH = 7) | XXX | |
| $NaH_2PO_4$ (10 mM; pH = 4.5) | XXX | |
| BORIC ACID (10 mM; pH = 4) | XXX | |
| POTASSIUM HYDROXIDE (1 M) | XXX | |

[a] Stability based on visual inspection with a microscope. The coated capillary terminus was immersed in the solution and sonicated for 1 minute.

[b] All solutions were aqueous, except for the alcohols.

μm o.d. X 50 cm length gold-coated capillary for more than 100 hours. This was accomplished in 10 sessions consisting of approximately 10 hours each. The ES onset voltage at the beginning of each session varied (randomly) from 2.7 kV to 3.3 kV (see Table 4.2). The voltage was maintained just above the onset in each session, resulting in an average of 3.1 ± 0.1 kV (uncertainties here and subsequently reflect the standard deviation of the mean). The counter-electrode collector current (see Figure 2.7) was recorded at 5 hour intervals, averaging 61 ± 17 nA. The rather large uncertainty in current (28% relative standard deviation) reflects slow, random drift (between 40 and 100 nA (see Table 4.2), rather than short-term instability within a single session. The short term collector current, measured over a 10 minute period, was estimated to be stable to within ± 2 nA. However, at the conclusion of 100 hours of testing, currents became erratic, and the set-up was disassembled. In removing the capillary from its platinum support, the gold coating was inadvertently scraped off by abrasion, terminating further evaluation of this capillary. It was subsequently determined that a faulty connection at the grounded counter electrode had caused the instability. The 100-hour benchmark was surpassed in a second longevity experiment lasting 102 hours. This experiment was performed under the exact same conditions as the first experiment except the counter electrode collector current and the ES voltage were recorded at intervals (for convenience) ranging from 6 to 13 hours. During the second experiment, onset voltages varied from 3.1 to 3.5 kV (average of 3.3 ± 0.10 kV) and collector currents ranged from 160 to 210 nA (average of 180 ± 20 nA) (see Table 4.3). Current stability is similar, but the average current is much higher than with the first emitter. The difference in average currents could be attributed to the variation in acetic acid

Table 4.2. Counter electrode current and needle voltage data for first capillary used to test long-term stability, spraying 10 mM acetic acid (pH 3.5) at 0.2 μL/minute.

| Time (hours) | Voltage (kV) | Current (nA) |
|---|---|---|
| 1 | 3.1 | 50 |
| 5 | 3.1 | 40 |
| 10 | 3.1 | 40 |
| 15 | 3.1 | 50 |
| 20 | 3.1 | 50 |
| 25 | 3.1 | 50 |
| 30 | 3.0 | 70 |
| 35 | 2.7 | 100 |
| 40 | 3.3 | 40 |
| 45 | 3.1 | 50 |
| 50 | 3.1 | 40 |
| 55 | 3.1 | 40 |
| 60 | 3.3 | 90 |
| 65 | 3.1 | 70 |
| 70 | 3.1 | 70 |
| 75 | 3.1 | 65 |
| 80 | 3.2 | 75 |
| 85 | 3.2 | 75 |
| 90 | 3.2 | 65 |
| 95 | 3.2 | 65 |
| 100 | 3.2 | 70 |

Table 4.3. Counter electrode current and voltage data for a second capillary used to test long-term stability, spraying 10 mM acetic acid (pH 3.5) at 0.2 μL/minute

| Time (hours) | Voltage (kV) | Current (nA) |
|---|---|---|
| 6 | 3.3 | 150 |
| 14 | 3.5 | 180 |
| 24 | 3.3 | 200 |
| 32 | 3.3 | 180 |
| 42 | 3.2 | 210 |
| 50 | 3.3 | 180 |
| 60 | 3.1 | 200 |
| 70 | 3.2 | 200 |
| 83 | 3.2 | 210 |
| 94 | 3.2 | 160 |
| 102 | 3.2 | 160 |

concentration from the two experiments. Solutions of acetic acid used to acquire the longevity data were prepared to be nominally 10 ± 0.1 mM (exact concentration was not determined) using a syringe to measure the acid volume. To determine whether this imprecision could account for the variation in collector current, two acetic acid solutions (9.49 mM and 10.47 mM) beyond the extremes of the precision range of the original solution, were prepared and sprayed. An average collector current of 190 ± 14 nA was obtained for the 9.49 mM acetic acid solution and an average collector current of 199 ± 5 nA was obtained for the 10.47 mM acetic acid solution with the same capillary used to acquire the second set of longevity data. The average of the currents used for the two extreme concentration ranges using the same capillary used for the second 100 hour longevity test are in good agreement with the average current from the second longevity experiment. Therefore, the differences in current observed for the two different longevity experiments can be attributed to differences in tip shape (all other parameters held constant).

Other capillaries used in un-timed MS applications (see below) have been estimated to approach the 100 hour benchmark. In general, the capillaries have remained useful until they have been accidentally scratched or broken through rough handling. This benchmark of 100 hours surpasses the lifetime of gold-coated capillaries prepared by simple vapor deposition within Smith's group (typical lifetimes of a few days). [249] The vapor deposited layer of gold with no undercoating suffers from poor adhesion and does not withstand a discharge (commonly encountered during the tuning process).

### 4.1.2 Spray Versatility

ES solutions sprayed using a dome-tipped stainless steel needle have typically consisted of methanol or solutions containing a large fraction of methanol (usually at least 50% by volume) to obtain stable spray. Stable spray is best described as a conical shaped mist of highly charged droplets that undergo solvent evaporation prior to striking the collector plate (or entering the instrument acceptance aperture). In the set-up of Figure 2.7, a steady collector current less than 1 μA was indicative of stable ES emission. Although methanolic solutions work well for conventional ES, they are not ideal for CE or for probing purely aqueous (no organic co-solvent) chemistry, such as natural conformations of biomolecules. Attempts at spraying purely aqueous solutions from a conventional ES emitter usually result in a "discharge" rather than stable spray. A discharge can be described as a spray that produces a counter electrode current much larger than 1 μA. Mass spectrometrically, a discharge results in an extremely large background in the low m/z range of the mass spectrum as a result of ionizing species within the atmospheric pressure region between the emitter and the entrance aperture of the instrument. A discharge suppresser, such as sulfur hexafluoride ($SF_6$), is a chemical species used to scavenge electrons. [67,92] The discharge suppresser is often delivered using a set-up similar to the nitrogen nebulizer arrangement shown in Figure 2.6. Using this arrangement, the discharge suppresser gas functions as an electron scavenger and a nebulizer. Although this arrangement works for spraying aqueous solutions from conventional ES emitters, the gain in sensitivity and reduction in background obtained from the use of small i.d. capillaries are not realized. The ability to spray a wide

variety of purely aqueous and sometimes high ionic strength buffers, without creating a discharge, is highly desirable. In order to assess the versatility of the gold-coated capillaries prepared as described in Chapter 2, a variety of solutions were sprayed using the bench-top "test stand" shown in Figure 2.7.

Plots of collector current as a function of needle potential, using a 25 μm i.d. capillary, shown in Figures 4.2 - 4.4, illustrate the distinct conditions necessary to sustain stable electrospray (plateaus below 1 μA) and the onset voltages for discharge (3-5 kV) in various solvent systems. Figure 4.4 contains data for a purely aqueous sample and contains only a single trace corresponding to the use of a 25 μm i.d. fused silica capillary. Corresponding data using a stainless steel needle could not be obtained due to the onset of discharge prior to stable spray of purely aqueous samples. The electric field strength generated between the ES emitter and the counter electrode depends on the outer diameter of the emitter, the geometry of the emitter and counter electrode, and the distance separating the emitter and counter electrode. From a "sharp" emitter, such as the tapered gold-tipped capillary, the electric field strength will be higher than for the larger o.d. dome-tipped stainless steel needle at the same needle potential. Therefore, the onset of a discharge will occur at lower voltages for the tapered gold-tipped capillary. As expected, with the separation distance held constant for the two emitters, the discharge onset voltage for the tapered silica capillary is lower than that observed with a "dome-tipped" stainless steel needle (with larger i.d. and correspondingly higher flow). [81] Nevertheless, using the Au tip capillary, there is in all cases a useful range of voltages where stable spray was observed without a discharge. The SS discharge onset voltage for the stainless steel (SS) needle was ≈ 4.6 kV. Stable spray was not observed from the SS needle prior to the

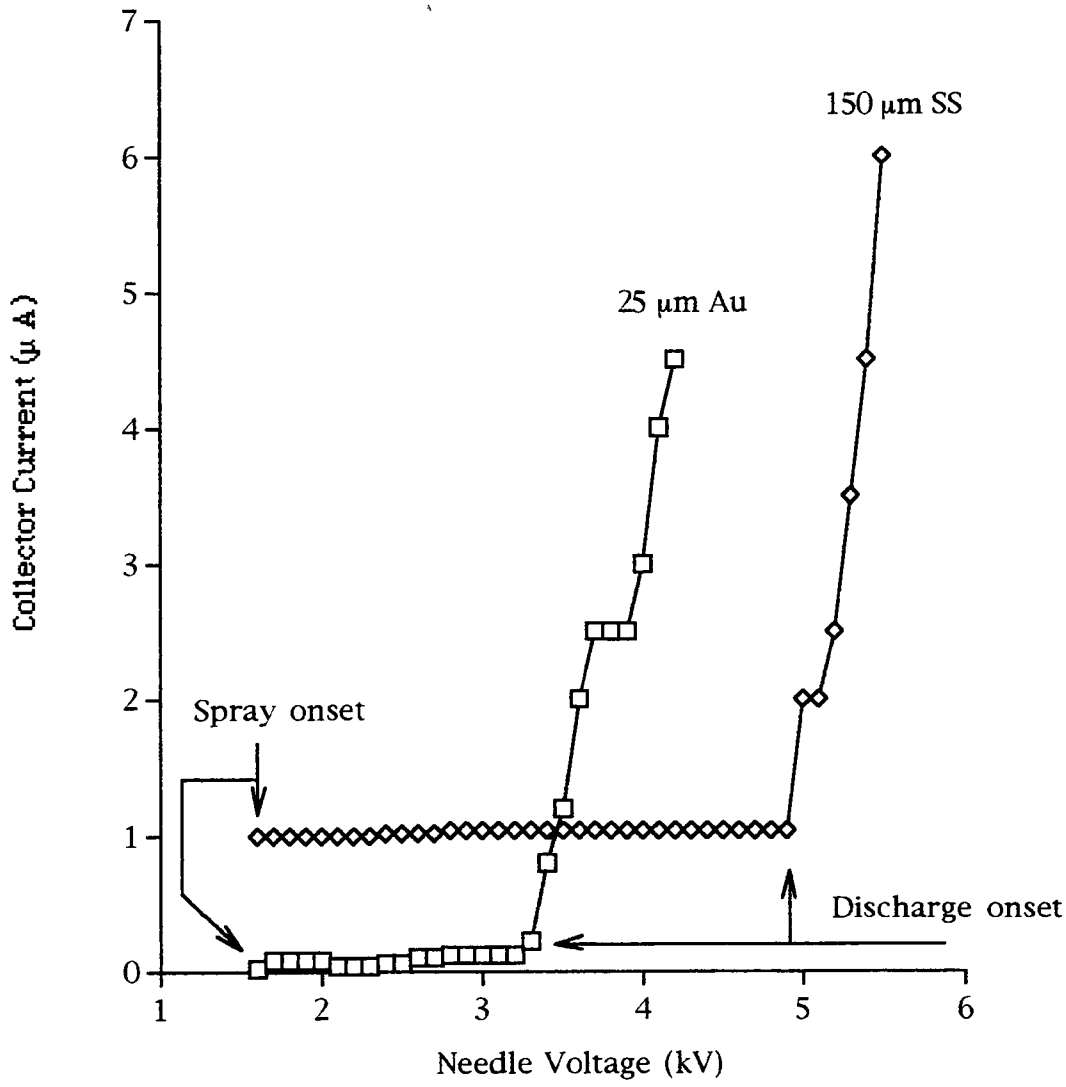



Figure 4.2. Collector current as a function of needle voltage while spraying methanol through a 25 μm i.d gold-coated capillary (Au) at a flow rate of 0.2 μL/minute and through a 150 μm i.d stainless steel needle (SS) at a flow rate of 1 μL/minute. The SS curve is offset +1 μA for clarity.

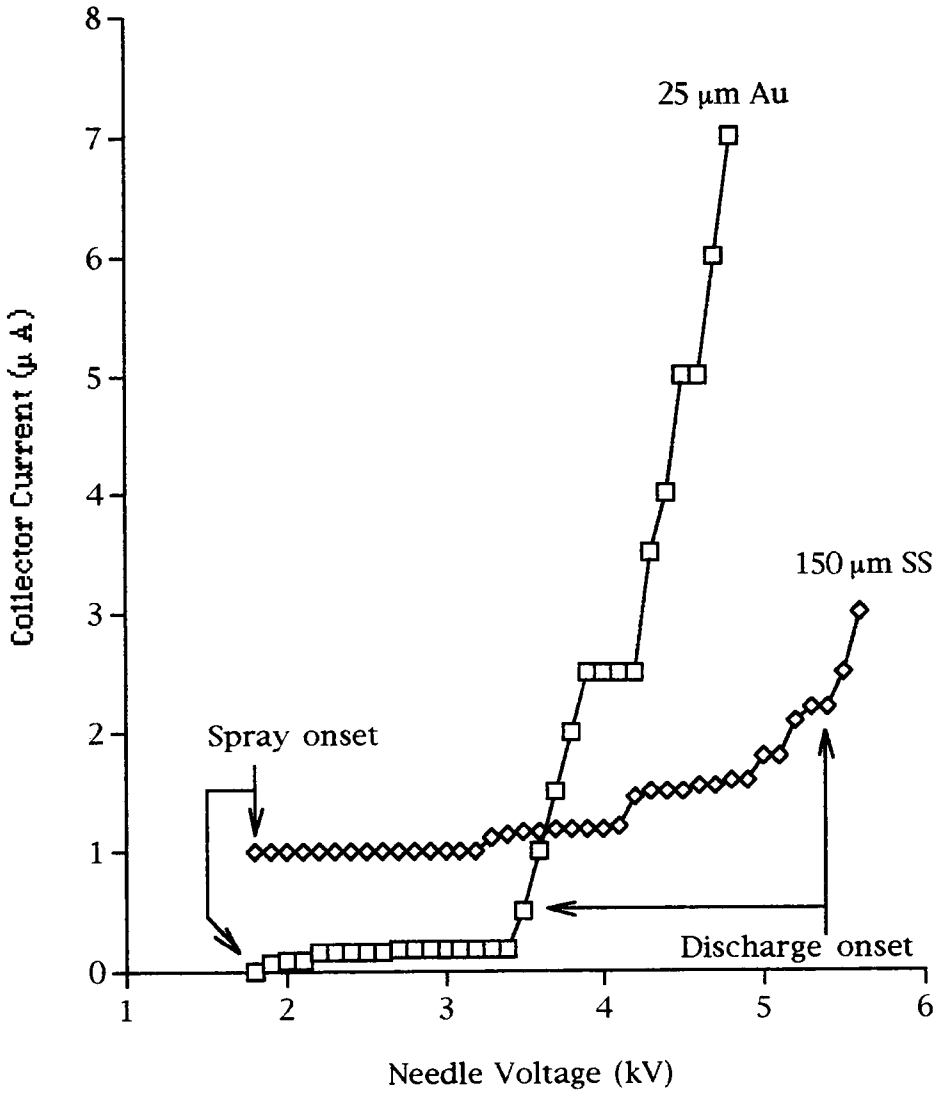



**Figure 4.3.** Collector current as a function of needle voltage while spraying 50:49:1 methanol:water:acetic acid (v/v/v) through a 25 μm i.d gold-coated capillary (Au) at a flow rate of 0.2 μL/minute and through a 150 μm i.d stainless steel needle (SS) at a flow rate of 1 μL/minute. The SS curve is offset +1 μA for clarity.

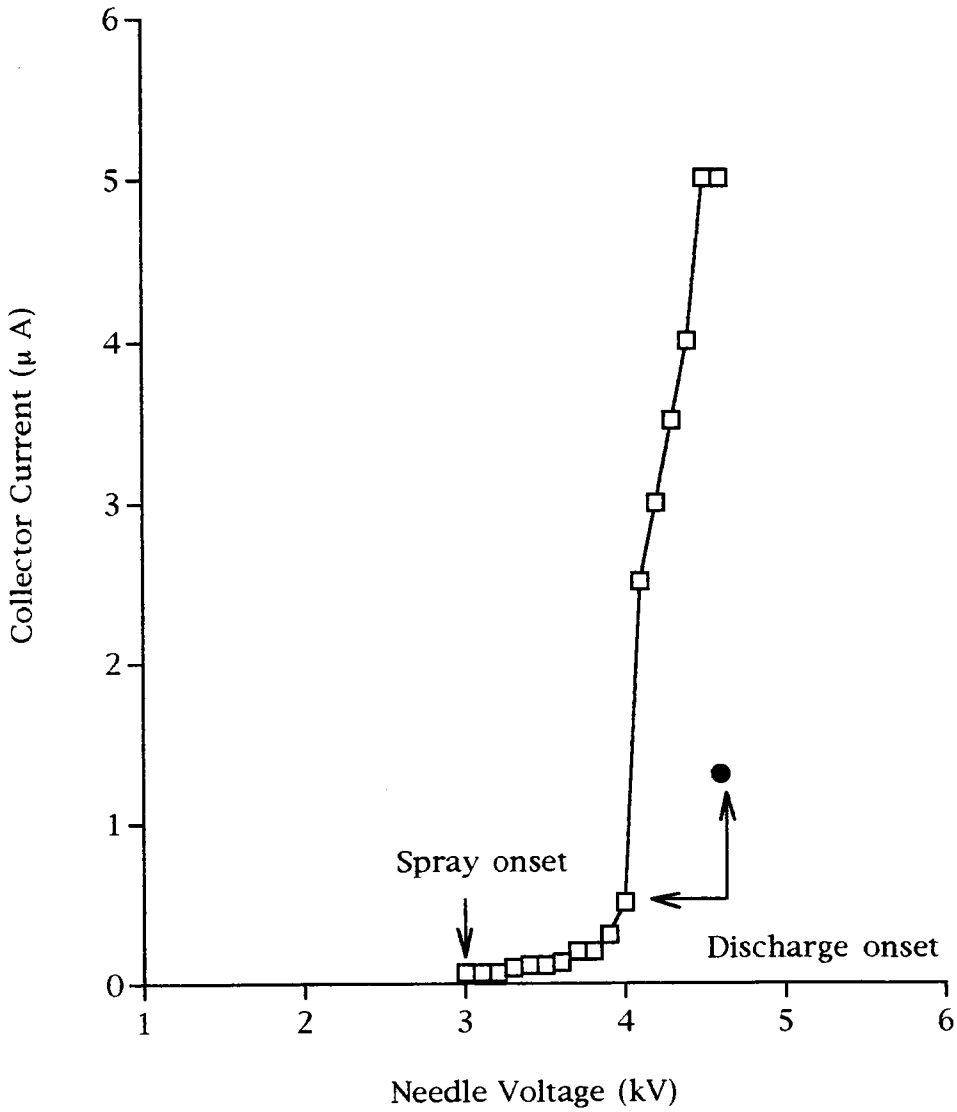



**Figure 4.4.** Collector current as a function of needle voltage while spraying pure water at a flow rate of 0.2 μL/minute through a 25 μm i.d gold-coated capillary and a flow rate of 1 μL/minute through a 150 μm i.d stainless steel needle (SS).

onset of a discharge (collector current ≥ 1μA). In addition to the solutions depicted in Figures 4.2-4.4, a stable spray was obtained with a wide variety of solutions (Table 4.4).

Finally, it is noteworthy that the data presented in Figures 4.2 - 4.4 were acquired using a single gold-coated capillary. The coating survived multiple discharges (evident from collector currents > 1 μA), indicative of its durability. Based on personal communication [249], other coated silica capillaries probably would not survive such treatment. While the capillaries described in this thesis are capable of withstanding a discharge, they do not survive a spark. Under the conditions that give rise to a spark, the gold is completely removed from the capillary tip.

## 4.2 Mass Spectrometric Applications

### 4.2.1 Continuous Infusion Experiments

While stable spray is important, a true test of the capillary performance is the generation of MS useful ions. Cytochrome C has been one of the widely used "test molecules" for assessing ES performance. Cytochrome C is a small electron-carrying heme protein containing 104 amino acid residues and having a nominal molecular weight of 12,367. ES has been used not only to determine its molecular weight, but also to probe its conformational changes. Chait *et al.* [77] have illustrated that the charge state distribution observed in the ES mass spectrum of cytochrome C is a function of solution pH. The number of protonatable basic amino acid residues available in the natural conformation of cytochrome C (a tightly bound species) is less than the

Table 4.4. Solutions used to test electrospray stability with 25 μm i.d. coated capillaries.

| Solution[a] | Concentration | Spray onset voltage (kV) (discharge onset voltage)[b] | Collector Current[c] (nA) |
|---|---|---|---|
| HPLC WATER | NEAT | 2.8 (4.1) | 50 |
| METHANOL | NEAT | 1.8 (3.5) | 30 |
| ACETIC ACID | 10 mM | 2.9 (3.5) | 70 |
| METHANOL/ WATER/ACETIC ACID | 50:49:1 (v/v/v) | 2.4 (3.6) | 300 |
| AMMONIUM ACETATE | 100 mM | 3.1 (NA) | 750 |
| $NaH_2PO_4$ | 10 mM | 3.0 (3.8) | 300 |
| $Na_2HPO_4$ | 10 mM | 3.0 (3.5) | 500 |
| $NaH_2PO_4$ | 50 mM | 3.0 (NA) | 250 |
| BORIC ACID | 100 mM | 2.8 (NA) | 500 |
| TRIS PHOSPHATE[d] | 75 mM | 3.1 (NA) | 1000 |

[a] All solutions were aqueous, except that labeled "methanol."

[b] Needle potential that produced a collector current greater than or equal to 1 μA.

[c] Collector current during stable spray.

[d] Buffer solution containing 75 mM Tris(hydroxymethyl)aminomethane and 10% methanol (v/v)

NA = not measured.

number of basic amino acid residues available in the denatured or unbound state. Since mass spectra are presented as a mass-to-charge ratio (m/z versus intensity), the appearance of the spectrum will change as a function of the number of charges per molecule. Proteins can be made to denature by changes in solution pH, solvent composition, and temperature.

The use of the gold-tipped capillaries for ES MS was initially evaluated by continuously infusing cytochrome C in aqueous solution containing 1% (v/v) acetic acid or in 75% methanol/24% water/1% acetic acid (v/v/v), as shown in Figures 4.5 and 4.6. As observed by Chait [64] and others, the natural conformation of cytochrome C can accommodate up to approximately 9 charges (protons), while the denatured conformation of cytochrome C will accommodate up to approximately 18 charges (see Figures 4.5 and 4.6). The spectra shown in Figure 4.5 from the methanolic solution indicate that the cytochrome C is in a denatured state, while the spectra shown in Figure 4.6 indicate that cytochrome C is in an undenatured state. Spectra were averaged over a 9 second period (ca. 33 scans) to simulate the peak width typically obtained for this compound by CE (using an acetic acid buffer and a 50 μm i.d. column treated with 3-aminopropyltriethoxysilane). [224] The flow rates indicated in the figure caption were those that provided the greatest electrospray stability (*i.e.*, the least amount of variation in total ion current from scan-to-scan). The variation in current was established during the instrument tuning process by monitoring the signal "on the fly" (no data collected) prior to the acquisition of data. The needle potential was held at the minimum voltage (onset voltage) necessary to maintain a stable spray for the flow rate being used. The 1 μL/minute flow rate used in these experiments for the SS needle is typical for conventional ES both at ORNL and in other

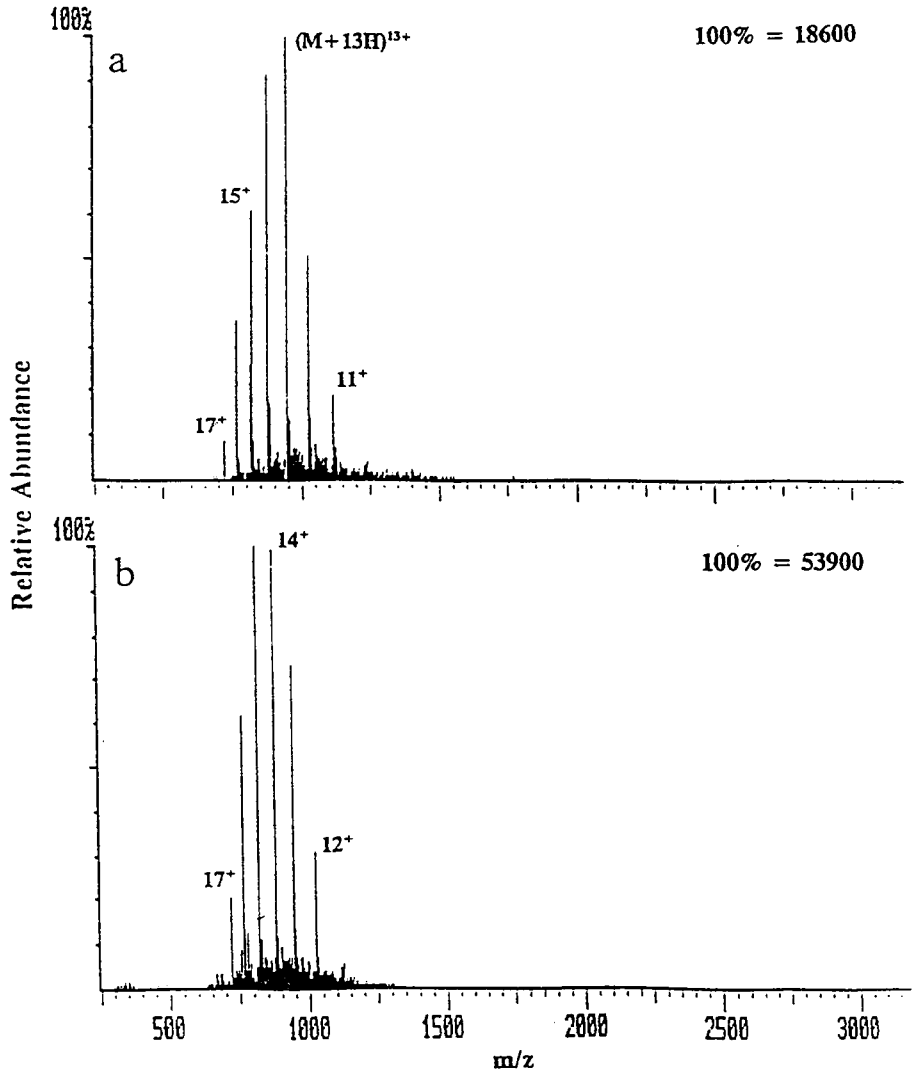



Figure 4.5. Electrospray ionization mass spectra of 21 μM cytochrome C in 75% methanol/24% water/1% acetic acid (v/v/v) using a (a) 32 gauge stainless steel needle and a flow rate of 1 μL/minute and (b) 10 μm i.d. gold-tipped capillary and a flow rate of 0.1 μL/minute. 3.2 picomoles of analyte were consumed using the SS needle and 0.32 picomoles of analyte were consumed using the Au-tipped capillary during the 9 second data averaging period. Numbers in the right hand corner represent absolute counts (of the most intense peak in the spectrum) in arbitrary units.

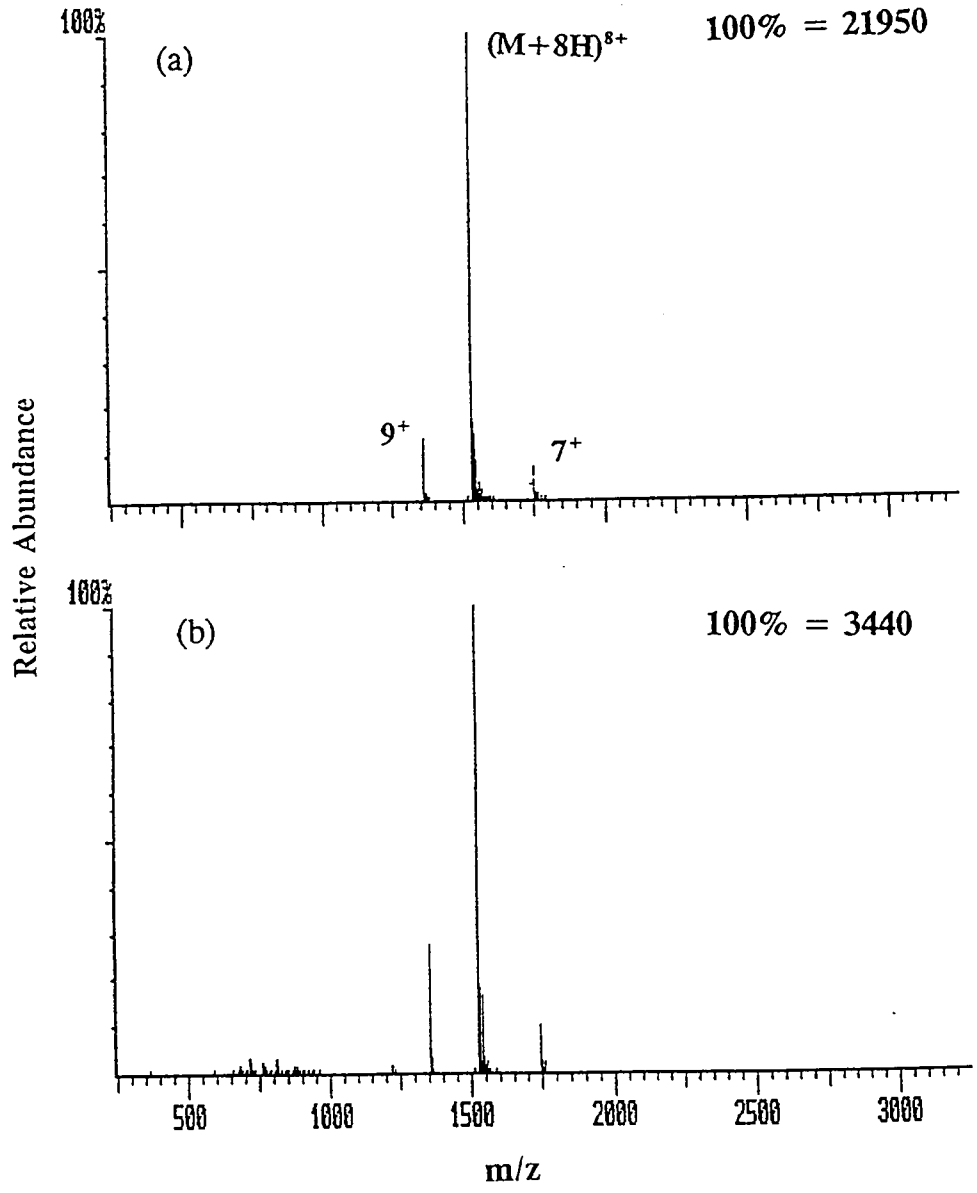



Figure 4.6. Electrospray ionization mass spectrum obtained from a 21 μM aqueous solution of cytochrome C using (a) a 32 gauge stainless steel needle with nitrogen nebulization and an infusion rate 1.0 μL/minute and (b) a 25 μm i.d. gold-tipped capillary and an infusion rate 0.1 μL/minute. Numbers in the upper right hand corner of the spectra represent absolute intensity in arbitrary units.

laboratories. Flow rates for SS needles usually range from 1 μL/minute to as high as 5 μL/minute depending upon the application. Flow rates for the fused silica capillaries have been reported to range from 0.05 to 0.1 μL/minute depending upon the capillary i.d. and the application.

Figure 4.5 compares the data obtained from the analyte at 21 μM concentration in the organic solvent solution using a 32 gauge needle (typical for infusion experiments in Ramsey's ORNL laboratory) and using a 10 μm gold-tipped capillary. The spectra are similar, with multiply charged molecular ions ranging from the $11^+$ to the $17^+$ charge state. This distribution of charge states indicates that the protein is in a denatured state as would be expected for solutions with a high methanol content. [58]

The total amount of sample consumed from the methanolic solution (Figure 4.5) using the 10 μm capillary was an order of magnitude lower than for the 32 gauge (100 μm i.d.) needle, while the intensity of the base peak was *ca.* 2.9 times greater resulting in an overall factor of 29 improvement. An overall increase in sensitivity (order of magnitude lower sample consumption, with a 6 fold increase base peak intensity) of a factor of 60 was observed when spraying a 21 μM solution of cytochrome C from aqueous solution (Figure 4.6). Such sensitivity enhancement derived from use of small i.d. capillaries has been observed elsewhere, and has been attributed to increased ionization efficiency (resulting from the formation of smaller droplets) and a decrease in mass flow (with a corresponding reduction in background). [83] For example, Smith *et al.* were able to detect 50 femtomoles of each component of a mixture of proteins using a 50 μm i.d. capillary, but were able to detect 600 attomoles of the same mixture using a 5 μm i.d. capillary. [84] A comparison of sensitivities for spraying 21 μM cytochrome C in 75% methanol/24% water/1% acetic acid

(v/v/v) using a 100 μm i.d. SS needle, and a 50, 25, or 10 μm gold-tipped capillary is provided in Table 4.5 below.

Table 4.5. A comparison of the sensitivity enhancement factors for spraying 21 μM cytochrome C in 75% Methanol/24% water/1% acetic acid from Au-tipped capillaries with varying inner diameter.

| Emitter | Sensitivity Enhancement Factor |
|---|---|
| 100 μm i.d. SS dome tipped needle | 1 |
| 50 μm i.d. gold-tipped capillary | 2 |
| 25 μm i.d. gold-tipped capillary | 4 |
| 10 μm i.d. gold-tipped capillary | 30 |
| 25 μm i.d. gold-tipped capillary | 60[a] |

[a] Sensitivity enhancement factor for spraying 21 μM aqueous solution of cytochrome C.

While the 10 μm i.d. capillary provided excellent sensitivities, plugging has precluded wide spread use.

Small changes in solvent composition have been shown to change the conformational state of cytochrome C. Comparison of Figure 4.6a with Figures 4.7 and 4.8 illustrate the effect of the solvent composition on the charge state distribution observed in the mass spectrum. The mass spectrum shown in Figure 4.7 was obtained by modifying an aliquot of the solution used to acquire the spectrum in Figure 4.6a (21 μM aqueous cytochrome C) to contain 20% (v/v) methanol. From the inset shown in Figure 4.7, it is clear that higher charge state cytochrome C (denatured) is enhanced in solution as a result of

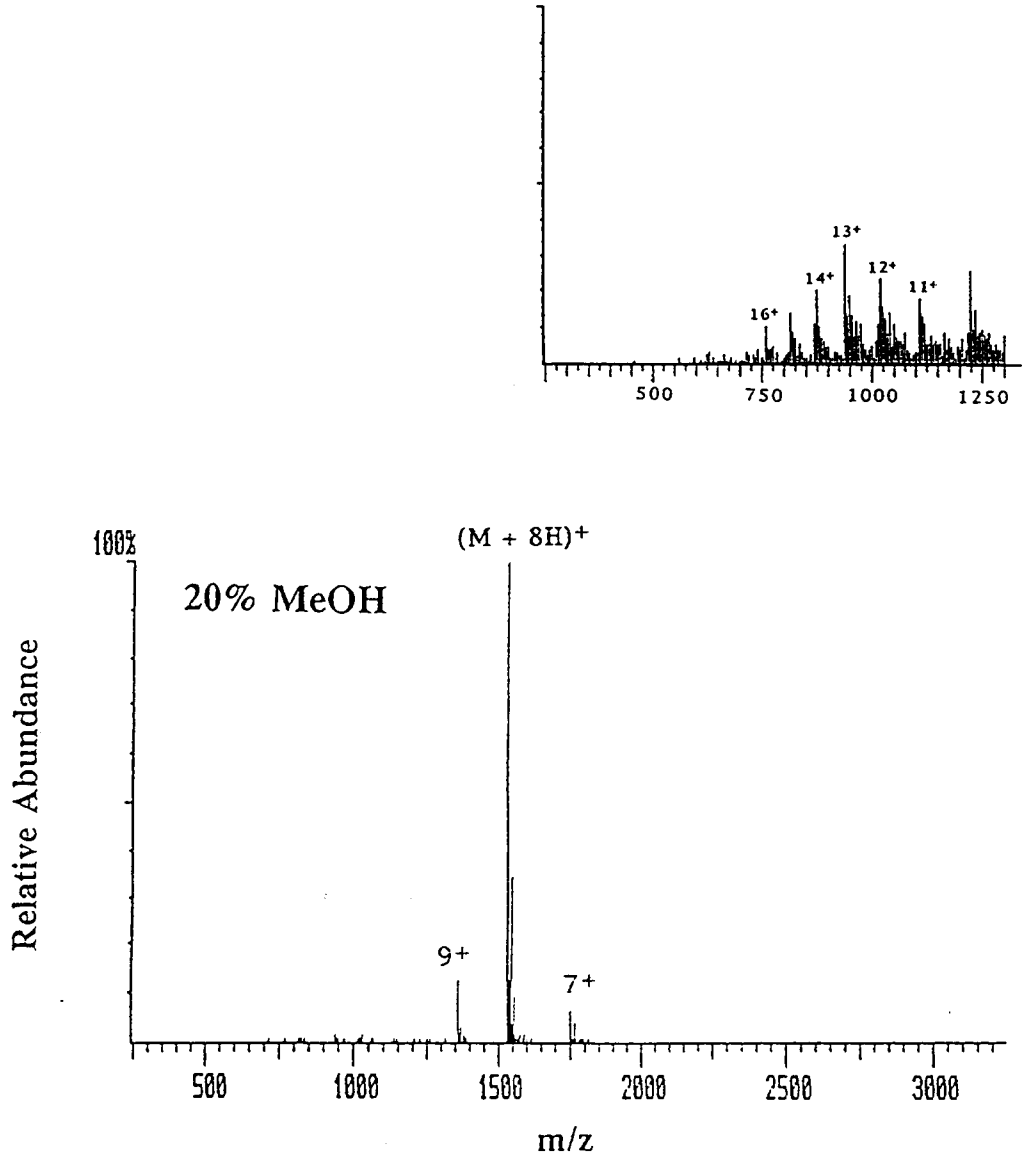



Figure 4.7. Electrospray ionization mass spectrum obtained from a 21 μM solution of cytochrome C in 80% water/20% methanol (v/v) using a 25 μm i.d. gold-tipped capillary and an infusion rate 0.1 μL/minute. The inset represents an 8X magnification of the low m/z region of the spectrum.

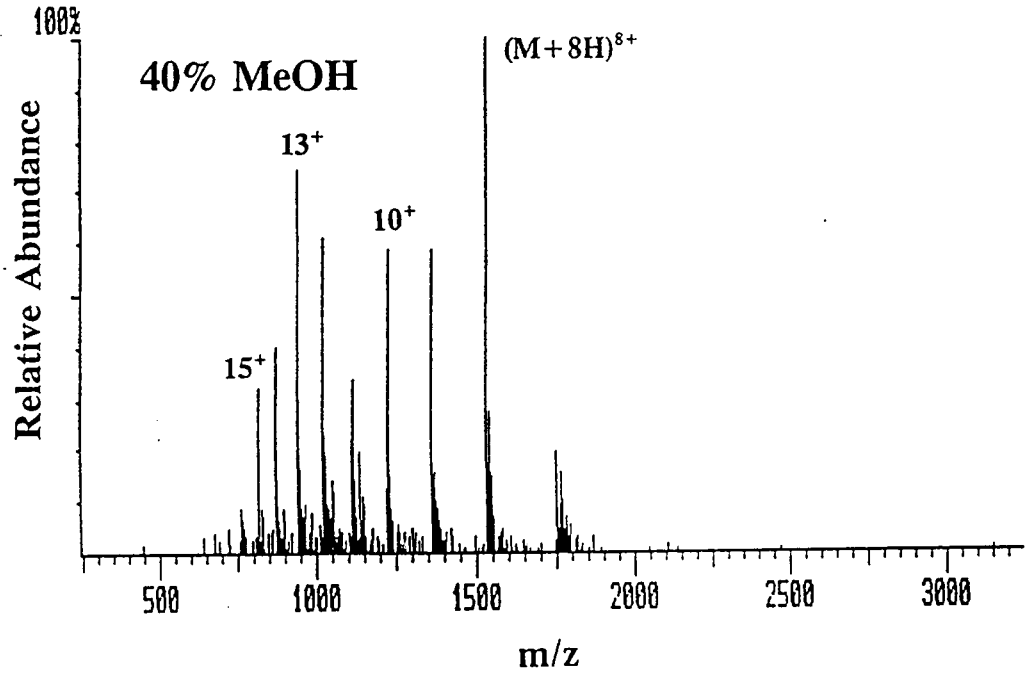



Figure 4.8. Electrospray ionization mass spectrum obtained from a 21 μM solution of cytochrome C in 60% water/40% methanol (v/v) using a 25 μm i.d. gold-tipped capillary and an infusion rate 0.1 μL/minute.

the addition of methanol to the solution. Figure 4.8 was obtained from a solution containing 40% (v/v) methanol. After the addition of 40% methanol, it is clear that a major portion of the cytochrome C has been converted to the denatured form of the protein. If the methanol is introduced as a sheath (resulting in 90% methanol from the 10:1 methanol:water flow ratio; Figure 4.9) rather than in the pre-mixed cytochrome C solution, the distribution of charge states is very similar to that observed for the methanolic solution of cytochrome C (Figure 4.5), suggesting that the denaturing process is rapid. A CE/ESI interface using the sheath flow design (for cytochrome C) has the effect of spreading the analyte signal over many possible channels, rather than a few possible channels using the aqueous solution (fewer charge states). Considering each charge state as an individual channel for ion signal, one can predict that the sensitivity and limit of detection for a given protein should be a function of the charge state distribution. For chromatographic techniques such as CE, addition of an organic co-solvent to the buffer or to the sheath can drastically degrade the sensitivity and limit of detection for proteins by distributing the analyte signal among several different charge states.

Although the effect of organic co-solvent on the CE/ESI experiment can be detrimental to sensitivity, the results are quite interesting from a solvation point of view. The small peaks that appear between the discrete large peaks of the 2 spectra shown in Figure 4.5 can be attributed to various degrees of solvation of the cytochrome C. The spectra shown in Figure 4.6 were acquired from a purely aqueous solution of cytochrome C and do not contain the characteristic "solvated" ions evident in the spectra of Figure 4.5. Careful observation of the spectra presented in Figures 4.5 and 4.6 suggest that the denatured cytochrome C is more solvated than the natural conformation of

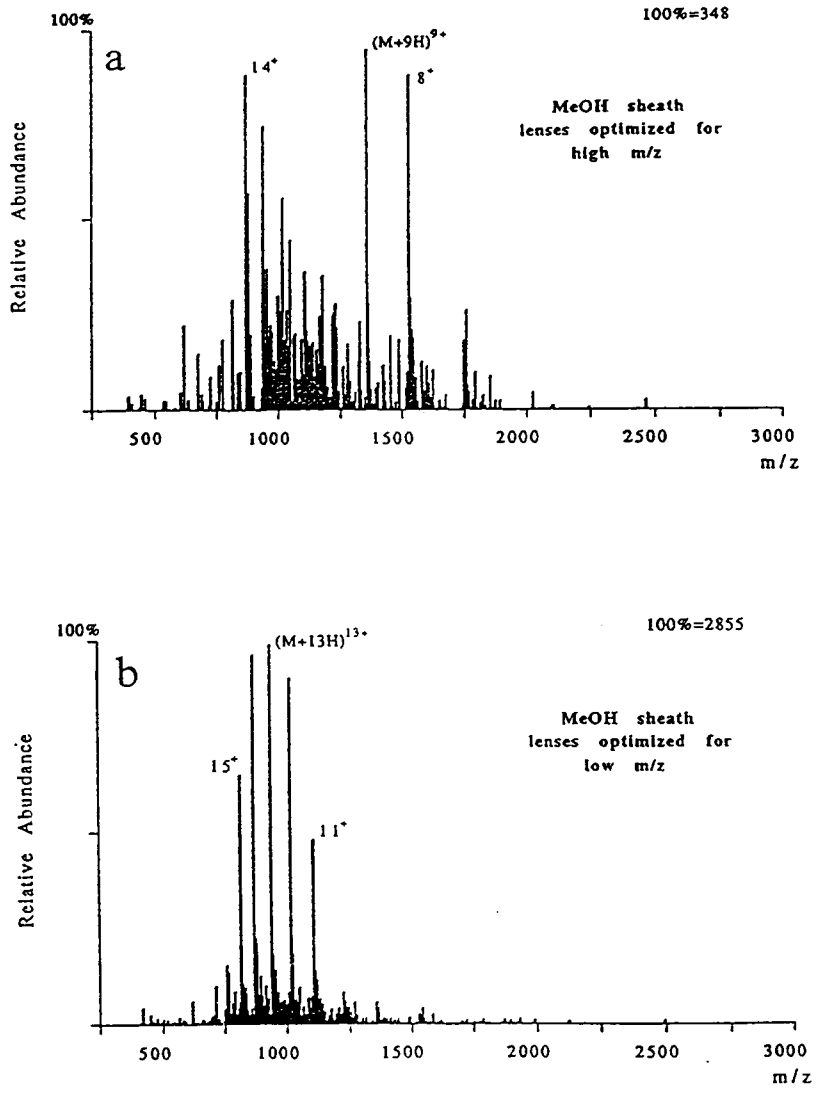



Figure 4.9. Electrospray ionization mass spectra obtained from a 21 μM aqueous solution of cytochrome C using the methanol sheath source shown in Figure 4.1. The interface was tuned to optimize signal intensity for (a) high m/z ions and (b) low m/z ions. The methanol was delivered at a flow rate of 1 μL/minute and the 21 μM aqueous cytochrome C solution was delivered at a flow rate of 0.1 μL/minute. Numbers in the upper right hand corner of the spectra represent absolute intensity in arbitrary units.

cytochrome C. It is possible to detect the presence of water or methanol by determining the mass separation of the smaller peaks located between the larger peaks. Methanol solvation peaks will be separated by a mass equal to 32/z (where z is the number of protons attached to the unsolvated peak) and water solvation peaks will be separated by a mass equal to 18/z. These experiments, however, did not provide the resolution necessary to determine contributions from the solvent clusters. An instrument capable of high resolution, such as the Fourier Transform (FT) ICR, would be ideal for these types of experiments. [250,251] Also, a peculiarity in tuning the ion trap interface has precluded any definitive statement about the extent to which cytochrome C is solvated. The appearance of the mass spectrum can be dramatically changed by minor changes in the tuning of the ion trap interface. Using an aqueous solution of cytochrome C and a gold-tipped capillary, the spectra shown in Figure 4.10 can be obtained. Figure 4.10a is a mass spectrum similar to that shown in Figure 4.5, and was obtained with the interface tuned to the high m/z species (low charge state). Using the exact same solution, and tuning to the low m/z species, a spectrum like that shown in Figure 4.10b can be obtained. Comparison of the absolute intensity numbers shown in the upper right hand corner of each spectrum indicates that only a small fraction of the aqueous analyte exists in the denatured state. Also, the only solvent present is water and the solvated peaks of the higher charge state species (i.e., the "noise" between peaks) are much larger than the solvated lower charge state species. This result suggests that the extent to which the ions are solvated is, perhaps, more dependent on the conformation of the protein than on the solvent. The denatured protein, having more accessible charge sites, and higher charge should be more extensively solvated.

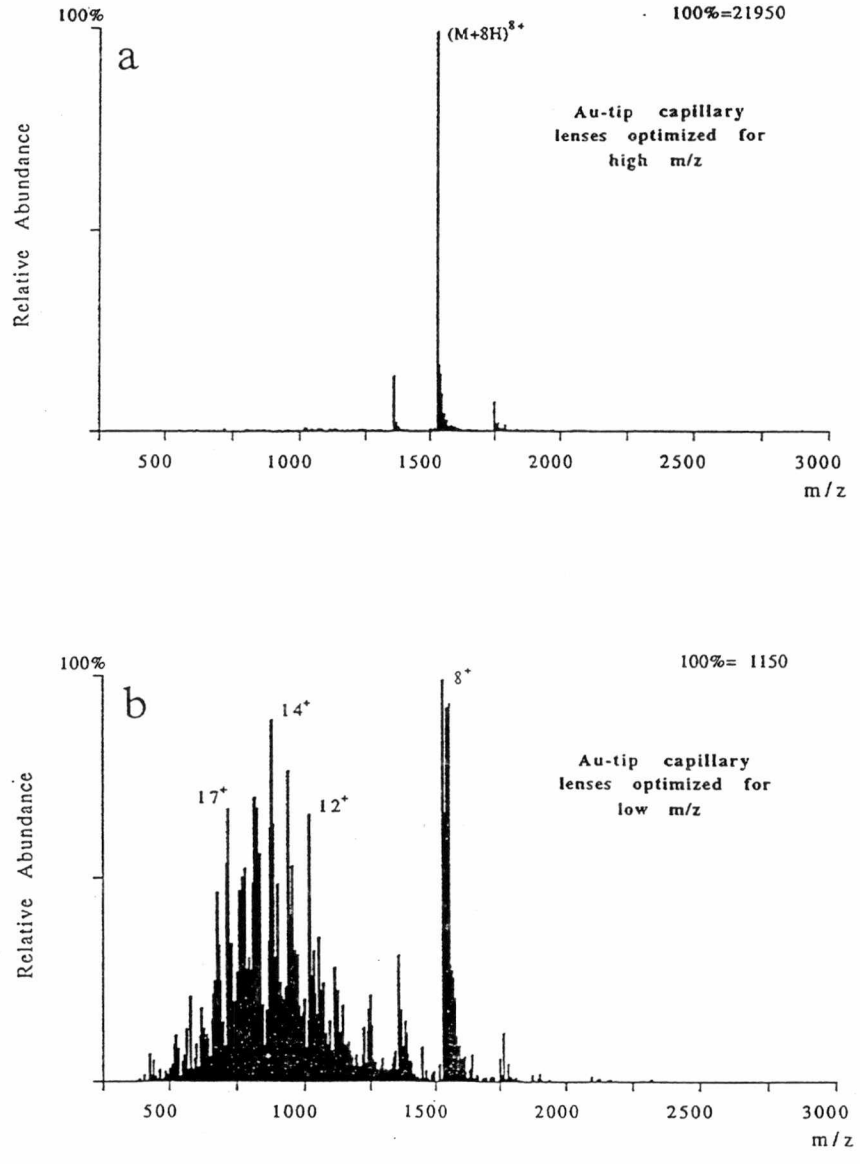



Figure 4.10. Electrospray ionization mass spectrum obtained from a 21 μM aqueous solution of cytochrome C using a 25 μm i.d. gold-tipped capillary and an infusion rate 0.1 μL/minute. The interface was tuned to optimize signal intensity for (a) high m/z ions and (b) low m/z ions. Numbers in the upper right hand corner of the spectra represent absolute intensity in arbitrary units.

### 4.2.2 Figures of Merit

The amount of material available for precious samples is often limited to extremely small volumes of solution. The ability to continuously infuse solution at low (relative to conventional ES) flow rates (such as 0.05 μL/minute) using the small i.d. capillaries is potentially advantageous and could lower limits of quantitation. For continuous infusion of 0.17 μM cytochrome C in acidified aqueous solution using the Au-tipped capillary, a detectable signal (with a S/N = 2) could be obtained from single scans using a 50 msec ion injection time into the ion trap, corresponding to 7 attomoles of sample consumed (Figure 4.11). The S/N was established by dividing the signal intensity average from 12 scans by the standard deviation of that average (avg./σ). A usable dynamic range (Figure 4.12) of three order of magnitude (minimum) could be obtained using continuous infusion of cytochrome C in acidified aqueous solution. The slope of the log/log plot shown in Figure 4.12 is 0.90 and should be 1.0 for a linear correlation. The log/log plot was necessary to illustrate the three orders of magnitude (a linear plot does not show this range clearly). The individual data points of Figure 4.12 were obtained by summing the intensity of the $8^+$ and $9^+$ charge states observed in the spectrum from an aqueous solution of cytochrome C. While low continuous infusion flow rates are appealing, even less material would be necessary for injection onto capillaries used for capillary electrophoresis. Therefore, the next logical step was to interface the gold-tipped ES capillaries with capillary electrophoresis. The next section describes preliminary CE/ES results.

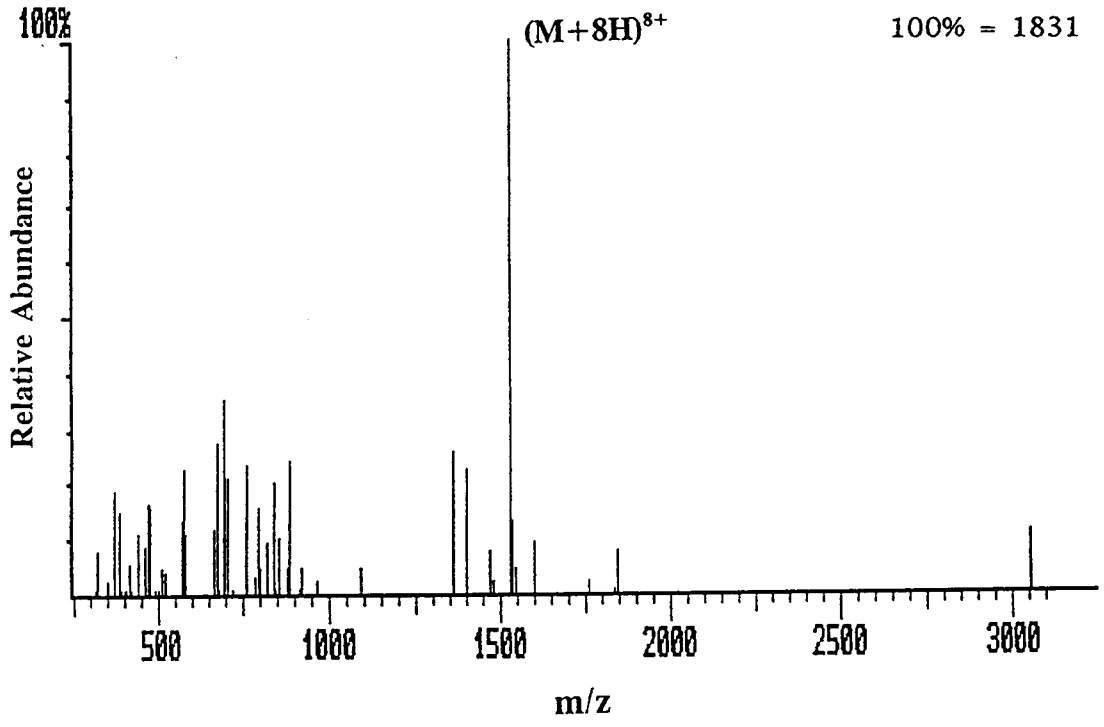



Figure 4.11. Single scan (50 msec injection time) mass spectrum of cytochrome C obtained from a 0.17 μM aqueous solution (1% acetic acid). The spectrum was acquired under continuous infusion conditions at a flow rate of 0.05 μL/minute using a 25 μm i.d. gold-tipped capillary.

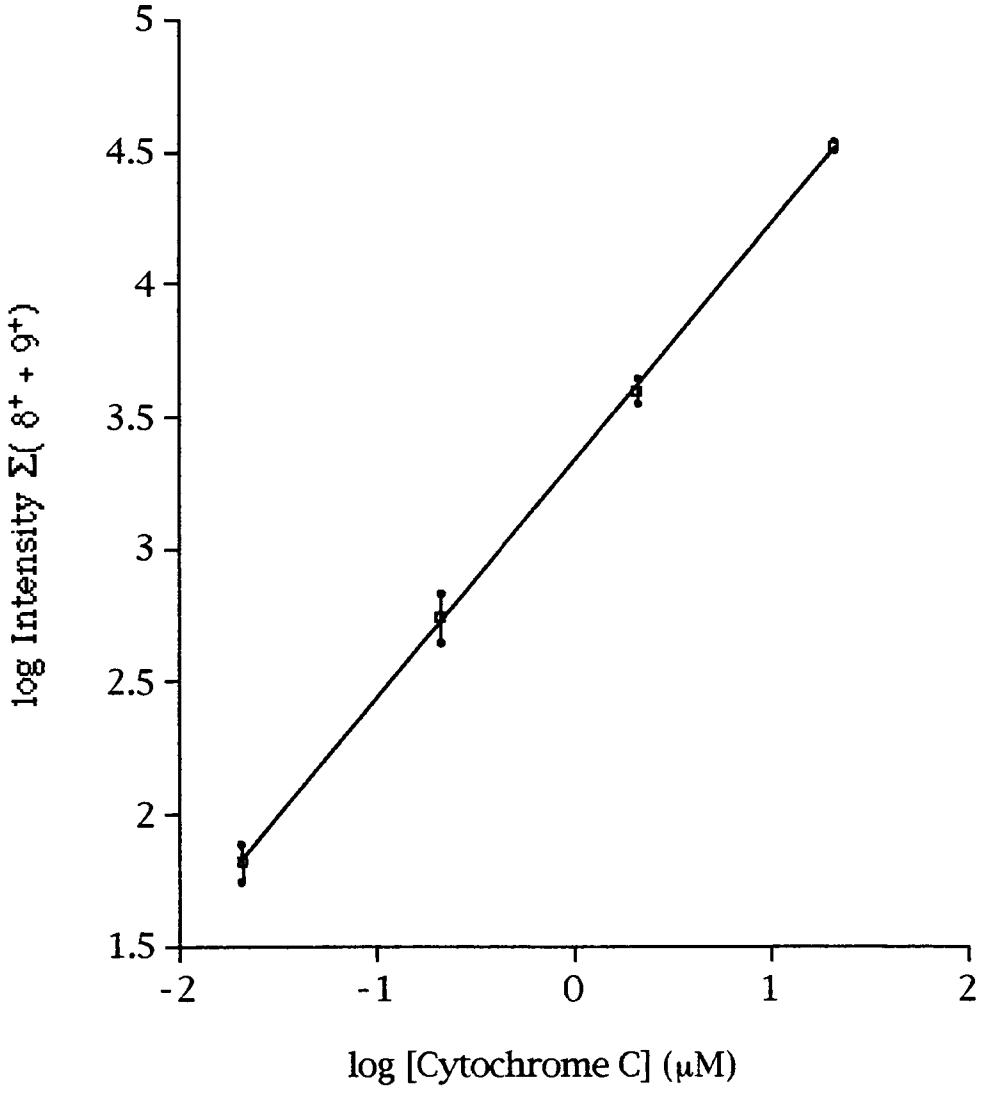



**Figure 4.12.** Plot of mass spectrometric response as a function of the cytochrome C concentration. A usable dynamic range of three orders of magnitude (minimum) is observed. All solutions were 99% water and 1% acetic acid. The line is described by the following equation: y = 0.90x + 3.33 with a correlation coefficient ($r^2$) of 0.9997.

### 4.2.3 CE/ES/MS

CE/ES is an approach to analyzing complex mixtures while consuming very little material. Figure 4.13 shows the total ion electropherograms (total ion signal as a function of time) obtained for aqueous solutions of leucine enkephalin varying in concentration from 9 to 45 μM. Quantities injected ranged from 17 to 710 femtomoles; a 50 μm i.d. gold-tipped column was employed. The S/B (estimated by dividing the intensity of the analyte peak by the intensity of the background peaks) in the mass spectrum (taken at the apex of the peak in the electropherogram) for the lowest quantity analyzed (Figure 4.14) is about 3. Assuming a linear calibration curve in this region, an injection of 11 femtomoles was estimated to be the limit of detection (S/N =2). Similar values have been reported for CE/ITMS using a 50 μm i.d. column and a liquid sheath interface. [83,93] Our column efficiency (theoretical plate number), however, was ca. 3 to 5 times lower, suggesting that a better limit of detection could be obtained by optimizing chromatographic (e.g., by coating the column interior) conditions to provide higher, narrower peaks. The use of smaller i.d. columns should enhance the sensitivity in CE/ES, as it did the continuous infusion experiments. Using a 50 μm i.d. gold-coated column with an interior coating of aminopropyltriethoxysilane and a 10 mM acetic acid buffer (pH 3.5) , a separation of leucine-enkephalin, xenopsin, neurotensin and bradykinin shown in the total ion electropherogram of Figure 4.15 could be obtained. The amount of each peptide injected and the CE conditions are provided in the figure caption. These peptides or various combinations of these peptides are often used as a test mixture for CE/ES MS. [93] Again, by optimizing CE conditions, it should be possible to improve the resolution.

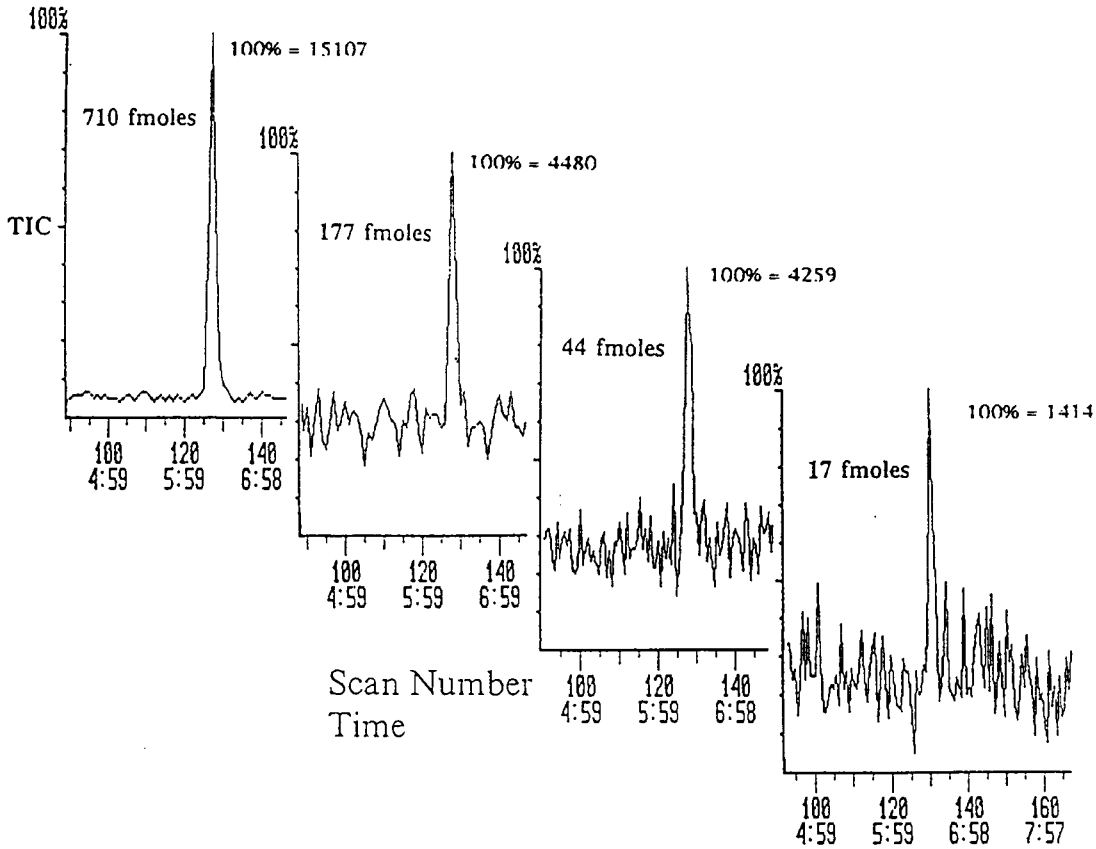



Figure 4.13. Total ion current electropherograms for multiple injections of leucine enkephalin on a 50 μm i.d. gold-tipped capillary.

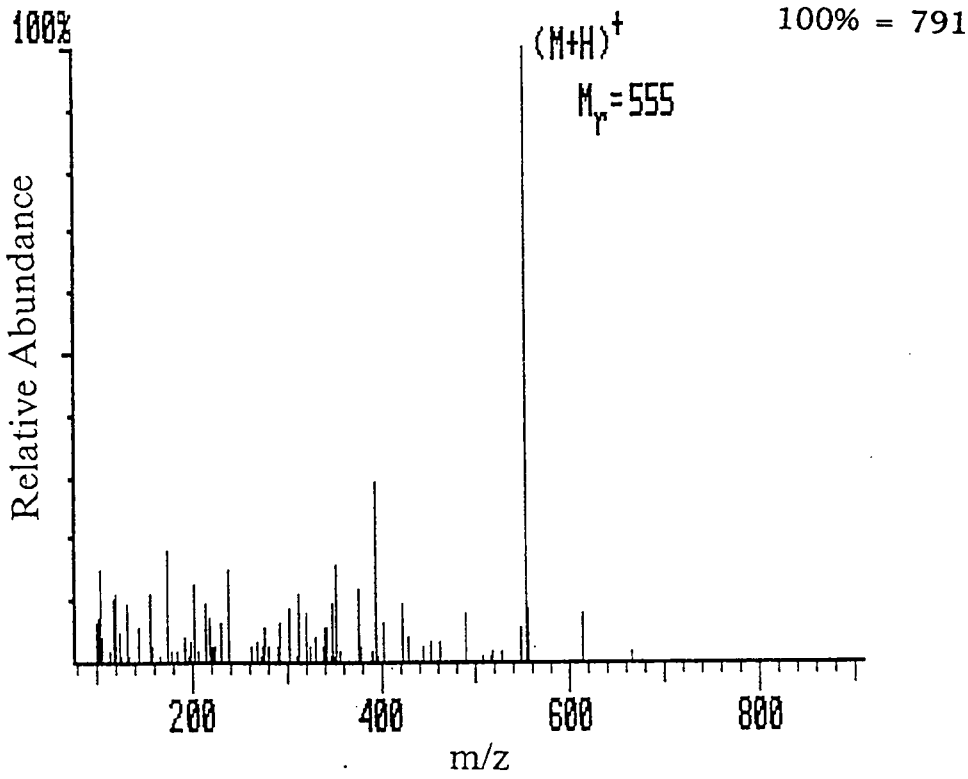



Figure 4.14. Electrospray ionization mass spectrum (single scan) from a 17 fmole injection of leucine enkephalin using capillary electrophoresis.

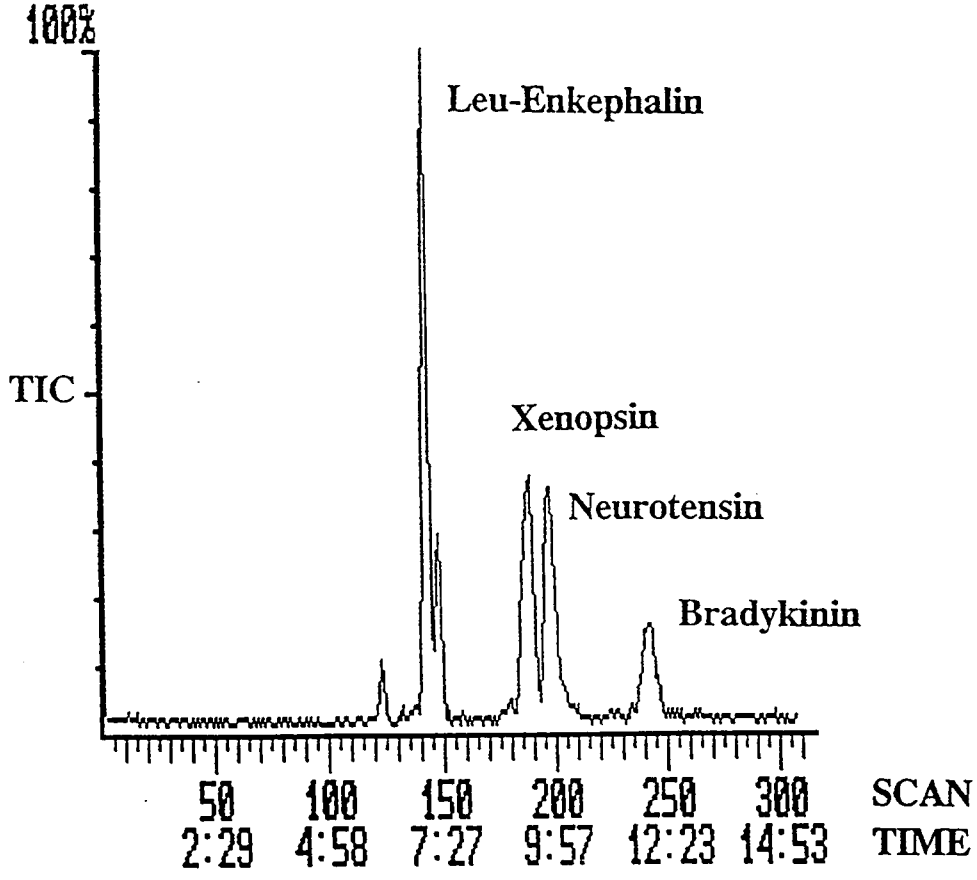



Figure 4.15. Total ion current (TIC) electropherogram for a single injection of a mixture of leucine-enkephalin (2.16 picomoles), xenopsin (730 femtomoles), neurotensin (622 femtomoles), and bradykinin (536 femtomoles) on a 50 μm i.d. gold-tipped capillary. Peptides were injected electrokinetically (6 seconds at 20 kV) from an aqueous solution onto a 60 cm long fused silica column. The CE voltage was maintained at 20 kV. The two peaks adjacent to Leu-Enkephalin (one before and one after) were not identified.

## 4.3 Conclusions

Gold-tipped capillaries prepared using an organofunctional silane to improve the adhesion of the gold film to the silica columns have been shown to be useful in ES MS and CE/ES MS, providing interfaces that are quite durable. They are capable of withstanding multiple discharges and have lifetimes that exceed 100 hr of operation. While not unique to this micro-electrospray source, some interesting observations were made when the solvent system was varied. Suggestions for future work in this area are presented in Chapter 6. The gold coating, unfortunately, did not survive normal EH operation. Several attempts to acquire EH data were not successful. A spark between the emitter and extractor electrode could be a possible explanation for why the gold layer was removed.

# Chapter 5

## Electrohydrodynamic Mass Spectrometry As A Probe of Solution Chemistry

Mass spectrometry (MS) offers an alternative approach to bulk phase methods of probing solvation which has proven capable of resolving individual solvent clusters in the gas-phase. For example, a free-jet vapor expansion can be used to sample or produce neutral clusters with very low internal energy, followed by electron ionization or photoionization MS to generate ion/solvent clusters. [181,183,184,185] By controlling cluster growth due to cooling during expansion, chemistry representative of vapor equilibria (as opposed to condensed-phase chemistry) can be probed for volatile solvents such as methanol and water. Although species ultimately detected are ionic, it is primarily the chemistry of neutral clusters which has been so characterized. High-pressure MS, on the other hand, has been a valuable probe of gas-phase ionic solvent cluster thermodynamics. [163,252] In these experiments, clusters are grown by gas-phase interactions between ions and solvent vapor at relatively high pressures. As with a jet expansion, cluster growth occurs in isolation from the influence of bulk solvent and counterions, so these studies also do not reflect condensed-phase ion solvation.

There are several MS "ionization" methods believed to sample ions directly from solution. Among these, fast atom bombardment (FAB), liquid secondary ion MS (LSIMS), [7,30] electrospray (ES), [58] and thermospray (TS) [253,254] MS are the most widely used for analytical MS of solutes. In each of these methods, there is substantial energy input either coincident with

sampling (in FAB and LSIMS) or during desolvation at relatively high pressure subsequent to sampling (in ES and TS). These processes are essential for the normal application of the methods, but can seriously complicate the relationship between clusters detected and those originally present in solution.

Such complications may be largely avoided in electrohydrodynamic (EH) MS, whereby "preformed" ions are desorbed directly from a liquid matrix by the action of a strong electric field ($10^6$ V/cm) applied to solutions contained in a metal capillary emitter located within an evacuated ion source. [97] The EH desorption process adds very little internal energy, resulting in simple mass spectra devoid of fragmentation, and often reflecting aspects of solution equilibria. [97,102,226] Ion/solvent clusters are often detected [97,226,119] and have been used as a primary ion source for liquid secondary ion MS. [204] In earlier work, [112] EH spectra obtained from mixed glycerol/water solutions appeared to reflect preferential solvation of $Na^+$ by glycerol. However, spectral stability and precision were poor, precluding firm conclusions about the distribution of ion/solvent clusters.

This chapter presents results obtained using the modified EH source described in Chapter 2. The modified source has provided improved performance for sampling volatile solutions. The present system still requires a small component of low-volatility solvent for stable emission. For the majority of the results presented in this chapter, a binary solvent system consisting of water and glycerol was therefore chosen again to test whether this method of creating gas-phase ion/solvent clusters accurately reflects selective condensed-phase ion/solvent interactions.

## 5.1 Preferential Solvation

As shown in Figure 5.1, the most intense peaks (labeled "A") in the spectrum of 40 mM HCl in 95/5 (v/v) water/glycerol correspond to the $[G_2 + H]^+$ and $[G_3 + H]^+$ clusters (where G = glycerol, $C_3H_8O_3$). In light of the relatively low (1.27 mole %) glycerol concentration, this dominance must result either from glycerol enrichment in the sampling region (resulting from preferential evaporation of water); from greatly differing instrumental responses to aqueous and glycerol clusters; or from preferred solvation of the proton by glycerol in the mixed solvent solution. Firm conclusions about the preferential solvation of the proton by glycerol require addressing each of these possibilities in turn.

The first and most obvious explanation for the more intense glycerol clusters, glycerol enrichment, was tested by selecting a solute that will preferentially accommodate water in the same 95/5 (v/v) water/glycerol solvent mixture. If glycerol enrichment at the emitter site is responsible for more intense glycerol clusters, then even a solute expected to prefer water should show a preference for glycerol, due simply to the unavailability of water at the emission site. The enthalpy of solvation of both $TMA^+$ and $TEA^+$ in water is more negative than the enthalpy of solvation in methanol (Table 5.1). The lower enthalpies of solvation in water indicate a stronger interaction of the ions with water (preferred solvation). The same trend in enthalpies should be true if glycerol (another alcohol) is used instead of methanol. Tetramethylammonium ($TMA^+$) and tetraethylammonium ($TEA^+$) were therefore selected to test for water depletion.

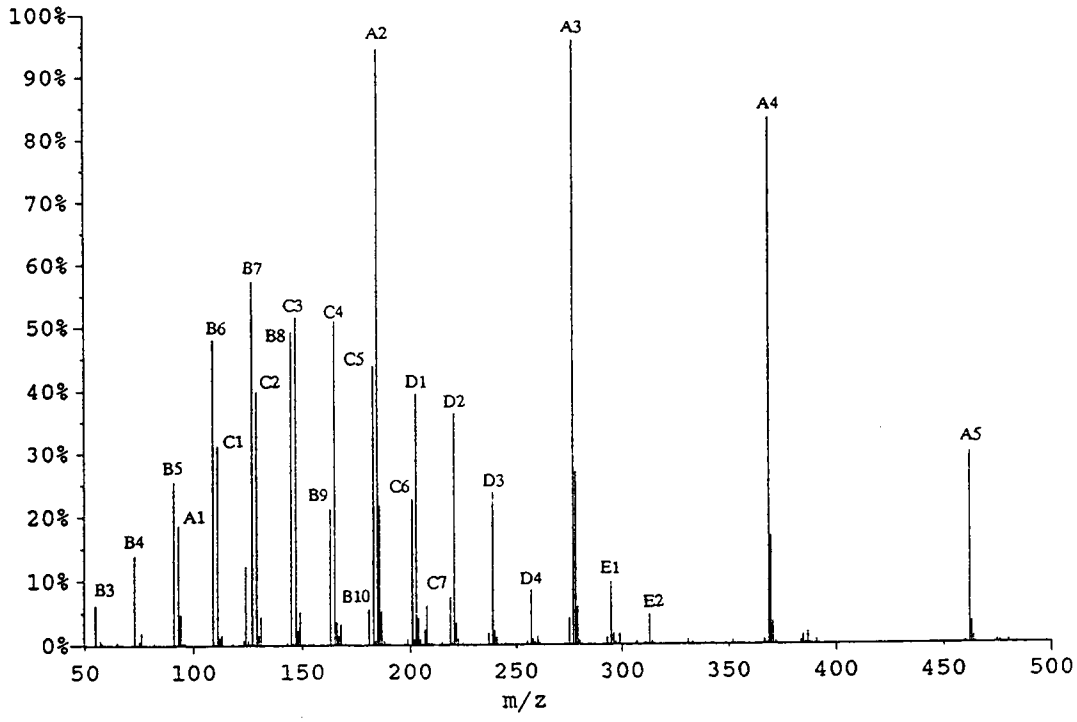



Figure 5.1. Electrohydrodynamic ionization mass spectrum of 40 mM HCl in 95% water / 5% glycerol (v/v). Clusters are labeled as follows: $A_n = [G_n + H]^+$; $B_n = [(H_2O)_n + H]^+$; $C_n = [G_1 + (H_2O)_n + H]^+$; $D_n = [G_2 + (H_2O)_n + H]^+$; $E_n = [G_3 + (H_2O)_n + H]^+$ (where G denotes glycerol). See Table 5.2 for list of ions and their relative abundance.

Table 5.1. Solvation enthalpies* (kJ $mol^{-1}$) of tetraalkylammonium ions in water and methanol at 25° C.

| tetraalkylammonium ion | water | methanol |
|---|---|---|
| tetramethylammonium ($TMA^+$) | -523.7 | -517.7 |
| tetraethylammonium ($TEA^+$) | -508.7 | -493.5 |

* Solvation enthalpies were obtained from reference [242].

The spectra of solutions containing tetramethylammonium ($TMA^+$) and tetraethylammonium ($TEA^+$) bromide (Figure 5.2) from a 95/5 (v/v) water/glycerol solvent mixture reveal that water clusters of $TMA^+$ and $TEA^+$ are more abundant than glycerol clusters of $TMA^+$ and $TEA^+$. This observation is consistent with known solution chemistry trends of these ions in water and alcohol solutions, [242] and indicates that water is the preferred solvent. Regardless of the solute, spectra containing peaks attributable to water clusters would not be observed (detected) if complete evaporation of water from the emitter region was occurring. Figures 5.1 and 5.2 do not, however, eliminate the possibility of preferential evaporation of water short of complete evaporation. Preferential evaporation of water may contribute to the appearance of the spectrum and precludes unambiguous interpretation.

The second possible explanation for the dominance of glycerol clusters in the spectrum shown in Figure 5.1 is related to grossly differing responses for the different clusters. Different responses for ions having different m/z could arise from either analyzer (transmission) or detector mass discrimination, or from sampling bias. Sector instruments usually do not exhibit mass discrimination over narrow mass ranges, such as that scanned here. Also, post-acceleration detection (Figure 2.9) decreases the chance for significant detector bias (which in any case would favor the lighter water clusters). In-flight desolvation (evaporation) can also contribute to transmission bias. Ions that experience solvent evaporation prior to exiting the ESA (Figure 2.9) will not be detected using the normal experimental conditions described in section 2.3. The results of experiments designed to characterize the in-flight evaporation are discussed later in this chapter.

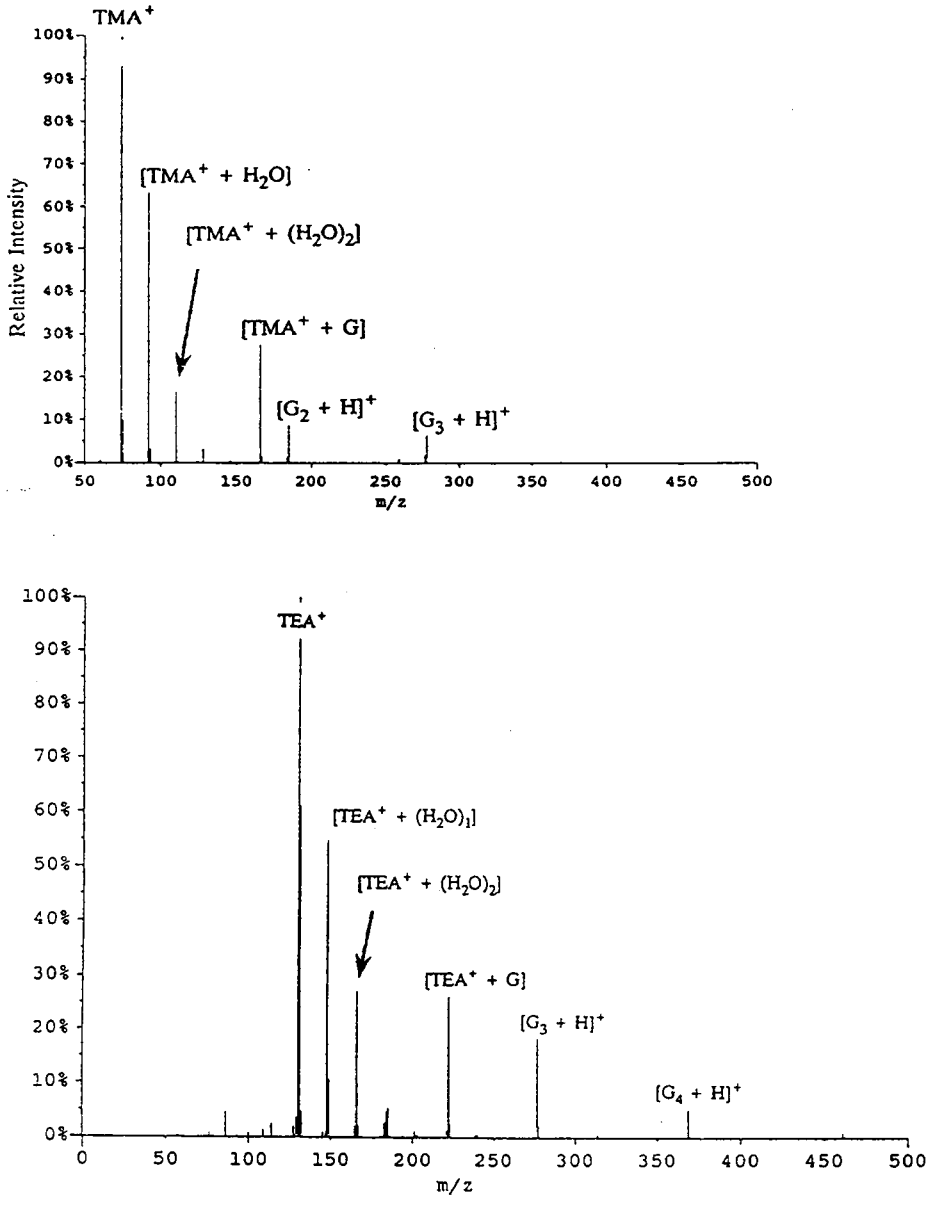



Figure 5.2. Electrohydrodynamic ionization mass spectrum of (a) 40 mM tetramethylammonium ($TMA^+$) bromide and (b) 40 mM tetraethylammonium ($TEA^+$) bromide in 95/5 (v/v) water/glycerol solvent mixture. Solvated peaks are labeled in the spectra (where G denotes glycerol).

They indicate that in-flight evaporation is extensive, in some cases, and complicates the quantitative interpretation of the cluster distributions. However, it does not appear to be sufficient to account for the dominance of glycerol clusters in Figure 5.1.

While the two sources of discrimination discussed above are unlikely to affect the measured cluster distribution, sampling bias resulting from differences in diffusion rates may be significant, as it has been observed in EH experiments. [107] For example, the sampling efficiency from a mixture of quaternary ammonium salts in glycerol increased from tetramethylammonium to tetrabutylammonium and then decreased for the tetrapentylammonium ion. [109] The differences in sampling efficiency resulted from the convolution of increased ion-solvent interactions (solvation) for the smaller quaternary ammonium ions and reduced mass transport of the larger quaternary ammonium ions to the emission site.

Boggess has shown that increasing flow (by using a syringe pump to deliver solution to the emitter tip) reduces this bias. [110] In a test to assess sampling bias due to mass transport in solution, a syringe pump was used to deliver solution to the emitter at flow rates of 7.5 and 10 μL/hour (compare with the vacuum induced flow at *ca.* 5 μL/hour for Figure 5.1). Table 5.2 lists the ions present at each flow rate and their relative abundances for comparison. Glycerol clusters are the most abundant in each experiment; bias due to mass transport is apparently not a problem. In any event, the bias would be against the larger solvent clusters (slower diffusion), which is not consistent with the spectrum shown in Figure 5.1 where the heavier glycerol clusters are the most intense. The distribution of the clusters is assessed in section 5.2 below.

Table 5.2. List of prominent ions appearing in EH mass spectra of 40 mM HCl in 95/5 (v/v) water/glycerol solvent mixture using a flow rate of 5, 7.5 and 10 μL/hour. Entries represent the average from at least 3 replicates and corresponding standard deviation (σ).

| Chemical Species | 5 μL/hr R.I. ± σ | 7.5 μL/hr R.I. ± σ | 10 μL/hr R.I. ± σ |
|---|---|---|---|
| $[(H_2O)_1 + H]^+$ | | 0.03 ± 0.01 | |
| $[(H_2O)_2 + H]^+$ | | 0.07 ± 0.02 | 0.05 ± 0.02 |
| $[(H_2O)_3 + H]^+$ | 0.09 ± 0.05 | 0.14 ± 0.04 | 0.13 ± 0.02 |
| $[(H_2O)_4 + H]^+$ | 0.18 ± 0.09 | 0.34 ± 0.09 | 0.33 ± 0.02 |
| $[(H_2O)_5 + H]^+$ | 0.27 ± 0.12 | 0.46 ± 0.12 | 0.48 ± 0.05 |
| $[(H_2O)_6 + H]^+$ | 0.48 ± 0.15 | 0.56 ± 0.13 | 0.60 ± 0.02 |
| $[(H_2O)_7 + H]^+$ | 0.57 ± 0.24 | 0.47 ± 0.15 | 0.57 ± 0.05 |
| $[(H_2O)_8 + H]^+$ | 0.47 ± 0.27 | 0.23 ± 0.09 | 0.47 ± 0.04 |
| $[(H_2O)_9 + H]^+$ | 0.21 ± 0.15 | 0.09 ± 0.03 | 0.26 ± 0.12 |
| $[(H_2O)_{10} + H]^+$ | 0.06 ± 0.05 | 0.03 ± 0.03 | 0.19 ± 0.12 |
| $[(H_2O)_{11} + H]^+$ | | | 0.09 ± 0.03 |
| $[G_1 + H]^+$ | 0.23 ± 0.10 | 0.24 ± 0.05 | 0.30 ± 0.10 |
| $[G_2 + H]^+$ | 0.94 ± 0.10 | (1.0) | (1.0) |
| $[G_3 + H]^+$ | 0.91 ± 0.11 | 0.94 ± 0.05 | 0.81 ± 0.04 |
| $[G_4 + H]^+$ | 0.53 ± 0.22 | 0.46 ± 0.04 | 0.31 ± 0.03 |
| $[G_5 + H]^+$ | 0.17 ± 0.12 | 0.13 ± 0.03 | 0.21 ± 0.02 |
| $[G_1 + (H_2O)_1 + H]^+$ | 0.32 ± 0.12 | 0.47 ± 0.07 | 0.44 ± 0.06 |
| $[G_1 + (H_2O)_2 + H]^+$ | 0.40 ± 0.14 | 0.59 ± 0.08 | 0.59 ± 0.02 |
| $[G_1 + (H_2O)_3 + H]^+$ | 0.47 ± 0.14 | 0.68 ± 0.08 | 0.73 ± 0.07 |
| $[G_1 + (H_2O)_4 + H]^+$ | 0.44 ± 0.12 | 0.51 ± 0.11 | 0.73 ± 0.07 |
| $[G_1 + (H_2O)_5 + H]^+$ | 0.37 ± 0.10 | 0.36 ± 0.12 | 0.63 ± 0.11 |
| $[G_1 + (H_2O)_6 + H]^+$ | 0.20 ± 0.08 | 0.15 ± 0.05 | 0.42 ± 0.11 |
| $[G_1 + (H_2O)_7 + H]^+$ | 0.07 ± 0.05 | 0.07 ± 0.01 | 0.21 ± 0.08 |
| $[G_1 + (H_2O)_8 + H]^+$ | | | 0.09 ± 0.04 |
| $[G_1 + (H_2O)_9 + H]^+$ | | | 0.05 ± 0.03 |

Table 5.2. continued.

| | | | |
|---|---|---|---|
| $[G_2 + (H_2O)_1 + H]^+$ | 0.35 ± 0.10 | 0.37 ± 0.11 | 0.52 ± 0.07 |
| $[G_2 + (H_2O)_2 + H]^+$ | 0.30 ± 0.11 | 0.27 ± 0.06 | 0.50 ± 0.10 |
| $[G_2 + (H_2O)_3 + H]^+$ | 0.20 ± 0.07 | 0.16 ± 0.03 | 0.35 ± 0.12 |
| $[G_2 + (H_2O)_4 + H]^+$ | 0.07 ± 0.02 | 0.08 ± 0.01 | 0.20 ± 0.06 |
| $[G_2 + (H_2O)_5 + H]^+$ | 0.05 ± 0.02 | 0.04 ± 0.02 | 0.14 ± 0.04 |
| $[G_2 + (H_2O)_6 + H]^+$ | | | 0.06 ± 0.02 |
| $[G_3 + (H_2O)_1 + H]^+$ | 0.03 ± 0.02 | 0.05 ± 0.01 | 0.11 ± 0.03 |
| $[G_3 + (H_2O)_2 + H]^+$ | 0.02 ± 0.03 | 0.05 ± 0.01 | 0.11 ± 0.04 |
| $[G_3 + (H_2O)_3 + H]^+$ | | | 0.04 ± 0.02 |
| $[G_3 + (H_2O)_4 + H]^+$ | | | 0.03 ± 0.01 |

The remaining and most interesting explanation for the appearance of the spectrum shown in Figure 5.1 is preferential solvation by glycerol. This explanation is consistent with both gas- and condensed-phase proton solvation chemistry, as follows: 1) Glycerol has a larger gas-phase proton affinity than water (Table 5.3); [181] if gas-phase equilibria pertain, protonated glycerol should dominate, as observed. 2) In solution, higher solvent polarizability generally results in stronger ion-solvent interactions at short distances; [255] thus, the more polarizable glycerol (Table 5.3) should again be favored, this time in the primary solvation shell. 3) The solvent dipole moment reportedly correlates with ion solvation at larger distances (secondary shell and beyond); [255] glycerol's larger dipole moment (Table 5.3) indicates that it should also be favored beyond the primary solvation shell. 4) Consistent with these expectations, electrochemically determined values of the molar free energy of transfer of a proton from water to mixed water/glycerol solution suggest that glycerol is more basic than water and is, therefore, the preferred solvent. [256,257,258,259,260]

Preferential solvation and the relative abundance of the ion/solvent clusters should be effected by changes in solution composition. If the solvent content of glycerol in the solution is increased, this should be reflected in the mass spectrum. This reflection is clearly evident in the spectrum (Figure 5.3) when the glycerol content is increased to 10% (v/v). The most dramatic change in the spectrum is the absence of water clusters. The absence of water clusters was also observed when $K^+$, $Na^+$, $Rb^+$, and $Cs^+$ were used as solutes in the 95/5 (v/v) water/glycerol solvent mixture (Figure 5.4). For example, the spectrum obtained from a solution containing 40 mM NaI in the 95/5 (v/v) water/glycerol solvent mixture is consistent with results obtained in earlier

Table 5.3. Solvent properties for water and glycerol.

| Parameter | Water | Glycerol |
|---|---|---|
| Proton Affinity (gas-phase) | 727 kJ $mol^{-1}$(a) | 874 kJ $mol^{-1}$(b) |
| Polarizability | 1.48 $Å^3$(a) | 8.14 $Å^3$(a) |
| Dipole Moment | 1.85 D(a) | 2.68 D(a) |

(a) from reference [126]

(b) from reference [181]

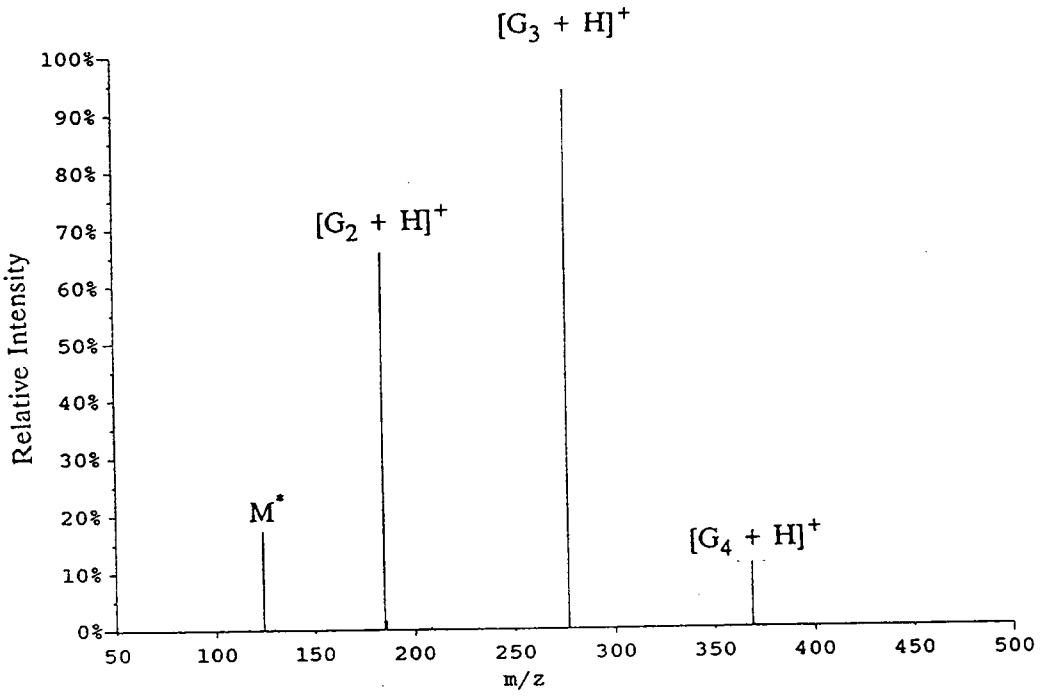



Figure 5.3. Electrohydrodynamic ionization mass spectrum of 40 mM HCl in a 90/10 (v/v) water/glycerol solvent mixture. Solvated peaks are labeled in the spectrum (where G denotes glycerol). Note the absence of water clusters. M* is a metastable decay product corresponding to the loss of one glycerol molecule from the trimer cluster ($[G_3 + H]^+ \rightarrow [G_2 + H]^+ + G$).

EH studies, [112] where clusters of the general formula $[Na^+ + (H_2O)_n]$ were detected only from 100% water solutions. The spectra shown in Figure 5.4 and results from Murawski [112] provide clear evidence for preferential solvation of the alkali cations by glycerol. In fact, the spectrum of the aqueous NaI solution containing only a small amount of glycerol is similar (contains only glycerol clusters) to the spectrum from a solution of NaI in 100% glycerol (Figure 5.5). Solvent clusters having the general formula $[G_n + Na]^+$ are present in both spectra, and clusters having the general formula $[G_n + H]^+$ are present in the spectrum from the aqueous solution. The protonated glycerol is a result of the slightly acidic (pH ≈ 6 as determined by narrow range pH indicator paper) water used in these experiments. The observation of protonated glycerol clusters is, again, consistent with both gas- and solution-phase data.

Another change in solution composition, such as acid concentration, should also have an effect on the appearance of the mass spectrum. In a series of experiments to test the effect of acid concentration on the appearance of the spectrum, the concentration of HCl was varied from 0 to 40 mM (similar to a titration experiment) while the total ionic strength was maintained at 40 mM by addition of NaI (the 40 mM total ionic strength is necessary to maintain stable ion emission). Starting with the 40 mM solution of NaI in 95/5 (v/v) water/glycerol, it is clear that protonated water clusters are not detected (see Figure 5.4b). Only ions resulting from sodium adducts of glycerol and protonated glycerol are detected. Only after reaching a concentration of approximately 20 mM HCl in the 95/5 (v/v) water/glycerol solution, are the hydrated clusters detected, even at low abundance (Figure 5.6). The "titration

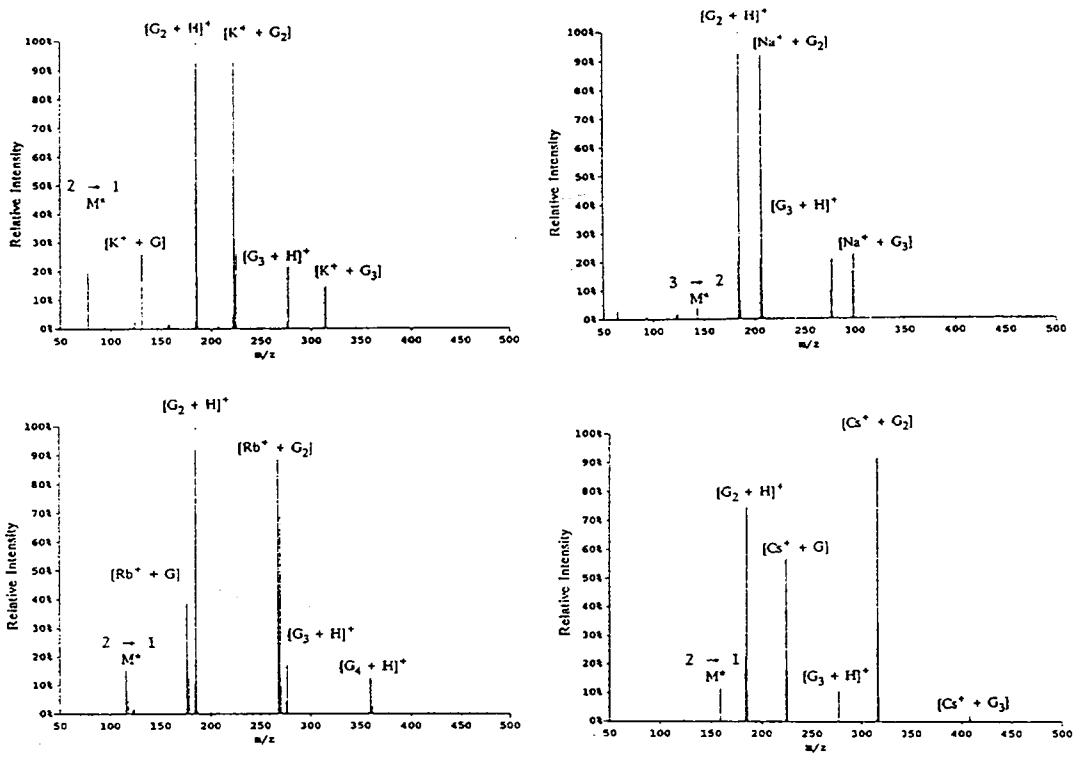



Figure 5.4. Electrohydrodynamic ionization mass spectrum of 40 mM (a) KI, (b) NaI, (c) RbI and (d) CsI in 95/5 (v/v) water/glycerol. Solvated peaks are labeled in the spectra (where G denotes glycerol). Note the absence of water clusters. M* represents metastable decay (n → n-1).

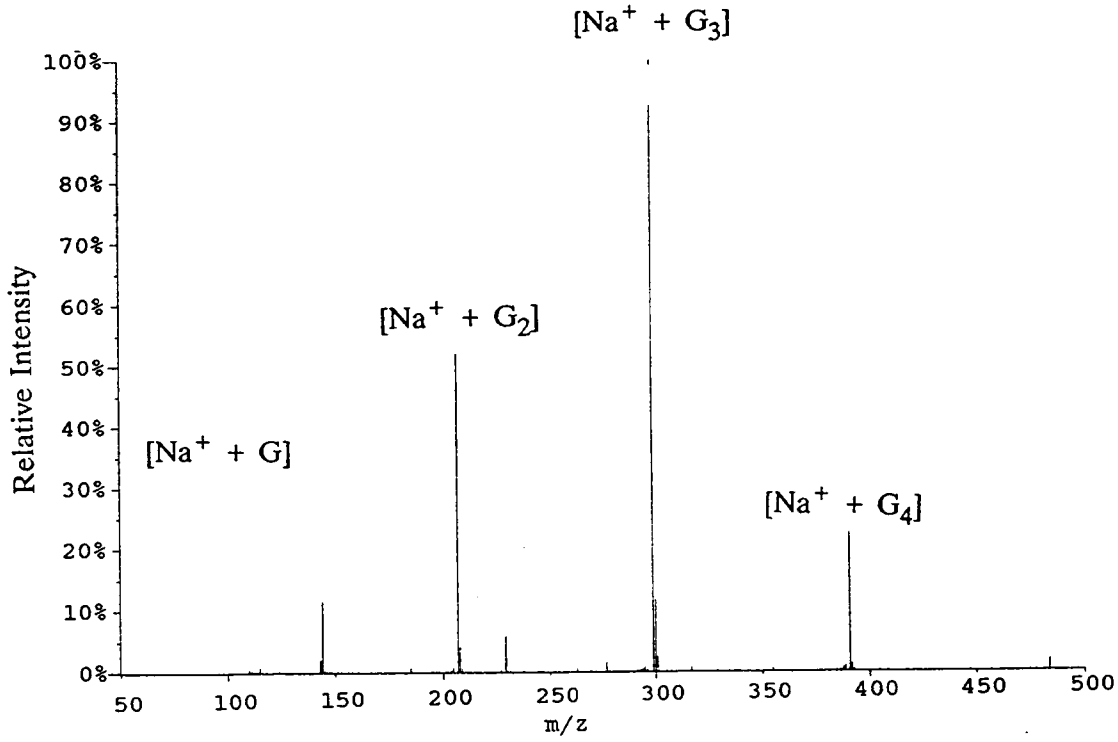



Figure 5.5. Electrohydrodynamic ionization mass spectrum of a 5 mol% NaI in 100% glycerol solution. Solvated peaks are labeled in the spectra (where G denotes glycerol). Note the absence of water clusters.

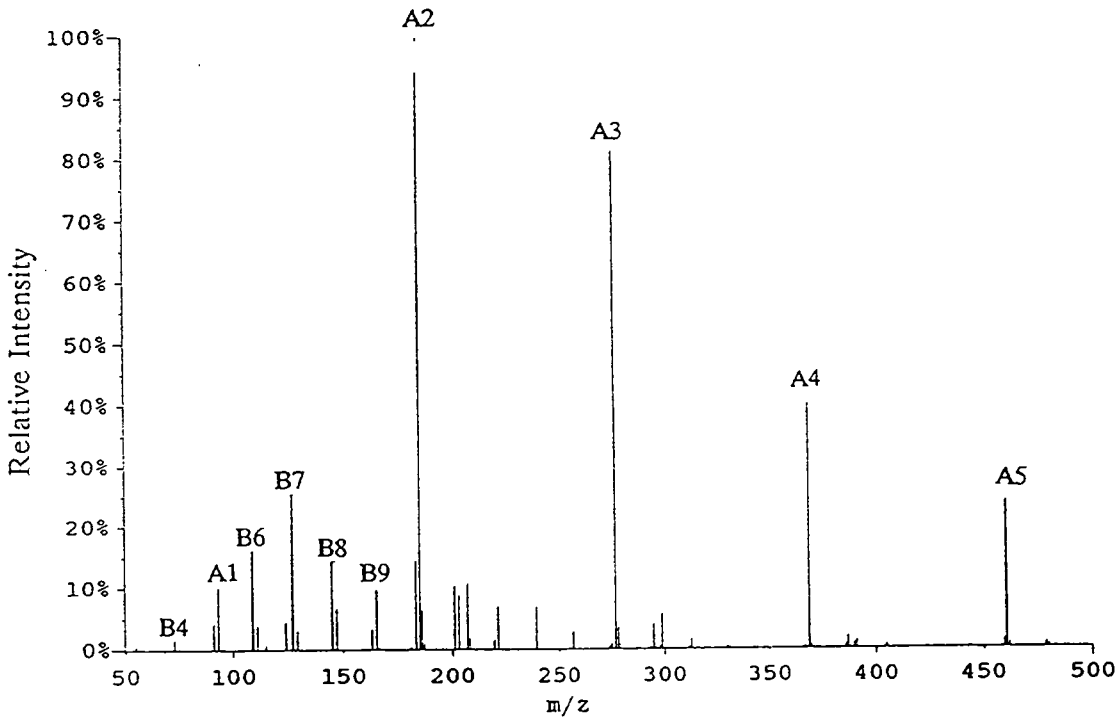



Figure 5.6. Electrohydrodynamic ionization mass spectrum of 18 mM HCl and 22 mM NaI in a 95/5 (v/v) water/glycerol solvent mixture. An = $[G + H]^+$; Bn = $[(H_2O)_n + H]^+$.

curve" shown in Figure 5.7 summarizes this behavior. The ordinate in the curve represents the ratio of the sum of protonated water cluster intensities ($\Sigma[(H_2O)_n + H]^+$) to the sum of the protonated glycerol cluster intensities ($\Sigma[G_n + H]^+$). The "end-point" appearance suggests that there should be some stoichiometric relationship among water, glycerol and proton concentrations. The amount of glycerol present in the 40 mM solution of HCl in 95/5 (v/v) water/glycerol is approximately 0.68 M, or 17 times more (on a molar basis) than the amount of protons, and the number of moles of water present is approximately 100 times more than the number of moles of glycerol; the acid is always the limiting reagent. The 40 mM solution of HCl in 90/10 (v/v) water glycerol contains approximately 34 times more glycerol than protons, and 50 times more water than glycerol. The solution containing 20 mM HCl in 95/5 (v/v) water/glycerol contains approximately 34 times more glycerol than protons, and approximately 100 times more water than glycerol. A comparison of the spectra obtained from the 40 mM solution of HCl in 90/10 (v/v) water/glycerol (Figure 5.3) and the 20 mM solution of HCl in 95/5 (v/v) water/glycerol (Figure 5.6) reveals that water clusters are present in the latter and not the former spectrum. This is true despite the glycerol to proton ratio remaining constant (34:1). The 20 mM solution of HCl in 95/5 (v/v) water/glycerol, however, also contains 20 mM NaI. Recall from above that the alkali cations have a glycerol solvent preference. Therefore, solvation of both sodium ions and protons can "consume" glycerol in the case of 20 mM HCl in 95/5 (v/v) water/glycerol solution. If sodium ion solvation is assumed to "consume" as much glycerol as does proton solvation, then the ratio of the amount of glycerol present to the amount of cations present becomes equal to the ratio for the 40 mM HCl solution in 95/5 (v/v) water/glycerol. Therefore,

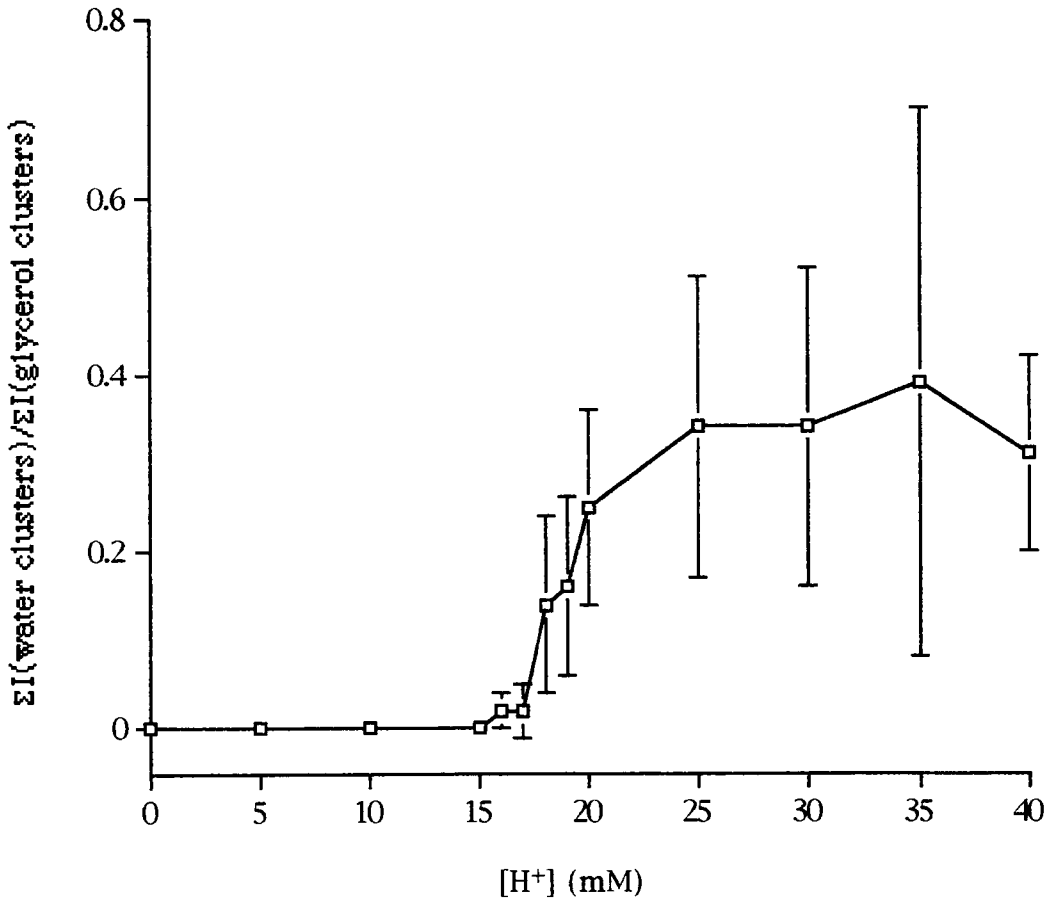



**Figure 5.7.** Plot of $\Sigma I[(H_2O)_n + H]^+$ divided by $\Sigma I[G_n + H]^+$ to illustrate that water clusters are detected after the addition of approximately 18 mM HCl to the 95/5 (v/v) water glycerol solution. Error bars represent the standard deviation of three replicates.

it is reasonable to detect protonated water clusters from the 20 mM solution of HCl in 95/5 (v/v) water/glycerol and not from the solution of 40 mM HCl in 90/10 (v/v) water glycerol. When the concentration of sodium ions is considered, the results obtained from varying the acid concentration and varying the glycerol concentration are consistent. Suggestions for future experiments designed to better ascertain the critical concentration of either glycerol or acid which induces the disappearance or appearance of the water clusters are described in Chapter 6.

Recall that a small amount of an involatile co-solvent (such as glycerol) is necessary for stable emission using the ion source configuration shown in Figure 2.11. Another involatile co-solvent commonly encountered in desorption ionization is thioglycerol. As a test to determine if ion/solvent clusters could be generated from a solution containing a co-solvent other than glycerol, thioglycerol (TG) was substituted. The spectrum obtained from a solution containing 40 mM HCl in 95/5 (v/v) water/thioglycerol contains ions attributable to protonated thioglycerol, protonated water and protonated water/thioglycerol clusters (Figure 5.8). Unlike the glycerol spectrum (Figure 5.1), the intensity contributions to each cluster here are difficult to determine unambiguously because thioglycerol is isobaric with $(H_2O)_6$ (both weigh 108 Daltons). Resolution on the basis of isotopic clusters is feasible, but requires better precision in intensity measurements than was obtained. However, inspection of the spectrum suggests that the contribution of the intensity from clusters having the general formula $[TG_n + (H_2O)_{6m} + H]^+$ to the intensity of clusters at m/z [108(n + m) + 1] for $m \neq 0$ or 1 can be neglected, based on the relative intensities of nearby clusters incorporating 1 - 5 more (or fewer) water molecules. It can thus be concluded that thioglycerol peaks are the most

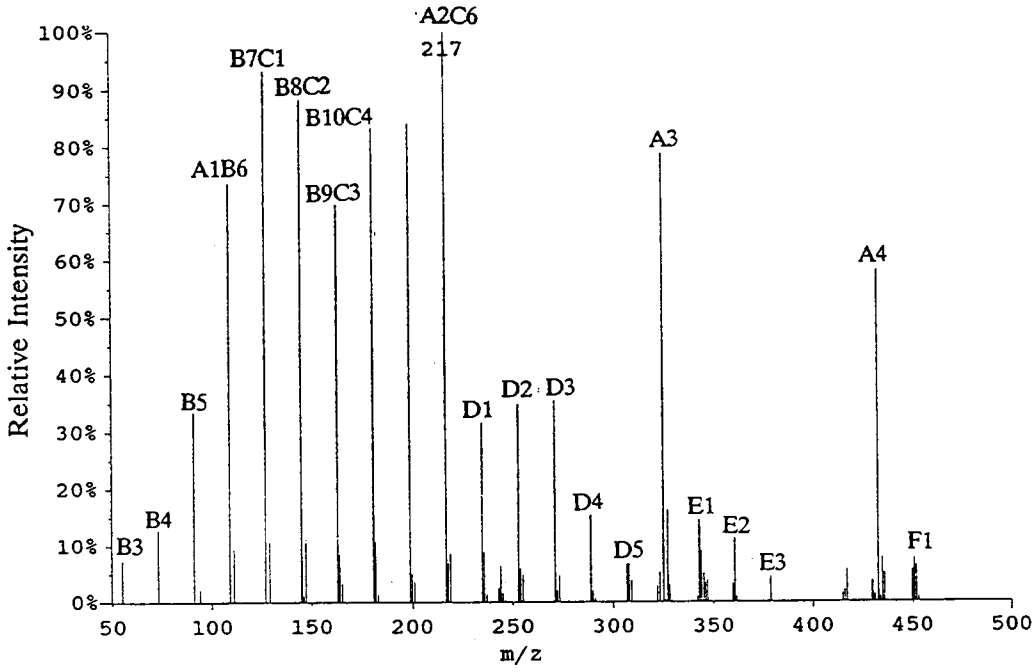



Figure 5.8. Electrohydrodynamic ionization mass spectrum of 40 mM HCl in a 95/5 (v/v) water/thioglycerol solvent mixture. $A_n = [TG_m + H]^+$; $B_n = [(H_2O)_n + H]^+$; $C_n = [TG + (H_2O)_n + H]^+$; $D_n = [TG_2 + (H_2O)_n + H]^+$; $E_n = [TG_3 + (H_2O)_n + H]^+$; $F_n = [TG_4 + (H_2O)_n + H]^+$.

intense in the spectrum, and that thioglycerol is the preferred solvent.

Qualitatively, EH spectra appear to reflect aspects of solution chemistry, such as preferential solvation. While qualitative information is useful, the next section will assess the potential of EH to provide quantitative information such as the distribution of ion/solvent clusters.

## 5.2 Cluster Distribution

Even if evaporation affects solvent concentrations, it is of interest to assess the cluster distributions within the individual series of Figure 5.1 to determine if they can be reconciled with predictions based on known thermodynamics, indicative of an equilibrium distribution, as suggested by their reproducibility. Each of the cluster series of Figure 5.1 is treated individually below.

Figures 5.9-5.11 show the effects of experimental conditions on the relative intensities of clusters having the general formulae $[(H_2O)_n + H]^+$, $[G_1 + (H_2O)_n + H]^+$, and $[G_2 + (H_2O)_n + H]^+$, respectively. If clusters are controlled by gas-phase equilibria, a change in flow rate (with a corresponding change in pressure) would be expected to affect the observed cluster distribution. The minimum attainable flow rate (using a 25 μm i.d. capillary) was the vacuum induced flow rate of 5 μL/hour. A syringe pump was used to increase the flow rate above the minimum vacuum-induced flow rate. Two separate flow rates (7.5 and 10 μL/hour) were used to determine how the observed distribution changes as a function of flow rate. These plots (Figures 5.9-5.11) illustrate that within experimental error, the distribution of ion/solvent clusters observed using different flow rates does not differ. The relative intensities of

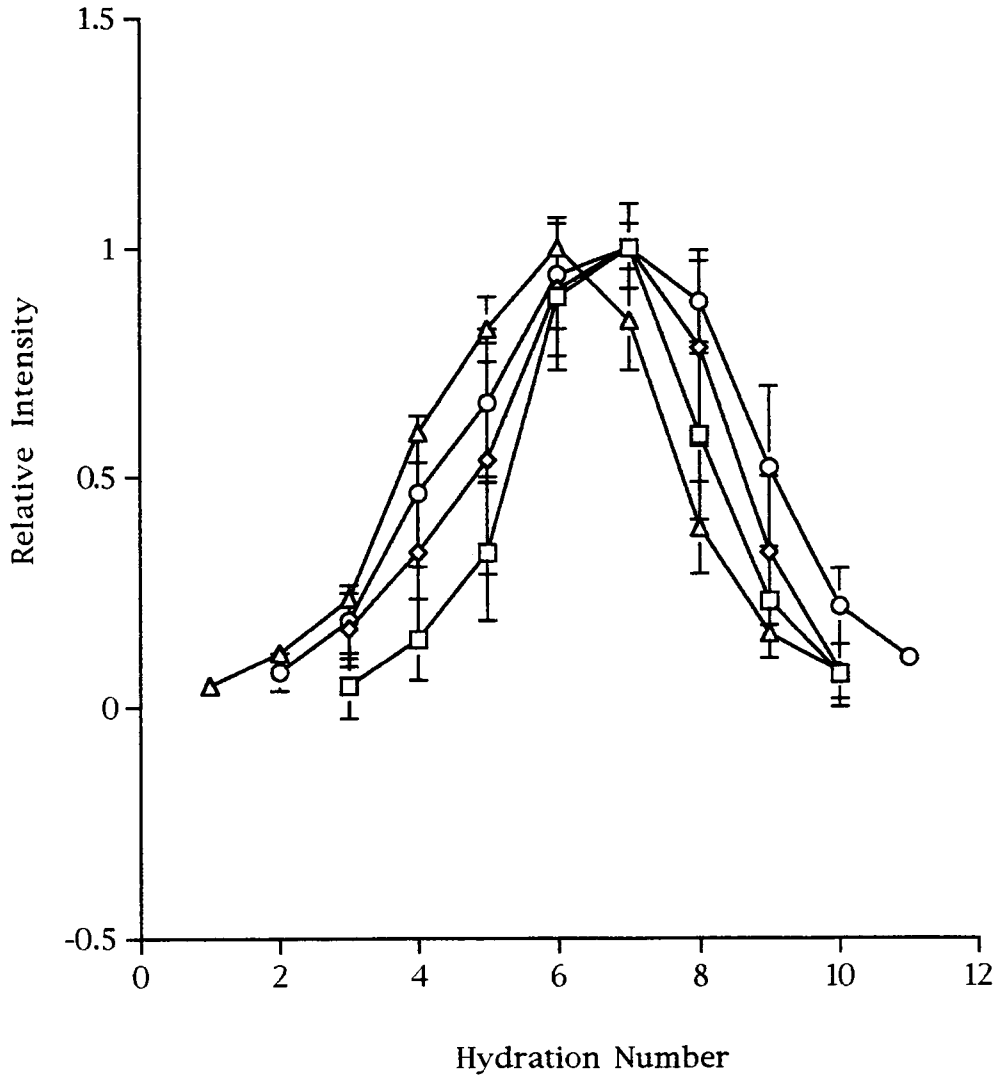



Figure 5.9. Plots of cluster relative intensity versus hydration number for the $[(H_2O)_n + H]^+$ series under different conditions of flow rate and accelerating voltage: ◊ = 5 μL/hour (8 kV needle potential); □ = 5 μL/hour (6 kV needle potential); Δ = 7.5 μL/hour (8 kV needle potential); o = 10 μL/hour (8 kV needle potential). Each series of clusters is normalized to the most abundant ion within that cluster.

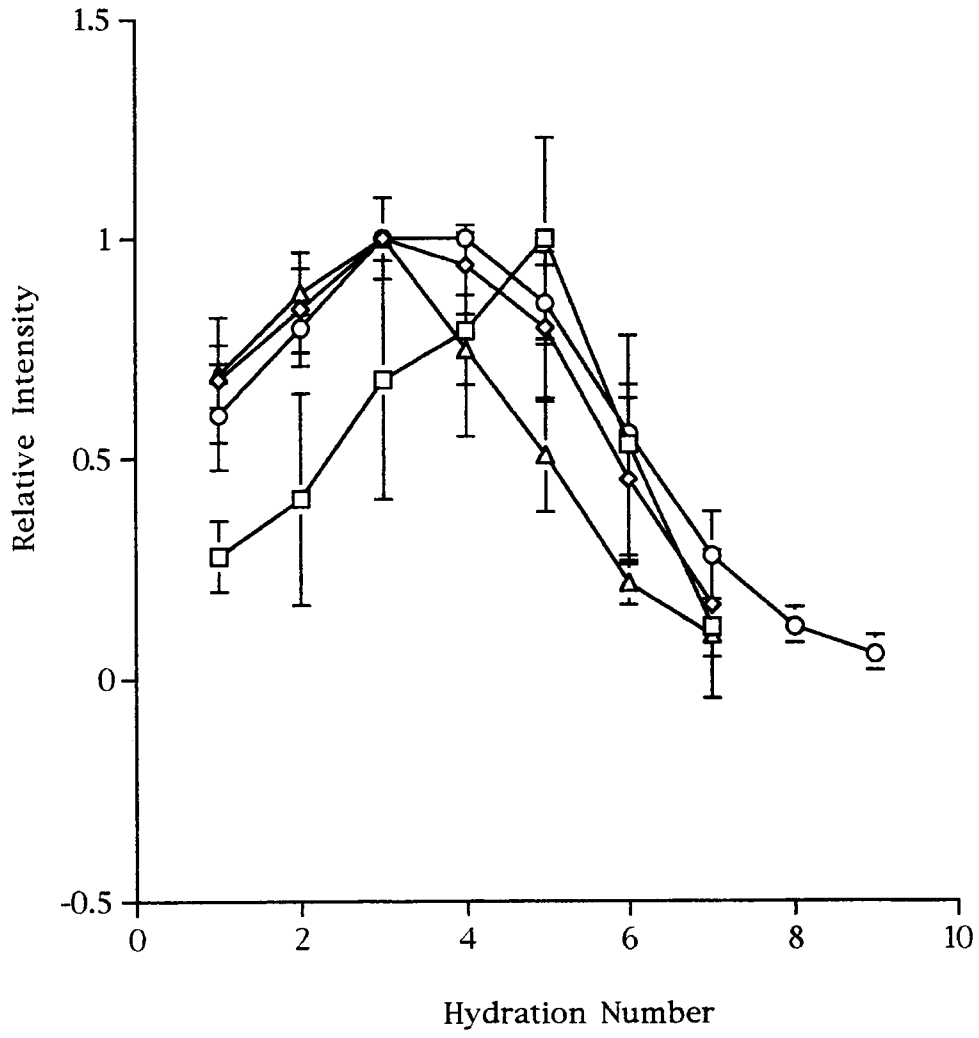



Figure 5.10. Plots of cluster relative intensity versus hydration number for the $[G + (H_2O)_n + H]^+$ series under different conditions of flow rate and accelerating voltage: ◊ = 5 μL/hour (8 kV needle potential); □ = 5 μL/hour (6 kV needle potential); Δ = 7.5 μL/hour (8 kV needle potential); o = 10 μL/hour (8 kV needle potential). Each series of clusters is normalized to the most abundant ion within that cluster.

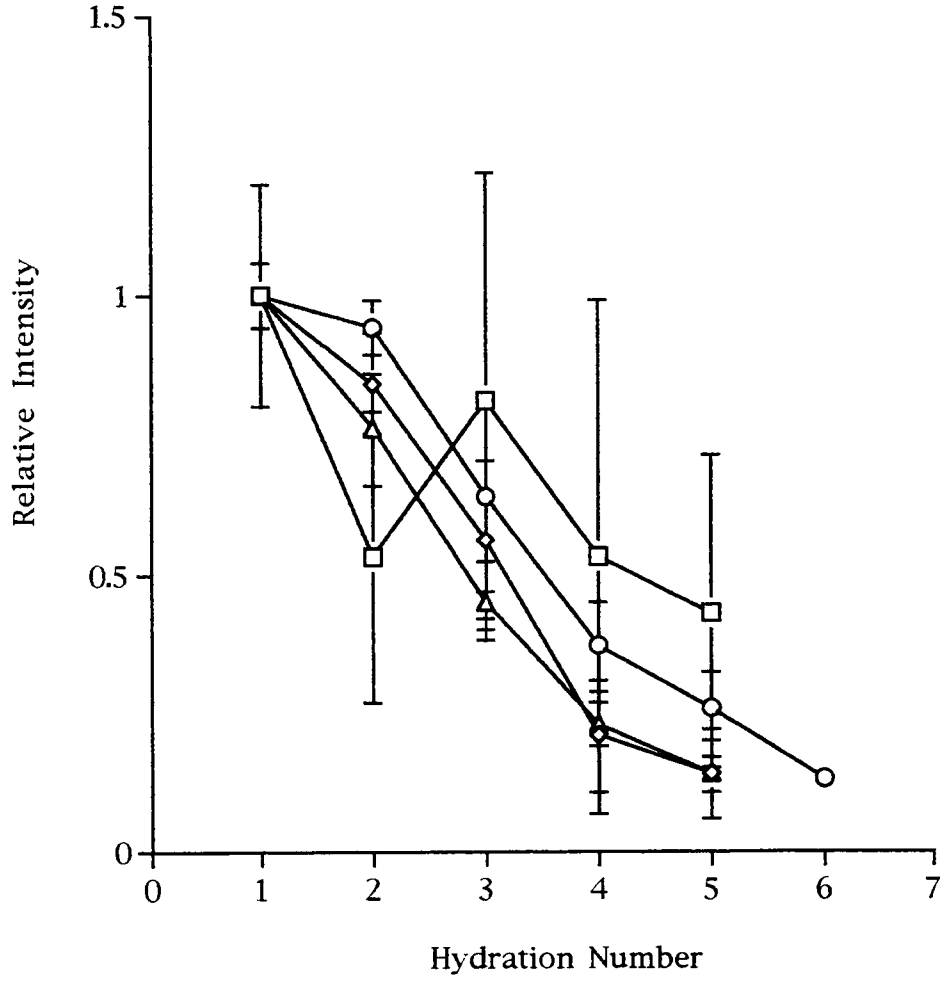



**Figure 5.11.** Plots of cluster relative intensity versus hydration number for the $[G_2 + (H_2O)_n + H]^+$ series under different conditions of flow rate and accelerating voltage: ◊ = 5 μL/hour (8 kV needle potential); □ = 5 μL/hour (6 kV needle potential); Δ = 7.5 μL/hour (8 kV needle potential); o = 10 μL/hour (8 kV needle potential). Each series of clusters is normalized to the most abundant ion within that cluster.

ion/solvent clusters observed using forced flow are provided in Table 5.2 for comparison with the vacuum induced flow rate data.

Another factor that might affect cluster distributions is the accelerating potential (and corresponding ion flight time). If certain ion/solvent clusters are less stable than others, an extended flight time would allow for dissociation or evaporation. The flight time of the ion/solvent cluster can be increased (over a rather narrow range) by decreasing the accelerating potential. Within experimental error, the distribution of ion intensities (Figures 5.9-5.11) at 6 kV (approximately 1.7 μsec flight time) does not differ from that at 8 kV (approximately 2.3 μsec flight time). It is worth noting that ion intensities observed from desorption ionization techniques typically fluctuate as much as 15 to 20% (RSD). The large error bars associated with the forced flow and 6 kV experiments can be attributed to a combination of typical errors associated with DI, amplified by working under non-ideal experimental conditions.

The low volatility of glycerol has precluded extensive gas-phase studies of glycerol clusters, so data for comparison with the "A" series of Figure 5.1 do not appear to be available. The EH source shown in Figure 2.11 requires a small amount of a low volatility co-solvent such as glycerol. This requirement actually makes EH ideally suited to study the solvent systems not amenable to gas-phase studies (low volatility solvents). Experiments utilizing the CID threshold approach described in section 1.4 to determine structure and thermodynamic information have not yet been done, but are suggested for future work in Chapter 6.

In contrast to glycerol, a great deal of information is available concerning water cluster distributions. This section will attempt to ascertain

whether the observed distribution of these clusters represents chemistry related to the gas-phase, solution-phase, or neither.

The series of protonated water clusters $[H^+(H_2O)_n]$ labeled "B" in Figure 5.1 extends from n = 3 to n = 10, with a maximum at n = 7. In contrast, there is a peak in a plot of free energy versus hydration number at n = 4 in the gas phase data that has been attributed the higher stability of this cluster, [261] and is considered to be indicative of a filled primary shell (see Figure 1.6). To assess whether the observed differences can be attributed to the effects of temperature and pressure on the gas-phase solvation equilibria of Reaction 5.1, the dependence of these equilibria on T and P was considered.

$$[H^+(H_2O)_n]_g = [H^+(H_2O)_{n-1}]_g + [H_2O]_g$$

Reaction 5.1

Assuming that relative signal intensities ($I_n$) are valid measures of relative abundances of corresponding clusters present at equilibrium (recall earlier discussion of low bias over a narrow mass range), the equilibrium constants for Reaction 1 can be written as follows:

$$K_{n,n-1} = \frac{I_{n-1}\ P_W}{I_n}$$

Equation 5.1

where $P_W$ represents the partial pressure of water and I indicates the EH spectral signal intensity of the subscripted cluster. This equation assumes that the I/P proportionality constant is the same for $I_{n-1}$ and $I_n$. From Equation 5.1

and the relationship of Equation 5.2 below:

$$\Delta G_{(n,n-1)} = -RT\ln K_{(n,n-1)}$$

Equation 5.2

(where R is the gas constant; 1.987 cal/mol K), a series of equations describing the temperature and pressure dependence of relative intensities can be derived (Equation 5.3):

$$\frac{I_n}{I_{n-1}} = \exp\left[\frac{\Delta G_{(n,n-1)}}{RT}\right] \times P_w$$

Equation 5.3

Equation 5.3 constitutes a family of non-linear equations in the variables $\Delta G$, T, and $P_w$, which can be solved (*e.g.*, using non-linear least squares) to determine a best fit for the experimentally observed intensity ratios. Values for $\Delta G_{n,n-1}$ are available through n = 8 from the literature, and are provided in Table 5.4 for convenience. [261] Using these values to calculate a best sum-squares fit of Equations 5.3 to the experimental intensity ratios for n = 2 to 8 (considering T and $P_w$ as independent variables) gives the response surface shown in part in Figure 5.12. There is a single minimum over the range T = 0 to 10,000 K and P= 0 to 2 atmospheres, occurring at 5495 K and 1.02 atmospheres. A temperature this high would indicate the presence of a discharge, inconsistent with the negligible fragmentation observed in EH. Since there is a rather strong temperature dependence, more reasonable temperatures would give very poor fits. Errors calculated using several temperatures and pressures are provided

Table 5.4. Gas phase thermodynamic data[a] for Reaction 5.1, involving protonated water clusters.

| n,n-1 | $\Delta G_{n,n-1}$ | $\Delta H_{n,n-1}$ | $\Delta S_{n,n-1}$ |
|---|---|---|---|
| 2,1 | 24.3 | 31.6 | 24.3 |
| 3,2 | 13.0 | 19.5 | 21.9 |
| 4,3 | 9.3 | 17.5 | 27.3 |
| 5,4 | 5.5 | 15.3 | 32.6 |
| 6,5 | 3.9 | 13.0 | 30.3 |
| 7,6 | 2.8 | 11.7 | 29.6 |
| 8,7 | 2.2 | 10.3 | 27.0 |

[a] Taken from reference [261]. Data are for 300 K and 1 atmosphere pressure. $\Delta G_{n,n-1}$, $\Delta H_{n,n-1}$ in kcal/mol and $\Delta S_{n,n-1}$ in cal/mol deg.

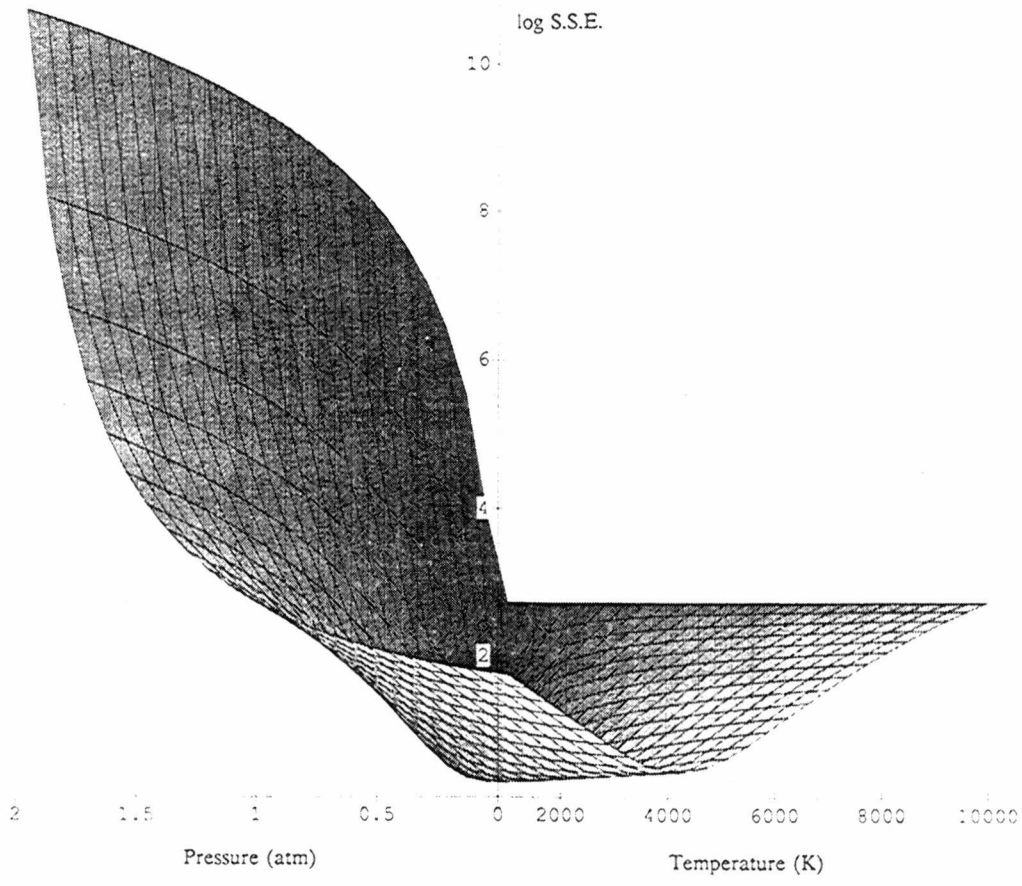



Figure 5.12. Sum-squares response surface showing the (log) sum squares error $[\Sigma(Y - \hat{Y})^2]$ for the fit of Equations 5.3 to the experimental intensity ratios using literature values of $\Delta G$ and indicated temperatures and pressures.

in Table 5.5 below.

Table 5.5. Calculated errors illustrating the poor fit at various temperatures and pressures.

| Temperature (K) | Pressure (atm) | S.S.E.[a] |
|---|---|---|
| 100 | $10^{-8}$ | $4.4 \times 10^{24}$ |
| 300 | $10^{-8}$ | 14.1 |
| 1000 | 0.01 | 9.63 |
| 5495 | 1.02 | 0.381[b] |

[a] S.S.E. = sum squares of errors. [b] Best non-linear least squares fit.

Thus, it may be concluded that the gas-phase equilibria of reaction 5.1 do not accurately represent the chemical system giving rise to the cluster distributions of Figure 5.1, given the assumption that ion intensity is proportional to the corresponding partial pressure.

An alternative explanation for the maximum at n = 7 in series "B" of Figure 5.1 could be a corresponding minimum in the free energy barrier to sampling clusters *from the bulk* (reaction 5.2):

$$[H^+(H_2O)]_{aq} \rightarrow [H^+(H_2O)_n]_g$$

Reaction 5.2

The required energy can be estimated from the energies of three processes (Figure 5.13): the endothermic removal of the core hydronium ion ($H_3O^+_{aq} \rightarrow H_3O^+_g$; $\Delta G_1$ = +101.2 kcal/mol;); [262,263,264] the endothermic removal of free solvent molecules from the bulk ($H_2O_{aq} \rightarrow H_2O_g$; $\Delta G_2$ = +2.04 kcal/mol for

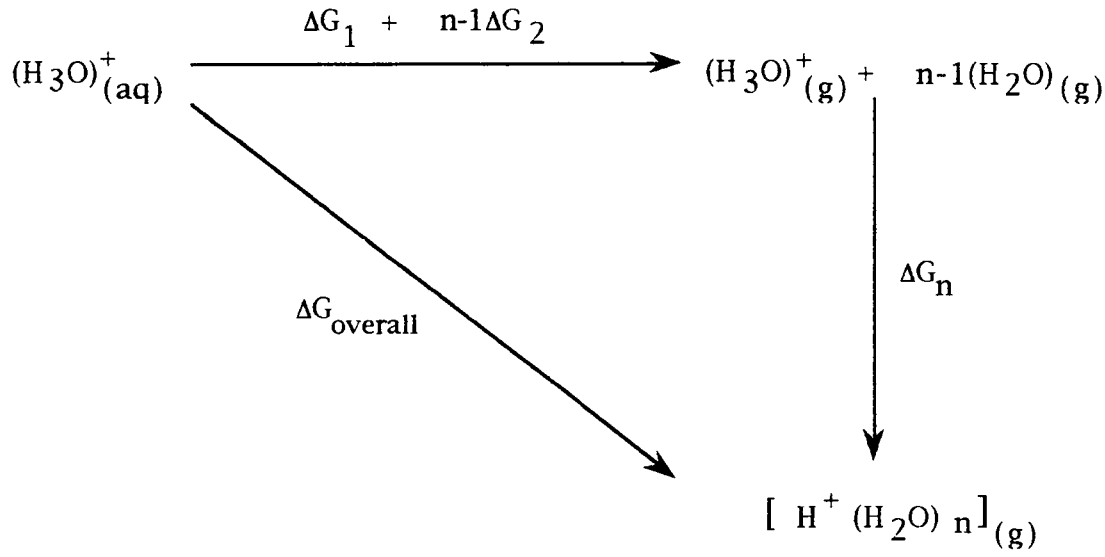



Figure 5.13. Free energy cycle for the removal of protonated water clusters from bulk solution.

each of n-1 water molecules [264]); and the exothermic gas-phase solvation of the core ion by n solvent molecules ($H_3O^+_g + (n-1)H_2O_g \rightarrow [H^+(H_2O)_n]_g$; $\Delta G_n < 0$; $\Delta G_n = -\sum_{i=2}^{n} \Delta G_{i\,i-1}$ using $\Delta G_{i,i-1}$ from Table 5.4). Thus $\Delta G_{overall} = \Delta G_1 + (n-1)\Delta G_2 + \Delta G_n$. This treatment assumes that the structure of the gas-phase solvated ion is independent of its route of formation. Again, thermodynamic data for $\Delta G_n$ is available only through n = 8. [181] Over this range, $\Delta G_{overall}$ shows a relatively smooth continuous decrease with increasing n, becoming roughly independent of n at approximately n = 6 (Figure 5.14). If the bulk desorption model is correct, the observed maximum in relative intensity must result from solvent structure favoring seven water molecules in close proximity to the proton (i.e., from high abundance of such a cluster), rather than an especially low barrier to removal of such a cluster. As shown above, the gas-phase $\Delta G$'s cannot predict such a distribution at reasonable T and P. One alternative explanation could be the reflection of bulk solvation.

Even if ions are sampled from a region representative of the bulk solution, unimolecular metastable desolvation after sampling may obscure the relationship between the measured mass spectrum and the relative abundance of solvent clusters present in solution. Evaporation in the second field-free region (FFR-2) of a Nier-Johnson instrument (Figure 2.9) like that used here would give rise to broadened peaks in the mass spectrum generally at non-integral mass-to-charge ratios m* given by equation 5.4 below (where $m_d$ and $m_p$ are masses after and before evaporation, respectively) [265]:

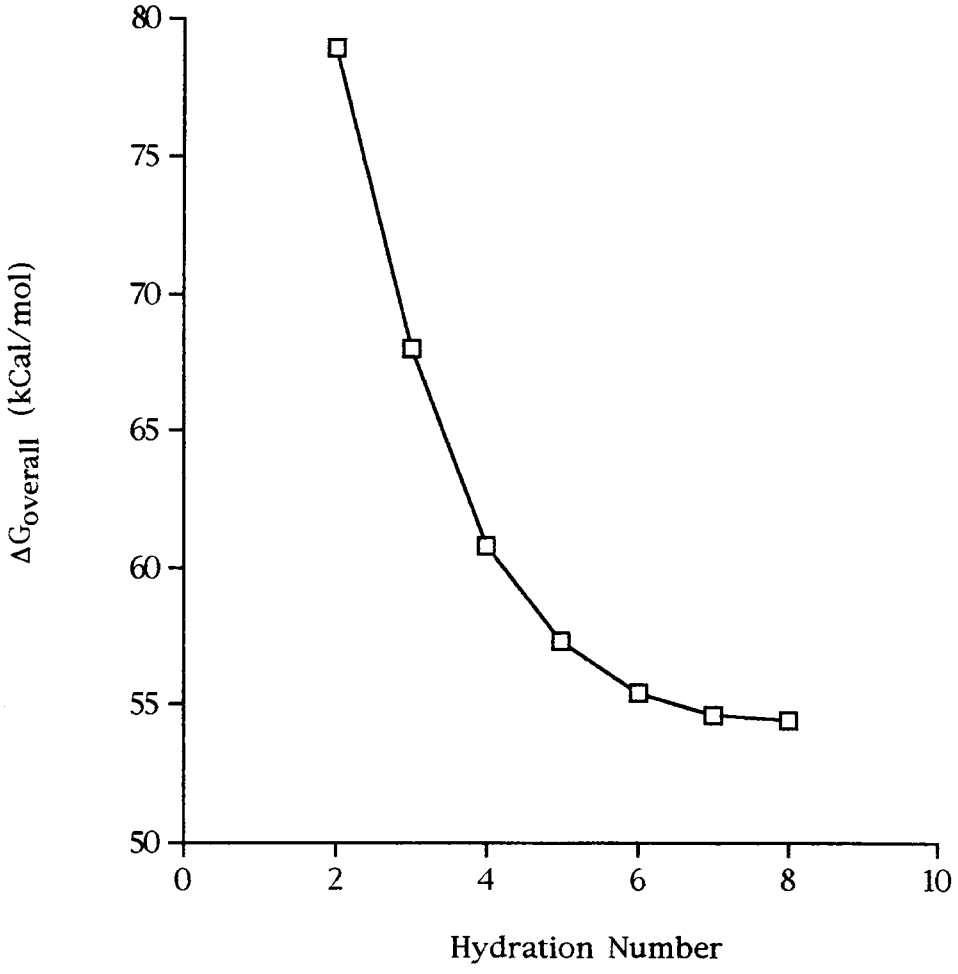



Figure 5.14. Free energy for removal of protonated water clusters $[(H_2O)_n + H]^+$ of varying n from bulk solution. Calculated from the free energy cycle using gas-phase $\Delta G$ values shown in Table 5.4.

$$m^* = \frac{m_d^2}{m_p}$$

Equation 5.4

Such peaks, which are readily attributable to metastable ions, are absent from the spectra of Figures 5.1 and 5.2. Products of more rapid evaporation (*e.g.*, in FFR-1) will reach the ESA with less than the nominal acceleration energy, and can be detected only *via* linked scans, [265] wherein the ESA is adjusted to account for the deficit in ion energy while the magnet is scanned. To test for evaporation in FFR-1, a linked scan was performed (see Chapter 2). In these experiments, the magnet (magnetic field strength represented by "B") and the ESA (electric field strength represented by "E") were scanned together (at constant B/E ratio) to detect the ions that experienced metastable decay prior to entering the ESA. The resulting metastable peak intensities (relative to the corresponding precursor intensity at full ion energy; average of at least 5 scans) and their corresponding energy (given by Equation 5.5 below) are listed in Table 5.6:

$$E_d = \frac{m_d}{m_p} \times E_p$$

Equation 5.5

where $E_d$ and $E_p$ are the fragment and precursor ion energies, respectively. The data of Table 5.6 indicate that most of the clusters experience the loss of at

Table 5.6. Metastable decay data for clusters from a 40 mM HCl solution in 95% water and 5% glycerol (v/v).

| Metastable Decay Reaction | R. I. ($\pm \sigma_n$) | Ion Energy (keV) |
|---|---|---|
| $[G_6 + H]^+ \rightarrow [G_6 + H]^+$ a | 1 ± 0 | 8.0 |
| $[G_6 + H]^+ \rightarrow [G_5 + H]^+$ | 1.32 ± 0.39 | 6.7 |
| $[G_6 + H]^+ \rightarrow [G_4 + H]^+$ | 0.57 ± 0.47 | 5.4 |
| $[G_6 + H]^+ \rightarrow [G_3 + H]^+$ | 0.30 ± 0.03 | 4.0 |
| $[G_5 + H]^+ \rightarrow [G_5 + H]^+$ a | 1 ± 0 (0.17) | 8.0 |
| $[G_5 + H]^+ \rightarrow [G_4 + H]^+$ | 2.51 ± 0.93 | 6.4 |
| $[G_5 + H]^+ \rightarrow [G_3 + H]^+$ | 0.83 ± 0.91 | 4.8 |
| $[G_4 + H]^+ \rightarrow [G_4 + H]^+$ a | 1 ± 0 (0.53) | 8.0 |
| $[G_4 + H]^+ \rightarrow [G_3 + H]^+$ | 1.88 ± 1.47 | 6.0 |
| $[G_4 + H]^+ \rightarrow [G_2 + H]^+$ | 0.13 ± 0.04 | 4.0 |
| $[G_3 + H]^+ \rightarrow [G_3 + H]^+$ a | 1 ± 0 (0.91) | 8.0 |
| $[G_3 + H]^+ \rightarrow [G_2 + H]^+$ | 0.48 ± 0.32 | 5.4 |
| $[G_2 + H]^+ \rightarrow [G_2 + H]^+$ a | 1 ± 0 (0.94) | 8.0 |
| $[G_2 + H]^+ \rightarrow [G_1 + H]^+$ a | 0.15 ± 0.08 | 4.0 |
| $[(H_2O)_9 + H]^+ \rightarrow [(H_2O)_9 + H]^+$ a | 1 ± 0 (0.21) | 8.0 |
| $[(H_2O)_9 + H]^+ \rightarrow [(H_2O)_8 + H]^+$ a | 2.45 ± 1.04 | 7.1 |
| $[(H_2O)_9 + H]^+ \rightarrow [(H_2O)_7 + H]^+$ | 0.11 ± 0.07 | 6.2 |
| $[(H_2O)_8 + H]^+ \rightarrow [(H_2O)_8 + H]^+$ a | 1 ± 0 (0.47) | 8.0 |
| $[(H_2O)_8 + H]^+ \rightarrow [(H_2O)_7 + H]^+$ | 1.35 ± 0.64 | 7.0 |
| $[(H_2O)_8 + H]^+ \rightarrow [(H_2O)_6 + H]^+$ | 0.19 ± 0.26 | 6.0 |
| $[(H_2O)_8 + H]^+ \rightarrow [(H_2O)_5 + H]^+$ | 0.07 ± 0.06 | 5.0 |
| $[(H_2O)_7 + H]^+ \rightarrow [(H_2O)_7 + H]^+$ a | 1 ± 0 (0.57) | 8.0 |
| $[(H_2O)_7 + H]^+ \rightarrow [(H_2O)_6 + H]^+$ | 0.56 ± 0.17 | 6.9 |
| $[(H_2O)_7 + H]^+ \rightarrow [(H_2O)_5 + H]^+$ | 0.07 ± 0.10 | 5.7 |
| $[(H_2O)_6 + H]^+ \rightarrow [(H_2O)_6 + H]^+$ a | 1 ± 0 (0.48) | 8.0 |
| $[(H_2O)_6 + H]^+ \rightarrow [(H_2O)_5 + H]^+$ | 0.29 ± 0.08 | 6.7 |
| $[(H_2O)_6 + H]^+ \rightarrow [(H_2O)_4 + H]^+$ | 0.04 ± 0.02 | 5.4 |

Table 5.6. continued.

| | | |
|---|---|---|
| $[(H_2O)_5 + H]^+ \rightarrow [(H_2O)_5 + H]^+$ [a] | 1 ± 0 (0.27) | 8.0 |
| $[(H_2O)_5 + H]^+ \rightarrow [(H_2O)_4 + H]^+$ | 0.43 ± 0.29 | 6.4 |
| $[(H_2O)_5 + H]^+ \rightarrow [(H_2O)_3 + H]^+$ | 0.05 ± 0.05 | 4.8 |
| $[(H_2O)_4 + H]^+ \rightarrow [(H_2O)_4 + H]^+$ [a] | 1 ± 0 (0.18) | 8.0 |
| $[(H_2O)_4 + H]^+ \rightarrow [(H_2O)_3 + H]^+$ | 0.26 ± 0.14 | 6.0 |
| $[(H_2O)_4 + H]^+ \rightarrow [(H_2O)_2 + H]^+$ | 0.31 ± 0.05 | 4.0 |
| $[G_1 + (H_2O)_4 + H]^+ \rightarrow [G_1 + (H_2O)_4 + H]^+$ [a] | 1 ± 0 (0.44) | 8.0 |
| $[G_1 + (H_2O)_4 + H]^+ \rightarrow [G_1 + (H_2O)_3 + H]^+$ | 1.40 ± 0.30 | 7.1 |
| $[G_1 + (H_2O)_4 + H]^+ \rightarrow [G_1 + (H_2O)_2 + H]^+$ | 0.10 ± 0.03 | 6.3 |
| $[G_1 + (H_2O)_4 + H]^+ \rightarrow [G_1 + (H_2O)_1 + H]^+$ | 0.06 ± 0.02 | 5.4 |
| $[G_1 + (H_2O)_4 + H]^+ \rightarrow [G_1 + (H_2O)_0 + H]^+$ | 0.14 ± 0.07 | 4.5 |
| $[G_1 + (H_2O)_3 + H]^+ \rightarrow [G_1 + (H_2O)_3 + H]^+$ [a] | 1 ± 0 (0.47) | 8.0 |
| $[G_1 + (H_2O)_3 + H]^+ \rightarrow [G_1 + (H_2O)_2 + H]^+$ | 0.81 ± 0.21 | 7.0 |
| $[G_1 + (H_2O)_3 + H]^+ \rightarrow [G_1 + (H_2O)_1 + H]^+$ | 0.08 ± 0.02 | 6.0 |
| $[G_1 + (H_2O)_3 + H]^+ \rightarrow [G_1 + (H_2O)_0 + H]^+$ | 0.10 ± 0.03 | 5.1 |
| $[G_1 + (H_2O)_2 + H]^+ \rightarrow [G_1 + (H_2O)_2 + H]^+$ [a] | 1 ± 0 (0.40) | 8.0 |
| $[G_1 + (H_2O)_2 + H]^+ \rightarrow [G_1 + (H_2O)_1 + H]^+$ | 0.76 ± 0.35 | 6.8 |
| $[G_1 + (H_2O)_2 + H]^+ \rightarrow [G_1 + (H_2O)_0 + H]^+$ | 0.67 ± 0.58 | 5.8 |
| $[G_1 + (H_2O)_1 + H]^+ \rightarrow [G_1 + (H_2O)_1 + H]^+$ [a] | 1 ± 0 (0.32) | 8.0 |
| $[G_1 + (H_2O)_1 + H]^+ \rightarrow [G_1 + (H_2O)_0 + H]^+$ | 0.61 ± 0.49 | 6.7 |

[a] Stable ion intensity included for comparison. Parenthetical numbers represent the relative intensity of the precursor ion in the full energy spectrum.

least 2, and sometimes 3, solvent molecules. In some cases, the intensity of the cluster with full accelerating energy is smaller than the intensity of the metastable cluster. This is not consistent with the expectation that very little internal energy is deposited into the clusters desorbed from solution, and again suggests that interpretation of the spectrum to reflect bulk solvation is difficult to quantitate. Since metastable decay or in-flight evaporation is a gas-phase process, the energies associated with these losses can be reconciled using the stepwise gas-phase free energy data from Kebarle. [261] The free energy changes in this case should be $\approx \Delta G_n$, and are listed in Table 5.7. The free energy data for metastable decay listed in Table 5.7 can be used to assess which clusters should experience in-flight desolvation given a fixed internal energy threshold. The metastable loss of 2 water molecules from the tetramer is the most endothermic process observed. Therefore, all other metastable decays with free energy less than 22.3 kcal/mol, should also occur and be detected. This is observed with the exception of two cases. The loss of 3 water molecules from the n = 7 cluster and the loss of 1 water molecule from the n = 3 cluster were not detected. Based on the detection of the loss of 2 water molecules from the tetramer, these products are energetically possible. One logical explanation for these anomalous results could be that the abundance of these clusters was simply too small to be detected. Another explanation, that could be tested by tandem mass spectrometry experiments, is the anomalous stability of the clusters that should have experienced in-flight evaporation (e.g., the n = 3 to n = 2 decay). Tandem mass spectrometric experiments utilizing collision induced dissociation to further probe the energetics and structure of clusters are suggested in Chapter 6.

Table 5.7. Metastable decay free energy for the loss of water from protonated water clusters. Calculated using gas-phase free energy data from Kebarle. [261]

| $[(H_2O)_n + H]^+ \rightarrow$ n | $[(H_2O)_{n-1} + H]^+ \rightarrow$ | $[(H_2O)_{n-2} + H]^+ \rightarrow$ | $[(H_2O)_{n-3} + H]^+$ |
|---|---|---|---|
| 2 | *24.3* [a] | | |
| 3 | *13.0* [a] | *37.3* [a] | |
| 4 | 9.3 | 22.3 | *46.4* [a] |
| 5 | 5.5 | 14.8 | *27.8* [a] |
| 6 | 3.9 | 9.4 | *18.7* [a] |
| 7 | 2.8 | 6.7 | *12.2* [a] |
| 8 | 2.2 | 5.0 | 8.9 |

[a] The italicized free energy values indicate that these decay products were not detected.

A better representation of the clusters leaving solution might be the sum of the intensities of the full energy stable ions and the metastable ions. Comparison of the protonated water cluster (having the general formula $H^+(H_2O)_n$) distribution observed from the stable full energy spectrum (data shown in Table 5.2) with that calculated from summing the metastable and stable cluster intensities reveals that the maximum is shifted to n = 8 (Figure 5.15). This shift in distribution is in a direction farther from gas phase equilibria and is consistent with the theory that EH spectra reflect solution chemistry.

Although there are no data in the literature available for comparison, it is interesting to examine the spectral distribution of mixed solvent clusters of water and glycerol having the general formula $[G_n + (H_2O)_m + H]^+$. A probe of these clusters would provide insight into not only the energetics of the interaction, but the structure of the cluster (a determination of the core ion). Figure 5.16 illustrates the variation of the number of water and glycerol molecules in the mixed solvent clusters. Incorporation of one glycerol molecule reduces the average hydration number (see figure caption for definition) by three, whereas the decrease is only about two when a second glycerol molecule is added. For the third (and subsequent) glycerol molecules, there appears to be a roughly one-for-one replacement. Such behavior would be consistent with glycerol activity as a tridentate or bidentate ligand competing for sites in the primary solvation sphere, followed by monodentate replacement of water in the more loosely bound outer sphere. Experiments utilizing a hybrid instrument capable of MS/MS to assess the relative stabilities of these clusters are suggested in Chapter 6.

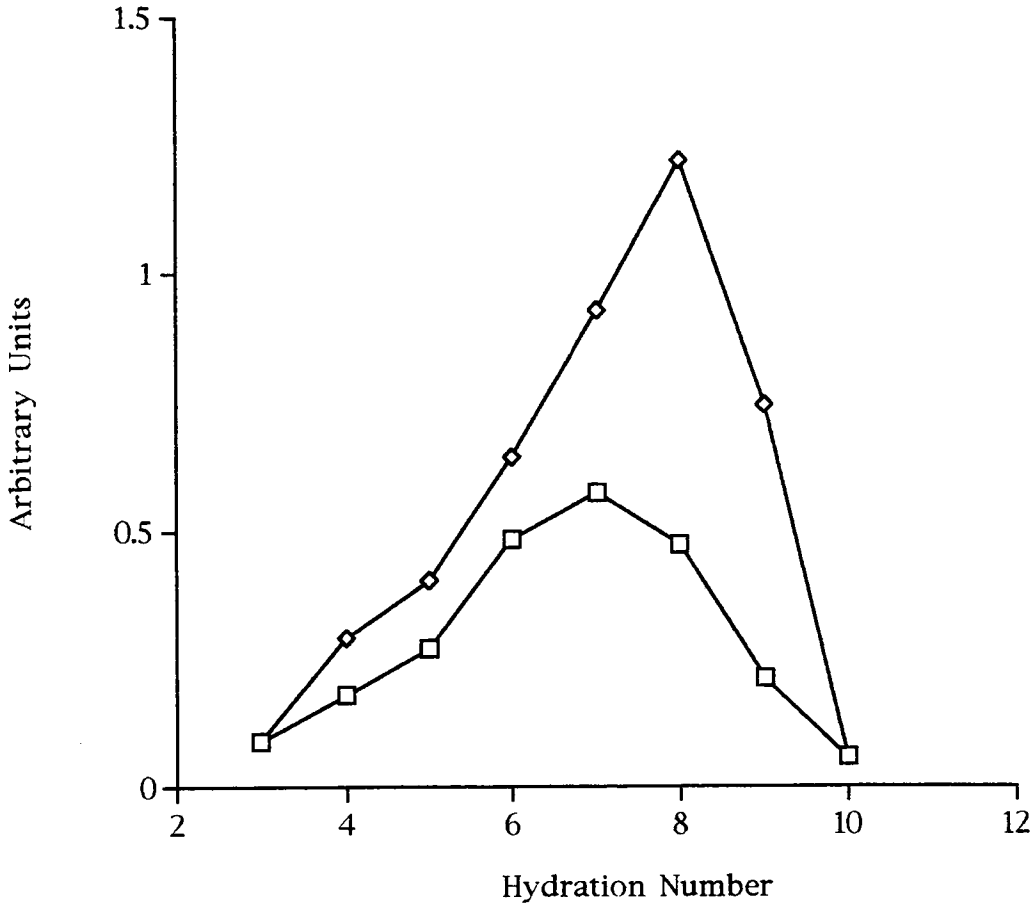



**Figure 5.15.** Comparison of the stable protonated water cluster distribution (□) with the corrected water cluster distribution (◊). The ordinate of the corrected distribution represents the sum of the stable full energy ion intensities and the metastable ion intensities.

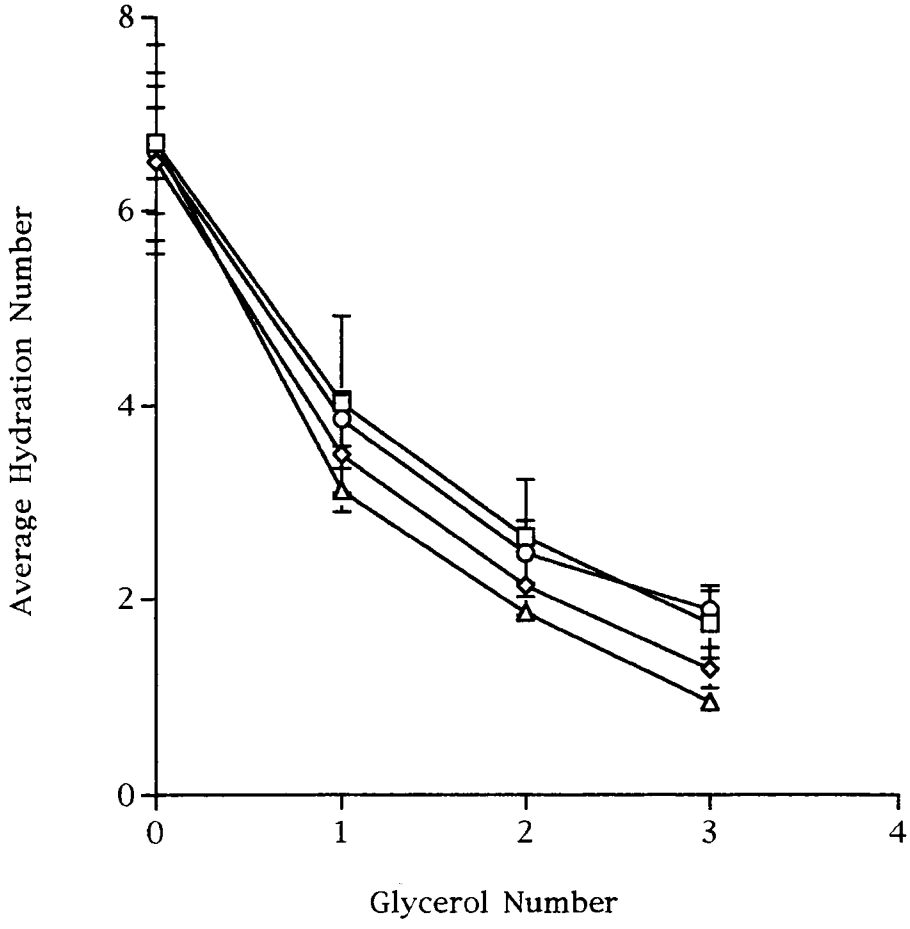



**Figure 5.16.** Dependence of the average proton hydration number on the number of glycerol molecules included in a mixed cluster under different conditions of flow rate and accelerating voltage: ◊ = 5 μL/hour (8 kV needle potential); □ = 5 μL/hour (6 kV needle potential); Δ = 7.5 μL/hour (8 kV needle potential); o = 10 μL/hour (8 kV needle potential). The average hydration number was calculated as follows: Average Hydration Number = $\frac{\Sigma n i_n}{\Sigma i_n}$

While the distributions of clusters from a glycerol solution are easily resolved and assessed, the isobaric interferences mentioned above make the distribution of clusters detected from a thioglycerol solution more difficult to assess. The distribution of water clusters up to n = 5 is unambiguous because of no overlap with thioglycerol clusters. This distribution is shown in Figure 5.17 and is similar to that observed in the spectrum obtained from water/glycerol (Figure 5.1) The distribution of thioglycerol clusters having the general formula $[TG_n + H]^+$ can also be determined if a simple and justifiable assumption is made. The peak at nominally 2 mass units higher than the monoisotopic cluster mass is due mainly to the $^{34}S$ isotope (4.4%) of thioglycerol. If the contribution to this peak from the $^{18}O$ (0.2%) isotope of water can be neglected, the intensity of the $^{34}S$ isotope peak can be used to determine the distribution of thioglycerol clusters having the general formula $[TG_n + H]^+$ (Figure 5.17). This distribution is similar to that observed from glycerol clusters and suggests a bi- or tridentate interaction with the proton.

The distribution of clusters having the general formula $[TG + (H_2O)_n + H]^+$ is more difficult to assess. For clusters of this series with $n \geq 6$, there is an overlapping contribution to intensity from clusters having the general formula $[TG_2 + (H_2O)_{n-6} + H]^+$. This overlap contributes to the $^{34}S$ isotope intensity since both cluster series contain thioglycerol. The distribution of clusters having the general formula $[TG + (H_2O)_n + H]^+$, for $n \leq 5$, can be estimated without this overlap, and is shown in Figure 5.18. The same consideration was given to the clusters having the general formula $[TG_2 + (H_2O)_n + H]^+$ and $[TG_3 + (H_2O)_n + H]^+$ and their distributions are also plotted in Figure 5.18. There do not appear to be any clear trends in the distributions

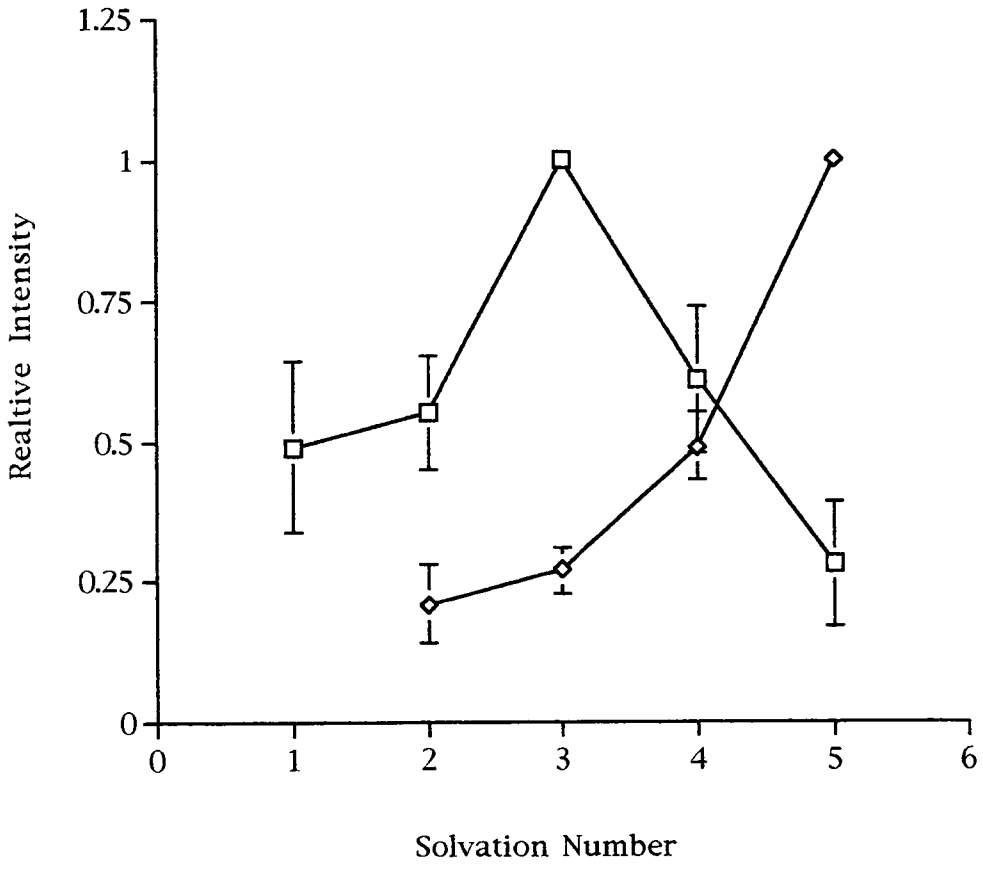



Figure 5.17. A plot of the distribution of water clusters having the general formula $[(H_2O)_n + H]^+$ up to n = 5 (◊) and the distribution of thioglycerol clusters having the general formula $[TG_n + H]^+$ (□) using the intensity of the $^{34}S$-containing isotope peak. Individual data points represent the average of 5 replicates and the error bars represent the standard deviation of the replicates.

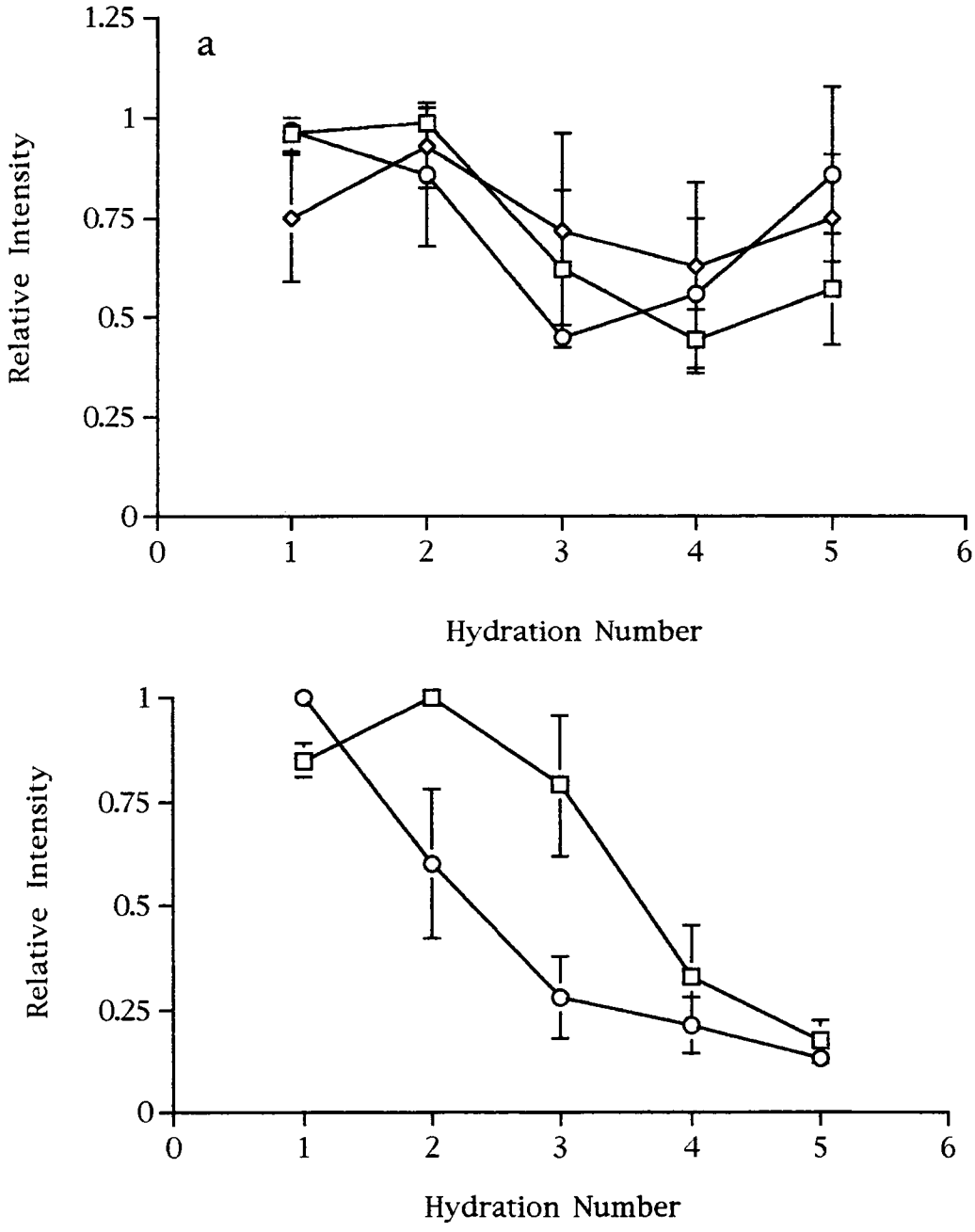



**Figure 5.18.** Plots of cluster relative intensity versus hydration number for the $[TG_m + (H_2O)_n + H]^+$ series using (a) the $^{34}S$ isotope peak to determine intensity and (b) the monoisotopic masses to determine intensity. The symbols represent the following clusters: ◊ = $[TG_1 + (H_2O)_n + H]^+$ ; □ = $[TG_2 + (H_2O)_n + H]^+$ ; o = $[TG_3 + (H_2O)_n + H]^+$. Each series of clusters is normalized to the most abundant ion within that series.

obtained using the $^{34}S$ isotope peak to determine the cluster intensity. The $^{34}S$ isotope peaks are much weaker (typically less than 10% of the base peak in the spectrum) than the monoisotopic peaks which could account for the variability in the data.

Assuming that the overlap of clusters having the general formulae $[TG_1 + (H_2O)_n + H]^+$ and $[TG_2 + (H_2O)_{n-6} + H]^+$ is negligible, the distribution of clusters can be determined from the monoisotopic mass intensities and is shown in Figure 5.18 for comparison with the distributions shown in Figure 5.17. There does appear to be a smooth trend in each distribution (similar to the trend observed for water/glycerol) if the overlap is neglected and the relative intensities of the monoisotopic peaks are plotted as a function of hydration number.

## 5.3 Conclusions

Although EH ionization does sample solvated species directly from solution, desolvation, unknown sensitivities, and the lack of suitable reference standards or reference data has complicated the relationship between the ion/solvent clusters observed in the mass spectrum and the species present in solution. Despite these complications in quantitative interpretation of the results, there is qualitative information, such as the appearance of the EH spectrum changing as a result of changes in solution composition (such as glycerol content and acid concentration) that indicates EH mass spectra are a reflection of solution chemistry. Furthermore, other evidence that solution chemistry dominates the appearance of the mass spectrum is the poor correlation of the observed distribution with the gas-phase distribution data from Kebarle. Therefore, the conclusion that gas-phase chemistry does not govern the observed distribution of clusters and that solution-phase chemistry is a likely alternative explanation, is reasonable. It is difficult to unambiguously conclude, however, that only solution-phase chemistry dominates. Recall that the gas-phase data represent equilibrium conditions, and the EH data are likely a "snapshot" in time that does not represent equilibrium conditions. Again, despite these complications in interpretation, EH has proven to be an approach capable of sampling ion/solvent clusters directly from solution.

Kebarle and others have been able to obtain thermodynamic data because of the ability to accurately control and change the temperature and pressure of the system. The EH source temperature is not known and the pressure reflects the entire source rather than the ionization region (local

pressure), which is probably much higher than the pressure gauge indicates. The gas-phase results from Kebarle, however, are not direct measures of solution-phase chemistry but are used to infer properties of solute/solvent interactions in solution. As already mentioned in section 1.4, the gas-phase measurements can impart an excess of internal energy, while EH has been noted to impart very little internal energy. Experiments suggested in Chapter 6 are designed to obtain MS/MS data for comparison of the relative solvation energies from EH with solvation energies from the gas-phase measurements obtained by Kebarle and others.

While original plans for this project included experiments from purely aqueous solutions, the EH source configuration shown in Figure 2.11 requires a small amount of a low volatility co-solvent such as glycerol or thioglycerol. Attempts at modifying the source to include a metallized fused silica capillary (similar to ES experiments but in vacuum) to eliminate the need for a co-solvent have not been successful. When the metallized capillary was used instead of positioning the fused silica capillary within the platinum emitter, the gold was removed resulting in no emission. This observation has been difficult to explain, but one possible explanation could be the field desorption of the gold from the fused silica capillary. Despite attempts to eliminate the glycerol co-solvent, it is not completely necessary to do so. In fact, there have been several mentions of the lack of sufficient literature references for comparison with results presented in this thesis. The current source configuration affords the acquisition of such data. Also, at least a binary solvent mixture is necessary to probe competitive solvation. The future work presented in Chapter 6 suggests using the VG ZAB-EQ instrument and CID to obtain thermodynamic and structural information.

# Chapter 6

## Conclusions and Suggestions for Future Work

This chapter describes potentially useful studies for extending the results obtained to date and presented within this dissertation. These suggestions are intended to help continue the research program already established in the field of solution chemistry probes using desorption ionization mass spectrometry.

As is clearly evident from the results of Chapter 3, the time dependence and hence, the sensitivity, can be dramatically affected by analyte surface activity and surface phenomena such as the Marangoni effect. Chapter 3 was limited to a very small set of analytes, including a "surfactant" and a "non-surfactant." Predicting the behavior and correcting for the behavior of secondary ion emission would be of paramount importance. For example, in a case where the experiment is sample limited (precious material), it would be necessary to optimize conditions to obtain the best possible sensitivity. Therefore, the small set of analytes used to establish that heterogeneous secondary ion emission from liquid samples should be extended to other classes of compounds commonly analyzed by FAB and LSIMS (such as biomolecules including amino acids and proteins). As illustrated in Chapter 3, the FAB studies should to be done in parallel with the corresponding ion imaging experiment as confirmation.

After establishing a protocol for determining whether or not an analyte will yield heterogeneous emission, it is necessary to take advantage of that information. Taking advantage of the heterogeneous emission is simple using

an imaging instrument, however, most laboratories using FAB and/or LSIMS are not equipped with an imaging instrument, rather they are equipped with a more conventional instrument such as the VG ZAB-EQ with a fixed acceptance aperture. While the acceptance aperture is fixed, the probe tip geometry and position can be varied to coincide with the secondary ion acceptance aperture of the analyzer. Therefore, careful design of probe tips for use on fixed secondary ion acceptance aperture instruments should bring the region of high intensity (discussed in Chapter 3) of secondary ion emission into focus early in the experiment, taking advantage of the increased secondary ion signal from heterogeneous emission.

Chapter 4 clearly illustrated the improved capabilities of continuous infusion electrospray ionization of both aqueous and methanolic solutions relative to conventional ES sources. The ability to spray purely aqueous solutions of proteins ranging in concentration from 21 μM to .21 nM extends the number of experiments potentially useful to biochemists. For example, biomaterials are often synthesized or extracted from natural materials at extremely small yields. The ability to spray concentrations of analyte in the nM region now makes available to many investigators mass spectral information not previously possible with FAB and/or LSIMS or even electrospray. Furthermore, the ability to spray and detect from purely aqueous samples allows further studies of what is thought to be the natural conformations of proteins. Also, the use of an instrument capable of high resolution (e.g., FT ICR) should provide some valuable information concerning the solvation of proteins. Preliminary evidence presented in Chapter 3 indicates that the protein is solvated, but poor mass resolution has precluded any definitive statements about which solvent is present.

An area that clearly needs to be improved is the CE/ESI. The CE/ESI results presented in Chapter 4 were accomplished using a 50 μm i.d. gold-tipped capillary. We have shown that to take advantage of the improved sensitivity of using the gold-tipped capillary, the i.d. must be as small as 25 μm i.d. or smaller. Therefore, repeating the experiments described in Chapter 4 using a 25 μm i.d. or smaller gold-tipped capillary should improve the mass spectrometric detectability. Also, it would be useful to improve the inner capillary coating to improve the chromatographic resolution and efficiency. A more complete inner coating will decrease the interaction of the positively charged biomolecules with the negatively charged silanol groups on the capillary wall. Improving the chromatographic resolution and efficiency will also have dramatic effect on the mass spectrometric detectability.

A study that has already been initiated is aimed at characterizing the pH of the electrospray plume. The electrospray process has long been thought to oxidize the solvent (usually methanol) generating protons and formaldehyde. A goal of the Cook research group has been to confirm, independent of mass spectrometry, that protons are being generated in the electrospray process. This study, which utilizes a pH sensitive fluorescent dye, should be pursued to confirm that protons are in fact being generated. The study should be extended to determine how the pH of the droplet changes as it travels farther from the emitter and evaporation occurs. If protons are being generated, the pH of the droplet must be changing as evaporation takes place during the electrospray process. It would be interesting to determine what the final pH of the droplet, prior to complete evaporation, actually is.

Another fundamental study that would further characterize the electrospray process involves determining if scattering of small (low m/z)

ions occurs within the electrospray plume. A short study that would address this issue involves the use of the bench-top electrospray apparatus and the secondary ion microprobe described in Chapter 2. Spraying a mixture of quaternary ammonium salts onto a LSIMS target and subsequently acquiring the secondary ion image of the target should provide useful information about the distribution of ions in the electrospray plume. If the theory of scattering of low m/z ions is correct, the intensity of secondary ions of low m/z should be greatest at the periphery of the "spray area" and the heavier m/z secondary ion intensity should be greatest in the center of the "spray area." Information about scattering within the electrospray plume could be useful in explaining differences in sensitivity observed in electrospray ionization mass spectrometry.

The results of the EH probe of solution chemistry presented in Chapter 5, like the FAB/LSIMS results of Chapter 3, are limited to a very small set of analytes. The majority of Chapter 5 addressed the results obtained for the apparent preferential solvation of the proton by glycerol in a mixture of water and glycerol in which water was the major solvent component (95 % v/v). In theory, EH ionization is well suited for probing solution chemistry. Thus far, the preliminary studies using the newly designed source have been difficult to interpret due to the convolution of thermodynamic factors and kinetic factors. Nonetheless, qualitative information about preferential solvation appears to be feasible. These studies should also be extended to include a wider variety of solutes and solvents such as biochemical species. Other mass spectrometric approaches to probing solvation are not capable of studying biochemicals because of the nature of the ionization event (biomolecules are typically non-volatile and fragile). EH is a soft ionization

technique capable of sampling non-volatile and fragile molecules from solution.

The results obtained from varying the acid concentration and from varying the glycerol concentration should be expanded to better ascertain the relationship between the critical amounts of water, glycerol, and protons necessary to observe water clusters. A series of titration data similar to that obtained for the 5 volume percent solution should be acquired over the glycerol concentration range 6 to 10 volume percent. The "endpoint" should shift to a higher acid concentration with increases in glycerol concentration and should provide useful insight into the critical stoichiometric ratios of water, glycerol, and protons that yields water clusters.

The gas phase approaches to probing ion/solvent interactions are limited to solvents having sufficient vapor pressure, such as water and methanol. While these solvents are certainly an important class, the non-volatile solvents such as glycerol and thioglycerol also represent an important class of solvents. EH is one approach to probing such solvent systems. In Chapter 5, the lack of reference data or information concerning thermodynamics, structure and dynamics for glycerol was mentioned several times. While the results presented in Chapter 5 are certainly useful and interesting, adapting the modified source to work on the VG ZAB-EQ would afford thermodynamic information not attainable on the MS-9 instrument. The ZAB-EQ is capable of mass selecting one of the ion/solvent clusters using the double focusing portion of the instrument and then subjecting that cluster to a region of high pressure where the clusters undergo collisions to remove solvent molecules. The energy of the collision can be controlled to provide information about the collision induced dissociation (CID) energy threshold.

This CID threshold, as mentioned in the introduction, can be used to determine thermodynamic values of non-equilibrium systems such as this. This approach could provide the step-wise thermodynamic data (e.g., free energy) that is currently not available for the less volatile solvent such as glycerol and thioglycerol.

# LIST OF REFERENCES

# LIST OF REFERENCES


1 Barber, M.; Bordoli, R.S.; Sedgwick, R.D.; Tyler, A.N. *J. Chem. Soc. Chem. Comm.* 1981, 325.

2 Yamashita, M.; Fenn, J.B. *J. Phys. Chem.* 1984, 88, 4451-4459.

3 Karas, M.; Bachmann, D.; Bahr, U.; Hillenkamp, F. *Int. J. Mass Spectrom. Ion Processes* 1987, 78, 53.

4 Evans, C.A., Jr.; Hendricks, C.D. *Rev. Sci. Instrum.* 1972, 43, 1527.

5 Aberth, W.; Straub, K.M.; Burlingame, A.L. *Anal. Chem.* 1982, 54, 2029.

6 Watson, J.T. *Introduction to Mass Spectrometry*, 2nd ed.; Raven Press, New York, 1985.

7 Burlingame, A.L.; Baillie, T.A.; Russell, D.H. *Anal. Chem.* 1992, 64, 467R.

8 Burlingame, A.L.; Boyd, R.K.; Gaskell, S.J. *Anal. Chem.* 1994, 66, 634R.

9 Benninghoven, A.; Jaspers, D.; Sichtermann, W. *Appl. Phys.* 1976, 11, 35.

10 Williams, D.H.; Bradley, C.; Bojesen, G.; Santikarn, S.; Taylor, L.C.E. *J. Am. Chem. Soc.* 1981, 103, 5700.

11 Forsberg, L.S.; Dell, A.; Walton, D.J.; Ballou, C.E. *J. Biol. Chem.* 1982, 257, 3555.

12 Whitney, J.; Lewis, S.; Straub, K.M.; Thaler, M.M.; Burlingame, A.L. *Proc. Jpn. Soc. Med. Mass Spectrom.* 1981, 6, 33.

13 Barber, M.; Bordoli, R.S.; Sedgwick, R.D.; Tyler, A.N. *Nature* 1981, 293, 270.

14 Pachuta, S.J.; Cooks, R.G. *Chem. Rev.* 1987, 87, 647.

15 Williams, D.H.; Findeis, A.F.; Naylor, S.; Gibson, B.W. *J. Am. Chem. Soc.*

1987, 109, 1980.

16 Sunner, J.; Morales, A.; Kebarle, P. *Anal. Chem.* **1988**, 60, 98.

17 Van der Peyl, G.J.Q.; Van der Zande, W.J.; Hoogerbrugge, R.; Kistemaker, P.G. *Int. J. Mass Spectrom. Ion Processes* **1985**, 67, 147.

18 Thompson, M.W. *Philos. Mag.* **1968**, 18, 377.

19 Sigmund, P. *Phys. Rev.* **1969**, 184, 383.

20 Biersack, J.P.; Haggmark, L.G. *Nucl. Instrum. Methods* **1980**, 174, 257.

21 Magee, C.W. *Int. J. Mass spectrom. Ion Processes* **1983**, 49, 211.

22 Applehans, A.D.; Delmore, J.E. *Anal. Chem.* **1989**, 61, 1087.

23 Aberth, W. *Anal. Chem.* **1986**, 58, 1221.

24 Winger, B.E.; Hand, O.W.; Cooks, R.G. *Int. J. Mass Spectrom. Ion Processes* **1988**, 84, 89.

25 Aberth, W.H.; Burlingame, A.L. *Anal. Chem.* **1988**, 60, 1426.

26 Reynolds, J.D.; Cook, K.D. *J. Am. Soc. Mass Spectrom.* **1990**, 1, 149.

27 Todd, P.J. *Org. Mass Spectrom.* **1988**, 23, 419.

28 Brown, S.M.; Busch, K.L. *Rapid Commun. Mass Spectrom.* **1988**, 2, 256.

29 Castro, M.E.; Mallis, L.M.; Russell, D.H. *J. Am. Chem. Soc.* **1985**, 107, 5652.

30 Fenselau, C.; Cotter, R.J. *Chem Rev.* **1987**, 87, 501.

31 Fenselau, C. *Anal. Chem.* **1982**, 54, 104A.

32 Sweetman, B.J.; Blair, I.A. *Biomed. Environ. Mass Spectrom.* **1988**, 17, 337.

33 Cook, K.D.; Todd, P.J.; Friar, D.H. *Biomed. Environ. Mass Spectrom.* **1989**, 18, 492.

34 De Pauw, E. *Mass Spectrom. Rev.* **1986**, 5, 191.

35 De Pauw, E.; Agnello, A.; Derwa, F. *Mass Spectrom. Rev.* 1991, 10, 283.

36 Barofsky, D.F.; Giessmann, U.; Barofsky, E. *Int. J. Mass Spectrom. Ion Phys.* 1983, 53, 319-322.

37 Field, F.H. *J. Phys. Chem.* 1982, 86, 5115-5123.

38 Cole, R.B.; Guenat, C.; Hass, J.R.; Linton, R.W. *Anal. Chem.* 1987, 59, 1930-1937.

39 Gale, P.J.; Bentz, B.L.; Chait, B.T.; Field, F.H.; Cotter, R.J. *Anal. Chem.* 1986, 58, 1070-1076.

40 Wong, S.S.; Röllgen, F.W. *Nucl. Inst. Methods* 1986, B14, 436-447.

41 Tuinman, A.A.; Cook, K.D. *J. Am. Soc. Mass Spectrom.* 1992, 3, 318-325.

42 Martin, S.A.; Costello, C.E.; Biemann, K. *Anal. Chem.* 1982, 54, 2362-2368.

43 Bolbach, G.; Viari, A.; Galera, R.; Brunot, A.; Blais, J.C. *Int. J. Mass Spectrom. Ion Processes* 1992, 112, 93-100.

44 Ligon, W.V.; Dorn, S.B. Int. *J. Mass Spectrom. Ion Processes* 1984, 57, 75-90.

45 Ligon, W.V.; Dorn, S.B. *Int. J. Mass Spectrom. Ion Processes* 1986, 78, 99-113.

46 Lacey, M.P.; Keough, T. *Rapid Commun. Mass Spectrom.* 1989, 3, 46-50.

47 Kleber, W. *Tech. Dig.* 1967, 9, 550.

48 Steiner, A.M.; Fuchs, H. *Seed Sci. Technol.* 1987, 15(3), 707.

49 Childs, R.E.; Mansout, N.N. *J. Propul. Power* 1989, 5, 641.

50 Dole, M.; Mach, L.L.; Hines, R.L.; Mobley, R.C.; Ferguson, L.P.; Alice, M.B. *J. Chem. Phys.* 1968, 49, 2240.

51 Mach, L.L.; Kralik, P.; Rheude, A.; Dole, M. *J. Chem. Phys.* 1970, 52, 4977.

52 Clegg, G.A.; Dole, M. *Biopolymers* 1971, 10, 821.

53 Teer, D.; Dole, M. *J. Polym. Sci.* 1975, 13, 985.

54 Dole, M.; Cox, Jr., H.L.; Gienec, *J. Adv. Chem. Serv.* 1973, No.125, 73.

55 Iribarne, J.V.; Thomson, B.A. *J. Phys. Chem.* 1976, 64, 2287.

56 Thomson, B.A.; Iribarne, J.V. *J. Chem. Phys.* 1979, 71, 4451.

57 Kebarle, P.; Tang, L. *Anal. Chem.* 1993, 65, 972A-986A.

58 Smith, R.D.; Loo, J.A.; Ogorzalek Loo, R.R.; Busman, M.; Udseth, H.R. *Mass Spectrom. Rev.* 1991, 10, 359-451..

59 Röllgen, F.W.; Bramer-Wegner, E.; Buttering, L. *J. Phys. Colloq.* 1984, 45, Supplement 12, C9-297.

60 Schmelzeisen-Redeker, G.; Buttering, L.; Röllgen, F.W. *Int. J. Mass Spectrom. Ion Processes* 1989, 90, 139.

61 Pfeifer, R.J.; Hendricks, C.D. *AIAA Journal* 1968, 6, 496.

62 Smith, D.P.H. *IEEE Trans. Ind. Appl.* 1986, IA-22(3), 527.

63 Tang, L.; Kebarle, P. *Anal. Chem.* 1993, 65, 3654-3668.

64 Chowdhury, S.K.; Chait, B.T. *Anal. Chem.* 1991, 63, 1660-1664.

65 Cheng, Z.L.; Siu, K.W.M.; Guevremont, R.; Berman, S.S. *J. Am. Soc. Mass Spectrom.* 1992, 3, 281-288.

66 Tang, L.; Kebarle, P. *Anal. Chem.* 1991, 63, 2709-2715.

67 Ikonomou, M.G.; Blades, A.T.; Kebarle, P. *J. Am. Soc. Mass Spectrom.* 1991, 2, 497-505.

68 Cole, R.B.; Harrata, K. *J. Am. Soc. Mass Spectrom.* 1993, 4, 546-556.

69 Fenn, J.B.; Mann, M.; Meng, C.K.; Wong, S.F.; Whitehouse, C. *Mass Spectrom. Rev.* 1990, 9, 37.

70 Lee, E.D.; Henion, J.D. *Rapid Comm. Mass Spectrom.* 1992, 10, 727.

71 Guevremont, R.; Siu, K.W.M.; Le Blanc, J.C.Y.; Berman, S.S. J. *Am. Soc. Mass Spectrom.* 1992, 3, 216-224.

72 Ikonomou, M.G.; Blades, A.T.; Kebarle, P. *Anal. Chem.* 1990, 62, 957-967.

73 Gatlin, C.L.; Turecek, F. *Anal. Chem.* 1994, 66, 712-718.

74 Goodlett, D.R.; Loo, R.R.O.; Loo, J.A.; Wahl, J.H.; Udseth, H.R.; Smith, R.D. *J. Am. Soc. Mass Spectrom.* 1994, 5, 614-622.

75 Ikonomou, M.G.; Kebarle, P. *J. Am. Soc. Mass Spectrom.* 1994, 5, 791-799.

76 Mirza, U.A.; Cohen, S.L.; Chait, B.T. *Anal. Chem.* 1993, 65, 1-6.

77 Chowdhury, S.K.; Katta, V.; Chait, B.T. *J. Am. Chem. Soc.* 1990, 112, 9012.

78 Wagner, D.S.; Anderegg, R.J. *Anal. Chem.* 1994, 66, 706-711.

79 Katta, V.; Chait, B.T. *Rapid. Comm. Mass Spectrom.* 1991, 5, 214.

80 LeBlanc, J.C.Y; Beuchemin, D.; Siu, K.W.M.; Guevremont, R.; Berman, S.S. *Org. Mass Spectrom.* 1991, 26, 831.

81 Gale, D.C.; Smith, R.D. *Rapid Comm. Mass Spectrom.* 1993, 7, 1017-1021.

82 Goodlett, D.R.; Wahl, J.H.; Udseth, H.R.; Smith, R.D. *J. Microcol. Sep.* 1993, 5, 57-62.

83 Wahl, J.H.; Goodlett, D.R.; Udseth, H.R.; Smith, R.D. *Electrophoresis* 1993, 14, 448-457.

84 Wahl, J.H.; Goodlett, D.R.; Udseth, H.R.; Smith, R.D. *Anal. Chem.* 1992, 64, 3194-3195.

85 Jorgenson, J.W.; Lukacs, K.D. *Science* 1983, 222, 266-272.

86 Olivares, J.A.; Nguyen, N.T.; Yonker, C.R.; Smith, R.D. *Anal. Chem.* 1987, 59, 1230-1232.

87 Smith, R.D.; Olivares, J.A.; Nguyen, N.T.; Udseth, H.R. *Anal. Chem.* **1988**, 60, 436-441.

88 Smith, R.D.; Barinaga, C.J.; Udseth, H.R. *Anal. Chem.* **1988**, 60, 1948-1952.

89 Lee, E.D.; Muck, W.; Henion, J.D.; Covey, T.R. *J. Chromatogr.* **1988**, 458, 313-321.

90 Pleasance, S.; Thibault, P.; Kelley, J. *J. Chromatogr.* **1992**, 591, 325-339.

91 Jorgenson, J.W.; Dohmeier, D.M.; Austell, T.L. Presented at Pittcon 1992, Pittsburgh Conference, New Orleans, LA, March 9-12, 1992.

92 Chowdhury, S.W.; Chait, B.T. *Anal. Chem.* **1991**, 63, 1660-1664.

93 Smith, R.D.; Wahl, J.H.; Goodlett, D.R.; Hofstadler, S.A. *Anal. Chem.* **1993**, 65, 574A-584A.

94 Dohmeier, D.M.; Austell, T.L.; Jorgenson, J.W. *Fourth International Conference on High Performance Capillary Electrophoresis*; Amsterdam, The Netherlands, Feb. 1992.

95 Van Berkel, G.J.; McLuckey, S.A.; Glish, G.L. *Anal. Chem.* **1992**, 64, 1586-1593.

96 Fang, L.; Zhang, R.; Zare, R.N. *Proceedings of the 41st ASMS Conference on Mass Spectrometry and Allied Topics*; San Francisco, CA, May 1993; 755A.

97 Cook, K.D. *Mass Spectrom. Rev.* **1986**, 5, 467.

98 Simons,D.S.; Colby, B.N.; Evans, C.A., Jr. *Int. J. Mass Spectrom. Ion Phys.* **1974**, 15, 291.

99 Stimpson, B.P.; Evans, C.A., Jr. *Biomed. Mass Spectrom.* **1978**, 5, 52.

100 Stimpson, B.P.; Evans, C.A., Jr. *Electrostatics* **1978**, 5, 411.

101 Lai, S.T.F.; Evans, C.A., Jr. *Org. Mass Spectrom.* **1978**, 13, 733.

102 Chan, K.W.S.; Cook, K.D. *J. Am. Chem. Soc.* **1982**, 104, 5031.

103 Man, V.F.; Lin, J.D.; Cook, K.D. *J. Am. Chem. Soc.* **1985**, 107, 4635.

104 Cook, K.D.; Chan, K.W.S. *Int. J. Mass Spectrom. Ion Processes* **1983**, 54, 135.

105 Chan, K.W.S.; Cook, K.D. *Anal. Chem.* **1983**, 55, 1306.

106 Lai, S.T.F.; Chan, K.W.S.; Cook, K.D. *Macromolecules* **1980**, 13, 953.

107 Cook, K.D.; Callahan, J.H.; Man, V.F. *Anal. Chem.* **1988**, 60, 706.

108 Callahan, J.H. *Ph.D. Thesis* **1986**, University of Illinois, Urbana, IL.

109 Callahan, J.H.; Hool, K.; Reynolds, J.D.; Cook, K.D. *Int. J. Mass Spectrom. Ion Processes* **1987**, 75, 291.

110 Boggess, W.C., Jr. *Ph.D. Thesis* **1994**, University of Tennessee, Knoxville, TN.

111 Reynolds, J.D.; Cook, K.D. *J. Am. Soc. Mass Spectrom.* **1990**, 1, 233-237.

112 Murawski, S.L.; Cook, K.D. *Anal. Chem.* **1984**, 56, 1015.

113 Murawski, S.L.; Cook, K.D. *34th Ann. Conf. Mass Spectrom. Allied Topics*, Cincinnati, June **1986**, 786.

114 Bel, P.; Cook, K.D. *35th Ann. Conf. Mass Spectrom. Allied Topics*, Denver, May **1987**, 786.

115 Salvato, S.W. *MS Thesis* **1995**, University of Tennessee, Knoxville, TN.

116 Dobychin, S.L.; Mil'man, B.L.; Turkin, M.Ya. *Zh Org. Khim.* **1978**, 14, 2221.

117 Dobychin, S.L.; Mil'man, B.L.; Turkin, M.Ya. *Teor. Eksp. Khim.* **1979**, 15, 429.

118 Mil'man, B.L.; Kuznetsov, M.A. *Zh. Org. Khim.* 1980, 16, 702.

119 Zolotoi, N.B.; Karpov, G.V.; Tal'roze, V.L.; Skurat, V.E.; Ramendik, G.I.; Vasyuta, Yu.V.; *Zh. Anal. Khim.* 1980, 35, 1461.

120 Zolotoi, N.B.; Karpov, G.V.; Tal'roze, V.L.; Skurat, V.E.; Ramendik, G.I.; Vasyuta, Yu.V.; *Zh. Anal. Khim.* 1980, 35, 1781.

121 Alexandrov, M.L.; Gall, L.N.; Krasnov, N.V.; Nikoleav, V.I.; Pavlenko, V.A.; Shkurov, V.A. *Int. J. Mass Spectrom. Ion Processes* 1983, 54, 231.

122 Alexandrov, M.L.; Baram, G.I.; Gall, L.N.; Grachev, M.A.; Knorre, V.D.; Krasnov, N.V.; Kusner, Yu. S.; Mirgorodskaya, O.A.; Nikoleav, V.I.; Shkurov, V.A. *Bioorg. Khim.* 1985, 11, 705.

123 Mahoney, J.F.; Perel, J.; Lee, T.D.; Legesse, K. *37th Ann. Conf. Mass Spectrom. Allied Topics*, Miami Beach, May 1989, 549.

124 Mahoney, J.F.; Perel, J.; Lee, T.D.; Legesse, K. *37th Ann. Conf. Mass Spectrom. Allied Topics*, Miami Beach, May 1989, 582.

125 Yakovlev, B.S.; Talrose, V.L.; Fenselau, C. *Anal. Chem.* 1994, 66, 1704-1707.

126 Marcus, Y. *Ion Solvation* Wiley Interscience: New York, 1985.

127 Ben-Naim, A. *Solvation Thermodynamics* Plenum Press: New York, 1987.

128 Conway, B.E. *Ionic Hydration in Chemistry and Biophysics* Elsevier: New York, 1981.

129 Murrell, J.N.; Boucher, E.A. *Properties of Liquids and Solutions* John Wiley & Sons Limted, New York, 1982.

130 Chuang, H.J.; Soong, L.L.; Leroi, G.E.; Popov, A. *J. Solution Chem.* 1989,

18, 759-768.

131 Sacco, A.; *Chem Soc. Rev.* 1994, 23(2), 129-136.

132 Coetzee, J.F.; Ritchie, C.D. *Solute-Solvent Interactions* (Vol. 2) Marcel Dekker, Inc.: New York, 1976.

133 Chazin, W.J. *Curr. Opin. Biotechnol.* 1992, 3(4), 326-332

134 Delpuech, J.J. *Analyt (London)* 1992, 117(3), 267-288.

135 Taniewska-Osinska, S. *Chem. Soc. Rev.* 1993, 21, 205.

136 Buckingham, A.D.; Legon, A.C.; Roberts, S.M.; *Princ. Mol. Recognit.* Blackies, Glasgow, UK (1993).

137 Maroncelli, M. *J. Mol. Liq.* 1993, 57, 1-37.

138 Enderby, J.E. *J. Phys.: Condens. Matter* 1991, 3(42), F87-90.

139 Owrutsky, J.C.; Raftery, D.; Hochstrasser, R.M. *Annu. Rev. Phys. Chem.* 1994, 45, 519-555.

140 Weitz, E.; Wells, J.R.; Ryther, R.J.; House, P. *ACS Symp. Ser.* 1993, 530 (Laser Chemistry of Organometallics), 147-163.

141 Goyal, S.; Schutt, D.L; Scoles, G. *Acc. Chem. Res.* 1993, 26(3), 123-130.

142 Mendolia, M.; Cai, H.; Farrington, G.C. Report 1992, Order No. AD-A260355, 53 pp. Avail.: NTIS From: Gov. Rep. Announce. Index (U.S.) 1993, 93(11), Abstr. No. 331,404.

143 Elsaesser, T.; Kaiser, W. *Annu. Rev. Phys. Chem.* 1991, 42, 83-107.

144 Syage, J.A. *Z. Phys. D.: At., Mol. Clusters* 1994, 30(1), 1-12.

145 Watanabe, I. *Anal. Sci.* 1994, 10(2), 229-239.

146 Schlick, S.; Alonso-Amigo, M.G.; Bednarek, J. *Colloids Surf., A* 1993, 72, 1-9.

147 Roozen, M.J.G.W.; Hemminga, M.A. *J. Phys. Chem.* 1990, 94, 7326-7329.

148 Meech, S.R. *Annu. Rep. Prog. Chem., Sect. C* 1991, Volume Date 1990, 87, 199-246.

149 Hirata, Y.; Matag, N. *Prog. React. Kinet.* 1993, 18(3), 273-308.

150 Auzanneau, I.; Combes, D.; Zwick, A. *J. of Raman Spec.* 1991, 22, 227-231.

151 Rowlen, K.L.; Harris, J.M. *Anal. Chem.* 1991, 63, 964-969.

152 Neilson, G.W.; Broadbent, R.D. *Chem. Phys. Lett.* 1990, 167, 429.

153 Neilson, G.W.; Enderby, J.E. *J. Phys. C.: Solid State Phys.* 1978, 11L625.

154 Neilson, G.W.; Enderby, J.E. *Adv. Inorg. Chem.* 1989, 34, 195.

155 Sima, J.; Labuda, J. *Comments Inorg. Chem.* 1993, 15(2), 93-108.

156 Stuve, E.M.; Kizhakevariam, N. *J. Vac. Sci. Technol., A* 1993,, 11(4, Pt. 2), 2217-2224.

157 Conway, B.E. *Chem. Soc. Rev.* 1992, 21(4), 253-261.

158 Doblhofer, K. *J. Electroanal. Chem.* 1992, 331(1-2), 1015-1027.

159 Philpott, M.R. Report 1991, TR-29; Order No. AD-A237 127, 19 pp. Avail.: NTIS From: Gov. Rep. Announce. Index (U.S.) 1991, 91(21), Abstr. No. 158,248.

160 Smith, B.B.; Hynes, J.T. Condens. Matter Phys. Aspects Electrochem., Proc. Conf. 1991, Meeting Date 1990, 436-448. Editors: Tosi, M.P.; Kornyshev, A.A.; Publisher: World Sci., Singapore, Singapore.

161 Izutsu, K. *Anal. Sci.* 1991, 7(1), 1-8.

162 Stamatovic, A.S.; Maerk, T.D. *Rapid. Comm. Mass Spectrom.* 1991, 5, 51-57.

163 Castleman, A.W., Jr. *Chem Rev.* 1986, 86, 589-618.

164 Castleman, A.W., Jr. *Int. J. Mass Spectrom. Ion Processes* 1992, 118/119, 167-189.

165 Kebarle, P.; Searles, S.K.; Zolla, A.; Arshadi, M.J. *J. Am. Chem. Soc.* 1967, 89, 6393.

166 Cunningham, A.J.; Payzant, A.D.; Kebarle, P. *J. Am. Chem. Soc.* 1972, 94, 7627.

167 Lau, Y.K.; Ikuta, S.; Kebarle, P. *J. Am. Chem. Soc.* 1982, 104, 1462.

168 Fehsenfeld, F.C.; Ferguson, E.E. *J. Chem. Phys.* 1973, 59, 6272.

169 Bohme, D.K.; Hemsworth, R.S.; Rundle, H.W.; Schiff, H.I. *J. Chem. Phys.* 1973, 58, 3504.

170 Ferguson, E.E.; Fehsenfeld, F.C.; Schmeltekopf, A.L. *Adv. At. Mol. Phys.* 1969, 5, 1.

171 Dunkin, F.C.; Fehsenfeld, F.C.; Schmeltekopf, A.L.; Ferguson, E.E. J. *Chem. Phys.* 1968, 49, 1365.

172 Fehsenfeld, F.C. *Int. J. Mass Spectrom. Ion Phys.* 1975, 16, 151.

173 Bowers, M.T.; Aue, D.H.; Webb, H.M.; McIver, R.T. *J. Am. Chem. Soc.* 1971, 93, 4314.

174 Henderson, W.G.; Taagepera, D.; Holtz, D.; McIver, R.T.; Beauchamp, J.L.; Taft, R.W. *J. Am. Chem. Soc.* 1972, 94, 4728.

175 McIver, R.T. *Rev. Sci. Instrum.* 1970, 41, 555.

176 McMahon, T.B.; Beauchamp, J.L. *Rev. Sci. Instrum.* 1972, 43, 509.

177 Xu, Y.; Jarvis, V.M.; Bostwick, D.E.; Moran, T.F. *Org. Mass Spectrom.* 1991, 26, 892-898.

178 Sunner, J. *Org. Mass Spectrom.* 1993, 28(8), 805-823.

179 Sunner, J.; Morales, A.; Kebarle, P. *Anal. Chem.* **1987**, 59(10), 1378-1383.

180 Todd, P.J. *J. Am. Soc. Mass Spectrom.* 1991, 2, 33-44.

181 Sunner, J.A.; Kulatunga, R.; Kebarle, P. *Anal. Chem.* **1986**, 58, 1312-1316.

182 Stace, A.J.; Shukla, A.K. *J. Am. Chem. Soc.* **1982**, 104, 5314-5318.

183 Ceyer, S.T.; Tiedmann, P.W.; Ng, C.Y.; Mahan, B.H.; Lee, Y.T. *J. Phys. Chem.* **1979**, 70, 2138.

184 Cook, K.D.; Jones, G.G.; Taylor, J.W. *Int. J. Mass Spectrom. Ion Phys.* **1980**, 35, 273.

185 Searcy, J.Q.; Fenn, J.B. *J. Chem. Phys.* **1974**, 61, 5282.

186 Dawson, P.H. *Int. J. Mass Spectrom. Ion Processes* **1982**, 43, 195.

187 Magnera, T.F.; David, D.E.; Michl, J. *Chem Phys. Lett.* **1991**, 182, 363.

188 Dalleska, N.F.; Honma, K.; Sunderlin, L.S.; Armentrout, P.B. J. *Am. Chem. Soc.* **1994**, 116, 3519-3528.

189 Dalleska, N.F.; Honma, K..; Armentrout, P.B. *J. Am. Chem. Soc.* **1993**, 115, 12125-12131.

190 Karpas, Z.; Eiceman, G.A.; Harden, C.S.; Ewing, R.G. *J. Am. Soc. Mass Spectrom.* **1993**, 4, 507-512.

191 Castleman, A.W., Jr.; Keesee, R.G. *Acc. Chem. Res.* **1986**, 19, 413.

192 Castleman, A.W., Jr.; Keesee, R.G. *Science* **1988**, 241, 36.

193 Aviyente, V.; Iraqi, M. Peres, T.; Lifshitz, C. *J. Am. Soc. Mass Spectrom.* **1991**, 2, 113-119.

194 Stace, A.J.; Moore, C. *Chem. Phys. Lett.* **1983**, 96, 80.

195 Mark, T.D.; Castleman. A.W., Jr. *Adv. At. Mol. Phys.* **1984**, 20, 65.

196 Boesl, U.; Weinkauf, R.; Schlag, E.W. *Int. J. Mass Spectrom. Ion Processes*

1992, 112, 121.

197 Echt, O.; Dao, P.D.; Castleman, A.W., Jr. *J. Chem. Phys.* 1985, 82, 4076.

198 Morgan, S.; Castleman, A.W., Jr. *J. Phys. Chem.* 1989, 93, 4544.

199 Lifshitz, C.; Louage, F. *J. Phys. Chem.* 1989, 93, 5633.

200 Lifshitz, C.; Louage, F. *Int. J. Mass Spectrom. Ion Processes* 1990, 101, 101.

201 Lifshitz, C.; Iraqi, M.; Peres, T. *Rapid Comm. Mass Spectrom.* 1990, 4, 485.

202 Wei, S.; Tzeng, W.B.; Castleman, A.W., Jr. *J. Chem. Phys.* 1990, 92, 332.

203 Wei, S.; Castleman, A.W., Jr. *Int. J. Mass Spectrom. Ion Processes* 1994, 131, 233-264.

204 Mahoney, J.F.; Cornett, D.S.; Lee, T.D. *Rapid Comm. Mass Spectrom.* 1994, 8, 403-406.

205 Kebarle, P. *Abstract of papers of the American Chemical Society* 1994, 207, Iss Mar, part I, PP 93-ANYL.

206 Blades, A.T.; Ikonomou, M.G.; Kebarle, P. *Anal. Chem.* 1991, 63, 2109-2114.

207 Blades, A.T.; Ikonomou, M.G.; Kebarle, P. *Anal. Chem.* 1991, 63, 1989-1998.

208 McLuckey, S.A.; Glish, G.L.; Asano, K.G.; Bartmess, J.E. *Int. J. Mass Spectrom. Ion Processes* 1991, 109, 171-186.

209 Anacleto, J.F.; Pleasance, S.; Boyd, R.K. *Org. Mass Spectrom.* 1992, 27, 660-666.

210 Cole, R.B.; Harrata, A.K. *Rapid Commun. Mass Spectrom.* 1992, 6, 536-539.

211 Douglas, D.J. Presented at the Winter Conference on Plasma Spectrochemistry, St. Petersburg, FL, January 1990, Paper IL-11.

212 Blades, A.T.; Jayaweera, P.; Ikonomou, M.G.; Kebarle, P. *J. Chem. Phys.* 1990, 92, 5900.

213 Jayaweera, P.; Blades, A.T.; Ikonomou, M.G.; Kebarle, P. *Int. J. Am. Chem. Soc.* 1990, 112, 2452.

214 Blades, A.T.; Jayaweera, P.; Ikonomou, M.G.; Kebarle, P. *Int. J. Mass Spectrom. Ion Processes* 1990, 101, 325.

215 Blades, A.T.; Jayaweera, P.; Ikonomou, M.G.; Kebarle, P. *Int. J. Mass Spectrom. Ion Processes* 1990, 102, 251.

216 Brutschy, B. *Chem. Rev.* 1992, 92, 1567-1587.

217 Grimm, C.C.; Short, R.T.; Todd, P.J. *J. Am. Soc. Mass Spectrom.* 1991, 2, 362-371.

218 Todd, P.J.; Short, R.T.; Grimm. C.C.; Markey, S.P. *Anal. Chem.* 1992, 24, 1871-1878.

219 Leibl, H. U.S. Patent 3,517,191.

220 Waltman, R.J.; Bargon, J.; Diaz, A.F. *J. Phys. Chem.* 1983, 87, 1459-1463.

221 Van Berkel, G.J.; Glish, G.L; McLuckey, S.A. *Anal. Chem.* 1990, 62, 1284.

222 McLuckey, S.A.; Glish, G.L; Van Berkel, G.J. *Anal. Chem.* 1991, 63, 1971.

223 McLuckey, S.A.; Van Berkel, G.J.; Goeringer, D.E.; Glish, G.L. *Anal Chem.* 1994, 66, 689A-695A.

224 Moseley, M.A.; Jorgenson, J.W.; Shabanowitz, J.; Hunt, D.F.; Tomer, K.B. *J. Am. Soc. Mass Spectrom.* 1992, 3, 289-300.

225 Goss, C.A.; Charych, D.H.; Majda, M. *Anal. Chem.* 1991, 63, 85-88.

226 Stimpson, B.P.; Simons, D.S.; Evans, C.A., Jr. *J. Phys. Chem.* 1978, 82, 660.

227 McEwan, C.N.; Layton, S.F.; Taylor, S.K. *Anal. Chem.* 1977, 49, 922.

228 Tuinman, A.A.; Cook, K.D. *J. Am. Soc. Mass Spectrom.* 1994, 5, 92-99.

229 Derwa, F.; DePauw, E.; Natalis, P. *Org. Mass Spectrom.* 1991, 26, 117.

230 Katritzky, A.R.; Watson, C.H.; Dega-Szafran, Zofia, Eyler, J.R. *J. Am. Chem. Soc.* 1990, 112, 2471.

231 Caprioli, R.M. *Anal. Chem.* 1983, 55, 2387-2391.

232 Todd, P.J.; Groenewold, G.S. *Anal. Chem.* 1986, 58, 895-899.

233 Heimenz, P.C. *Principles of Colloid and Surface Chemistry*, 2nd ed.; Marcel Dekker, Inc.: New York, 1986.

234 Adamson, A.W. *Physical Chemistry of Surfaces*, 2nd ed.; Wiley Interscience: New York, 1967.

235 McBain, J.W.; Swain, R.C. *Proc. R. Soc. London* 1936, A154, 608-618.

236 Evanoff, J.E.; Harris, W.E. *Can. J. Chem.* 1978, 56, 574-577.

237 Ligon, W.V. *Int. J. Mass Spectrom. Ion Phys.* 1983, 52, 189.

238 Standing, K.G.; Chait, B.T.; Ens, N.; McIntosh, G.; Beavis, R. *Nucl. Inst. Methods* 1982, 198, 33.

239 Kriger, M.S.; Cook, K.D.; Short, R.T.; Todd, P.J. *Anal. Chem.* 1992, 64, 3052-3058.

240 Boggess, B.; Cook, K.D. *J. Am. Soc. Mass Spectrom.* 1994, 5, 100.

241 Tanford, C. *The Hydrophobic Effect: Formation of Micelles and Biological Membranes*; John Wiley & Sons, New York, 1973.

242 de Visser, C.; Somsen, G. *J. Chem. Thermodyn.* 1972, 4, 313.

243 Shahgholi, M. *Ph.D. Thesis* 1993, University of Tennessee,

Knoxville, TN.

244 Woolf, L.A.; Weingartner, H. *Faraday Trans.* **1982**, 17, 41.

245 Mittal, K.L.; Botherel, P., ed., *Surfactants in Solution*, Vol. 4, Plenum Press, New York, NY, 1986.

246 Benninghoven, A.; Rudenaur, F.G.; Werner, H.W. *Secondary Ion Mass Spectrometry*; Wiley: New York, 1987; pp 726-727.

247 Barber, M.; Bell, D.; Eckersley, M.; Morris, M.; Tetler, L. *Rapid Commun. Mass Spectrom.* **1988**, 2, 18-21.

248 Kriger, M.S.; Cook, K.D.; Ramsey, R.S. *Anal. Chem.* **1995**, 67, 385-389.

249 personal communication with Dr. S. Hofstadler.

250 Beu, S.C.; Senko, M.W.; Quinn, J.P.; Wampler, F.M., III; McLafferty, F.W. *J. Am. Soc. Mass Spectrom.* **1993**, 4, 557-565.

251 Winger, B.E.; Hofstadler, S.A.; Bruce, J.E.; Udseth, H.R.; Smith, R.D. *J. Am. Soc. Mass Spectrom.* **1993**, 4, 566-577.

252 Kebarle, P. *Ann. Rev. Phys. Chem.* **1977**, 28, 445-476.

253 Vestal, M. *Mass Spectrom. Rev.* **1983**, 2, 447-480.

254 Alexander, A.J.; Kebarle, P. *Anal. Chem.* **1986**, 58, 471-478.

255 Karplus, M.; Porter, R.N. *Atoms and Molecules* W.A. Benjamin, Inc.: California, 1970.

256 Khoo, K.H. *J. of the Chemical Society Faraday Trans I* **1972**, 68, 554-563.

257 Khoo, K.H. *J. of the Chemical Society Faraday Trans I* **1973**, 69, 1313-1319.

258 Taniewska-Osinska, S.; Woznicka, J.; Bartel, L. *Thermochimica Acta* **1981**, 47, 65-69.

259 Roy, R.N.; Gibbons, J.J.; McGinnis, T.; Woodmansee, R. *Cryobiology* 1985, 22, 578-588.

260 Bandopadhyaya, S.; Lahirir, S.C. *J. Ind. Chem. Soc.* 1978, LV, 1286-1292.

261 Grimsrud, E.P.; Kebarle, P. *J. Chem. Soc.* 1973, 95(24), 7939-7943.

262 Lias, S.G.; Leibman, J.F.; Levin, R.D. *J. Phys. Chem. Ref. Data 13* 1984, 695.

263 Krestov, G.A. *Thermodynamics of Solvation* Ellis Horwood: New York, 1991.

264 Wagman, D.D.; Evans, W.H.; Parker, V.B.; Schumm, R.H.; Halow, I.; Bailey, S.M.; Churney, K.L.; Nuttall, R.L. *J. Phys. Chem. ref. Data 11, Supl. 1* 1982.

265 Cooks, R.G.; benyon, J.H.; Caprioli, R.M.; Lester, G.R. *Metastable Ions*; Elsevier: Amsterdam, 1973.

# VITA

Michael Scott Kriger, son of Glenn and Judy Kriger, was born in Miami, Florida on October 12, 1966. He graduated from Winter Park High School in Winter Park, Florida in May 1984. In the fall of 1984, he entered Flagler College in St. Augustine, Florida. He later transferred to the University of Central Florida in 1985. Scott graduated from the University of Central Florida in December, 1989 with a Bachelor of Science degree in chemistry. Scott entered graduate school at the University of Tennessee in the spring of 1990 to conduct research under the direction of Professor Kelsey D. Cook.

As a graduate student, Scott received funding from a Science Alliance Fellowship, a Scholarly Activity and Research Incentive Fund award, a teaching assistantship in general chemistry in 1990, 1993, and 1994, and as an instructor of quantitative analysis in the summer of 1994. Scott also worked as a graduate research assistant for Professor Kelsey D. Cook in 1991, 1992, and 1993.

Scott married Amanda in June of 1992 and became the proud father of Sarah Meghan in January, 1995. Scott has accepted a senior scientist position with Hoffmann-La Roche and will relocate with his family to Florence, South Carolina.

Scott is a member of the American Chemical Society (1989), the American Society for Mass Spectrometry (1990), the East Tennessee Mass Spectrometry Discussion Group (1991), and Sigma Xi Scientific Society (1994).

Scott has co-authored the following presentations and publications:

(1) "Effect of MS Matrix Solvent on the Kinetics of Peptide Hydrolysis by Carboxypeptidase-Y"
Shahgholi, M.; Kriger, S.; Rao, S.; Murawski, S.; Bel, P.; Cook, K. *Proceedings of the 39th ASMS Conference on Mass Spectrometry and Allied Topics*, May 1991, Nashville,TN.

(2) "Time Dependence and Surface Phenomena of Secondary Ion Emission From Solution"
Kriger, M.S.; Cook, K.D.; Short, R.T.; Todd, P.J. *Proceedings of the 40th ASMS Conference on Mass Spectrometry and Allied Topics*, June 1992, Washington, D.C.

(3) "Secondary Ion Emission from Solutions: Time Dependence and Surface Phenomena"
Kriger, M.S.; Cook, K.D.; Short, R.T.; Todd, P.J. *Analytical Chemistry*, 1992, 64, 3052-3058.

(4) "Conductive Tapered Microcapillary Emitters for Electrospray and Electrohydrodynamic Mass Spectrometry"
Cook, K.D.; Kriger, M.S. *Patent under consideration by the University of Tennessee Research Corporation.*

(5) "Evaluation of a Sheathless Capillary Electrophoresis/Electrospray Ionization Interface on an Ion Trap Mass Spectrometer"
Kriger, M.S.; Ramsey, R.S.; Cook, K.D. *Proceedings of the 42nd ASMS Conference on Mass Spectrometry and Allied Topics* May 1994, Chicago, IL.

(6) "Electrohydrodynamic Mass Spectrometry as a Probe of Solution Chemistry: Proton Solvation in Water/Glycerol"
Kriger, M.S.; Cook, K.D. submitted to the *Journal of Physical Chemistry.*

(7) "Durable Gold-Coated Fused Silica Capillaries for Use in Electrospray Mass Spectrometry"
Kriger, M.S.; Ramsey, R.S.; Cook, K.D. *Anal. Chem.* 1995, 67, 385-389.